Role of associated rhoptry proteins in *Toxoplasma gondii* invasion

Ben Chaabene, Rouaa

UNIVERSITÉ DE GENÈVE
FACULTÉ DE MEDECINE
Section de médecine fondamentale
Département de Microbiologie
Prof. Dominique Soldati-Favre
et Médecine Moléculaire
Dr. Gaelle Lentini

Role of associated rhoptry proteins in *Toxoplasma gondii* invasion

THÈSE

présentée aux Facultés de médecine et des sciences de l'Université de Genève
pour obtenir le grade de Docteur ès sciences en sciences de la vie,
mention Sciences biomédicales

par

Rouaa BEN CHAABENE
de
Bizerte (Tunisie)

Thèse N° 207

GENÈVE
2023

Scientific output

The work presented in the thesis resulted in the following peer reviewed article and reviews:

- Lentini, G. †, **Ben Chaabene, R**. †, Vadas, O. †, Ramakrishnan, C., Mukherjee, B., Mehta, V., Lunghi, M., *et al.* (2021), "Structural insights into an atypical secretory pathway kinase crucial for *Toxoplasma gondii* invasion.", *Nature Communications*, England, Vol. 12 No. 1, p. 3788, doi: 10.1038/s41467-021-24083-y. (→ **See chapter 3.1**)

  †These authors contributed equally to the work

- **Ben Chaabene, R**., Lentini, G. and Soldati-Favre, D. (2021), "Biogenesis and discharge of the rhoptries: Key organelles for entry and hijack of host cells by the Apicomplexa.", *Molecular Microbiology*, Vol. 115 No. 3, pp. 453–465. *Review* (→ **See Annex 1**)

- **Ben Chaabene, R**. and Soldati-Favre, D. (2023), "The Lytic Cycle of Human Apicomplexan Parasites.", in Bradshaw, R.A., Hart, G.W. and Stahl, P.D. (Eds.), *Encyclopedia of Cell Biology (Second Edition)*, Academic Press, Oxford, pp. 356–370. *Review* (→ **See Annex 2**)

Manuscript in preparation:

- **Ben Chaabene, R**., *et al.* "*Toxoplasma gondii* RAP1 is critical for rhoptry discharge and invasion." **(In preparation)** (→ **See chapter 3.3 and 3.4**)

Other contributions during my PhD, but not presented in the thesis, resulted in the following publications in peer reviewed scientific journals:

- Hugo, B., **Ben Chaabene, R**., Ricarda, S., Bohumil, M., Baptiste, M.J., Tim-Wolf, G., Tobias, S., *et al.* (2020), "The ZIP Code of Vesicle Trafficking in Apicomplexa: SEC1/Munc18 and SNARE Proteins", *MBio*, American Society for Microbiology, Vol. 11 No. 5, pp. e02092-20, doi: 10.1128/mBio.02092-20.

Acknowledgment

First, I would like to say a huge thank you to “the big boss” **Dominique** for everything. Thank you for giving me the opportunity to work on such great projects in such an amazing environment. Thank you for all the guidance and hours of brainstorming. Thank you for your tireless patience and continuous support, and for finding a way to pick me up whenever I lose my way.

I would like to warmly thank **Gaëlle** “la boss” for being such a great supervisor and an awesome friend. Thank you for sharing with me all your knowledge about the field and for sticking up with me (I know it was not that easy) throughout all these years. Thank you for always believing in me. You are such an inspiration, and I will be grateful for life.

I would like to also thank the **thesis committee members** who accepted to review my work and evaluate my PhD thesis.

I couldn’t have wished for a better lab, with the perfect blend of craziness, fun, and science. I walked into this lab in September 2017, and I was warmly welcomed by everyone, and it took a few hours to realize how incredibly crazy this place is. Besides all the fun, the commitment to research and the amount of scientific discussions we can have in the lab, are astonishing. Thank you all for the great memories, for all the laughters we shared, for all the top-secret events we had, for the hepatic cirrhosis and diabetes I am getting in the future, for the good and very bad music played in the P2 and for every mental support when needed. You made this place a second home for me. I will take a few lines to express my thanks to…

Sunil, for being my best friend through it all and for all the memories in and outside the lab; **Hugo**, my beer mate, my crazy *****, for all the hangovers and the crazy memories (The kilimanjara); **Nicolas**, for your crazy mood that makes me laugh and the escape games we managed to solve; **Caty**, for being our minister of happiness and for always finding time for each and everyone, **Jean-Ba**, mon vieux préféré, for your big heart and for being my favorite superhero in the lab; **Matteo**, for bringing some calm and peacefulness to the lab; **Aarti**, for dealing with all my Abishtu and for always taking care of me; **Joachim**, Jo Jo, for just being you, the calm and crazy, and for never calling the HR department; **Mary**, for bringing all the joy to the P2 dance

floor; Shu, my Shu Shu, for your great spirit and making sure that I'm always well fed in the lab; **Rémy**, for the great discussions and your joyful presence; **Oscar**, our protein purification God, for the support and the tireless discussions during RON13 project (RONthirTEAM); **Bohumil**, for always being there when needed; **Alessandro**, for being my first mentee, for your great work and your joyful smile; **Albert** (or is it Alter?), my Albertito, for being a great neighbor in the lab and a good friend; **Romuald**, for trying your best so I don't kill you and the great laughters we had together; **Gloria**, for your nice spirit and the good vibes; **All the rest of the Soldati lab**, the previous and the current members, and all members of **the Brochet lab**, for all the apéros we had, all the dinners and events and for making my PHD a great memory that I will always cherish.

I want to thank the whole **MIMOL department** for such great fun and memories. I met some amazing people who became great friends of mine. **Joao, Aurélia, Ines (x2), Mariana, Natalia** and **Yugo,** thank you for being such great friends, for all the great memories and the Ibiza nights. I couldn't have survived this without you. Big thanks to the secretariat, **Dylan, Doris, Luli** and **Hani** for your great work and for always being there when needed. **Manel**, thank you for always trying to help and for smoothening my stay.

Thanks to all the people I met through the **PhD program** and the **PhD association**. It was such great pleasure meeting every single one of you. A big thanks to my friends with whom I had the great pleasure to work with in our Biosounds podcast.

I want to specially thank my "**Geneva family**" and all these people who made my life here feels quite like home. **The Silvermits**, my dear besties, thank you for being in my life. **The Labrigas,** thanks for all the support and fun memories. **Chris,** for your great book suggestions, **Esteban,** for being an awesome D&D Master. All my boardgaming friends and especially **Dino**, thanks for being such a good friend and for all the fun times. **Rania** and **Mouna**, my first friends here in Genava, thank you for the wonderful time. Many thanks to all the rest of my friends and people who were once part of my life.

A special thank for my non biological twin, **Foufou**, for being my best friend since we were born and for always having my back.

I would love to thank you all again, and many others whom I haven't named, for being part of my life and this journey. I will never forget you!

I like to thank all members of **my family**, for the endless support and all the sacrifices along these years. **My parents**, Raoudha and Khaled, for everything they have done for me and their endless love. **My brother**, Riadh, for always being there for me. I'm proud of you. **My grandmother**, Radhia, for being my safe space and for loving me unconditionnaly. My aunts, **Tati Maha** and **Tati Ishraf**, for being such amazing role models and for being always there for me. All of you and everyone that I haven't named, thank you so much and I love you all.

Last but not the least, to the most important person in my life. For nothing would have been possible without you in my life. For being my rock throught all this journey. For dealing with my ups and downs and for always picking me up and pushing me forward. You make me a better person everyday. I can't even thank you enough. I love you so much **Safa,** my Wifie. And thank you to my baby cat, **Tesla**, for always making me smile with your goofiness, and for keeping me company when I was writing this PhD thesis.

Thank you, Thank you so much!!

Abstract

The unicellular eukaryote *Toxoplasma gondii* commonly parasitizes humans and other vertebrates, and approximately one third of the human population is chronically infected. This opportunistic pathogen is an obligate intracellular parasite that belongs to the phylum of Apicomplexa, which also includes *Cryptosporidium* and *Plasmodium* species and numerous other human and veterinary pathogens.

For an obligate intracellular parasite, host cell invasion is a vital event to survive, replicate and spread. Rhoptries are specialized apical secretory organelles conserved in the Apicomplexa phylum that play a critical role in the establishment of the intracellular niche. Rhoptry proteins fall into two categories based on their localization in the sub-compartments of the organelle: rhoptry neck proteins (RONs) and rhoptry bulb proteins (ROPs). Some of these proteins critically participate in invasion (RONs) and subversion of host cellular function (ROPs). In addition to proteins, rhoptries contain lipids and membranous materials (Dubremetz, 2007) that contribute to the formation of the parasitophorous vacuole membrane (PVM) to sustain invasion and to hijack host functions crucial for maintaining the infection (Boothroyd and Dubremetz, 2008). During invasion, a set of rhoptry proteins form a RON complex that is indispensable for the formation of the moving junction (MJ), a structure at the interface between host and parasite plasma membrane which is critical for parasite invasion and serves as a support to propel it inside the host cell (Alexander *et al.*, 2005; Besteiro *et al.*, 2009; Lebrun *et al.*, 2005; Mital *et al.*, 2005).

The thesis project was aiming to identify novel components implicated in rhoptry discharge. The first part of the thesis focused on TGGT1_321650 that was previously identified as a substrate of ASP3, an aspartyl protease essential for rhoptry secretion (Dogga *et al.*, 2017). TGGT1_321650 encodes a rhoptry neck protein, RON13 predicted to be fitness-conferring (Sidik *et al.*, 2016). RON13 possesses a transmembrane spanning segment, a predicted Serine/Threonine kinase domain and a large C-terminal extension. Biochemical characterization of the enzyme and resolution of its tridimensional structure at atomic resolution by cryo-electron microscopy reveal that RON13 is an atypical S/T kinase. Phenotypical investigations showed that parasites lacking RON13 or expressing an inactive RON13 kinase can secrete their rhoptry content but cannot form

the MJ, resulting in a severe defect in invasion. Comparative phosphoproteomics between wild type and RON13 depleted parasites, led to the identification of numerous RON13 susbtrates. Mainly ROPs and RONs are phosphorylated by RON13, including the RON complex. Collectively, RON13 activity is instrumental for RON complex assembly at the MJ, justifying its role in invasion.

Recent studies based notably on cryo-electron tomography, have shed light on the structural and molecular players of the rhoptry secretion apparatus, however the molecular mechanisms that timely and spatially orchestrate organelle discharge are far from being fully understood. To fill up in part this gap of knowledge, we scrutinized 7 predicted fitness conferring proteins found in the rhoptry fraction by localization of organelle proteins by isotope tagging (LOPIT) (Barylyuk *et al.*, 2020). The second part of the thesis was dedicated to the characterization of TGGT1_242820, that codes for a 22 kDa Rhoptry Associated Protein (RAP1). RAP1 is located at the rhoptry bulb and at the rhoptry tip and shows a dynamic localization following invasion. Conditional depletion of RAP1 results in a severe block in rhoptry discharge leading to an impairment in invasion.

Résumé

Toxoplasma gondii est un parasite eucaryotique unicellulaire qui infecte couramment les animaux à sang chaud et notamment les humains avec environ un tiers de la population humaine chroniquement infectée. Cet agent pathogène opportuniste est un parasite intracellulaire obligatoire appartenant au phylum des Apicomplexes qui comprend également les espèces telles que *Cryptosporidium* et *Plasmodium* et un certain nombre d'autres agents pathogènes d'importance vétérinaire.

Pour ce parasite intracellulaire obligatoire, l'invasion de la cellule hôte est un événement vital pour survivre, répliquer et se propager. Les rhoptries sont des organelles sécrétoires apicales, conservées dans le phylum des Apicomplexes et jouant un rôle critique dans l'établissement du parasitisme. Les protéines des rhoptries se divisent en deux catégories en fonction de leur localisation dans les sous-compartiments de l'organite : les protéines du col des rhoptries (RONs) et les protéines du bulbe des rhoptries (ROPs). Certaines de ces protéines participent de manière critique à l'invasion (RONs), et à la subversion de la fonction cellulaire hôte (ROPs). Les rhoptries contiennent également des matériaux membranaires et des lipides (Dubremetz, 2007) qui contribuent à la formation de la membrane de la vacuole parasitophore afin de soutenir l'invasion et de détourner les fonctions de l'hôte cruciales pour l'infection (Boothroyd and Dubremetz, 2008). Durant l'invasion, un ensemble de protéines des rhoptries forment un complexe RON qui est indispensable pour la formation de la jonction mobile, une structure à l'interface entre la membrane plasmique de l'hôte et celle du parasite qui est critique pour l'invasion du parasite et sert de support pour le propulser à l'intérieur de la cellule hôte (Alexander *et al.*, 2005; Besteiro *et al.*, 2009; Lebrun *et al.*, 2005; Mital *et al.*, 2005).

Le projet de thèse avait pour but d'identifier de nouveaux composants impliqués dans la sécrétion des rhoptries. La première partie de la thèse est concentrée sur TGGT1_321650 qui a été précédemment identifié comme un substrat de ASP3, une aspartyle protéase essentielle pour la sécrétion des rhoptries (Dogga *et al.*, 2017). TGGT1_321650 code pour une protéine du col des rhoptries, RON13, qui possède un domaine transmembranaire, un domaine sérine/thréonine kinase prédit et une large extension C-terminal. L'expression de RON13 recombinante dans des

cellules d'insecte a permis la caractérisation biochimique de l'enzyme et de résoudre sa structure tridimensionnelle à une résolution au niveau atomique, par microscopie cryo-électronique. Des études biologiques ont révélé que les parasites dépourvus de RON13 ou exprimant une version inactive de la kinase sont capables de sécréter le contenu des rhoptries mais ne peuvent pas former de jonction mobile, ce qui entraîne un grave défaut d'invasion. La phosphoprotéomique comparative entre les parasites de type sauvage et ceux dépourvus de RON13 a conduit à l'identification de nombreuses protéines ROPs et RONs, y compris le complexe RON, comme substrats de cette kinase. Collectivement, l'activité de RON13 est instrumentale pour l'assemblage du complexe RON à la jonction mobile, et peut expliquer son rôle dans l'invasion.

Des études récentes, basées notamment sur la tomographie cryo-électronique, ont identifié les acteurs structurels et moléculaires de l'appareil de sécrétion des rhoptries ; cependant, les mécanismes moléculaires qui orchestrent de manière temporelle et spatiale la décharge des organelles sont loin d'être entièrement compris. Pour combler en partie ce manque de connaissances, nous avons examiné 7 protéines prédites essentielles, et trouvé dans la fraction des rhoptries par localisation des protéines organellaires grâce au marquage isotopique (LOPIT) (Barylyuk *et al.*, 2020). La deuxième partie de la thèse a été consacrée à la caractérisation de TGGT1_242820, qui code pour une protéine associée aux rhoptries de 22kDa (RAP1). La déplétion conditionnelle de RAP1 entraîne un blocage sévère de la sécrétion des rhoptries conduisant à une déficience de l'invasion. RAP1 n'est pas sécrétée dans la cellule hôte mais s'accumule à l'extrémité des rhoptries et montre une localisation dynamique pendant l'invasion.

Table of Contents

List of abbreviations

Acβ Adenylate cyclase β

ADP Adenosine diphosphate

AIP Aro-intercating protein

ALIX ALG-2 interacting protein X

AMA Apical membrane antigen

AP1 Adaptor protein 1

APH Acylated pleckstrin homology protein

APR Apical polar ring

ARM Armadillo motif

ARO Armadillo repeat only protein

ASP Apical sushi protein

ASP Aspartyl protease

ATc Anhydrotetracyclin

ATP Adenosine triphosphate

AV Apical vesicle

BBB Blood-brain barrier

BDCP BEACH domain-containing protein

BIPPO 5-Benzyl-3-isopropyl-1H-pyrazolo[4,3-d] pyrimidin-7(6H)-one

BSA Bovine serum albumin

Ca^{2+} Calcium ions

cAMP Cyclic adenosine monophosphate

CDC50 Cell division control protein 50

CDPK Calcium-dependent protein kinase

cGMP Cyclic guanosine monophosphate

cGMP Cyclic adenosine monophosphate

CIN85 Cbl-interacting 85 kDa protein

CNS Central nervous system

CRMP Cystein repeats modular protein

CSCHAP Coccidian Specific CORVET/HOPS Associated Protein

CTD C-terminal domain

CTE C-terminal extension

CytD Cytochalasin D

DAG Diacylglycerol

DAPI 4',6-diamidino-2-phenylindole

DGK Diacylglycerol kinase 1

DHFR Dihydrofolate reductase

DiCre Dimerizable Cre

DMEM Dulbecco's Modified Eagle Medium

DOC2 Double C2 protein

DrpB Dynamin-related protein B

EBA Erythrocyte binding antigen

EE Early endosomes

ELC Endosome-like compartment

EM Electron microscopy

ER Endoplasmic reticulum

ET Electron tomography

F-actin Filamentous actin

FER Ferlin proteins

FIB-SEM Focused ion beam-scanning electron microscopy

GAC Glideosome-associated connector

GBP Guanylate binding protein

GC Guanylate cyclase

GLURP Glutamate rich protein

gRNA guide RNA

GPI Glycosylphosphatidylinositol

GRA Dense granules proteins

GTP Guanosine triphosphate

HFF Human foreskin fibroblast

HtrA High temperature requirement A

HXGPRT Hypoxanthine-xanthine-guanine phosphoribosyl transferase

IAA Indole-3-acetic acid (auxin)

ICMAP Intraconoidal microtubule-associated proteins

ICMT Intraconoidal microtubules

IFA Immunofluorescence assay

IFNγ Gamma interferon

IMC Inner membrane complex

IMP Intramembranous particles

IP_3 Inositol triphosphate

IRG Immunity-related GTPases

IVN Intravacuolar network

K^+ Potassium ions

mAiD mini-auxin degron

MIC Microneme proteins

MJ Moving junction

MPA Mycophenolic acid

MTOC Microtubule organization center

MVs Microtubule-associated vesicles

MW Molecular weight

Myo Myosin heavy chain

Myr Myc-regulation genes

ND Non-discharge

NDP ND partner

PA Phosphatidic acid

PAT Putative pantothenate transporter

PBS Phosphate-buffered saline

PCR Preconoidal rings

PH Plekstrin-homology

PIP2 Phosphatidylinositol 4,5 biphosphate

PI-PLC Phospholipase C

PKA cAMP-dependent protein kinase

PKG cGMP-dependent protein kinase

PLP1 Perforin-Like Protein 1

PM Plasma membrane

PTM Post-translational modification

PV Parasitophorous vacuole

PVM Parasitophorous vacuole membrane

RA Rhoptry-associated adhesin

RAP1 Rhoptry-associated protein 1

RASP Rhoptry Apical Surface Protein

RBC Red blood cell

RDF Rhoptry discharge factor

RON Rhoptry neck proteins

ROP Rhoptry bulb proteins

ROPK ROP kinase

RSA Rhoptry secretory apparatus

SAG Surface antigen glycoprotein

SDS Sodium dodecyl sulfate

SNARE Soluble N-ethylmaleimide-sensitive-factor attachment protein receptor

snRNA Small nuclear ribonucleoprotein

SPMT Subpellicular microtubules

SRS SAGs related sequence

SRTLR Sortlilin-like receptor

STAT Signal Transducer and Activator of Transcription

SUB1 Microneme Subtilisin Protease 1

TAILS Terminal amino isotopic labeling of substrates

TEM Transmission electron microscopy

TEMED Tetramethylethylenediamine

TFP Transporter facilitator protein

TGN Trans-golgi network

TMD Transmembrane domain

U-ExM Ultrastructure expansion microscopy

UGO Unique GC organizer

UPRT Uracil phosphoribosyltransferase

VAC Vacuolar compartment

VSP Vacuolar protein sorting-associated protein

WHO World Health Organization

WRD Tryptophan-rich protein

XA Xanthine

1. Introduction

1.1. The phylum of Apicomplexa

Apicomplexan parasites form a phylum of single-celled eukaryotes that include a large number of notorious pathogens of animals and humans, with 6000 identified species, making it a pressing clinical and economic burden (Adl *et al.*, 2012). These parasites have adopted an intracellular lifestyle, a strategy that is effective for microorganism's survival. This mechanism allows these pathogens to hide from the host immune system, avoid clearance and access the host metabolites and nutrients. Apicomplexans are grouped with the ciliates and dinoflagellates, under the Alveolata superphylum (Adl *et al.*, 2012). The phylum is divided into three main groups: gregarines, coccidia and hematozoa **(Figure 1.1)**. Gregarines comprise several subgroups: archigregarines, eugregarines, neogregarines and Cryptosporidia (Votypka *et al.*, 2016). For a long time, *Cryptosporidium* was classified in the coccidia group, but it was formally transferred to the gregarines group after confirming its close relationship with these parasites (Ryan *et al.*, 2016).

Gregarines are considered the "primitive" apicomplexan parasites infecting the intestine of a wide repertoire of invertebrates and lower vertebrates. Transmission of these pathogens occurs by the oral ingestion of oocysts. Sporozoites escape the oocysts, attach to the intestine, and develop epicellulary (Leander, 2008). Due to its medical and veterinary importance, *Cryptosporidium spp.* is the most studied pathogen in this group. *Cryptosporidium parvum* is responsible for severe intestinal diseases and it is the leading cause of diarrhea-associated mortality in children and immunocompromised patients worldwide (Khalil *et al.*, 2018).

Hematozoa subclass is composed of Haemosporidia (*Plasmodium spp.)* and Piroplasmida (*Babesia spp.* and *Theileria spp.*). *Plasmodium spp.* are the causative agent of malaria in humans and animals. *Plasmodium falciparum* is the deadliest form of human malaria, responsible for the death of 627,000 person annually, most of them are young children in sub-Saharan Africa (WHO World Malaria Report 2021). *Plasmodium vivax*, *Plasmodium malariae*, *Plasmodium knowlesi* and *Plasmodium ovale* also cause benign and severe forms of malaria in humans while other species

like *Plasmodium berghei* causes murine malaria. Both *Babesia spp.* and *Theileria spp.* are responsible for tick-borne diseases in animals and have high consequences on livestock industry.

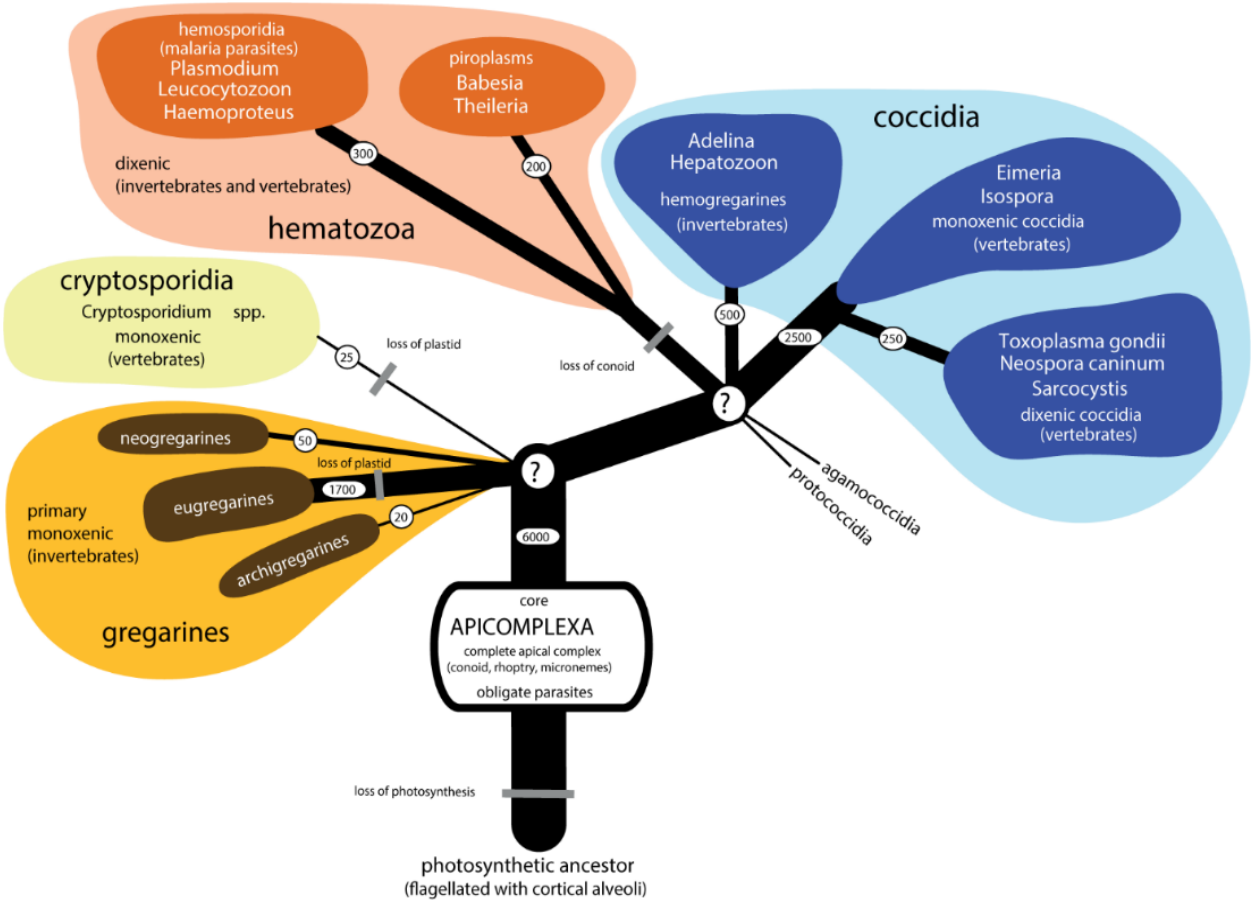

Figure 1.1 **Phylogenetic tree of Apicomplexa.** Numbers and branch thickness represent number of species. Modified from (Votypka *et al.*, 2016).

The coccidian subclass, groups a number of cyst-forming pathogens with widespread prevalence and impact on animal and human health. This group includes parasites that infect cattle and life-stocks like *Eimeria* (the causative agent of chicken coccidiosis), *Neospora* (causing disease in cattle), *Sarcocystis* (causing disease in sheep) and *Besnoitia spp* (causes skin lesion in domestic animals). *Toxoplasma gondii* is the most studied coccidian pathogen and represents an important model organism for Apicomplexa. *T. gondii* causes toxoplasmosis, one of the most common

infections in humans and warm-blooded animals. With a prevalence estimated at 30% in humans and more than 60% in birds and wild rodents, it represents a major threat in the agriculture sector (Tenter *et al.*, 2000). Even though the acute infection is often well controlled by a healthy immune system, the parasite reaches immune-privileged sites such as the eye, brain (where the parasite persists as cysts) or the placenta and can infect the fetus. Therefore, immunocompromised/immunosuppressed patients are most vulnerable to the development of acute toxoplasmosis upon a new infection or reactivation of cysts. Fatally, *T. gondii* can cause encephalitis, retinochoroiditis and hydrocephalus in congenitally infected children.

Apicomplexan pathogens share several unifying morphological features (dos Santos Pacheco *et al.*, 2020) as well as the conservation of many apicomplexan specific genes (Janouškovec *et al.*, 2019). Despite all these common features, these parasites infect a wide range of distinctive hosts, occupy specific niches, and have divergent strategies to ensure their survival and transmission.

1.2. Ultrastructure of *Toxoplasma gondii*

Members of Apicomplexa possesses the typical features of eukaryotic cells such as a nucleus, the endoplasmic reticulum (ER), a Golgi apparatus, and a single tubular mitochondrion **(Figure 1.2)**. The parasite is enclosed by a pellicle composed of the plasma membrane (PM) associated to an inner membrane complex (IMC). The IMC is a double membrane system composed of flattened membranous sacs or vesicles, positioned underneath the PM. The IMC is underlined by a meshwork of intermediate-like filaments called the alveolin network. Most of the apicomplexan parasites possess a peculiar non-photosynthetic plastid-like organelle called the apicoplast, which hosts essential metabolic pathways, making it a drug target of choice (McFadden and Yeh, 2017).

Like all other apicomplexan parasites, *T. gondii* is a highly polarized cell. The apical and basal poles contain highly complex structures. The apical complex, which gives the name of this phylum, is conserved among Apicomplexa. This structure is composed of cytoskeletal elements

and secretory organelles. The cytoskeletal part harbors the apical polar ring (APR), a structure that presumably serves as a microtubule organizing center (MTOC), nucleating the twenty-two subpellicular microtubules (SPMTs) of *T. gondii*. The SPMTs cover two third of the parasite length and give it its distinctive crescent shape **(Figure 1.2)**. An additional tubulin-rich structure, the conoid, is a dynamic organelle located on top of the APR (Hu, Roos, et al., 2002; Morrissette and Sibley, 2002). The conoid moves through the APR (extrude) during invasion in a calcium-dependent manner (del Carmen *et al.*, 2009; Mondragon and Frixione, 1996; Monteiro *et al.*, 2001).

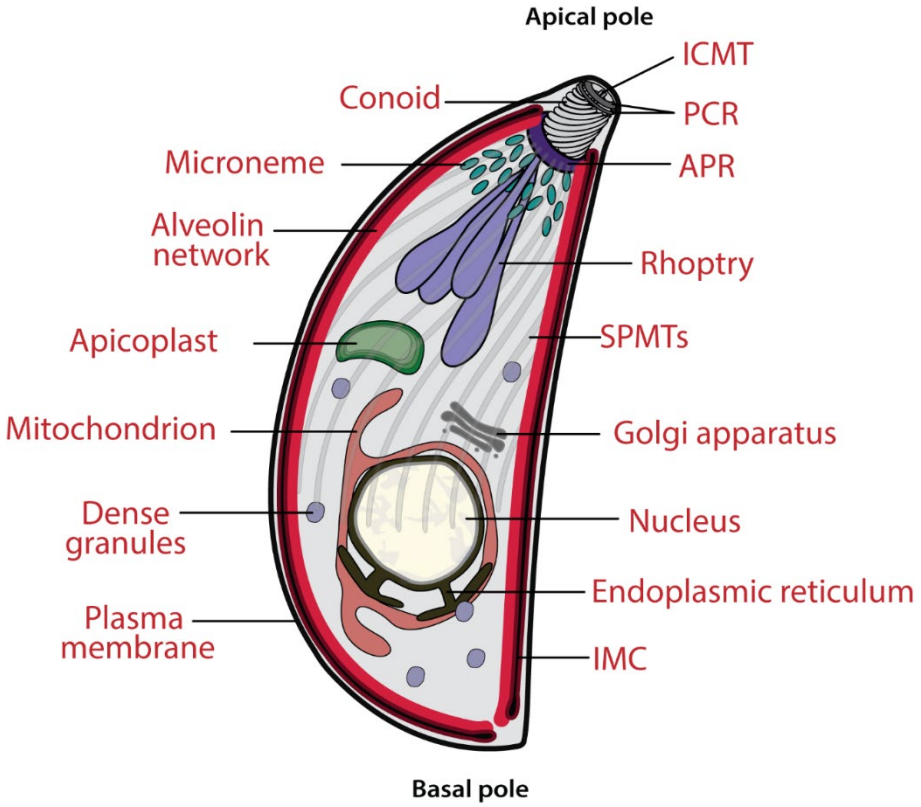

Figure 1.2 **Schematic representation of *Toxoplasma gondii* ultrastructure**. Modified from (ben Chaabene and Soldati-Favre, 2023).

In coccidians, the conoid is composed of a cone made of spiraling tubulin fibers, is topped by two preconoidal rings (PCRs) and and a pair of intraconoidal microtubules (ICMTs) are found in the

center of the structure (dos Santos Pacheco *et al.*, 2020). For a long time, it was thought that *Plasmodium* species are devoid of conoid. Recently, a reduced conoid was observed using ultrastructure expansion microscopy (U-ExM) and cryo-electron tomography (cryo-ET) (Bertiaux *et al.*, 2021; Ferreira *et al.*, 2022). However, this conoid was present only in ookinetes.

The secretory organelles found in the apical complex of *T. gondii* are named rhoptries and micronemes **(Figure 1.2)**. These two organelles differ both in shape and in function, and are required for host cell invasion, egress, and establishment of an intracellular lifestyle. Micronemes are small, rod-shaped organelles and about 50 to 100 micronemes can be found at the apical pole of *T. gondii* tachyzoites. Micronemes contain proteins including adhesins, proteases and perforins that are secreted in a calcium-dependent manner by the fusion of the organelle with the PM. Microneme proteins (MICs) are needed for the parasite motility, invasion, and egress from the infected host cell (Dubois and Soldati-Favre, 2019). In contrast, rhoptries are much larger, club-shaped organelles (8 to 12 per parasite) that cluster together at the apical pole and are critical for parasite invasion and host cell modulation (Ben Chaabene et al., 2021). Conventional transmission electron microscopy (TEM) of ultra-thin sections showed that the organelle is organized in two sub-compartments, a long narrow neck that appears uniformly electron dense, and a basal portion called bulb with a honeycomb appearance (Dubey *et al.*, 1998). Another type of secretory organelles, the dense granules, are found randomly dispersed within the cytosol. They have a spherical-shaped structure and appear electron dense in TEM, hence their name (Ferguson DJP, 2013). The dense granule proteins are important for the remodeling of the vacuolar niche and the modulation of the host cellular function (Griffith *et al.*, 2022).

1.3. Life cycle and lytic cycle of *Toxoplasma gondii*

1.3.1. Life cycle

T. gondii has a complex life cycle that consists of several developmental stages: the sporozoite stage in oocysts shed in the feces of the definitive host (felids), the tachyzoite stage and the cyst-forming bradyzoite stage within the intermediate hosts (Delgado *et al.*, 2022) **(Figure 1.3)**. Sexual replication of *T. gondii* is accomplished within the definitive host where the parasites undergo merogony following the invasion of the intestinal epithelial cells (Hunter and Sibley, 2012). The merozoites produced proceed to gametogony to generate the sexual forms, the male microgamete and female macrogamete.

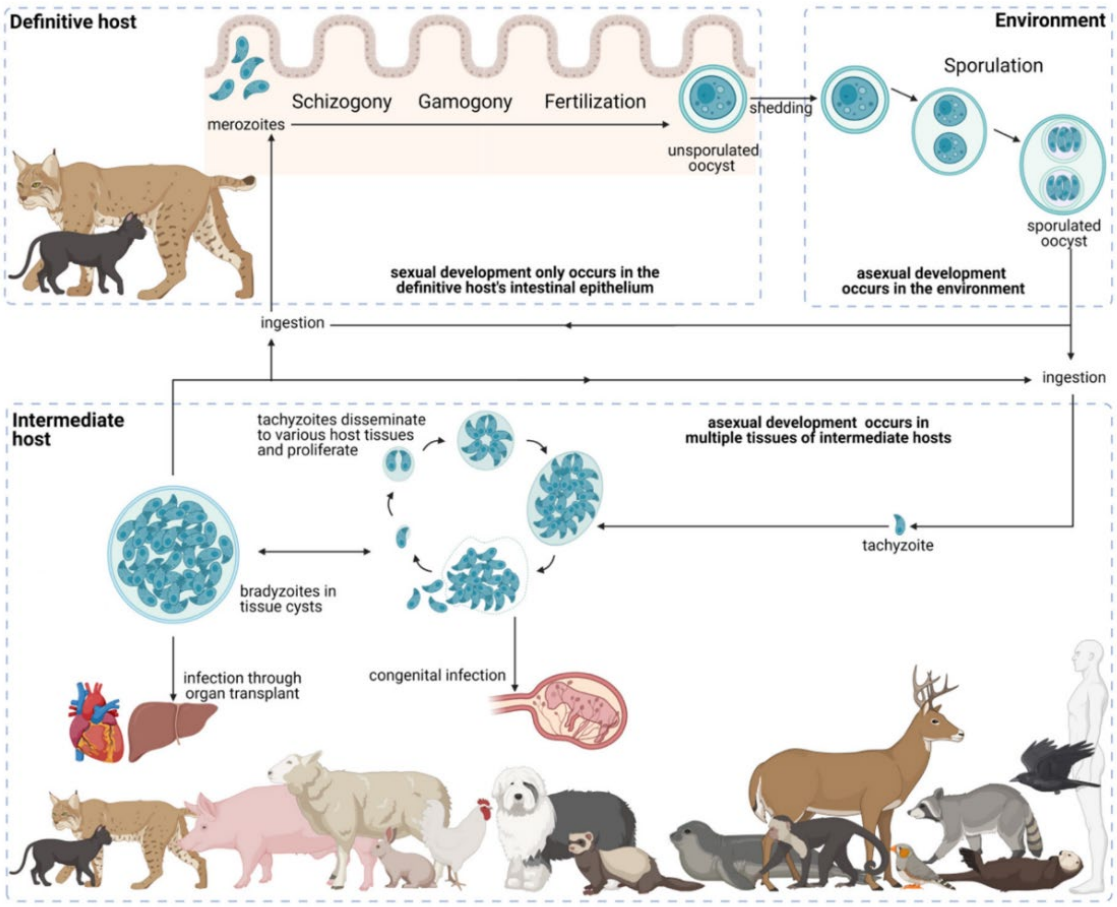

Figure 1.3 **Life cycle of *Toxoplasma gondii*.** Modified from (Delgado *et al.*, 2022).

The fertilization of macrogamete occurs after the release of the bi-flagellated microgametes and generates oocysts. In the environment, the oocysts sporulate and become infective via ingestion of contaminated food or water, starting the asexual replication of the parasites in intermediate hosts. Sporozoites infect the intestine and rapidly multiply to produce highly replicative tachyzoites capable of invading host cells and initiate new lytic cycles **(Figure 1.3)**.

Tachyzoites can disseminate throughout the host body, by infecting migratory immune cells via a "Trojan horse" strategy (Drewry and Sibley, 2019), and be responsible for the acute phase of infection, though this phase is usually quelled by the host's immune defenses. However, the parasite can escape clearance by invading immune-deprived sites and differentiates into the slow replicating bradyzoites that form tissue cysts, leading to the chronic form of the infection. Tissue cysts are frequently localized in the brain and skeletal muscles, where they persist usually asymptomatically during the entire life of the host (Weiss and Kim, 2000).

The life cycle is completed upon predation of the intermediate host by a member of the felid family. Several drugs are efficient against the replicative tachyzoites. However, no effective drugs are available against the slow growing cyst forming bradyzoites, hindering an efficient treatment of chronically infected patients or animals. Additionally, tissue cysts are infectious through carnivorism, which is a unique feature of *Toxoplasma* among the coccidia group, allowing a horizontal infection between intermediate hosts without going through sexual reproduction. This represents one of the key determinants of the high infection rate of *T. gondii* and play a role in the clonal expansion of the parasite into three major clonal lineages (Su *et al.*, 2003). Type I strains (typified by RH and PLK) are highly virulent, while type II (typified by ME49) and type III (typified by CTG) are less virulent. These differences in virulence are partially attributed to different alleles of virulence factors secreted into the host cell during invasion (Hunter and Sibley, 2012) **(detailed in chapter 1.6).**

1.3.2. Lytic cycle

The fast-replicating tachyzoite is the most studied stage due to its simple cultivation in laboratory tissue culture. *T. gondii* tachyzoite can be maintained and amplified asexually through several

lytic cycles in many types of nucleated cells. This cycle requires several critical steps, starting with the gliding motility of the parasite and attachment to the host cell followed by invasion and simultaneous formation of the parasitophorous vacuole (PV) **(Figure 1.4)**. The human fibroblasts (HFF) are primary cells that become quiescent and are frequently used to passage the parasites. The PV, a protective niche within the host cell cytoplasm, is essential for the parasite proliferation and dissemination. Parasites undergo several cycles of multiplication and eventually actively egress from the host by lysis of the parasitophorous vacuole membrane (PVM) and the host PM. Freshly egressed parasites immediately infect neighboring cells to initiate a new lytic cycle **(Figure 1.4)**.

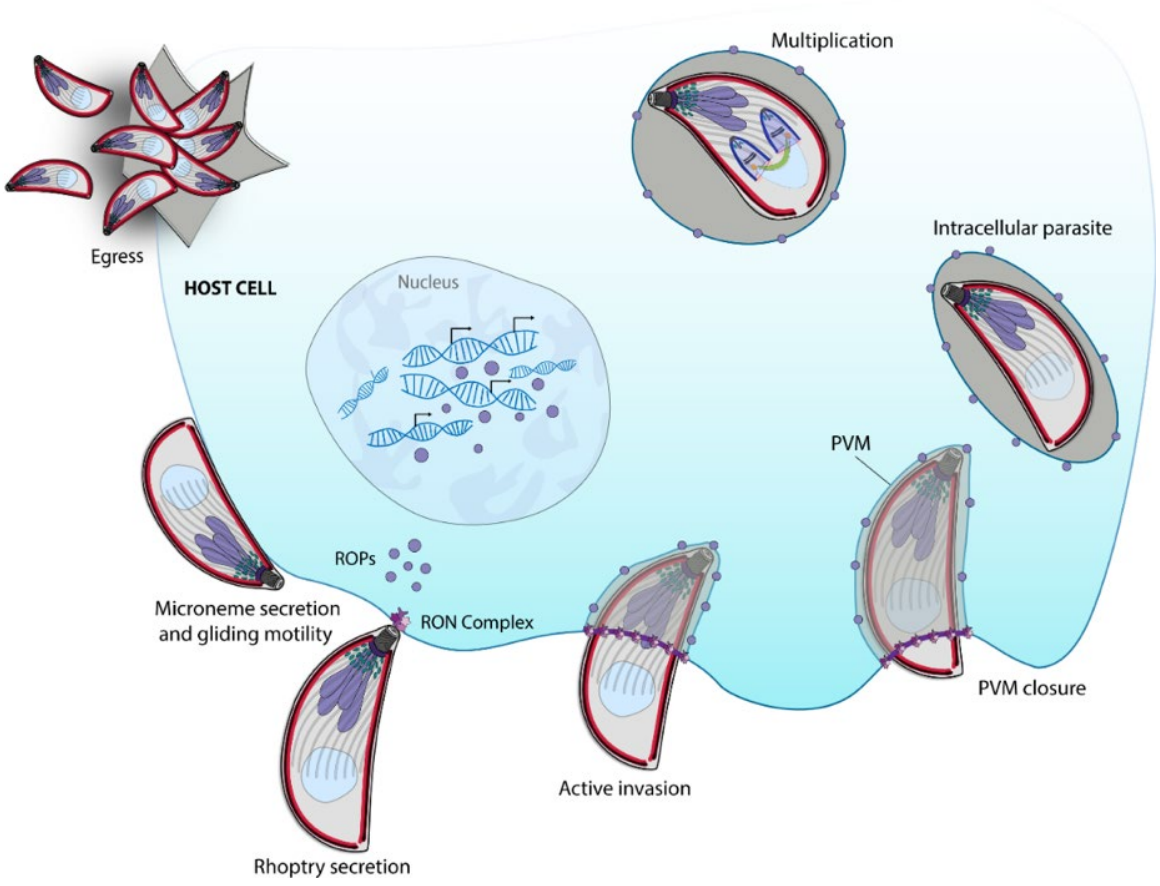

Figure 1.4 **Lytic cycle of *Toxoplasma gondii*.** Modified from (Ben Chaabene et al., 2021).

To multiply, *T. gondii* tachyzoites engage in cycles of internal budding process called endodyogeny (*endo*-inside, *dys*-two, *genesis*-creation), where two daughter cells are formed within the mother cell that will eventually be lost (Hu, Mann, *et al.*, 2002) **(Figure 1.5)**. This process is highly synchronized among the parasites of the same vacuole and initiates as soon as the parasite infects the host cell, inside the PV.

The first steps of parasite division are replication of the centrioles, elongation of the Golgi apparatus and apicoplast. Then, the daughter cell conoid and MTOC are assembled forming the nucleating points for the daughter IMCs and SPMTs (Nishi *et al.*, 2008). The elongation of the IMC guarantees the separation between the mother material and the forming daughter cells. This is trailed by sequential segregation of the nucleus, ER, Golgi apparatus, apicoplast and the mitochondrion. In contrast, the secretory organelles are mainly made *de novo* in each forming daughter cell (Nishi *et al.*, 2008) **(Figure 1.5)**.

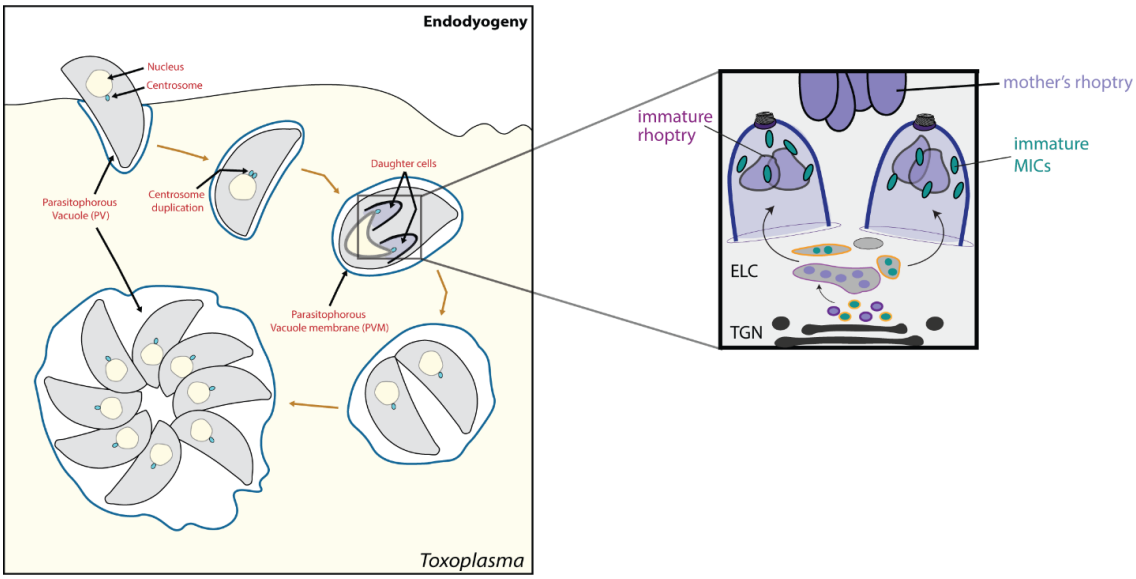

Figure 1.5 **Endodyogeny in *T. gondii*.** Intracellular parasite divides by endodyogeny producing two daughter cells inside the mother cell. Pro-rhoptries and pro-micronemes are sorted inside vesicles emerging from the trans-Golgi network (TGN). The content of these vesicles is processed in the endosome-like compartment (ELC) before forming the immature organelles. Image modified from (ben Chaabene and Soldati-Favre, 2023).

Additionally, daughter micronemes are also recycled from the mother in an actin dependent manner (Periz *et al.*, 2019). Eventually, the cytoskeleton and non-inherited materials of the mother cell are disassembled and degraded in the residual body, a compartment that connect all the parasites inside the vacuole (Muñiz-Hernández *et al.*, 2011). Finally, the PM of the mother cell covers the two emerging daughter cells whereas the mitochondrion forms a continuum via the residual body between the two formed parasites (Nishi *et al.*, 2008).

1.4. Secretory organelles

To undergo successful lytic cycles, members of Apicomplexa rely on their secretory organelles that play a crucial role in the parasite survival. Some content of these organelles also modulates the host cell innate defense and interfere with the host signaling, conferring resistance to host cell defenses. Invasion and egress are defining features of this phylum and secretory organelles similar to micronemes and rhoptries are present in other branches of alveolates (Gubbels and Duraisingh, 2012; dos Santos Pacheco *et al.*, 2020), suggesting their existence before the emergence of intracellular parasitism.

1.4.1. Micronemes

Micronemes are composed of a wide repertoire of proteins with transmembrane and soluble proteins including adhesins, proteases and perforins (Dubois and Soldati-Favre, 2019) that critically participate in motility, invasion, and egress. Two distinct populations of micronemes were observed by super-resolution microscopy and they appear to be trafficked differently (Kremer *et al.*, 2013). In *Plasmodium spp.* this characteristic is more prominent with the existence of a microneme-like organelles that are exclusively involved in egress whereas the “classical” microneme organelles are only important for motility and invasion (Singh *et al.*, 2007; Yeoh *et al.*, 2007). In *Toxoplasma,* micronemes accumulate under the conoid or at its periphery but recently, some micronemes were also observed inside the conoid (Gui *et al.*, 2022; Mageswaran *et al.*, 2021; Segev-Zarko, Dahlberg, Sun, Pelt, Sethian, *et al.*, 2022).

1.4.1.1. Microneme exocytosis

Microneme exocytosis is driven by the fusion of the organelles with the parasite PM. Even though apicomplexan genomes encode for some of the highly conserved eukaryotic component of the exocytosis machinery, it was recently showed that they play a role in organelle trafficking rather than exocytosis (Ayong *et al.*, 2011; Hugo *et al.*, 2020; Shinuo *et al.*, 2021). This indicates that microneme exocytosis rely on different effectors and might follow an unconventional mechanism of fusion. Microneme exocytosis is triggered upon a complex signaling cascade that involves several molecular components (Bisio and Soldati-Favre, 2019) **(Figure 1.6)**.

The first described extrinsic signal that triggers microneme secretion is the drop of potassium (K^+) levels. This is sensed by the parasite through the activation of phospholipase C (PI-PLC) that raises the intracellular concentration of calcium (Ca^{2+}). The cGMP-dependent protein kinase (PKG) (Brown *et al.*, 2017) phosphorylates key enzymes forming phosphatidylinositol 4,5 biphosphate (PIP2) that is next converted by PI-PLC (Brochet *et al.*, 2014) into inositol triphosphate (IP3) and diacylglycerol (DAG) (Singh *et al.*, 2010). IP3 binds its receptors in the ER inducing the release and increase of Ca^{2+} in the cytosol.

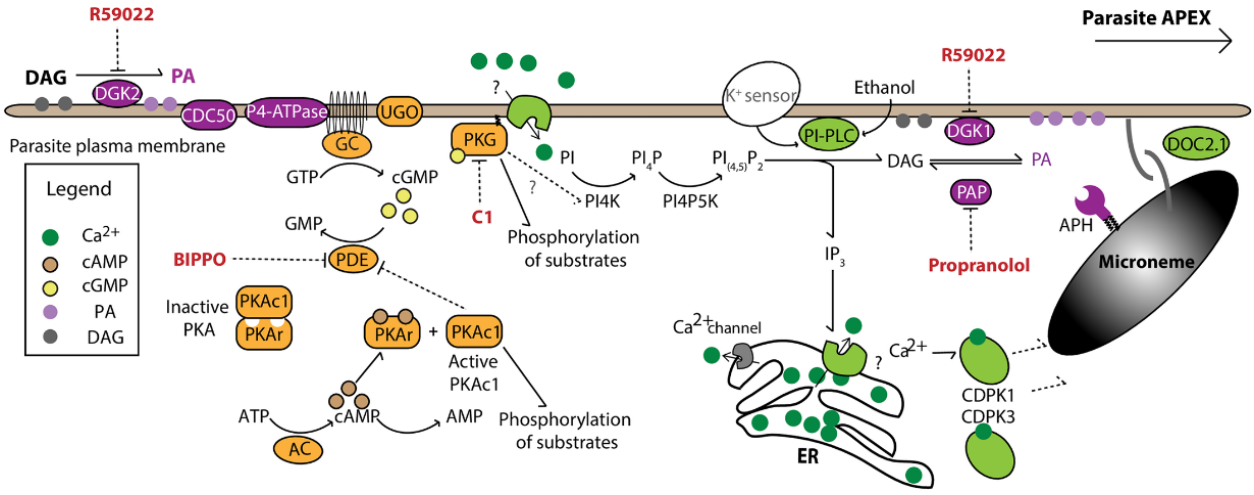

Figure 1.6 **Schematic representation of the signaling pathways leading to microneme exocytosis.** Pathways involving phosphatidic acid is shown in purple, cyclic nucleotides as cGMP, cAMP in orange, and calcium in green. Common inducers and inhibitors of microneme secretion used in research are highlighted in red (Bisio and Soldati-Favre, 2019).

The diacylglycerol kinase 1 (DGK1) converts DAG to phosphatidic acid (PA), essential for microneme exocytosis. PA is also important for the activation of a complex composed of CDC50-P4ATPase-GC-UGO (Bisio *et al.*, 2019). This complex is found at the parasite PM and participate in the sensing of multiple signals and in the stability and localization of the guanylate cyclase (GC) (Bisio *et al.*, 2019). GC converts guanosine triphosphate (GTP) to cyclic guanosine monophosphate (cGMP) that is an important effector in microneme secretion. On its turn, cGMP activates PKG that mobilizes calcium. Another important factor is cyclic adenosine monophosphate (cAMP) that activates protein kinase A (PKA) that phosphorylate several components of the glideosome, the machinery that powers motility and invasion (Jacot *et al.*, 2014; Jia *et al.*, 2017). Calcium-dependent protein kinases (CDPKs), mainly CDPK1, play a fundamental role in microneme secretion (Lourido *et al.*, 2010).

Other microneme exocytosis effectors were identified in both *Toxoplasma* and *Plasmodium spp.* In *Plasmodium,* parasites lacking the DOC2 (double C2) protein are unable to secrete micronemes (Farrell *et al.*, 2012) whereas in *Toxoplasma,* DOC2 seems to play a broader role since the disruption of TgDOC2 leads to a block of microneme, rhoptries and dense granules secretion (Tagoe *et al.*, 2021). Additionally, orthologues of the calcium sensing Ferlin proteins (FER) were discovered in Apicomplexa. These proteins have a role in vesicle fusion and membrane trafficking by binding to phospholipids and calcium. FER1 and FER2 are conserved across apicomplexan parasites whereas FER3 is only found in Coccidia (Coleman *et al.*, 2018). Disruption of TgFER1 leads to a complete block in microneme maturation and exocytosis (Tagoe *et al.*, 2020). Several putative transporters are as well required for microneme exocytosis, but their precise function is still unclear. Transporter facilitator protein 1 (TFP1) plays a critical role in micronemes maturation and exocytosis (Hammoudi *et al.*, 2018). In *P. berghei,* a putative pantothenate transporter (PAT) is required for the secretion of microneme-like organelles called osmiophilic bodies (Kehrer *et al.*, 2016). Additionally, a microneme acetylated protein APH (Acylated Pleckstrin Homology domain containing protein), conserved across Apicomplexa, is crucial for microneme exocytosis. APH is located to the surface of micronemes and recognize PA at the surface of the parasite PM

and with DOC2 triggers the fusion of micronemes with the PM (Darvill *et al.*, 2018; Farrell *et al.*, 2012) **(Figure 1.6)**.

Microneme exocytosis can be triggered by intrinsic factors (parasite derived) or extrinsic signals (host end environment derived). All these factors will lead to the elevation of calcium level, triggering the signaling cascade for microneme exocytosis.

1.4.1.2. Role of micronemes in parasite egress

Following multiple rounds of replication, parasites eventually exit the host cell by lysing the PVM and the host PM. This active process of egress requires the conoid extrusion (del Carmen *et al.*, 2009), exocytosis of micronemes and activation of the actomyosin system (Caldas *et al.*, 2018). The perforins secreted by micronemes permeabilize the PVM and the host cell PM and help the motile parasites to mechanically rupture the fragilized PVM (Kafsack *et al.*, 2009). Several inducers that converge to a rise in cGMP and intracellular Ca^{2+} triggering microneme exocytosis and stimulate egress (Bisio *et al.*, 2019). The damage delt to the host PM leads to a drop in intracellular K^{+}, which is sensed by the parasite causing the release of intracellular calcium and triggering egress (Moudy *et al.*, 2001). Acidification of the PV can also trigger the secretion of micronemes and activate perforin-like protein 1 (PLP1) that forms a pore complex in membranes (Kafsack *et al.*, 2009; Roiko *et al.*, 2014). PLPs are expressed in different life stages and can contribute to the lysis of different cell membranes (Garg *et al.*, 2020; Sassmannshausen *et al.*, 2020). DGK2, a protein that accumulates inside the PV, produces PA and plays a role in egress as a “molecular clock” that triggers the exit of the parasite roughly 48h after invasion (Bisio *et al.*, 2019).

1.4.2. Rhoptries

The following section is largely inspired from our review on the rhoptries that can be found in **Annex 1** (ben Chaabene *et al.*, 2021)

1.4.2.1. Ultrastructure of rhoptry organelles

Rhoptries constitute a hallmark feature of the Apicomplexa phylum. They are large, club-shaped organelles that localize to the apical end of the parasite. These organelles are highly conserved across the Apicomplexa, but their number and content vary between different species across the phylum as well as between different developmental stages in the same specie. In *Plasmodium*, merozoites and sporozoites possess only two rhoptries whereas ookinete stage lacks them entirely (Kats *et al.*, 2006). *Cryptosporidium* sporozoites harbor one rhoptry (Tetley *et al.*, 1998) and *Theileria parva* merozoite has six (Shaw and Tilney, 1992). *T. gondii* tachyzoites contain 10-12 rhoptries of ~2-3 µm in length, whereas bradyzoites possess only 1 to 3 such organelles.

In *T. gondii*, the rhoptries are clustered together at the apical end, and two distinctive compartments define the fine structure of the rhoptry organelle, a rhoptry neck and a rhoptry bulb, **(Figure 1.7)**.

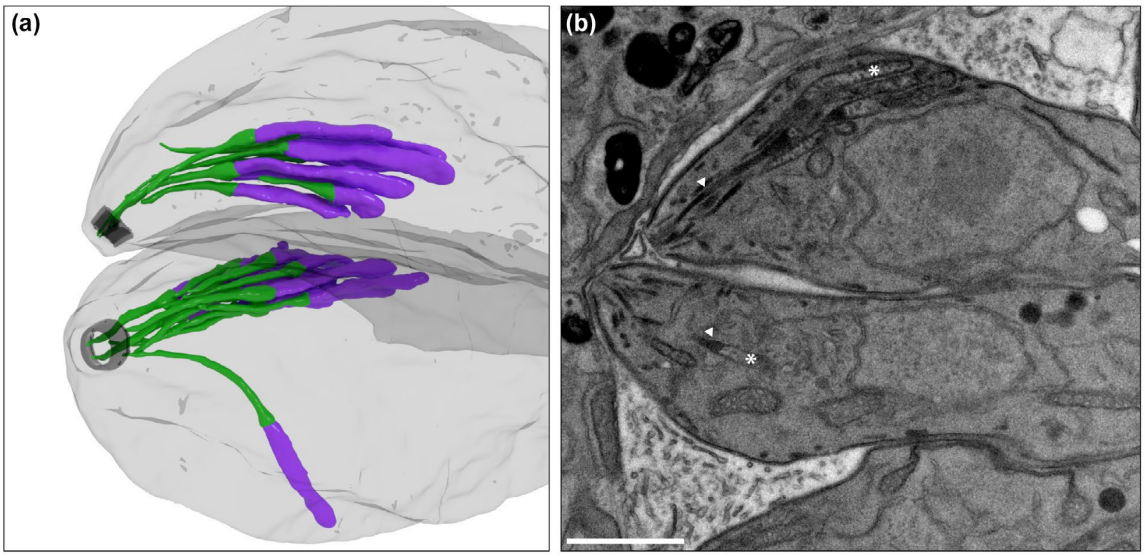

Figure 1.7 **Ultrastructure of rhoptry organelles.** A. 3D reconstruction from FIB-SEM images showing clustered rhoptries at the apical pole of two intracellular parasites. The retracted conoid is colored in black. Rhoptry neck (green) and bulb (purple) are colored. We can observe a couple of rhoptries traversing the conoid. The plasma membrane is colored in shaded grey. B. Transmission electron microscopy (TEM) image of two intracellular parasites showing the electron dense neck (arrowhead) and electron-lucent bulb (asterisk). Scale bar = 1um. Image from (ben Chaabene *et al.*, 2021).

Some of the rhoptry neck proteins (RONs) are secreted first during invasion and are critical for the formation of the MJ, a structure that serves as a support to propel the parasite into the host cell. The RONs are well conserved across the Apicomplexa, in accordance with a conserved role of these proteins in the formation of the MJ and the invasion process across the phylum. The rhoptry bulb proteins (ROPs) are more divergent. They include effector molecules important for the virulence of the parasite and proteins and membranous material involved in the formation and maturation of the PVM **(see section 1.6)**. Interestingly, intramembranous particles (IMPs) were detected on metal replicas of freeze-fractured tachyzoites and were found on the rhoptry membrane with a high density in the rhoptry bulb **(Figure 1.8)** (Lemgruber *et al.*, 2011). One hypothesis was that these particles represent specific surface domains which might interact with the cytoskeleton of the parasite and then strongly anchor the rhoptries at the apical end (Bannister *et al.*, 2000; Lemgruber *et al.*, 2011). It is not yet fully understood how the rhoptries are clustered together and anchored to the cytoskeleton, however Armadillo repeats only protein (ARO) is important for the clustering and apical anchoring of the rhoptry organelles **(see Section 1.4.2.4)** (Mueller *et al.*, 2013, 2016).

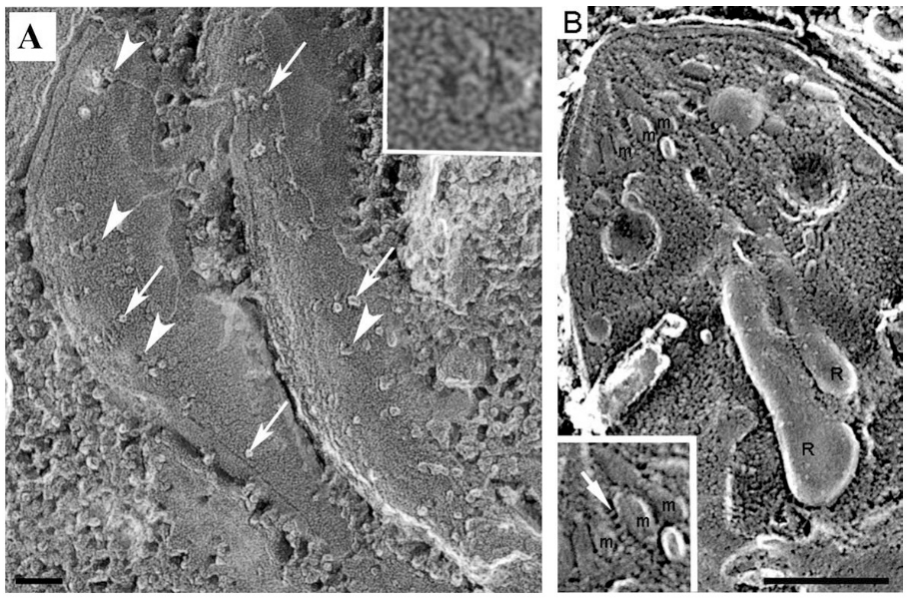

Figure 1.8 **Metal replica of freeze-fractured tachyzoites.** (A) Visualized IMPs (white arrows) are spread over the whole organelle surface. Pore-like structures (arrowheads/Inset) are observed throughout the bulb region. (B) Micronemes (m) are connected with tiny filaments (inset). Scale bars A= 5200 nm, B= 5400 nm (Lemgruber *et al.*, 2011).

A third sub-compartment of the rhoptries connecting the neck to the bulb was observed and exhibits an intermediate electron density (Lemgruber *et al.*, 2011). So far, two proteins have been identified to localize to this intermediate region – ARO-interacting protein (AIP) and adenylate cyclase β (Acβ). It is not fully understood how the rhoptry proteins are targeted to their respective sub-compartments making the organelle even more complex to understand. Using Cryo-ET to visualize the apical complex of *T. gondii* and *C. parvum*, it was observed that luminal helical filaments are shaping the rhoptry neck (Mageswaran *et al.*, 2021). The neck can be divided to an anterior and posterior part, where the helical filaments are differently organized giving a different rhoptry width for each compartment **(Figure 1.9).** Rhoptry biogenesis is a complex process that required synthesis, trafficking, and maturation of the rhoptry content together with mechanisms that ensure proper organelle shaping and anchoring.

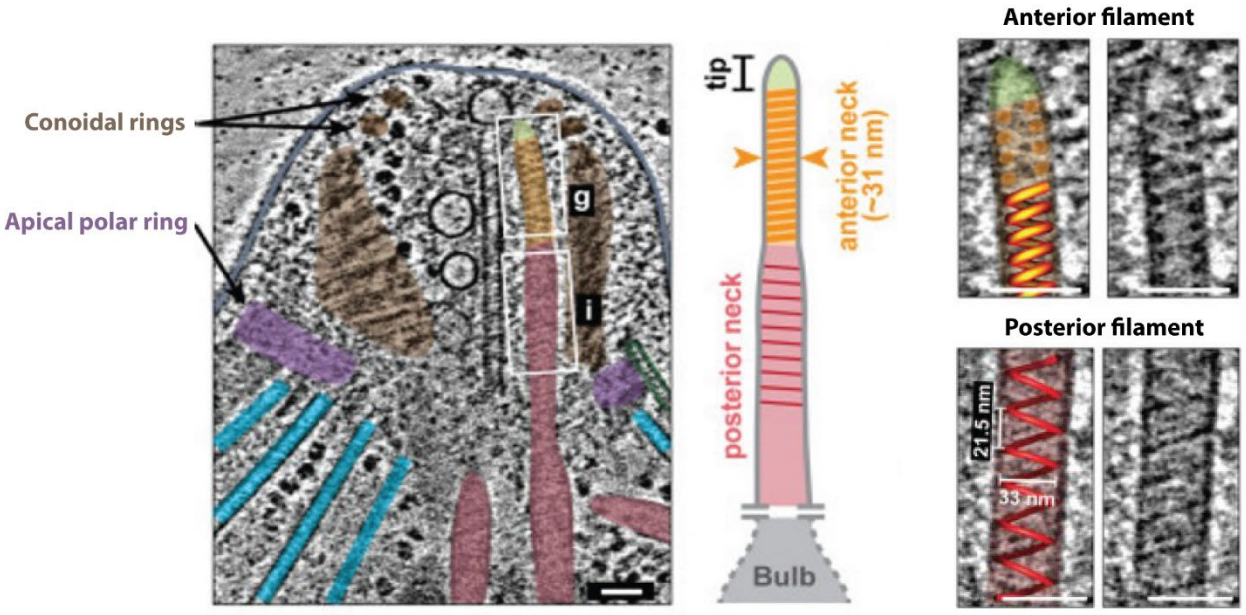

Figure 1.9 **The luminal filaments shape the rhoptry neck in *T. gondii*.** Figure modified from (Mageswaran *et al.*, 2021).

1.4.2.2. Rhoptry biogenesis and trafficking

During endodyogeny, the rhoptries are inherited from the mother parasite but are formed *de novo* (Nishi *et al.*, 2008). The fate of the maternal rhoptries is still a mystery, and they might

either be degraded or in part recycled and participate to the newly formed rhoptry as it has been shown for the IMC (Ouologuem and Roos, 2014).

Rhoptries production derives from vesicles originated from the Golgi apparatus that traffics through the early endosomes (EE) and forms the immature organelle called pre-rhoptries **(Figure 1.10)** (Dubremetz, 2007). The pre-rhoptries develop to mature organelles by condensation of rhoptry content and at the same time, elongation of the neck to adopt the distinctive club-shaped structure. Inside the pre-rhoptries, the lumen holds heterogenous dense material that include ROPs and RONs, according to electron microscopy (EM) analysis (Dubremetz, 2007) as well as lipids and membranous material. Proteolytic maturation of the pro-rhoptry proteins happens in the pre-rhoptries. Mature rhoptry organelles are then anchored to the apical pole of mature parasites. In addition, rhoptries are acidic organelles and have possibly evolved from endocytic and secretory pathways (Ngo *et al.*, 2004; Shaw *et al.*, 1998).

Intensive functional investigations of conserved eukaryotic molecules have unraveled the trafficking pathways of micronemes and rhoptry proteins (Venugopal and Marion, 2018). The membrane trafficking system is a well-conserved mechanism in all eukaryotes and is central to the sub-compartmentalization of cells. In Apicomplexa, several conserved endocytic trafficking proteins are implicated in the biogenesis and transport of the secretory organelles as well as of the IMC. This includes the Sortilin-like receptor (SRTLR) (Hallee *et al.*, 2018; Sloves *et al.*, 2012), adaptor protein 1 complex (AP1) (Venugopal *et al.*, 2017), Rab GTPases (Rab5A and RAB5C) and vacuolar protein sorting-associated proteins (VSP) **(Figure 1.10)** (Hugo *et al.*, 2020; Morlon-Guyot, el Hajj, *et al.*, 2018; Morlon-Guyot *et al.*, 2015; Sakura *et al.*, 2016). Disruption of these cargo proteins impairs the biogenesis of rhoptries and micronemes reflecting a common dependence on a post-Golgi endosomal machinery.

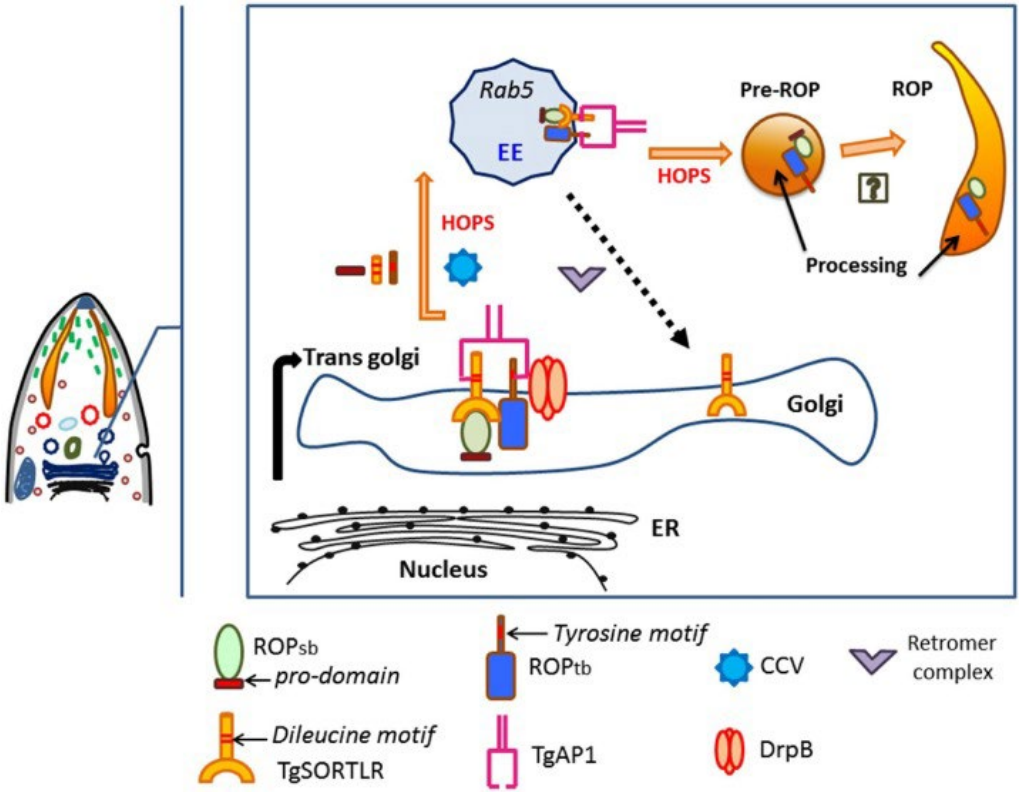

Figure 1.10 **Schematic representation of the sorting and trafficking of rhoptry proteins during biogenesis.** (Venugopal and Marion, 2018).

SRTLR was identified in *T. gondii* and *P. falciparum* as a key cargo receptor to transport newly synthesized rhoptry and microneme proteins from the Golgi to the endosomal related compartment (Sloves *et al.*, 2012). The conditional depletion of TgSRTLR leads to the formation of parasites lacking micronemes and rhoptries (Sloves *et al.*, 2012). In *T. gondii*, AP1 functions as a hetero-tetrameric complex composed of four subunits and is involved in biogenesis of rhoptries and micronemes but not dense granules (Venugopal *et al.*, 2017). AP1 interacts with regulator of clathrin and plays a role in the anterograde secretory pathway of rhoptry proteins form the Golgi. AP1 is also implicated in the maturation process of pre-rhoptry compartments to an apically anchored mature organelle (Venugopal *et al.*, 2017). TgAP1 is linked to the C-terminal tail of SORTLR, suggesting a role during the trafficking of MICs and rhoptry proteins via a clathrin-dependent process from the Golgi (Sloves *et al.*, 2012). The endosomal tethering complexes

CORVET and HOPS are conserved in most apicomplexan parasites (Jimenez-Ruiz *et al.*, 2016; Morlon-Guyot *et al.*, 2015). These tethering complexes are essential for early to late endosome trafficking, lysosome biogenesis and the endo-lysosomal trafficking process (Nickerson *et al.*, 2009; Spang, 2016). In *T. gondii,* the vacuolar compartment (VAC) represents the lysosome, and its cathepsin proteases mediate the proteolytic cleavage of ingested proteins (Zhicheng *et al.*, 2014). Depletion of some VSPs in *T. gondii* has an impact on the biogenesis and trafficking of micronemes, rhoptry, and dense granule proteins. Conditional depletion of Vsp9 leads to the mis-sorting of rhoptry, micronemes and dense granule proteins (Sakura *et al.*, 2016). Vsp11 is a common subunit of HOPS and CORVET as well as Vsp18, Vsp16 and Vsp33 (Morlon-Guyot, el Hajj, *et al.*, 2018; Morlon-Guyot *et al.*, 2015). Conditional knock down of Vsp11 leads to the mis-localization of Rab7 and a defect in micronemes, rhoptries and dense granules biogenesis (Morlon-Guyot *et al.*, 2015). Two subunits belonging to the interacting network of Vsp11, BEACH domain-containing protein (BDCP) and Vsp8 were recently identified (Morlon-Guyot, el Hajj, *et al.*, 2018). Depletion of Vsp8 affects the biogenesis of dense granules, rhoptries and a subset of micronemes. In contrast, BDCP has a restricted function affecting only the biogenesis of rhoptries. In absence of BDCP, rhoptries undergo morphological aberrations which results in a defect in invasion due probably to a defect in rhoptry secretion (Morlon-Guyot, el Hajj, *et al.*, 2018).

The dynamin related protein B (DrpB) is located to the cytoplasm close to the Golgi and plays a crucial role in the biogenesis of rhoptries and micronemes (Breinich *et al.*, 2009). Additionally, a putative transporter localized to the rhoptry membrane, TFP2, also plays a role in the morphology of the rhoptries. In absence of TFP2, the rhoptries adopt an elongated shape without any impact on the abundance, processing, or secretion of rhoptry content or the organelles clustering and apical positioning (Hammoudi *et al.*, 2018).

Altogether, further investigation of the mechanism of targeting and sorting of the rhoptry proteins is necessary. This might uncover the contribution of novel protein complexes or perhaps other unknown trafficking signatures and motifs.

1.4.2.3. Processing and maturation of rhoptry proteins

The trafficking and function of the secretory proteins are highly controlled by post translational modifications (PTMs) that help in contributing to a greater complexity and functional diversity of the proteome from a small number of genes. One of the critical PTMs is proteolytic maturation, which is an irreversible modification that consists of cleaving peptide or iso-peptide bonds of a protein by proteases. Proteolytic processing serves to modify the biological activity of the protein, which could involve the cleaving of the first methionine after translation, the removal of the protein transmembrane domain (TMD) or the signal peptide from nascent proteins, the cleavage of pro-peptide to activate the protein, or the proteolysis leading to complete degradation. Proteases are classified into seven broad categories based on the principal catalytic residue of the active site: Threonine proteases, Serine Proteases, Glutamic proteases, Cysteine proteases, Aspartic proteases, Asparagine proteases and Metalloproteases (Dou and Carruthers, 2011; Dowse *et al.*, 2008; M. Santos *et al.*, 2012; Roiko and Carruthers, 2009).

Rhoptry and microneme proteins are mostly synthesized as large precursors (pre-pro-proteins) that are processed to give mature, active proteins that reach the organelles *via* the classical secretory pathway from the ER to Golgi before being sorted inside the endosome-like compartment (ELC). Often, the pro-domain found in the N-terminal end functions as a targeting determinant and is cleaved during the trafficking through the post-Golgi compartment to the respective organelles. The cleavage of rhoptry proteins was shown to occur at a putative cleavage site harboring the consensus sequence SϕXE (ϕ is hydrophobic, X is any amino acid) (Miller *et al.*, 2003), as has been experimentally confirmed for several ROPs. Alternatively, some ROPs lack this consensus motif and are still cleaved. RONs also possess several SϕXE motifs and are also cleaved along the secretory pathway (Besteiro *et al.*, 2009). Although subtilisin protease (SUB) SUB2 was initially presumed to be the major protease responsible for processing rhoptry proteins, it is now known that an aspartyl protease (ASP) ASP3 is responsible for the cleavage of many ROPs and RONs, as well as MICs (Dogga *et al.*, 2017).

ASPs constitute a family of enzymes, highly conserved and found in all kingdoms of life. These proteins were shown to have a critical role in the virulence of many pathogens such as HIV-1, *Candida albicans* and *Plasmodium spp.*, making them an interesting drug target. The activity of the protease requires an acidic environment, which restrict their localization in the cell. A comprehensive phylogenetic and bioinformatic analysis showed that Apicomplexa ASPs cluster into six clades, with protein members of each clade sharing similar biological features (Shea *et al.*, 2007) **(Figure 1.11)**.

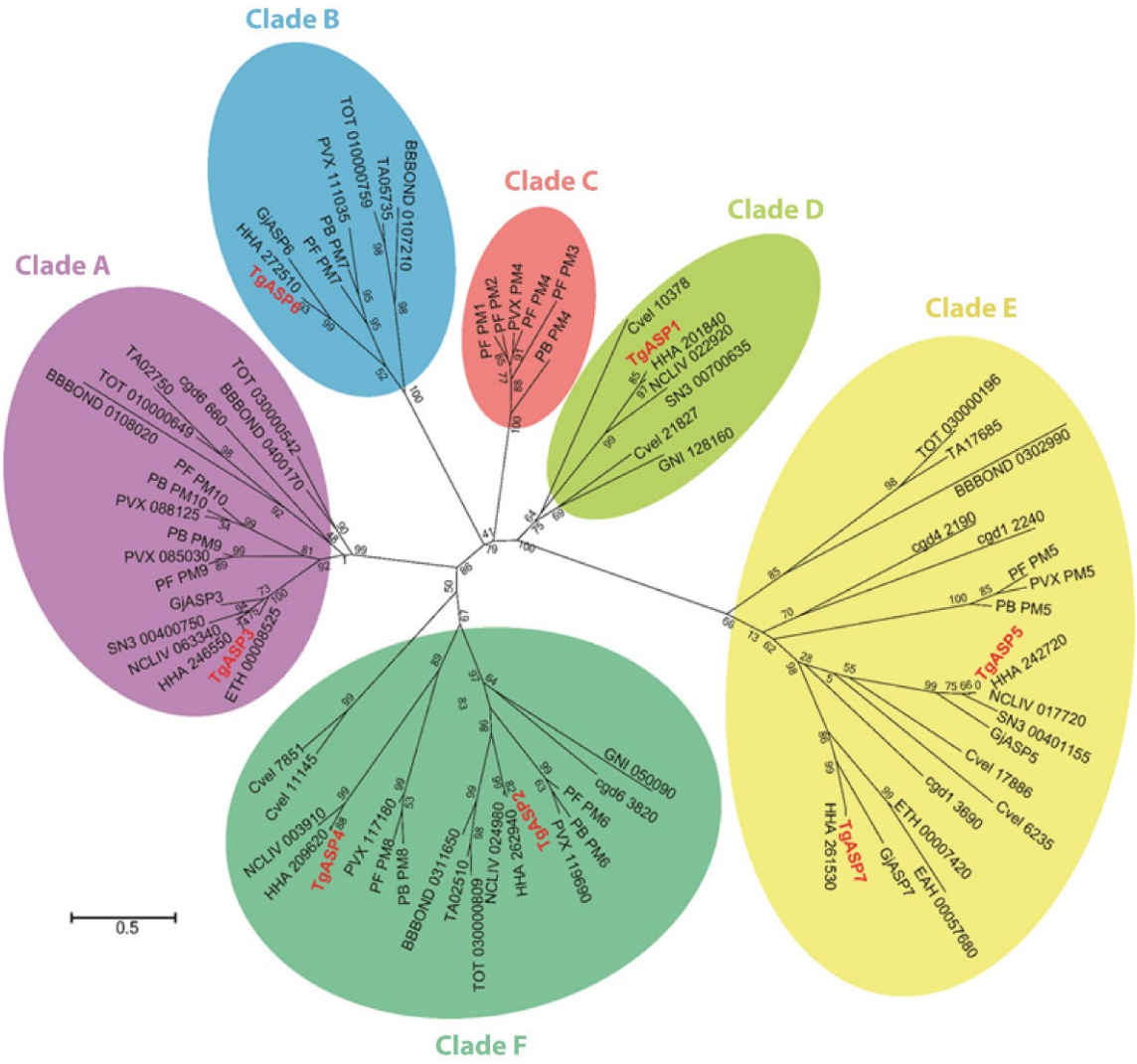

Figure 1.11 **Phylogeny of Apicomplexan aspartyl proteases** (Dogga *et al.*, 2017).

P. falciparum encodes ten putative ASPs called plasmepsins (PM) and clade C is specific to *Plasmodium* and groups four proteases **(PM I-IV, clade C)** expressed during the erythrocytic stage and are responsible for the degradation of the hemoglobin in the food vacuole, a compartment absent in *T. gondii* (Coombs *et al.*, 2001).

While degradation of hemoglobin in *P. falciparum* is an essential process for the parasite, individual deletion of each of these plasmepsins do not affect parasite growth, therefore indicating that there is a redundancy between members of this family. Another plasmepsin, (**PMV, clade E)**, was shown to be involved in protein export by cleaving *Plasmodium* export element protein (PEXEL) found at the surface of the infected red blood cell (RBC) (Boddey *et al.*, 2010; Russo *et al.*, 2010; Sleebs *et al.*, 2014). Plasmepsin IX and X **(PM IX-X, clade A)** have been recently characterized as essential factors in multiple life cycle stages of *Plasmodium* parasites. They have been shown to be responsible for the maturation of microneme and rhoptry proteins and absence of these proteases results in a defect in invasion and egress (Pino *et al.*, 2017).

T. gondii genome encodes seven aspartyl proteases (TgASP1-7), with only TgASP1, TgASP3 and TgASP5 being significantly expressed in the tachyzoite stage. These seven ASPs contain conserved motifs (DTG/DTG or DTG/DSG) harboring the two catalytic aspartic acid residues, the pro-region, a polyproline loop and a β-hairpin flap that closes over the active site and controls substrate access and specificity (Shea *et al.*, 2007). ASP1 is a coccidian-specific protease, albeit non-essential, as parasites depleted in this enzyme are still viable in vitro and exhibit normal virulence *in vivo* (Polonais *et al.*, 2011). ASP5 has been shown to be a maturase of GRAs and plays an important role in the trafficking of effectors to the PVM (Hammoudi *et al.*, 2015). ASP3 localizes to the ELC and acts as an essential maturase involved in the pre-exocytosis processing of MICs and rhoptry proteins ROPs and RONs (Dogga *et al.*, 2017). Conditional depletion of ASP3 leads to a defect in processing of numerous MICs and rhoptry proteins and results in a defective rhoptry discharge, invasion, and egress. ASP3 is phylogenetically related to PfPMIX and PfPMX and the phenotypes observed have been attributed to its function as a maturase of microneme and rhoptry proteins (Dogga *et al.*, 2017; Nasamu *et al.*, 2017; Pino *et al.*, 2017). TgASP3 substrates

were identified by comparing the terminal amino isotopic labelling of substrates (TAILS) between WT and ASP3-depleted parasites. However, the ASP3 substrates responsible for the defects observed, have not been identified yet. Recently, it was observed that the rhoptry neck was morphologically aberrant and does not localize to the tip of the parasite in ASP3 depleted parasites (Lentini *et al.*, 2021). This phenotype can explain the drastic invasion defect observed in the absence of ASP3. An antimalarial compound based on a hydroxyethylamine scaffold (49c) was designed and used to target the malaria PfPMII (Boss *et al.*, 2003; Ciana *et al.*, 2013). However, 49c has been shown to interfere with several stages of *Plasmodium* parasites at subnanomolar concentration by targeting PfPMIX and PfPMX. Similarly, 49c was shown to kill *T. gondii* by blocking egress and rhoptry discharge and inhibiting rhoptry and microneme protein processing, thus recapitulating the phenotype observed upon depletion of TgASP3 (Dogga *et al.*, 2017).

1.4.2.4. Rhoptry organelles positioning

The apical positioning of rhoptry organelles is crucial for the secretion of their content and eventually a successful invasion. ARO is essential for the apical anchoring and clustering of the rhoptries (Beck et al., 2013; Mueller et al., 2013). ARO is composed of five predicted armadillo motif (ARM) and is anchored to the rhoptry membrane by N-terminal myristylation and palmitoylation (Beck *et al.*, 2013; Frenal *et al.*, 2013). Each ARM repeat is important for the proper folding and functioning of ARO and individual ARM deletions showed that ARO requires all its repeats motifs to bring the rhoptries to the apical pole (Mueller *et al.*, 2016). In *T. gondii*, depletion of ARO leads to dispersed rhoptries all over the cytosol eventually resulting in an accumulation of membranous structure of rhoptry origin (Mueller *et al.*, 2016). Pull-down analysis identified several partners of ARO such as the motor protein Myosin F (MyoF), ACβ and AIP. MyoF is essential for the apical positioning of rhoptries suggesting that this process is actomyosin-dependent (Mueller *et al.*, 2013). AIP and ACβ are not essential for parasite survival and are not directly linked to ARO essential functions (Lemgruber *et al.*, 2011; Mueller *et al.*,

2016). The trans-genera functional complementation between *T. gondii* and *P. falciparum* indicates that ARO is functionally conserved across Apicomplexa (Mueller *et al.*, 2016). The crystal structure of PfARO shows five highly flexible ARM repeats which allow the protein to accommodate simultaneous interactions with multiple binding partners (Geiger *et al.*, 2020). Similarly, to its *T. gondii* ortholog, PfARO also interacts with PfACβ and PfAIP but in contrast to TgAIP, PfAIP is essential for parasite survival (Geiger *et al.*, 2020). This difference may reflect a compensation of other proteins in *T. gondii* in absence of TgAIP or additional functions in *P. falciparum*.

Another coccidian protein, CORVET/HOPS Associated Protein (CSCHAP), was identified in *T. gondii* and showed to play an important role in the apical positioning of rhoptries (Morlon-Guyot, Berry, *et al.*, 2018). In contrast to ARO, this protein does not affect the clustering of the organelle. CSCHAP possess two microtubule binding domains that might play a role in the anchoring of rhoptries to the ICMTs (Morlon-Guyot, Berry, *et al.*, 2018).

1.4.3. Dense granules

Dense granules are secretory organelles conserved in Apicomplexa, they contain dense granule proteins (GRAs) that play an important role in the modulation of the host cell expression (Griffith *et al.*, 2022) and the remodeling of the PVM, PV and the intravacuolar network (IVN), a network of highly curved membrane tubules inside the PV that connects parasites to one another (Mercier *et al.*, 2002; Travier *et al.*, 2008). Dense granules are not located apically but rather dispersed in the cytosol. GRAs are secreted after host cell invasion and then constitutively secreted during the lytic cycle (Carruthers and Sibley, 1997). These proteins play a critical role in the differentiation to bradyzoites (Griffith *et al.*, 2022). The processing of GRAs and its importance in the trafficking of these proteins to the PVM and beyond has been well characterized (Coffey *et al.*, 2015; Curt-Varesano *et al.*, 2016; Hammoudi *et al.*, 2015). Some GRAs proteins exhibit intrinsically disordered domains, and their unfolded state might help them crossing the PVM through the translocon (Hakimi *et al.*, 2017; Hakimi and Bougdour, 2015).

In contrast to rhoptries and micronemes, dense granules emerge from the Golgi as mature organelles. ASP5 belongs to **Clade A** along with plasmepsin PMV **(Figure 1.11)** and is responsible for the cleavage of several GRAs in the Golgi (Coffey *et al.*, 2015; Curt-Varesano *et al.*, 2016; Hammoudi *et al.*, 2015). The disruption of TgASP5 inhibits the processing of several GRAs, which results in a disruption in their export beyond the PV without affecting their secretion (Coffey *et al.*, 2015).

1.5. Host cell invasion

The following section is largely inspired from our reviews on the rhoptries and on the lytic cycle of Apicomplexa that can be found in **Annex 1 and 2** (ben Chaabene *et al.*, 2021; ben Chaabene and Soldati-Favre, 2023).

For an obligate intracellular parasite like *T. gondii*, invasion is a vital event. Host cell entry happens as fast as ~30 seconds and it is a multistep process driven by the parasite. Gliding motility is an indispensable feature for invasion. This substrate-dependent mode of locomotion requires the actomyosin machinery of the parasite, located underneath the PM and named the glideosome (Frenal *et al.*, 2017). The invasion process is highly conserved across the phylum. The first step required for a successful invasion is the attachment of the parasite to the host cell PM, mediated by members of glycosylphosphatidylinositol (GPI)-anchored surface antigen glycoproteins (SAGs) related sequence (SRS) (Jung *et al.*, 2004; Manger *et al.*, 1998). These proteins are present abundantly on the surface of the parasite and bind specifically to the host cell receptors. The secretion of the MICs when the parasite is extracellular is crucial for this step. Some of the secreted MICs include transmembrane adhesins that recognize and interact with carbohydrates on the surface of the host cell (Reiss *et al.*, 2001), mediating a more intimate attachment (Frenal *et al.*, 2017). Immediately after, an unknown signaling cascade triggers the discharge of the rhoptries. Secreted rhoptry proteins co-opt with MICs for the invasion process and with GRAs for the PVM establishment and host cell modulation. Some RONs form a complex

composed of RON2, RON4, RON5 and RON8 in the organelle. Once secreted into the host cell, the complex remains associated with the cytosolic face of the host PM by interacting with the host cortical cytoskeleton (Bichet *et al.*, 2014). One member of this complex, RON2 is a transmembrane protein embedded in the host PM and interacts with the microneme protein called apical membrane antigen 1 (AMA1) on the parasite's surface (Alexander *et al.*, 2005; Besteiro *et al.*, 2009; Lebrun *et al.*, 2005; Mital *et al.*, 2005). This RONs-AMA1 complex establishes the MJ, a strong link between the parasite and the host cell which is critical for invasion. The apico-basal translocation of the RONs-AMA1 complex is powered by the actomyosin system, with the glideosome-associated connector (GAC) connecting the MJ to the parasite F-actin (Bichet *et al.*, 2014; Jacot *et al.*, 2016).

As the parasite enters the host cell, the host PM invaginates and forms the PVM, which ultimately pinches off without leaving any breach into the host PM (Pavlou *et al.*, 2018; Suss-Toby *et al.*, 1996). The PVM serves as a hub for parasite effector proteins ROPs and GRAs, that subvert the host cell functions, and protect the intracellular parasites from the host cell immune response (Griffith *et al.*, 2022). The PVM is also important for acquisition of many essential nutrients, through a pore-like system, mediated by GRAs (Desai and Rosenberg, 1997; Gold *et al.*, 2015; Schwab *et al.*, 1994) **(See section 1.6)**.

In *Plasmodium spp.* several other proteins are involved in invasion. A rhoptry bulb protein called rhoptry-associated adhesin (PfRA) is conserved across several malaria parasites and is indispensable for invasion. This protein is secreted inside the host cell and translocate to the merozoite surface interacting with the sialic acid on the infected RBC membrane (Anand *et al.*, 2016). Other proteins are known to interact with sialic acid mediating parasite entry through the sialic acid-dependent pathway, such as the erythrocyte binding antigen (EBA) EBA-175 (Sim *et al.*, 1994), EBA-181 (Gilberger *et al.*, 2003), EBA-140 (Jiang *et al.*, 2009) and Rh1 (Triglia *et al.*, 2005). Additionally, rhoptry neck proteins Rh1, Rh4 and Rh5 acts as adhesins and bind to the host cell receptors to ensure invasion (Duraisingh *et al.*, 2003; Hayton *et al.*, 2008; Triglia *et al.*, 2009). Finally, RhopH complex, composed of a member of the RhopH1/CLAG family, RhopH2 and

RhopH3, is secreted during invasion and inserted in the PVM (Ito *et al.*, 2017). This complex plays a critical role in invasion and nutrient uptake (Ito *et al.*, 2017; Ling *et al.*, 2003).

1.5.1. Building the Moving Junction

An important step in invasion is the formation of the MJ, the tight apposition between the host cell PM and the parasite, visualized for the first time in invading *Plasmodium* using electron micrography (Aikawa *et al.*, 1978). Initially, the MJ looks more like a punctate focus that rapidly resolves into a ring-like structure that moves toward the basal pole of the parasite simultaneously with the invagination of the PM of the host and the engulfment of the invading parasite (Straub *et al.*, 2011). Even though the morphological details of this process were described about 40 years ago, the molecular features of the MJ were solved quite recently. The MJ is also crucial for the establishment of a non-fusogenic PV in most apicomplexan parasites, by excluding host proteins from the forming PVM, that is originated predominately from the host PM (Charron and Sibley, 2004). This stripping of host proteins is critical for the survival of the parasite inside the host by preventing host lysosomes from fusing with the PVM (Sinai, 2014). The striking feature of the MJ is that it is formed by the combination of micronemes (AMA1) and rhoptries proteins (RONs complex) and these components are highly conserved across the phylum and essential for parasite survival **(Figure 1.12)** (Alexander *et al.*, 2005; Lamarque *et al.*, 2011; Mital *et al.*, 2005; Straub *et al.*, 2011; Yap *et al.*, 2014). RON2, RON4 and RON5 are conserved across the Apicomplexa, while RON8 is specific to the Coccidia (Straub *et al.*, 2009). AMA1 is a type I transmembrane microneme protein that is translocated, upon invasion, on the parasite surface towards the rear end. AMA1 interacts directly with RON2 anchored to the host PM and this binding does not require other RONs. This interaction generates a firm and irreversible link between the parasite and the host PM (Lamarque *et al.*, 2014). While RON2 C-terminal end interacts with the N-terminal ecto-domain of AMA1 on the parasite surface, RON2 N-terminal part is located within the host cytosol and binds to the other RONs (RON4/RON5/RON8) (Tonkin *et al.*, 2011). RONs complex cooperatively interact with several host cytoskeletal structures such as CIN85, CD2AP and the ESCRT-I components ALIX and TSG101, and together contribute to the

solid bridging interaction with the parasite **(Figure 1.12)** (Besteiro *et al.*, 2009; Guerin *et al.*, 2017).

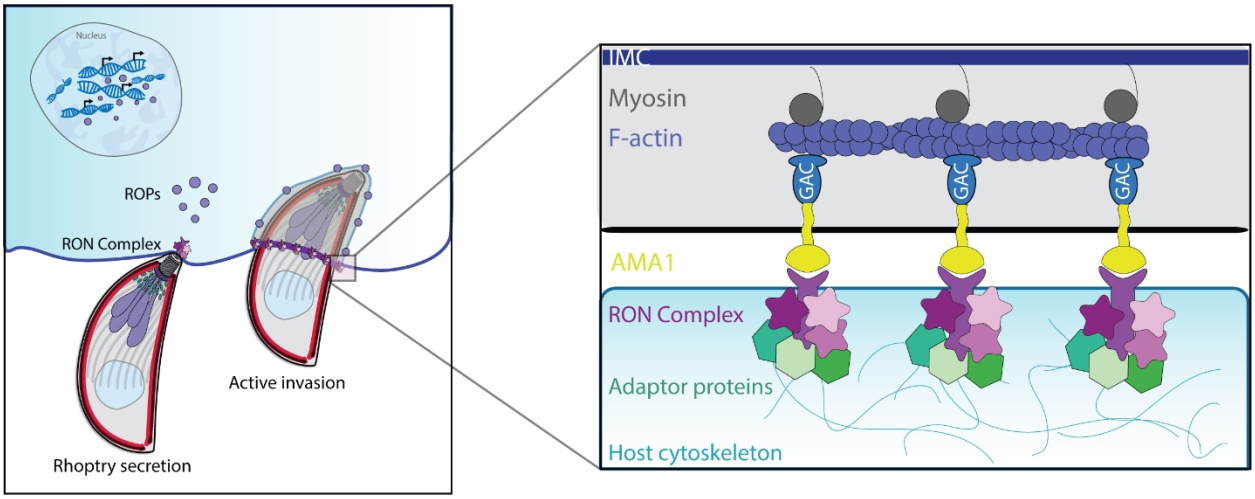

Figure 1.12 **Schematic representation of the moving junction organization.** The RONs complex is secreted and inserted in the host plasma membrane and interact with AMA1 via the RON2 C-terminal end forming the moving junction. From the host cytosolic part, the RONs complex interact with cytoskeleton structure establishing a firm interaction between both cells. Image modified from (ben Chaabene *et al*., 2021).

The RON complex is already formed in the rhoptry organelle but achieve its function only during invasion when it interacts with AMA1. In *T. gondii,* RON5-deficient parasites result in the degradation of RON2 and the mistargeting of RON4 during rhoptry biogenesis, suggesting the importance of RON5 in the stability and targeting of these proteins, respectively (Beck *et al.*, 2014). Additionally, RON2 and RON4, also play a critical role in the stabilization on the MJ complex. Thus, depletion of either RON2, RON4, or RON5 is sufficient to induce a defect in the stability and targeting of the others whereas RON8 is not influenced and localizes correctly to the rhoptries and MJ (Beck *et al.*, 2014; Lamarque *et al.*, 2014; Wang *et al.*, 2017). Concerning the role of AMA1 in the formation and stability of the MJ, studies have shown that in AMA1-depleted tachyzoites, the MJ is still formed (Bargieri *et al.*, 2013; Giovannini *et al.*, 2011). However, this observation might result from an adaptation of the parasite as an upregulation of AMA1 and RON2 paralogs was observed in AMA1-KO tachyzoites, that cooperate to support invasion (Lamarque *et al.*, 2014; Parker *et al.*, 2016).

A putative homolog of RON4 called RON4L1, is an additional member of the MJ complex and associate with the cytosolic face of the host PM during invasion (Guérin *et al.*, 2017). In RON4, RON2 or RON5 knock-down parasites, RON4L1 is normally expressed and localizes to the MJ during invasion suggesting the presence of a redundancy in the components of the MJ and probably additional components that remain to be discovered.

In *Plasmodium spp.*, a second complex plays a role in the formation of the MJ. SURFIN4.2 is a merozoite rhoptry neck protein that is exported to the infected RBC surface (Mphande *et al.*, 2008; Winter *et al.*, 2005). This protein interacts with RON4, and a parasite surface protein called GLURP for glutamate rich protein, giving the name SURGE to the complex (Quintana *et al.*, 2018). SURFIN4.2 tryptophan-rich domain (WRD) is predicted to bind cytoskeleton proteins such as spectrin and actin linking the PM of the parasite to the RBC cytoskeleton (Zhu *et al.*, 2017).

In conclusion, the MJ, containing AMA1-RONs complex and maybe several other proteins that remain to be identified, plays a central part during invasion. Understanding how this complex, with its numerous interactions, is established will help to cast light on the intricate mechanism of invasion and provides a deep insight about the process of PVM formation and closure.

1.5.2. The rhoptry secretion machinery

In the recent years, we started to have a clearer idea about how rhoptry discharge works and several molecular players and structures were identified and characterized. Even though some aspect of this step is not fully understood yet, the machinery of rhoptry secretion appears highly specialized and complex to ensure such a tightly regulated secretion. This process is linked to microneme secretion (Kessler *et al.*, 2008) and requires a contact between the parasite and a host cell (Carruthers and Sibley, 1997). Depletion of MIC8 was associated to a defect in invasion and rhoptry discharge confirming the link between the two subsequent microneme and rhoptry secretion events (Kessler *et al.*, 2008). Recently, two novel micronemal proteins MIC15 and

MIC14 were also showed to be important for rhoptry secretion and renamed rhoptry discharge factor 1 (RDF1) and rhoptry discharge factor 1 (RDF2), respectively (Possenti *et al.*, 2022).

Although *T. gondii* possess several rhoptry organelles, only two rhoptries are discharged during invasion. These two are seen with their neck traversing the conoid and are primed and docked to the apical tip of the parasite (Paredes-Santos *et al.*, 2012). Following their discharge, rhoptries are observed empty (Lebrun *et al.*, 2005) and smaller (Paredes-Santos *et al.*, 2012) which means that they do not fuse with the PM upon invasion. This accentuate the difference between the unique mechanism of rhoptry discharge from the exocytosis of micronemes where empty micronemes are never observed as the organelles fuse entirely with the parasite PM. A successful rhoptry discharge relies on secreting their content into the host cell while dealing with several physical barriers (rhoptry membrane, parasite PM and host cell PM). For this, the parasite needs either to form a pore or to fuse its membrane with the host PM. Previous data on patch-clamp experiments showed a break at the host PM prior to invasion that can correspond to the rhoptry secretion step (Suss-Toby *et al.*, 1996). The ultrastructure of the elements surrounding the primed rhoptries were first identified using focused ion beam-scanning electron microscopy (FIB-SEM) (Paredes-Santos *et al.*, 2012). It was only recently that, the 3-dimentional (3D) structure and composition of these elements were described in detail using cryo-electron microscopy (Cryo-EM) and Cryo-ET (Aquilini *et al.*, 2021; Mageswaran *et al.*, 2021; Segev-Zarko, Dahlberg, Sun, Pelt, Kim, *et al.*, 2022; Theveny *et al.*, 2022) **(Figure 1.13)**. It was shown that the primed rhoptries are aligned along a pair of ICMTs and are not in direct apposition with the parasite PM but their neck reaches an apical vesicle (AV) located underneath the PM at the tip of the parasite and previously described in *Toxoplasma* (Paredes-Santos *et al.*, 2012; Porchet-Hennere and Nicolas, 1983), *Sarcocystis* (Porchet and Torpier, 1977) and *Eimeria* (Dubremetz and Torpier, 1978) **(Figure 1.13-A)**. The AV differs in shape and size from one parasite to another. It is circular in *P. falciparum*, ellipsoid in *Toxoplasma*, and teardrop-shaped in *Cryptosporidium* (Mageswaran *et al.*, 2021; Martinez *et al.*, 2022). Additionally, along one of the ICMTs, three to six lined up microtubule-associated vesicles (MVs) were described and thought to be involved in replenishing

the AV and enabling successive rounds of rhoptry discharge (Paredes-Santos *et al.*, 2012). Indeed, MVs and ICMTs are only present in parasites that harbors more than two rhoptries, thus they are absent in *Cryptosporidium* and *Plasmodium*. Along the second ICMT, fibrous material with an unknown composition and function was observed. The role of the ICMTs was tentatively assigned to rhoptry discharge (Nichols and Chiappino, 1987), but their function is still not understood. To date, only one protein has been localized to the ICMTs, named ICMAP1, and postulated to have a role in their stabilization (Heaslip *et al.*, 2009). In *T. gondii,* the docked rhoptry neck was shown to be connected to the AV through a tip density of unknown composition (Aquilini *et al.*, 2021; Mageswaran *et al.*, 2021) **(Figure 1.13-B)**.

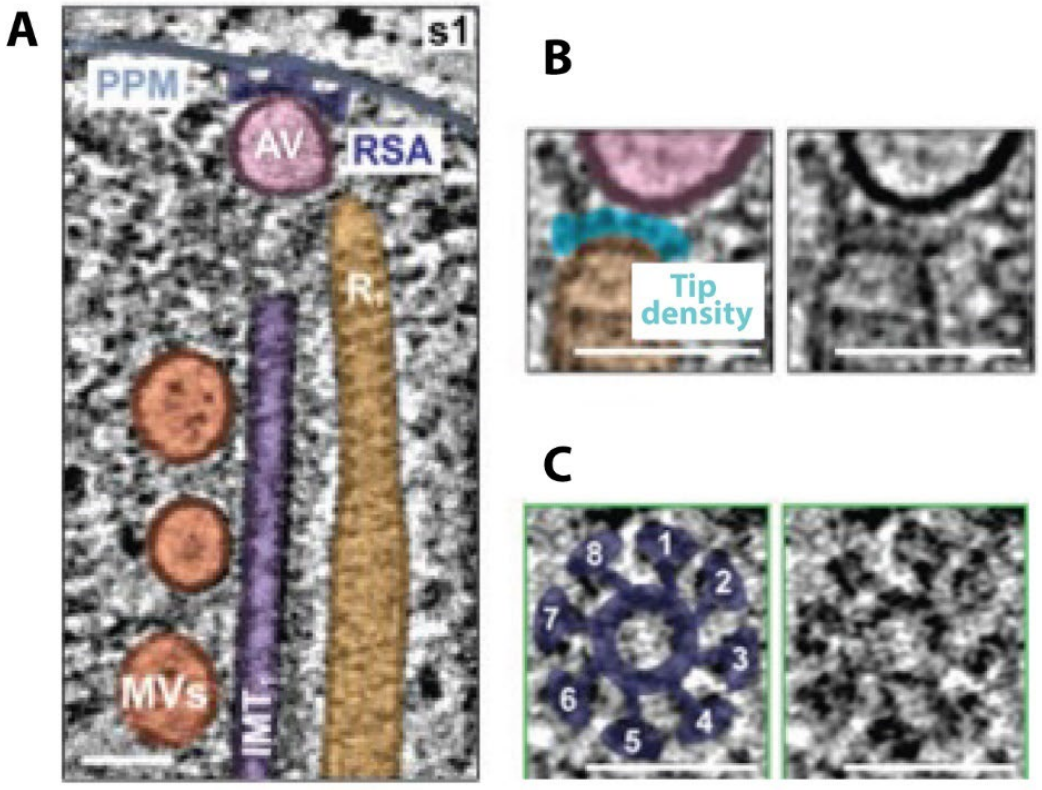

Figure 1.13 **The AV and the rhoptry secretory apparatus. A.** A rhoptry neck (yellow) is shown docked to the AV (pink). The ICMTs are shown in purple. Running alongside the ICMT, 3 MVs are observed (orange). **B.** Rhoptry neck is associated to the AV through a density (cyan) at their tip. **C.** Top view of the rosette showing eight-fold rotational symmetry. Figures modified from (Mageswaran *et al.*, 2021).

Above the conoid and the AV, the PM is decorated by a protein structure composed of IMPs, called the "rosette" (Dubremetz, 2007) **(Figure 1.13-C)**. This structure is conserved across the Apicomplexa and is also found in distant organisms like ciliates, where the rosette is found at the contact site with defensive secretory organelles called mucocysts in *Tetrahymena* and trichocysts in *Paramecium*, suggesting a conserved secretion mechanisms across evolution (Aquilini *et al.*, 2021; Plattner and Kissmehl, 2003).

All these elements are functionally linked to rhoptry discharge in *T. gondii* (Aquilini *et al.*, 2021), *C. parvum* (Mageswaran *et al.*, 2021) and in *P. falciparum* (Martinez *et al.*, 2022). Unlike the rosette that is conserved across the superphylum of Alveolates, the AV is only found in Apicomplexa. This might be an adaptation of organisms towards parasitism adding an additional complexity to this discharge mechanism and can also be the reason why in Apicomplexa, rhoptry content can be discharged inside the host cell in contrast to other organisms that secrete the content extracellularly. A complex composed of Non-discharge (Nd) proteins was previously described in *Paramecium tetraurelia* and shown to be important for trichocysts exocytosis and rosette formation (Lefort-Tran *et al.*, 1981). These proteins are conserved in Apicomplexa, Ciliates and Dinoflagellates. Recently, this complex was functionally described in *T. gondii* and *P. falciparum* (Aquilini *et al.*, 2021). In *T. gondii*, parasites depleted in TgNd6 or TgNd9 are unable to secrete the rhoptries and additionally, TgNd9 depletion leads to a defect in the rosette assembly (Aquilini *et al.*, 2021) and the AV anchoring (Mageswaran *et al.*, 2021). However, in *P. falciparum*, only depletion of PfNd9 leads to a defect in rhoptry secretion (Aquilini *et al.*, 2021). TgNd6 and TgNd9 are found in the cytoplasm, however, TgNd6 also accumulates at the tip of the parasite underneath the rosette (Aquilini *et al.*, 2021). Moreover, Nd partners identified by co-immunoprecipitation, NdP1 and NdP2, are also part of the complex and they are important for the rosette formation in *T. gondii* and for mucocysts secretion in the Ciliate *Tetrahymena thermophilia* (Aquilini *et al.*, 2021). Collectively, the rosette belongs to a multicomponent structure named the rhoptry secretory apparatus (RSA) conserved across Apicomplexa (Mageswaran *et al.*, 2021; Martinez *et al.*, 2022) **(Figure 1.14)**. The RSA is composed of a central

density, 3 anchors and a center channel located between the AV and the parasite PM **(Figure 1.14 A)**. The central density is exposed to the extracellular side while sitting on a cytoplasmic structure (plug) and on the central channel located between the AV and the plug. The central density might be involved in the formation of a pore-like structure at the PPM. Together, anchor I and the central density, represents the apical rosette. Anchor II and anchor III are attached to the AV and might play a role in its anchoring but also its prevention from a spontaneous fusion. During rhoptry discharge, the torque motion of anchor I could amplify the twist between anchor II and III, thus pulling the AV closer to the PPM for fusion **(Figure 1.14 A)**.

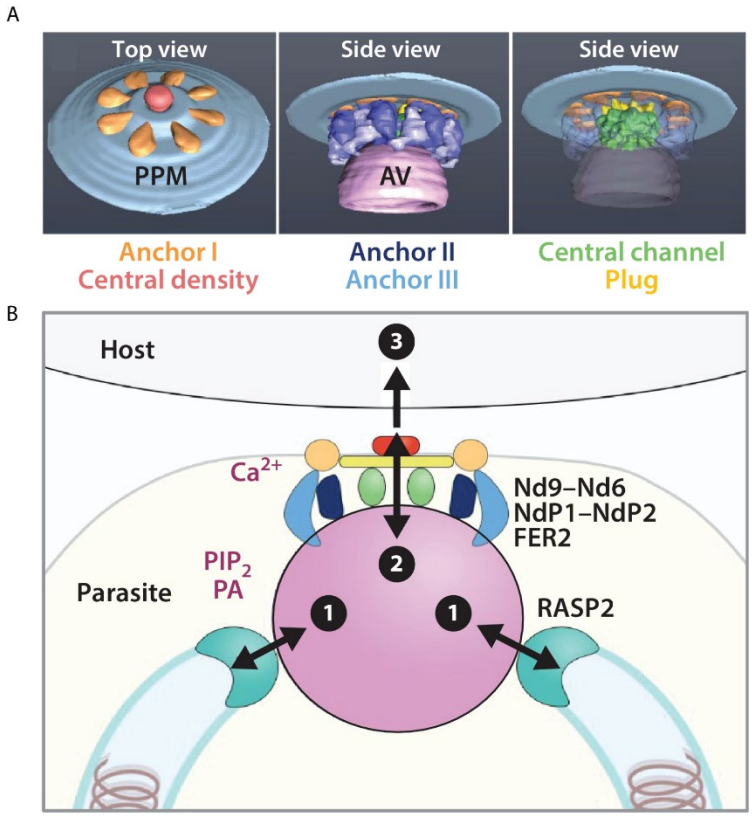

Figure 1.14 ***Toxoplasma* secretion machinery. (A)** A 3D representation of the parasite plasma membrane (PPM), the AV and RSA. **(B).** Schematic representation of the Key players in rhoptry secretion. 1) RASP2 mediates the fusion between the rhoptries and the AV. 2) The Alveolata-specific complex composed of Nd6, Nd9, NdP1, NdP2 and FER2, plays a role in the assembly of the RSA and the fusion of the AV with the PPM. 3) The third step is the fusion or the pore formation between the PPM and the host PM. This step is still not understood and how the rhoptry content is discharged inside the host cell is still unknown. Image modified from (Cova et al., 2022).

The RSA structures are different between *Toxoplasma, Plasmodium* and *Cryptosporidium* reflecting an adaptation mechanism for their specific invaded hosts (Mageswaran *et al.*, 2021; Martinez *et al.*, 2022). The RSA is believed to play a role in the docking of the AV to the parasite PM, allowing their fusion and the rhoptry discharge. Using ARO depleted parasites, it was also shown that the rosette, AV, MVs and the ICTMs were present at the tip of the parasites in absence of docked rhoptries showing that the machinery of secretion located at the parasite PM does not require the docking of the secretory organelles (Aquilini *et al.*, 2021).

It was always thought that rhoptry discharge was a calcium-independent process, unlike microneme secretion that is linked to the intracellular Ca^{2+} oscillations. Recently, a series of proteins possessing calcium-dependent function were identified as key factors for rhoptry secretion. Depletion of FER2 in *Toxoplasma* leads to a defect in invasion and rhoptry discharge (Coleman *et al.*, 2018). However, the role of calcium is still unclear in this process. FER2 was recently described as part of the TgNd6 and TgNd9 complex (Aquilini *et al.*, 2021) **(Figure 1.14 B)**. Additionally, FER2 was also identified in *Tetrahymena,* and its depletion leads to a defect in mucocysts release (Sparvoli *et al.*, 2022) confirming the conservation of this machinery.

A family of rhoptry apical surface proteins (RASPs) were identified in *Toxoplasma* and *Plasmodium.* These RASPs localize at the tip of the rhoptry neck, and they play a role in organelle secretion (Suarez *et al.*, 2019). RASP1, RASP2 and RASP3 interact together forming a complex in *Toxoplasma*. Parasites depleted in RASP2 have a severe defect in invasion due to a block in rhoptry secretion, while no defect was observed in the morphology or positioning of the organelle (Suarez *et al.*, 2019). In *Plasmodium*, PfRASP2 is also called PfCERLI1 and localizes to the rhoptry bulb with a similar phenotype as observed in *T. gondii* (Liffner *et al.*, 2020). RASP2 contains a PH-like domain and a C2 lipid binding domain that might contribute to the fusion of rhoptries to the AV by binding to PA and PIP2 (Suarez *et al.*, 2019) **(Figure 1.14 B)**. PA was already described as a lipid mediator in the microneme exocytosis (Bullen and Soldati-Favre, 2016) and PIP2 accumulation is important for membrane fusion (Martin, 2015). The proposed hypothesize

is that RASP2 binds to the accumulated PIP2 and PA following microneme secretion and contribute to the docking of the rhoptries and fusion with the AV (Suarez *et al.*, 2019).

Another family of proteins was recently identified in *Toxoplasma* and plays a role in rhoptry discharge (Possenti *et al.*, 2022; Singer *et al.*, 2022; Sparvoli *et al.*, 2022). Cysteine repeat modular proteins (CRMPs) were also described in *Tetrahymena* and are required for mucocysts release (Sparvoli *et al.*, 2022). In *Toxoplasma*, CRMPs are dispersed within the parasite cytosol similar to Nd proteins, although the signal is more apical and partially overlap with microneme proteins. Unlike Nd proteins, CRMPs are not required for the rosette assembly, and they accumulate at the secretion site transiently just prior to the invasion (Sparvoli *et al.*, 2022). CRMPs contain a carbohydrate-binding domain known to bind to sialic acids suggesting that they may bind to host ligands at the PM surface and act as sensors to ensure timely coordination of rhoptry discharge.

1.6. Role of ROPs and GRA in subversion of host cell functions and virulence *in vivo*

The genome of *Toxoplasma* contains around 8000 genes with 159 predicted as kinases. This represents 2% of the genome and it includes 108 kinases and 51 pseudokinases (Peixoto *et al.*, 2010). All members of Apicomplexa possess a family of CDPKs that are also found in plants. These kinases are important for the proper regulation of multiple pathways related to parasite motility, invasion, replication, and egress. Their absence from the human genome, makes them suitable drug targets (Billker *et al.*, 2009). In addition, apicomplexan parasites possess some specific set of kinases namely FIKK kinases and ROP kinases (ROPKs). Kinases function by catalyzing the transfer of a phosphoryl group from adenosine triphosphate (ATP) to the hydroxyl group of a given substrate. Kinase substrates can be peptides, small molecules or even the kinase itself (autophosphorylation). The flexibility and reversibility of phosphorylation explains its selection as the most general pathway adopted by eukaryotic organisms. Depending on the

phosphorylated residue, kinases can be separated to categories – Serine kinases, threonine kinases and tyrosine kinases (Cohen, 2002).

FIKK kinases are atypical kinases specific to the Apicomplexa phylum (Ward *et al.*, 2004) with no orthologs in any other eukaryotes. The FIKK designation comes from the fact that these proteins contain four residues motif (Phe-Ile-Lys-Lys) in their catalytic domain (Ward *et al.*, 2004). Among all the FIKK kinases, only one of them, FIKK8, is present in all apicomplexan parasites, except *Theileria Spp.* and *Babesia bovis* (Talevich *et al.*, 2011). However, *P. falciparum* have an expanded number of FIKKs, with 21 identified kinases (Ward *et al.*, 2004), making their characterization very promising for the development of anti-malarial drugs. In *Toxoplasma*, FIKK8 is found in the posterior end of the parasite and is dispensable for the lytic cycle of the parasite (Skariah *et al.*, 2016). *In P. falciparum*, most FIKK kinases are exported to the host cell membrane during parasite intracellular growth. These exported FIKKs have a role in the remodeling of the infected RBC as well as the pathogenicity and virulence of the parasite.

In *T. gondii*, proteomic analysis of purified rhoptries identified more than 30 proteins (Bradley *et al.*, 2005). Some of these rhoptry proteins harbor specialized functions such as kinases, proteases and phosphatases. ROPKs are the largest group of ROPs found so far, only conserved in coccidia, and possess a conserved serine/threonine (S/K) kinase domain (el Hajj *et al.*, 2006). Several proteins of the ROPKs family do not possess the catalytic triad necessary for phosphorylation activity and are referred to as pseudo-kinases. Several ROPKs and pseudo-kinases are important mediators in modulating the host cell for the parasite's benefit (Boothroyd and Dubremetz, 2008).

The numbers of ROPKs vary across these different strains with 37 genes in type I, 55 in type II and 38 in type III (Peixoto *et al.*, 2010; Talevich *et al.*, 2012). A few ROPKs were functionally characterized in *Toxoplasma* and shown to be responsible for parasite virulence and pathogenesis, namely ROP5, ROP16, ROP17 and ROP18 (Saeij *et al.*, 2006, 2007; Taylor *et al.*, 2006). The activity of these kinases is crucial for hijacking the host-signaling pathways. ROP16 is

secreted in the cytosol of the host cell at the time of invasion and translocate to the host cell nucleus. In type I strain **(Figure 1.15)**, ROP16 activates signal transducer and activator of transcription 3 (STAT3) and STAT6 that lead to the repression of *T. gondii*-induced pro-inflammatory cytokines (Ong *et al.*, 2010; Saeij *et al.*, 2007; Yamamoto *et al.*, 2009). Moreover, in type I strains, expression of ROP5, a pseudo-kinase, is linked with a high level of virulence (Behnke *et al.*, 2011). The combined activity of ROP5 and ROP18 phosphorylates immunity related GTPases (IRGs) Irga6 and Irgb6, blocking their recruitment to the PV surface for parasite clearance (Fentress *et al.*, 2010; Steinfeldt *et al.*, 2010). These two rhoptry proteins were shown to form a complex with ROP17 at the PVM surface. In type II strains **(Figure 1.15)**, point mutations of ROP5, ROP18 and ROP16 produce variant kinases that are less active, leading to a weaker control of host immune response. Type III strains **(Figure 1.15)**, like type I, secrete ROP16 and induce a prolonged activation of STAT6 and STAT3 (Ong *et al.*, 2010). However, type III parasites express an inactive form of ROP18 and thus fail to block the recruitment of IRGs to the PV and succumb to IRG-mediated intracellular killing (Fentress *et al.*, 2010; Melo *et al.*, 2011; Steinfeldt *et al.*, 2010).

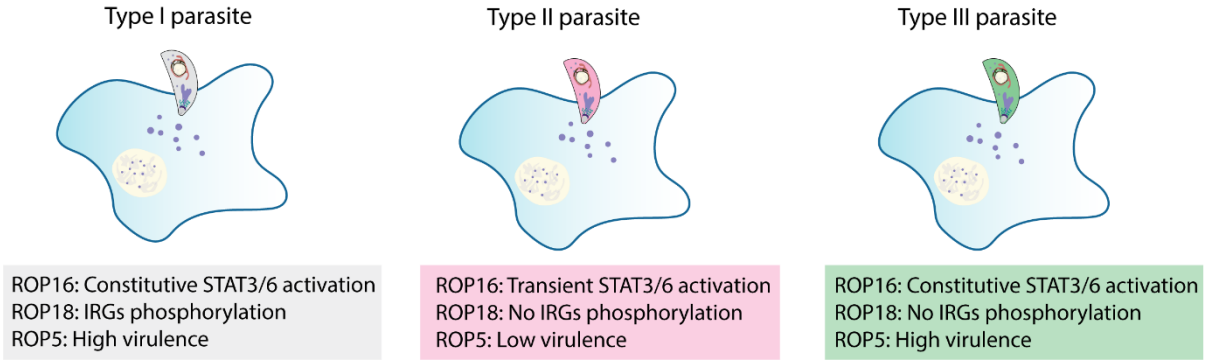

Figure 1.15 **Host functions affected by rhoptry proteins. A.** In type I parasites, ROP16 and ROP18 are secreted into the host cell and are responsible for the phosphorylation of STAT3/6 (constitutively) and IRGs, respectively. In this strain, ROP5 is secreted and responsible for a high virulence. **B.** Type II parasites express a less active ROP16, leading to a transient phosphorylation of STAT3/6. ROP18 is expressed as an avirulent form, therefore no IRGs phosphorylation. ROP5 alleles expressed in this strain are associated with low virulence. **C.** In type III strains, ROP16 induce a constitutive phosphorylation of STAT3/6 whereas ROP18 is inactive. ROP5 alleles expressed are associated with a high virulence. Adapted from (Melo *et al.*, 2011).

ROP54, is a pseudo-kinase effector, secreted into the host cell and traffics to the cytoplasmic face of the PVM playing a role in the modulation of host immune response in type II strain (Kim *et al.*, 2016). Guanylate Binding Proteins (GBPs) belong to a class of gamma interferon (IFN-γ)-dependent immunity-related loading protein, which are important during *T. gondii* infection (Yarovinsky, 2014) and several are loaded onto the PVM and play a critical role in parasite clearance (Yamamoto *et al.*, 2012). ROP5 and ROP18 can block GBP1 loading (Degrandi *et al.*, 2007; Selleck *et al.*, 2013) while ROP54 is involved in modulating the loading of GBP2 (Kim *et al.*, 2016). Depletion of ROP54 display a significant increase in GBP2 loading causing a decrease in virulence in mice (Kim *et al.*, 2016). Contrary to what is observed in *T. gondii,* none of the *Plasmodium* ROPs have a kinase activity and all these paradoxes in ROPs functionality is probably due to the very different host cells in which parasites reside. In *Plasmodium*, ROPs were shown to be involved in rhoptry biogenesis, invasion, PV formation, and host cell modification (Kats *et al.*, 2006).

A serine protease found in rhoptry bulb called DegP, belongs to the high temperature requirement A (HtrA) family and is conserved in most Apicomplexa except for rodent malaria parasites (Arenas *et al.*, 2010). Type II strain *T. gondii* parasites lacking this protease, show a significant decrease in acute virulence in immune-competent mice whereas in immunodeficient mice, the parasite lacking DegP kill efficiently the mice suggesting a role of this rhoptry protease in immune evasion and the establishment of lethal infection (Lentini *et al.*, 2017).

Tissue cysts are frequently localized in the brain and skeletal muscles, where they persist usually asymptomatically during the entire life of the host. The cyst matrix is a highly complex environment composed of distinctive layers, vesicular and tubular structures (Lemgruber *et al.*, 2011). The regulation of these structures and their cargo remains poorly investigated and the role of protein kinases in controlling the development of these structures remain largely unexplored. The genes coding for the members of the ROPK family showed a differential expression between the tachyzoite stage and the bradyzoites stage and even between different

type strains of *Toxoplasma* (Peixoto *et al.*, 2010). Despite their ROP nomenclature, a subset of ROPK family proteins do not localize to the rhoptries. ROP21 and ROP27 are localized to a small vesicular structure and secreted constitutively into the cyst matrix in bradyzoites (Jones *et al.*, 2017). Depletion of these two kinases results in a reduction of cyst burden *in vivo*.

Toxoplasma infection causes severe disease in immunocompromised patients and can cause encephalitis when crossing the blood-brain barrier (BBB) and invading the central nervous system (CNS). *T. gondii* is one of the few pathogens to cross the BBB and this is achieved by hijacking leucocytes and using them as a Trjan horse (Courret *et al.*, 2006; Harker *et al.*, 2015; Konradt *et al.*, 2016). It is believed that infected leukocytes deliver the parasites across the endothelial barrier via the extravasation, an integrin-dependent adhesion process (Ley *et al.*, 2007). However, an integrin-independent migration of leukocytes is possible within tissues, and it is mediated through the activation of the Rho/ROCK pathway (Lammermann *et al.*, 2008). The activation of this pathway in infected monocytes is mediated by ROP17 (Drewry *et al.*, 2019). It forms a complex with ROP5 and ROP18 at the PVM, but the activation of the Rho/ROCK pathway seems independent from the complex (Etheridge *et al.*, 2014). Mice infected by ROP17-deficient parasites shows a decrease in monocyte tissue migration which leads to a slower dissemination of the parasite and prolonged mice survival suggesting that *T. gondii* infection reprogram the monocytes to migrate through tissues in an integrin-independent manner, promoted by ROP17-dependent phosphorylation (Drewry *et al.*, 2019). The kinase activity of ROP17 is also important for the translocation of GRA proteins across the PVM (Panas *et al.*, 2019).

GRA proteins are also important effectors for the modulation of the cell host immune system. Secretion of GRAs occurs at the end of invasion following PV formation. These proteins are found post-secretion inside the PV, at the PVM, or delivered into the host cell and can modulate its genes expression and cellular functions**.**

GRA16, GRA18 and GRA24 are translocated across the PVM and localize to the host cytosol where they subvert host cell signaling pathway. A translocon system formed by a complex of Myc-

regulation genes (MYR) proteins allows the movement of GRAs (Marino *et al.*, 2018). ROP17 is essential for the translocation of GRAs proteins probably by the phosphorylation of the component of the translocon machinery (Marino *et al.*, 2018). The first example of interaction between GRAs and rhoptry proteins, is the binding of GRA7 to the rhoptry complex ROP18/ROP4/ROP5/ROP8 increasing the turnover of IRGs and controlling the acute infection (Alaganan *et al.*, 2014; Dunn *et al.*, 2008). Additionally, GRAs play a role in the maturation of the PV into a metabolically active compartment and its transformation into a cyst wall (Griffith *et al.*, 2022). Recently it was demonstrated that GRAs proteins are also important for *T. gondii* dissemination by exploiting the trafficking of parasitized macrophages (ten Hoeve *et al.*, 2022). GRA28 cooperates with the host chromatin remodelers driving the chemotactic migration of infected macrophages.

Altogether, the synchronized activity of ROPs and GRAs demonstrate that *Toxoplasma* is a master manipulator that uses its wide repertoire of effectors to hijack many cellular functions and disseminate undetectably, making it one of the best invaders.

1.7. Phosphorylation of rhoptry proteins

In the previous section, we have seen that the parasite uses secreted kinases to target host cellular pathways, thus affecting parasite pathogenicity and virulence. In addition, apicomplexan parasites also rely on protein phosphorylation to modulate their own biology.

Previous phosphoproteomic analysis on intracellular and extracellular *Toxoplasma* and *Plasmodium spp.* showed that several parasite proteins are phosphorylated including rhoptry proteins **(Table 1)**. Interestingly, the RON proteins involved in the formation of the MJ, are highly phosphorylated **(Table 1 highlighted in blue)** (Nebl *et al.*, 2011; Treeck *et al.*, 2011). However, the functional relevance of these phosphorylations and the implicated kinases are not known.

Gene ID	Protein description	LOPIT localization	CRISPR score Tg	Number of phosphorylated residues
TGME49_300100	rhoptry neck protein RON2	rhoptries 1	-4.63	3
TGME49_223920	rhoptry neck protein RON3	rhoptries 1	-4.41	4
TGME49_311470	rhoptry neck protein RON5	rhoptries 1	-4.34	4
TGME49_294770	Armadillo/beta-catenin family repeat-containing protein	nucleus - chromatin	-3.54	10
TGME49_297960A	rhoptry neck protein RON6	rhoptries 1	-3.48	3
TGME49_306060	rhoptry neck protein RON8	rhoptries 1	-3.26	5
TGME49_230350	hypothetical protein	rhoptries 2	-3.25	4
TGME49_210820	hypothetical protein	rhoptries 2	-2.68	8
TGME49_225200	hypothetical protein	rhoptries 1	-2.54	2
TGME49_261440	ARM repeats containing protein	rhoptries 2	-2.10	2
TGME49_279420	hypothetical protein	rhoptries 1	-1.96	7
TGME49_202200	hypothetical protein	rhoptries 1	-1.41	1
TGME49_225860	hypothetical protein	rhoptries 1	-1.35	9
TGME49_254070	hypothetical protein	rhoptries 2	-1.03	3
TGME49_315490	rhoptry protein ROP10	rhoptries 1	-0.96	4
TGME49_229010	rhoptry neck protein RON4	rhoptries 1	-0.93	21
TGME49_258360	hypothetical protein	rhoptries 1	-0.89	3
TGME49_315220	rhoptry protein ROP14	rhoptries 2	-0.78	4
TGME49_294790	hypothetical protein	rhoptries 2	-0.59	8
TGME49_229500	hypothetical protein	rhoptries 2	-0.58	2
TGME49_305250	hypothetical protein	rhoptries 2	-0.51	5
TGME49_241000	hypothetical protein	rhoptries 2	-0.34	4
TGME49_310010	rhoptry neck protein RON1	rhoptries 1	-0.34	19
TGME49_312150	hypothetical protein	rhoptries 2	-0.23	1
TGME49_312270	rhoptry protein ROP13	rhoptries 1	-0.13	3
TGME49_259700	hypothetical protein	rhoptries 2	-0.04	1
TGME49_253100	hypothetical protein	rhoptries 2	0.10	2
TGME49_211290	rhoptry protein ROP15	rhoptries 1	0.16	1
TGME49_246178	hypothetical protein	rhoptries 2	0.20	5
TGME49_227810	rhoptry kinase family protein ROP11 (incomplete catalytic triad)	rhoptries 1	0.25	2
TGME49_258660	rhoptry protein ROP6	rhoptries 2	0.28	2
TGME49_285290	hypothetical protein	rhoptries 2	0.30	5
TGME49_314500	subtilisin SUB2	cytosol	0.30	1
TGME49_297070	hypothetical protein	rhoptries 2	0.31	3
TGME49_261740	hypothetical protein	rhoptries 1	0.31	1
TGME49_222100	hypothetical protein	rhoptries 1	0.35	2
TGME49_225330	hypothetical protein	rhoptries 1	0.39	1
TGME49_263220	rhoptry kinase family protein ROP21	cytosol	0.48	6
TGME49_261750	rhoptry neck protein RON10	rhoptries 2	0.52	6
TGME49_225320	hypothetical protein	rhoptries 2	0.64	1
TGME49_270200	hypothetical protein	rhoptries 2	0.65	7
TGME49_247520	hypothetical protein	rhoptries 1	0.68	6
TGME49_244250	hypothetical protein	rhoptries 1	0.79	4
TGME49_243730	rhoptry protein ROP9	rhoptries 1	0.85	4
TGME49_205250	rhoptry protein ROP18	rhoptries 1	0.89	9
TGME49_318525	hypothetical protein	rhoptries 1	0.93	6
TGME49_264600	hypothetical protein	rhoptries 2	0.95	1
TGME49_304740	rhoptry kinase family protein ROP35	dense granules	1.10	2
TGME49_262730	rhoptry protein ROP16	rhoptries 1	1.11	2
TGME49_291960	rhoptry kinase family protein ROP40 (incomplete catalytic triad)	rhoptries 1	1.13	3
TGME49_258580	rhoptry protein ROP17	rhoptries 1	1.29	3
TGME49_252360	rhoptry kinase family protein ROP24 (incomplete catalytic triad)	rhoptries 1	1.34	1
TGME49_294630	hypothetical protein	rhoptries 2	1.55	31
TGME49_214080	toxofilin	rhoptries 1	1.56	10
TGME49_309590	rhoptry protein ROP1	rhoptries 1	1.59	7
TGME49_203990	rhoptry protein ROP12	rhoptries 1	1.63	5
TGME49_262050	rhoptry kinase family protein ROP39	rhoptries 2	1.97	3
TGME49_218270	hypothetical protein	rhoptries 2	2.01	3
TGME49_295110	rhoptry protein ROP7	rhoptries 1	n.a.	7
TGME49_266100	rhoptry kinase family protein ROP41	n.a.	n.a.	2

Table 1 **List of phosphorylated rhoptry proteins.** In blue are highlighted proteins of the RON complex.

Also, whether phosphorylation of rhoptry proteins occurs either along the trafficking route, in the rhoptry lumen or post-secretion, needs to be determined. ROP4, is a pseudo-kinase, secreted from the parasite during invasion and localizes to the PVM (Carey *et al.*, 2004). This protein is phosphorylated on several residues in infected host cells; however, no phosphorylation is observed in extracellular parasites. Interestingly, pro-ROP4 is not phosphorylated in contrast to mature ROP4. These observations indicate that (1) the protein maturation and conformation is important for the phosphorylation, (2) the protein and ATP might be in separate compartment within the parasite, and (3) some secreted effectors are substrates of host and/or parasite kinases that are activated at a certain timepoint of the infection (Carey *et al.*, 2004).

The extensive phosphorylation of rhoptry proteins, indicates that PTM could be an important trigger of a signaling cascade that eventually leads to rhoptry secretion, formation of the MJ and invasion. This phosphorylation might as well play an important role in the modulation of host cell cytoskeleton during invasion. *T. gondii* tachyzoites possess an actin-binding protein, toxofilin, that localizes to both the bulb and the neck of the rhoptry and is secreted in the host cytoplasm early during invasion (Delorme-Walker *et al.*, 2012; Gonzalez *et al.*, 2009). Upon secretion, toxofilin binds to host cell actin and accelerates actin filament turnover, which results in a looseness of the host cell cytoskeleton network at the site of entry and facilitates the entry of the parasite. Interestingly, toxofilin contains 10 phosphorylation sites (Serine and Threonine) and it was reported that phosphorylation of the Serine 53 residue is required for its activity on actin remodeling (Delorme et al., 2003; Delorme-Walker et al., 2012). The kinase responsible for this phosphorylation is still unknown, though a casein kinase II activity was suggested to play a role (Delorme *et al.*, 2003).

2. Aim of the PhD thesis

The phylum of Apicomplexa groups some of the most significant pathogens of humans and animals alike, causing considerable threat to health and welfare. Rhoptries are specialized secretory organelles conserved in Apicomplexa and play a central role in the establishment of parasitism. Rhoptry content includes proteinaceous as well as membranous materials that are secreted into the host cell in a highly regulated manner during parasite invasion. Some of the rhoptry neck proteins form the RON complex that critically participates in the formation of the MJ. A set of the rhoptry bulb proteins are associated with the membranous materials and contribute to the formation of the PVM while others are targeted to different host cell compartment including the nucleus, to subvert cellular functions. Despite the advance in our understanding of the biogenesis, trafficking and secretion of these organelles, many questions remain opened.

The overall goal of the thesis was to better understand the mechanism of rhoptry discharge and parasite invasion and to characterize novel proteins important for these steps.

The main objectives of the thesis project were:

- **Characterization of the ASP3 -dependent processing of the rhoptry neck protein RON13 and functional dissection of this atypical kinase**.
- **Identification of novel rhoptry proteins predicted to be essential**.
- **Functional characterization of a novel rhoptry protein RAP1.**

3. RESULTS

3.1. Structural insights into an atypical secretory pathway kinase crucial for *Toxoplasma gondii* invasion

During invasion, rhoptries discharge their content into the host cell. Once secreted, the RONs complex composed of RON2, RON4, RON5 and RON8, remains associated on the cytosolic face of the PM by interacting with the host cortical cytoskeleton (Bichet *et al.*, 2014) and assembles with AMA1 that is located at the parasite's surface post microneme-secretion (Alexander *et al.*, 2005; Mital *et al.*, 2005). This RONs-AMA1 complex forms the MJ that serves as a support to propel the parasite into the host cell.

T. gondii ASP3 is an essential maturase residing in the ELC and involved in the pre-exocytosis processing of several MICs, RONs and ROPs (Dogga *et al.*, 2017). Conditional depletion of ASP3 leads to a severe defect in rhoptry discharge resulting in an invasion defect of 90%. However, the unprocessed substrate of ASP3 responsible for the phenotype is not known.

RON13 (TGGT1_321650) is a substrate of ASP3 identified by TAILS analysis. RON13 is a rhoptry neck protein that possess one transmembrane spanning segment and a predicted serine/threonine kinase domain. Based on a global CRISPR/Cas9 genome-wide analysis (Sidik *et al.*, 2016), RON13 was assigned a negative fitness score of -2.57, suggestive of a central role in parasite survival.

The main findings of this work are summarized as follow:

- RON13 is essential for parasite survival.
- The invasion is largely impaired in absence of RON13.
- Parasite depleted in RON13 can secrete their micronemes and rhoptries but are unable to form a MJ.
- RON13 play a role in host cell viability.

- The kinase activity of RON13 is central to its function.
- Many RONs and ROPs were identified as substrates of RON13 via phosphoproteome analysis.
- RON13 auto-phosphorylation is important for its kinase activity.

Author contributions for this work:

G.L. and **R.B.C.** performed all the biological and functional experiments. B. Mu. performed the initial experiments, related analysis, and conceptualization. R.V. and O.V. expressed and purified the proteins. C.R., J.G., and A.B.H. generated and analyzed the phosphoproteomes. B. M. generated and documented the electron microscopy images. V.M.K. and V.M. perforemed and processed the cryo-EM data, built, and refined the atomic model. M.L. performed all mouse experiments. G.L. and D.S.-F. wrote the manuscript with input from all authors.

nature COMMUNICATIONS

ARTICLE

https://doi.org/10.1038/s41467-021-24083-y OPEN

Structural insights into an atypical secretory pathway kinase crucial for *Toxoplasma gondii* invasion

Gaëlle Lentini[1,8], Rouaa Ben Chaabene[1,8], Oscar Vadas[1,8], Chandra Ramakrishnan[2], Budhaditya Mukherjee[1,7], Ved Mehta[3], Matteo Lunghi[1], Jonas Grossmann[4,5], Bohumil Maco[1], Rémy Visentin[1], Adrian B. Hehl[2], Volodymyr M. Korkhov[3,6✉] & Dominique Soldati-Favre[1✉]

Active host cell invasion by the obligate intracellular apicomplexan parasites relies on the formation of a moving junction, which connects parasite and host cell plasma membranes during entry. Invading *Toxoplasma gondii* tachyzoites secrete their rhoptry content and insert a complex of RON proteins on the cytoplasmic side of the host cell membrane providing an anchor to which the parasite tethers. Here we show that a rhoptry-resident kinase RON13 is a key virulence factor that plays a crucial role in host cell entry. Cryo-EM, kinase assays, phosphoproteomics and cellular analyses reveal that RON13 is a secretory pathway kinase of atypical structure that phosphorylates rhoptry proteins including the components of the RON complex. Ultimately, RON13 kinase activity controls host cell invasion by anchoring the moving junction at the parasite-host cell interface.

[1] Department of Microbiology and Molecular Medicine, University of Geneva, Geneva, Switzerland. [2] Institute of Parasitology, University of Zurich, Zurich, Switzerland. [3] Institute of Biochemistry, ETH Zurich, Zurich, Switzerland. [4] Functional Genomic Center Zurich, ETH Zurich and University of Zurich, Zurich, Switzerland. [5] The Swiss Institute of Bioinformatics, SIB, Lausanne, Switzerland. [6] Paul Scherrer Institute, Villigen, Switzerland. [7] Present address: School of Medical Science and Technology, IIT Kharagpur, India. [8] These authors contributed equally: Gaëlle Lentini, Rouaa Ben Chaabene, Oscar Vadas. ✉email: volodymyr.korkhov@psi.ch; dominique.soldati-favre@unige.ch

Toxoplasmosis is a zoonotic infectious disease caused by the protozoan parasite *Toxoplasma gondii*, a member of the Apicomplexa phylum. Specialized apical secretory organelles called rhoptries and micronemes crucially participate in gliding motility and active host cell entry of these obligate intracellular parasites. Micronemes secrete surface-exposed transmembrane adhesins (MICs) linked to the actomyosin system that promote traction for motility and invasion. Rhoptries inject proteins across the host cell plasma membrane (PM)[1], some acting as receptors during host cell invasion and others as effectors to subvert host cellular functions[2]. These club-shaped organelles contain rhoptry bulb proteins (ROPs) in the enlarged base that are segregated from rhoptry neck proteins (RONs) at the thin neck connected to the apical tip of the parasite. After injection, the RON complex (composed of RON2, 4, 5, and 8) is inserted in the host PM and binds to the microneme protein AMA1 on the parasite surface, forming a multiprotein complex that contributes to the formation of the moving junction (MJ)[3,4]. On the host cytoplasmic side, the RON complex interacts with several host adaptor proteins presumably linking the MJ with the host cortical actin[5]. Powered by the parasite actomyosin system[6], the MJ translocates toward the posterior end of the invading parasite, where the PM-derived parasitophorous vacuole membrane (PVM) is sealed[7,8]. Of relevance, the rhoptries also discharge membranous materials that participate in the PVM formation[9]. Once inside the host cell, *T. gondii* tachyzoite survival relies on an expanded coccidian lineage-specific family of secreted ROP kinases and pseudo-kinases (ROPKs)[10,11] acting as key virulence factors[12]. The RON complex is heavily phosphorylated[13]; however, the functional relevance of this posttranslational modification and the kinase(s) implicated are not known. Here, we identified and characterized a rhoptry-resident kinase RON13 that phosphorylates several rhoptry proteins, including the RON complex. RON13 kinase activity stabilizes the RON complex at the MJ to ensure successful invasion.

Results

Proteolytic maturation of RON13. Most ROPs/RONs as well as MICs are synthetized as pre-pro-proteins and are processed in the endosomal-like compartment by the aspartyl protease ASP3 ref. [14]. ASP3-depleted parasites are unable to invade host cells, notably due to a severe defect in rhoptry discharge. Among the identified ASP3 substrates[14] the TGGT1_321650 gene product (here referred to as RON13) is predicted to be a kinase. RON13 localizes to the rhoptry neck[14] and deletion of the gene is fitness-conferring based on a genome-wide CRISPR-Cas9 screen[15]. Ultrastructure expansion microscopy (U-ExM) revealed that RON proteins present two types of localizations, previously undistinguishable by conventional microscopy. RON2 and RON4 are found all along the neck of the organelles, while RON13 and RON9 localize at the extreme tip of the rhoptry neck (Fig. 1a and Supplementary Fig. 1a, b). Upon ASP3 depletion, the localization of RON13 and other RONs is altered with a disappearance of the neck and sliding of the bulbous part of the organelle closer to the conoid (Fig. 1a and Supplementary Fig. 1a, b). Focused ion beam scanning electron microscopy (FIB-SEM) analysis confirmed that the rhoptry necks are morphologically aberrant and do not extend to the apical tip of the parasite (Fig. 1b, Supplementary Fig. 1b, and Supplementary Movies 1 and 2). RON13 is a substrate of ASP3 and consequently, in the absence of the protease, RON13 is not processed anymore and accumulates as a membrane-anchored, largely insoluble pro-protein (Fig. 1c, d and Supplementary Fig. 1c). Taken together the aberrant rhoptry morphology and content organization in ASP3-depleted parasites provide a rationale for the previously reported defect in rhoptry discharge[14] (Fig. 1e).

The topology of the RON13 at the rhoptry membrane was examined in RON13-YFP-expressing parasites. Processed RON13 localizes to the rhoptry lumen as demonstrated by the lack of detection of RON13-YFP by cytosolic anti-YFP nanobodies (Fig. 2a and Supplementary Fig. 2a). To determine if RON13 is secreted, RON13 was fused to beta-lactamase (RON13-BLA) and intracellular lactamase activity was used as a sensitive readout for rhoptry secretion in the host cell[16]. Cells infected by RON13-BLA parasites do not show any detectable lactamase activity (Fig. 2b–e and Supplementary Fig. 2b–e). In addition, RON13 is neither associated with e-vacuoles nor with the RON complex post-secretion in invading parasites, supporting the notion that RON13 is not secreted into the host cell during invasion but is instead active in the parasite (Supplementary Fig. 2f, g).

RON13 is an active kinase. RON13 is a 153 kDa type II transmembrane protein with a putative serine/threonine kinase domain and a large luminal carboxy-terminal extension (CTE) with no identifiable structural motif (Fig. 1d). Phylogenetic analysis showed that RON13 belongs to the ROPK clade (Supplementary Fig. 3)[11]. It has a bilobal kinase domain organization and possesses the motifs characteristic of active eukaryotic protein kinases (ePKs; Supplementary Data. 1). The canonical HRD catalytic triad of ePKs differs in RON13 with an HFD motif conserved among all the coccidian orthologues of RON13 (Supplementary Data 2). RON13 is an active kinase as demonstrated by the intense autophosphorylation activity of the recombinant RON13 protein (rRON13k; Fig. 3a–c). The kinase activity is stimulated by the addition of Mg^{2+} or Mn^{2+}, and is insensitive to the broad-spectrum kinase inhibitor staurosporine (Fig. 3c), similarly to the Fam20C secretory pathway kinase[17]. In addition, ATP hydrolysis activity was detected (Fig. 3d). The catalytic activity was completely abolished by introducing a single amino acid change (D595A) in the catalytic HFD motif (rRON13dk), validating the importance of this conserved kinase motif for enzymatic activity (Fig. 3a–c).

RON13 has an atypical kinase structure. To gain insight into the function and regulation of RON13 kinase, its three-dimensional structure was resolved at 3.1 Å resolution by single-particle cryo-EM (Fig. 4a, Supplementary Fig. 4a–i, Supplementary Table 1, and Supplementary Movie 3). The RON13 kinase domain is similar to ePKs, but contains an α-helical N-lobe insertion (NLI; Fig. 4b, c) present exclusively in RON13 coccidian orthologues (Supplementary Data 1 and 2). Unlike ROPKs that also reside in the rhoptries, RON13 lacks an α-helical N-terminal extension (Fig. 4d)[10,18]. The kinase C-lobe structure contains all the motifs required for ATP transfer to the substrate, as well as a ROPK-specific disulfide bond[10]. Another unique feature of RON13 is its CTE, composed of 550 amino acids, that shares no sequence homology with any other proteins (Supplementary Data 1 and 2). The CTE is mainly composed of α-helices clamping the kinase domain C-lobe (Fig. 4b). Of note, the CTE is essential for RON13 folding and stability as neither expression of the kinase domain alone, nor proteolytic cleavage to separate the kinase domain from the CTE of rRON13 yielded a functional RON13 kinase. Although the proteolytic cleavage was efficient, as observed on denaturing/reducing SDS–PAGE analysis, both the kinase domain and the CTE remained attached and could not be separated by addition of high salt concentrations. Cleaved rRON13 behaved exactly as WT rRON13 when analyzed by size-exclusion chromatography, further emphasizing the strong interaction between RON13 kinase domain and the CTE (Supplementary

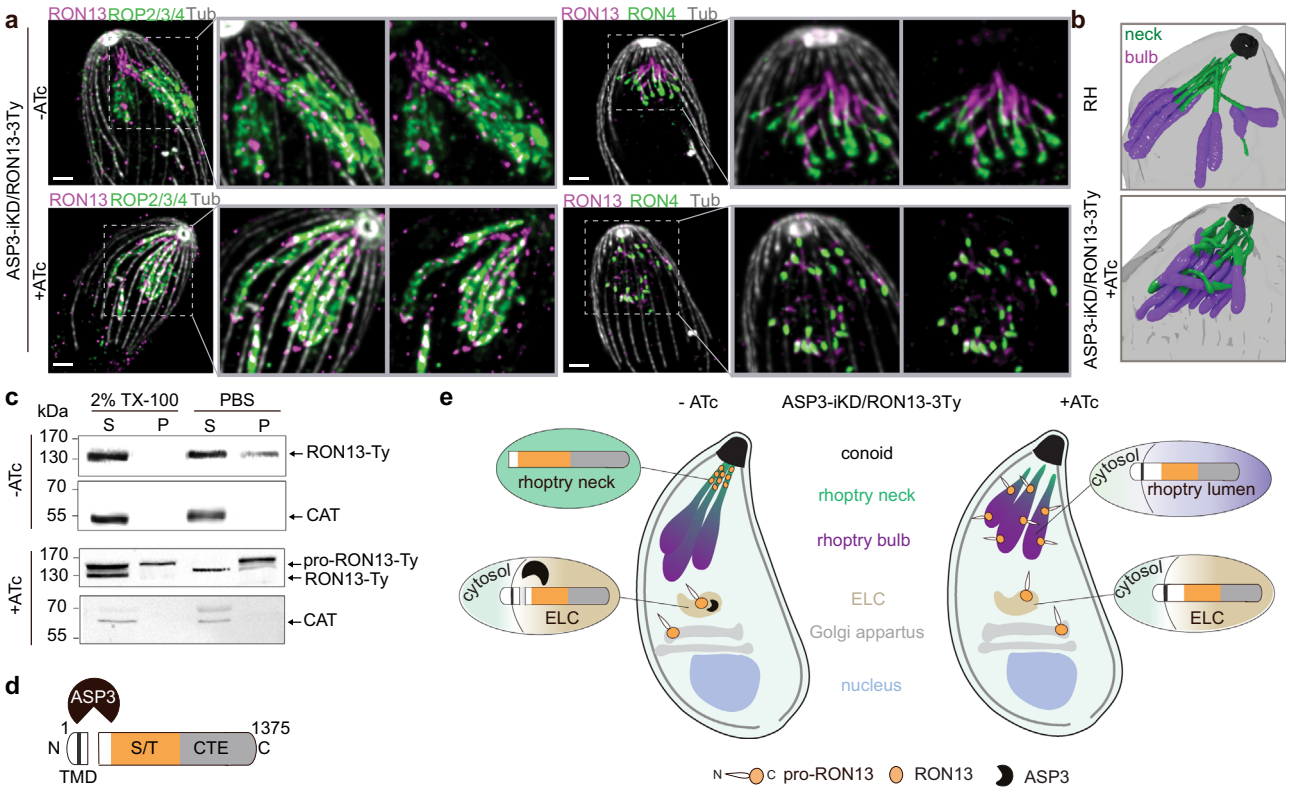

Fig. 1 RON13 is a RON kinase processed by ASP3. a U-ExM images of rhoptries from ASP3-iKD/RON13-3Ty extracellular parasites ± anhydrotetracycline (ATc). RON4 (green) and ROP2/3/4 (green) antibodies are used to visualize the neck and the bulb of the rhoptries, respectively. RON13-3Ty (magenta) is detected by anti-Ty antibodies. The subpellicular microtubules (gray) are stained with α/β anti-tubulin antibodies. Scale bar = 2 µm. Image representative of three biologically independent experiments. **b** 3D reconstruction from FIB-SEM images of the apical part of RH (control) and ASP3-iKD parasites treated 48 h with ATc. The neck (green) and the bulb (violet) of the rhoptries are colored. The conoid (black) and the PM (gray) are depicted. $n = 1$ biologically independent experiment. **c** Solubility of RON13 in ASP3-iKD/RON13-3Ty parasites ±ATc. Catalase is a marker of the soluble fraction. Samples derived from the same experiment and gels were processed in parallel. Image representative of three biologically independent experiments. **d** Scheme of RON13 protein and its cleavage by ASP3 just downstream the transmembrane domain (TMD). S/T serine/threonine kinase domain (orange), CTE C-terminal extension (gray). **e** Scheme representing the fate of RON13 in presence or in absence of ASP3. Without processing by ASP3, RON13 remains insoluble and mistargeted to the body of morphologically aberrant rhoptries. ELC endosome-like compartment. Source data are provided as a Source data file.

Fig. 5a, b). Analysis of RON13 electrostatic potential highlighted a rather extended positively charged groove lying on one side of the kinase that may be involved in protein–protein interactions, but did not provide strong hints to the role the CTE plays (Supplementary Fig. 5c).

RON13 is critical for invasion and virulence. To assess the role of RON13 kinase in *T. gondii*, knockdown parasites (RON13-KD) were generated by replacing the endogenous promoter with an anhydrotetracycline (ATc) repressible promoter (Supplementary Fig. 6a). The promoter swapping resulted in RON13 gene knockdown even without ATc treatment (Supplementary Fig. 6b, c). RON13-KD parasites were severely impaired in their lytic cycle and in host cell invasion (Fig. 5a–c and Supplementary Fig. 6d), but not affected in intracellular replication or egress from host cells (Supplementary Fig. 6e, f). Despite numerous attempts, a complete deletion of the gene could not be obtained. The kinase activity is important for RON13 function as complementation with the dead kinase mutant (RON13-KD/ron13dk) failed to fully rescue the phenotype. In contrast to ASP3-iKD[14], RON5-iKD[19] or ARO-iKD[20] parasites previously reported to be unable to secrete their rhoptries, rhoptry discharge into the host cell was unaffected in RON13-KD parasites, when assayed by empty vacuole formation (e-vacuoles)[9] or by ROP16-dependent host cell STAT6 phosphorylation[21] (Fig. 5d–g). Likewise, microneme secretion was unaffected in RON13-depleted parasites (Fig. 5h). These results indicate that the invasion defect of RON13-KD parasites is not explained by a defect in rhoptry discharge. Of note, infection with RON13-KD parasites resulted in a premature damage of the host cell monolayer, a phenomenon not observed with RON4-KO parasites that display otherwise a comparable invasion defect (Fig. 5i, j and Supplementary Fig. 6g). Remarkably, RON13-KD parasites lost virulence in mice (Fig. 5k) along with a failure to elicit a protective immune response (Supplementary Fig. 6h and Supplementary Table 2). Such inability to trigger immune protection has been previously reported in mutant parasites defective in secretion of rhoptry contents[20,22]. In contrast, RON13-KD/ron13dk parasites were avirulent, but still able to induce seroconversion and protection in the infected animals challenged with the lethal RH strain (Fig. 5k and Supplementary Fig. 6h). Taken together, the presence of RON13 appears to favor host cell survival and is necessary to mount a protective immune response.

RON13 phosphorylates mainly RONs. RON13 substrate identification was undertaken using comparative phosphoproteome analyses of wt (RH) versus RON13-KD (dataset 1), as well as RON13-KD/ron13wt versus RON13-KD/ron13dk (dataset 2; Fig. 6a). A total of 14,681 phosphosites (mainly phosphoserines) in 3012 proteins were identified in the quadruplicate experiments.

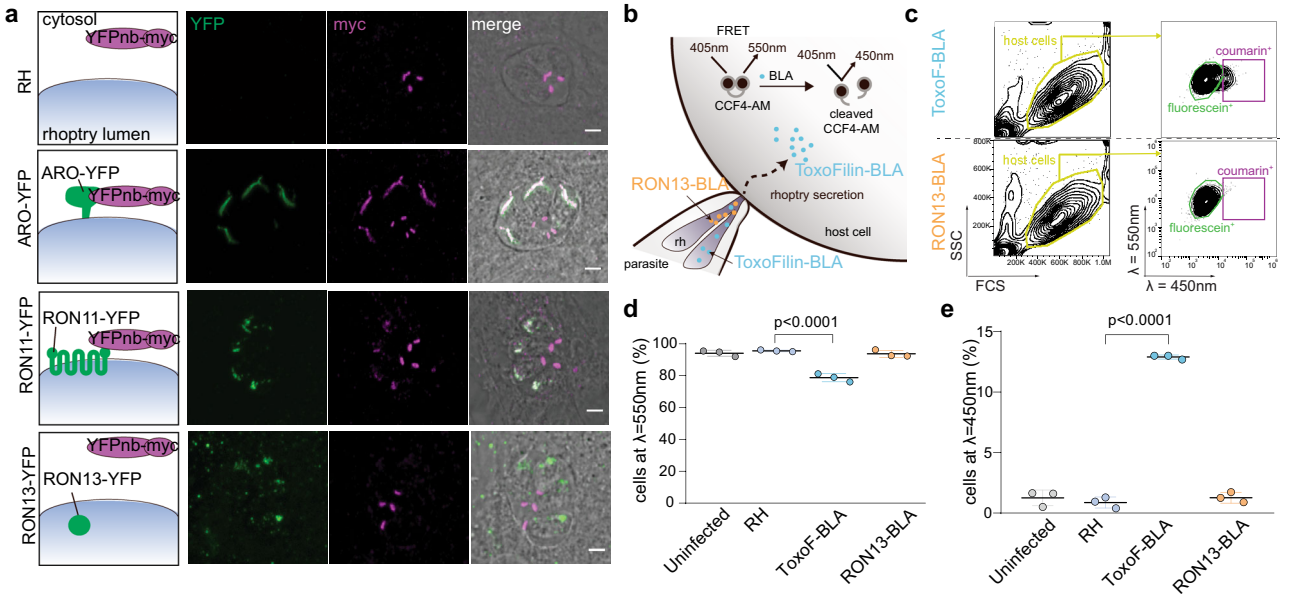

Fig. 2 RON13 is a luminal rhoptry protein that is not secreted during invasion. a IFAs of RH-, ARO-YFP- (green), RON11-YFP- (green), or RON13-YFP- (green) expressing parasites transiently transfected with cytosolic nanobodies targeting YFP fused to a myc-tag (YFPnb-myc). ARO is a protein associated with the cytosolic face of the rhoptry membrane and RON11 is a type III transmembrane protein with its C-terminal domain exposed in the parasite cytoplasm. The myc signal (magenta) observed at the basal part of the parasite is unspecific. Left panels show the schematic topology of the proteins and their ability to bind the cytosolic YFPnb-myc. Scale bar = 2 µm. Image representative of three biologically independent experiments. **b** Principle of the experimental design for the FRET-based rhoptry secretion assay used to determine if RON13 (orange) is secreted into the host cell during the invasion. Toxofilin (blue) is a soluble rhoptry protein secreted into the host cell. **c** Gating strategy for quantification of fluorescein$^+$ cell (green gate; $\lambda = 550$ nm) and coumarin$^+$ cell (violet gate; $\lambda = 450$ nm) frequency for RON13-BLA- and Toxofilin-BLA-infected cell monolayer (yellow gate) analyzed by flow cytometry. **d**, **e** Frequency of fluorescein$^+$ cells ($\lambda = 550$ nm, **d**) or coumarin$^+$ cells ($\lambda = 450$ nm, **e**) in each condition (mean ± SD; $n = 3$ biologically independent experiments). Statistical significance was assessed by a one-way ANOVA significance with Tukey's multiple comparison. Source data are provided as a Source data file.

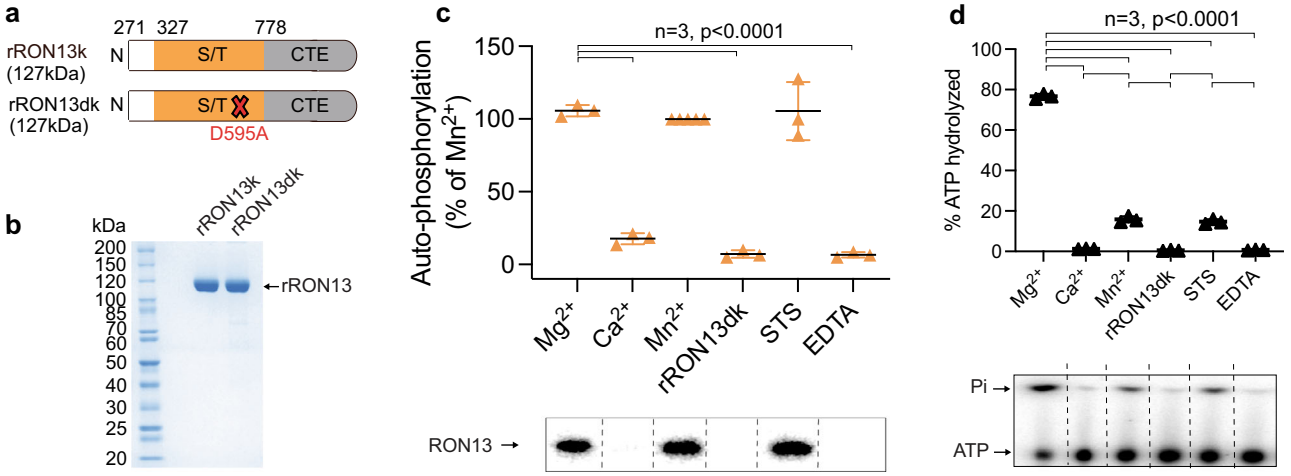

Fig. 3 Recombinant RON13 is active in vitro. a Scheme of recombinant RON13 kinase (rRON13k) and RON13 dead kinase (rRON13dk), in which kinase activity is abrogated by introducing the mutation D595A. **b** Coomassie-stained gel of purified rRON13k and RON13dk produced in insect cells. **c** Radioactive RON13 kinase activity assays based on rRON13k autophosphorylation. Radiograph is shown below the graph. Densitometry data (mean ± SD; $n = 3$ biologically independent experiments) were normalized to rRON13k in presence of Mn^{2+}. Statistical significance was determined using a two-tailed paired *t* test. STS staurosporine. **d** ATP hydrolysis during kinase reactions, as measured by TLC analysis (mean ± SD; $n = 3$ biologically independent experiments). Autoradiograph showing both non-hydrolyzed ATP (ATP) and inorganic phosphate (Pi) is shown below the graph. *P* values were determined by a two-tailed paired *t* test. Source data are provided as a Source data file.

The overlap with a previous study[13] is partial mainly due to differences in sample size, as well as in the experimental settings. The enrichment of phosphopeptides by immunoprecipitation done in this study allowed the detection of low abundance peptides leading to the identification of new phosphoproteins[13] (Supplementary Data 3 and Supplementary Fig. 7a, b). Over 220 phosphopeptides corresponding to 171 phosphoproteins showed a >4-fold difference in abundance in wt compared to RON13-KD (dataset 1). Dataset 2 revealed 196 differentially phosphorylated proteins between the complemented strain RON13-KD/ron13wt and

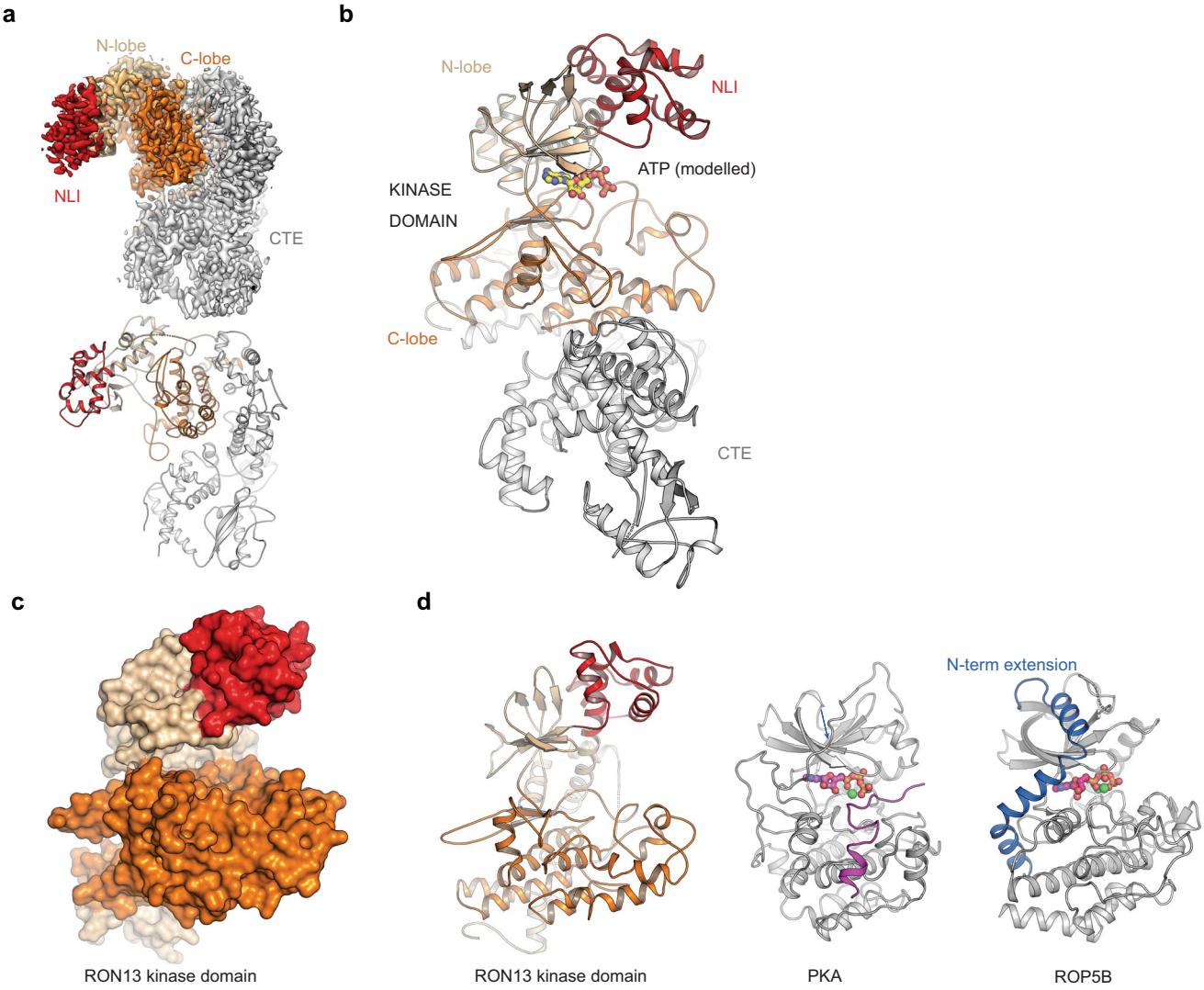

Fig. 4 Structure of RON13. a Cryo-EM density map determined by single-particle analysis at a resolution of 3.1 Å (top), and the corresponding views of the atomic model of rRON13dk. The kinase domain and the C-terminal extension (CTE) are colored in orange and gray tones. **b** Domain organization of RON13. The position of the ATP-binding site is indicated by the ATP ligand modeled into the active site (absent in the experimentally determined density map). The N-lobe insertion (NLI, red) and the C-terminal extension (CTE, gray) are color-coded. **c** Surface representation of RON13 kinase domain at 3.1 Å resolution. **d** Comparison of RON13 kinase domain structure with other kinases. PKA from *Mus musculus* (PDB ID: 1atp) is complexed with MnATP and an inhibitory peptide (violet). ROP5B from *T. gondii* bound to ATP (PDB ID: 3q60) contains a ROP-specific N-terminal extension (blue).

RON13-kD/ron13dk. Overall 42 proteins (63 phosphopeptides) are common to both datasets (Fig. 6b, Supplementary Fig. 7c, and Supplementary Data 4). We defined phosphopeptides as highly probable targets of RON13, when these were upregulated in both datasets, i.e., in wt versus RON-13KD, as well as RON13-KD/ron13wt versus RON13-KD/ron13dk. According to the spatial data obtained from hyper LOPIT[23], most of the proteins hits are predicted to localize to the rhoptries (Fig. 6c, d and Supplementary Fig. 7d, e). Dataset 2 uncovered an increased phosphorylation of proteins from microneme, apicoplast and inner membrane complex likely attributable to the ~3-fold higher level of RON13 in RON13-KD/ron13wt parasites compared to wt (Supplementary Data 4). It is plausible that the overexpression of RON13 in the RON13-KD/ron13wt parasites led to mis-trafficking and thus to increased exposure of RON13 to targets outside of the rhoptries. A large proportion of the deduced RON13 substrates consists of previously annotated or predicted ROPs and RONs based on fractionation or transcriptomic data[23,24] (Supplementary Data 5). Analysis of the phosphopeptide sequences led to the identification of a RON13 substrate consensus motif ExxxxxExxxNx**S**QSSxx-xAxE (Supplementary Fig. 7f).

Of interest, three autophosphorylation sites were identified on RON13: Thr379 and Ser381 within the NLI in proximity to the ATP-binding site (N-lobe) and Thr703 closer to the activation loop (C-lobe; Fig. 7a, b). Mutation of these residues to alanine (phosphonull mutant, ron13pn) abolishes autophosphorylation in vitro, whereas mutation to aspartic acid (phosphomimetic mutant, ron13pm) does not impact RON13 autophosphorylation, suggesting that other residues than the ones identified are targeted (Fig. 7c). The complemented RON13-KD/ron13pm parasites showed a mild defect in invasion (Supplementary Fig. 8a–c), suggesting a modest contribution of RON13 autophosphorylation to its function. Taken together comparative phosphoproteomics reveals that RON13 phosphorylates rhoptry proteins in situ, including the components of the RON complex.

RON4 is a substrate of RON13. RON4 which plays a critical role in MJ formation is differentially phosphorylated in both datasets.

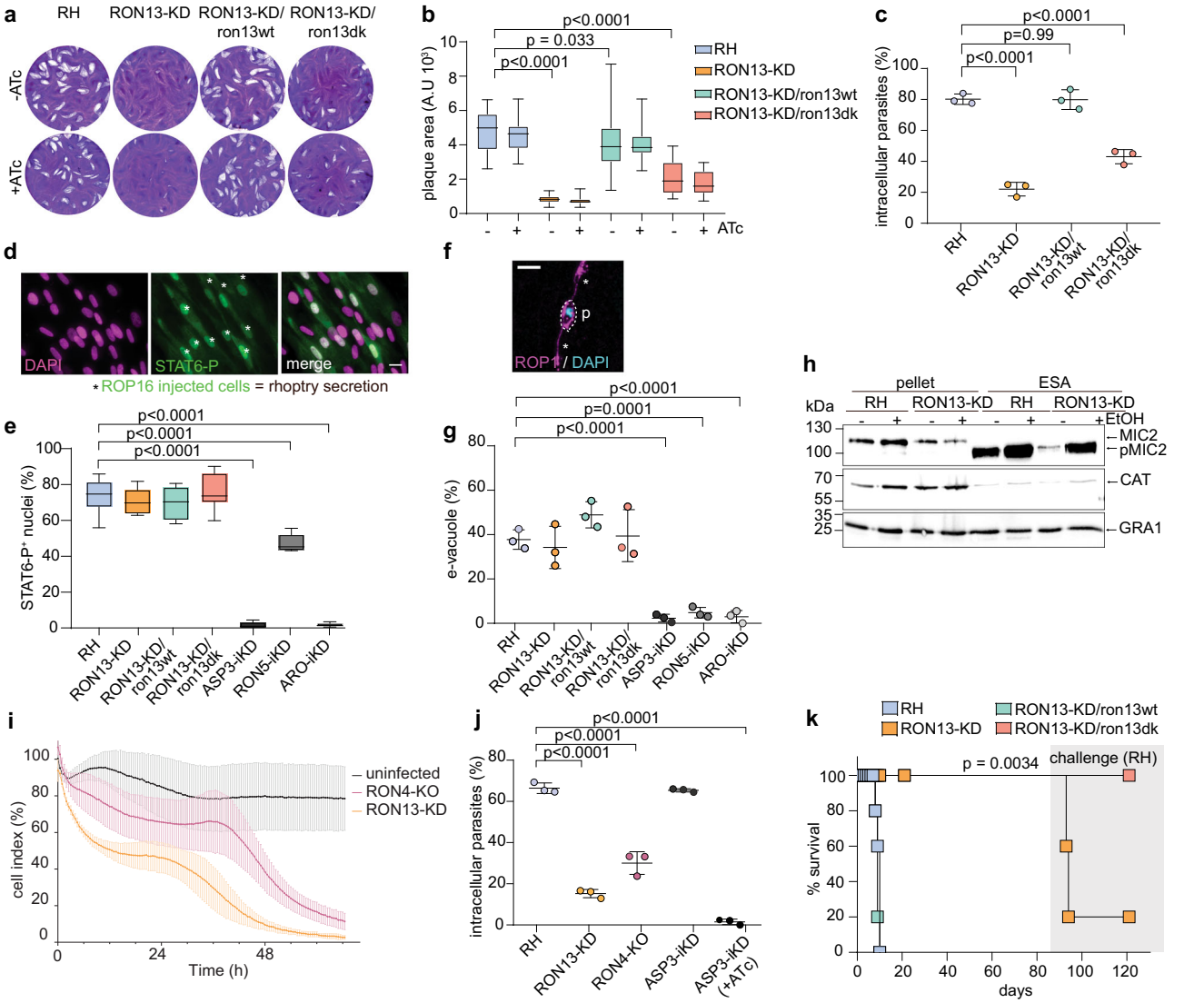

Fig. 5 RON13 is critical for invasion. a Plaque assays of different parasite strains (±ATc) showing that depletion of RON13 impairs the parasite lytic cycle (no plaque), a phenotype that is fully rescued by complementation with an active RON13 kinase. Image representative of three biologically independent experiments. **b** Quantification of plaque assays for RH, RON13-KD, and complemented RON13-KD/ron13wt or RON13-KD/ron13dk parasites (±ATc). Data are presented as box and whiskers plot (median with min to max, $n = 3$ biologically independent experiments). Statistical significance was assessed by a two-way ANOVA significance with Tukey's multiple comparison. **c** Invasion assay (+ATc) showing a strong invasion defect when RON13 kinase is absent or inactive *P* value were determined by a one-way ANOVA significance with Tukey's multiple comparison. (Mean ± SD; $n = 3$ biologically independent experiments). **d** IFA showing a representative field of the rhoptry secretion test using phosphor-STAT6 as a readout with fibroblast nuclei stained in DAPI (magenta) and ROP16-injected cells stained with anti-phospho-STAT6 (STAT6-P) antibody (green, asterisks). Scale bar = 25 µm. Image representative of three biologically independent experiments. **e** Phospho-STAT6 assays assessing the ability of the parasite to secrete the rhoptry protein ROP16 into the host cell that phosphorylates host STAT6 in the nucleus. Data are presented as box and whiskers plot (median with min to max, $n = 3$ biologically independent experiments). Statistical significance was assessed by a two-way ANOVA significance with Tukey's multiple comparison. **f** Representative IFA of the e-vacuole assay to assess rhoptry secretion when invasion is blocked by cytochalasin D. A parasite (p) secreting e-vacuoles ROP1$^+$ (asterisks) is depicted. Parasite DNA is visualize using DAPI (blue). Scale bar = 5 µm. Image representative of three biologically independent experiments. **g** E-vacuole assays assessing the ability of the parasites to secrete the rhoptry protein ROP1 into the host cell (mean ± SD; $n = 3$ biologically independent experiments). Statistical significance was assessed by a one-way ANOVA significance with Tukey's multiple comparison. **h** Microneme secretion of extracellular parasites stimulated with 2% ethanol to assess the release of MIC2 in culture supernatant. pMIC2 processed MIC2, ESA excreted–secreted antigens. GRA1 is used as a control for constitutive secretion from dense granules. Samples derived from the same experiment and gels were processed in parallel. Image representative of three biologically independent experiments. **i** Kinetic assay representing the cell index of HFF infected with different parasite strains. (Mean ± SD; $n = 3$ biologically independent experiments). **j** Invasion assay showing that RON13-KD and RON4-KO parasites are defective in invasion. *P* values were determined by a one-way ANOVA significance with Tukey's multiple comparison (mean ± SD; $n = 3$ biologically independent experiments). Statistical significance was assessed by a one-way ANOVA significance with Tukey's multiple comparison. **k** Virulence of different strains in mice. Surviving mice at 84 days post infection were challenged with RH parasites (gray shaded). ($n = 5$ biologically independent animals). *P* values were determined by a Mantel–Cox test. Source data are provided as a Source data file.

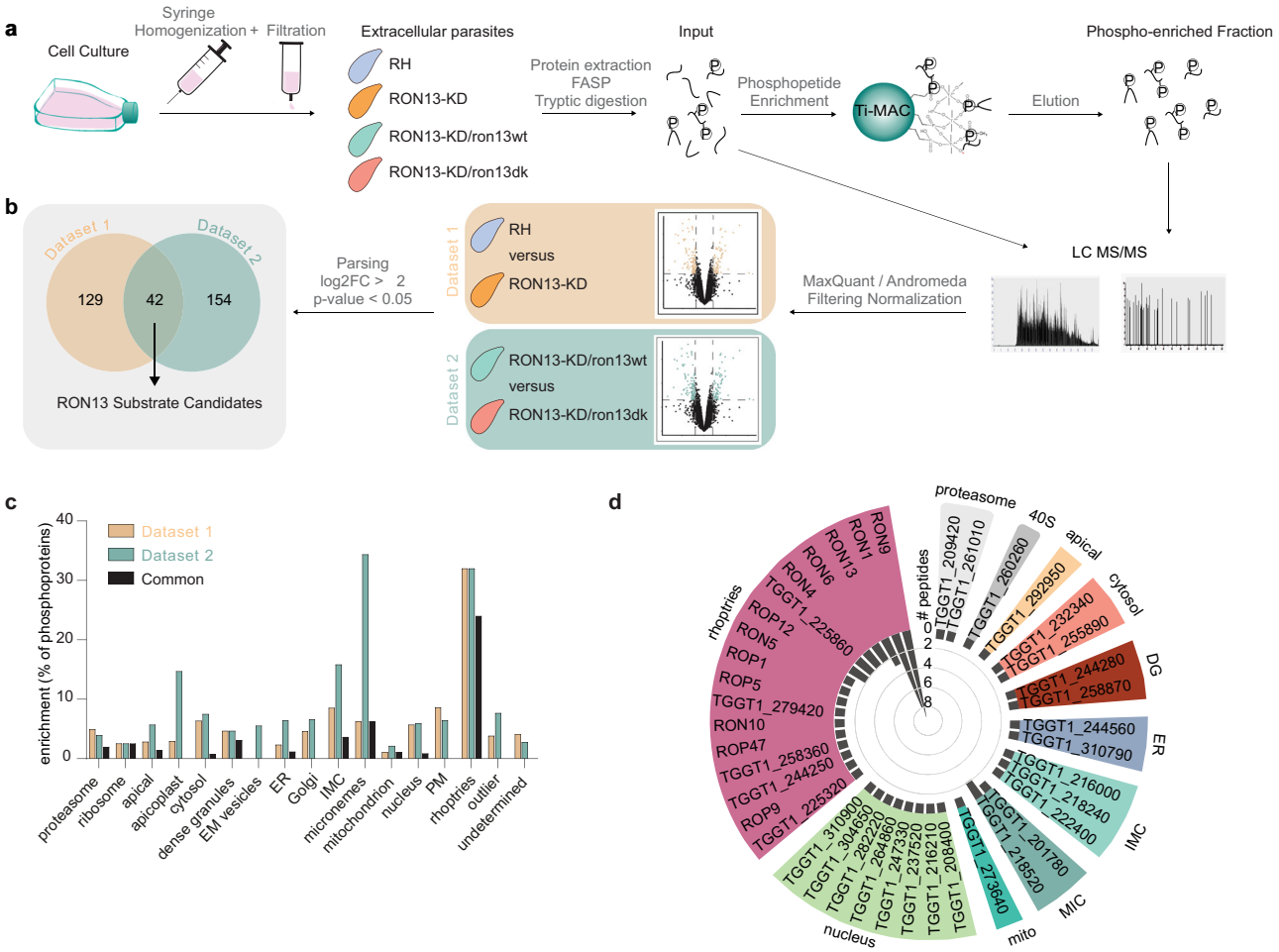

Fig. 6 Rhoptry proteins are the major substrate of RON13. a Workflow of the shotgun approach and phosphoproteome analysis used to identify RON13 substrates. Samples were prepared for each strain from four independent experiments ($n = 4$ biologically independent experiments). RH (blue) RON13-KD (orange) RON13-KD/ron13wt (green) RON13-KD/ron13dk (salmon). **b** Venn diagrams of the phosphoproteins found in datasets 1 and 2. **c** Bar graph showing the percentage of phosphoproteins from datasets 1 and 2 relative to the total number of phosphoproteins, according to their predicted localization[23]. EM endomembrane, IMC inner membrane complex. **d** Polar plot of the number of phosphopeptides found in both datasets (common) binned by gene IDs and clustered, according to their predicted subcellular localizations[23]. Source data are provided as a Source data file.

To validate it as a direct substrate, recombinant RON4 (rRON4) produced in insect cells was purified and its phosphorylation by rRON13 tested in vitro. Compared to the generic kinase substrate myelin basic protein (MBP) or autophosphorylation, rRON4 serves as a much better substrate, while maintaining the same ion preferences as observed with autophosphorylation (Fig. 7d, e), strongly suggesting that RON4 is an endogenous substrate. The phosphorylation status of rRON13 clearly influenced its RON4-directed phosphotransferase activity with the phosphonull mutant (rRON13pn) showing a twofold increased activity, whereas phosphomimetic significantly downregulating RON4 phosphorylation status (Fig. 7c). Thus, RON13 autophosphorylation directly influences substrate phosphorylation in vitro. Next, hydrogen/deuterium eXchange-mass spectrometry (HDX-MS)[25] was applied to map the interaction sites between RON13 with RON4. HDX-MS can monitor protein dynamics based on the rate of exchange of protein amide protons with the solvent. Comparison of rRON13 dynamics alone and in presence of an excess of rRON4 (Fig. 7f) identified a single region protected from H/D exchange by RON4 (amino acids 377–390; Fig. 7g, Supplementary Fig. 9a, b, Supplementary Data 6, and Supplementary Table 3). As the only rRON13 region showing differential HDX rate upon addition of RON4 is small compared to the overall rRON13 structure, this suggests that the RON13–RON4 interaction is transient. Of relevance, this region is surface-exposed within the NLI and comprises two of the autophosphorylation sites, Thr379 and Ser381 (Fig. 7h). These results validate the direct interaction between rRON4 and rRON13, and identify the NLI as a substrate-recognition region.

RON13-KD parasites are unable to assemble the MJ. As previously stated, the majority of RON13-KD parasites were defective in host cell entry and remained extracellular (~90%; Fig. 8a). However, among the minor subpopulation of invading parasites, the typical ring-shaped MJ was observed in <14% of the events (Fig. 8b). For most of the RON13-KD- and RON13-KD/ron13dk-invading parasites, the MJ components RON2/4/8 were absent or abnormally distributed at the host–parasite interface (Fig. 8b, c). Importantly, prior to secretion, the RON complex is properly processed, assembled, and accurately targeted to the neck of the rhoptries (Fig. 8d). Furthermore, co-immunoprecipitation experiments of RON4 confirmed that the intact RON complex is still able to associate to the microneme protein AMA1 (Fig. 8e and Supplementary Table 4). Consequently, RON13-catalyzed phosphorylation is a prerequisite for the stabilization of the MJ at

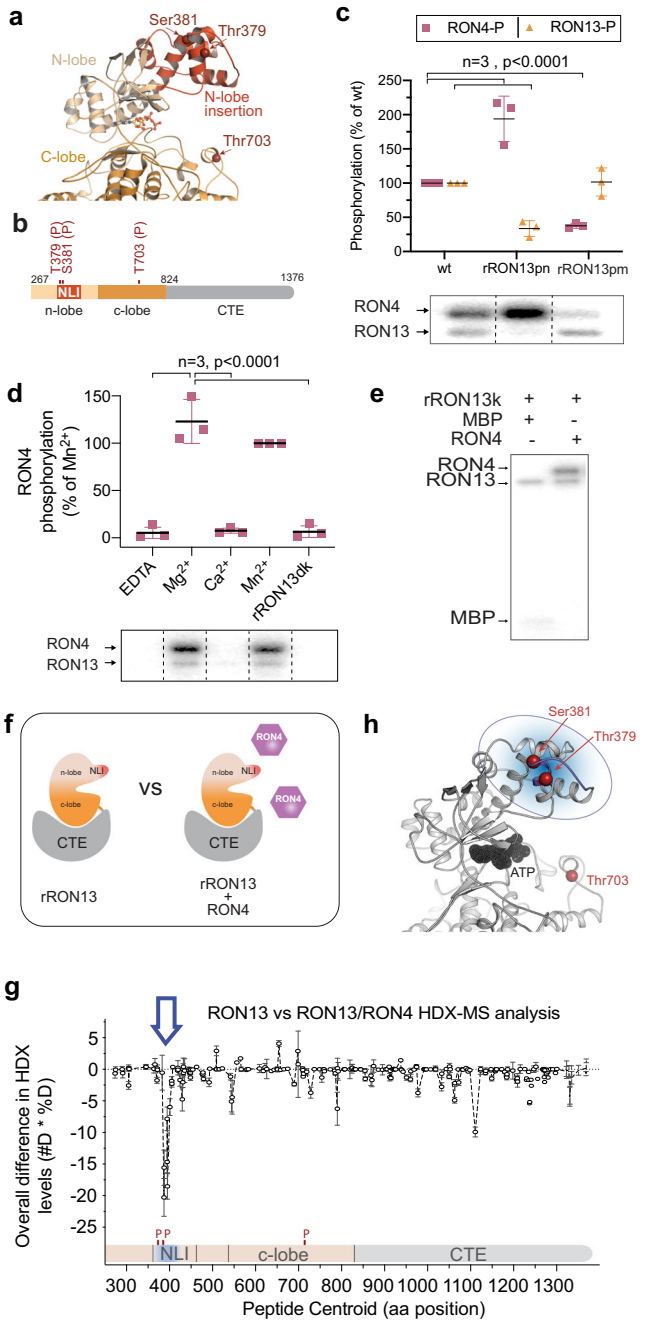

Fig. 7 RON4 is a direct substrate of RON13. a Partial view of the RON13 structure highlighting the autophosphorylation sites (arrows, red). Kinase domain (orange tones). NLI (N-lobe insertion). **b** Schematic representation of RON13 structure organization highlighting the autophosphorylated residues (red) mutated in this study. The kinase domain and the C-terminal extension (CTE) are colored in orange and gray tones. **c** Radioactive kinase activity assays comparing RON4 phosphorylation and RON13 autophosphorylation for different rRON13 phospho-mutants; phosphonull (RON13pn) and phosphomimetic (RON13pm). Autoradiograph of a representative radioactive kinase assay is shown below the graph. Data shown as mean ± SD normalized to wt ($n = 3$ biologically independent experiments). *P* values were determined using a two-tailed paired *t* test. **d** Radioactive kinase activity assays characterizing the influence of ions on rRON4 phosphorylation by RON13. Densitometry data (mean ± SD; $n = 3$ biologically independent experiments) were normalized to RON4 phosphorylation in presence of Mn^{2+}. Statistical significance was determined using a two-tailed paired *t* test. **e** Autoradiograph from a radioactive kinase activity assays in presence of MBP (left) or RON4 (right) as a substrate. **f** Schematic representation of the two states analyzed by HDX-MS. The kinase domain and the C-terminal extension (CTE) are colored in orange and gray tones. NLI (red). RON4 (violet). **g** Differences in HDX rates between rRON13dk alone and in the presence of RON4. A single region encompassing amino acids 377–390 is protected by RON4, indicating the contact site between the two proteins. Data shown as mean ± SD; $n = 3$ biologically independent experiments. **h** RON13 kinase domain highlighting the RON4-binding site (residues 377–390; blue) identified by HDX-MS. This region corresponds to the NLI and encompasses the two phosphosites Thr379 and Ser381. Source data are provided as a Source data file.

the parasite/host interface without destabilizing the RON complex prior secretion. Of note, autophosphorylation of RON13 does not influences the correct assembly of the RON complex at the MJ post-secretion (Supplementary Fig. 10a, b). Identified as an endogenous RON13 substrate, modification of RON4 phosphorylation status alone is not sufficient to prevent MJ formation. Indeed, RON4 phosphonull (RON4pn) and RON4 phosphomimetic (RON4pm) mutant parasites (Fig. 9a–c) showed an unaltered lytic cycle and host cell invasion (Fig. 9d–f). In accordance with these observations, in both RON4 phosphomutant parasites, the stabilization of the RON complex at the MJ is unaffected and even if dispensable, we observed the recruitment of the host adaptor protein ALIX to the MJ[5] (Fig. 9g–j). Overall, these results suggest a pleiotropic role of RON13 in the phosphorylation of each of the components of RON complex that together contribute to the success of host cell invasion.

Discussion

RON13 is an atypical kinase possessing a unique NLI within the kinase domain that participates in substrate recognition. It harbors a large CTE critical for proper folding that is conserved among the coccidians. Comparisons of RON13 CTE structure to other proteins in the protein data bank did not reveal any clear match (only superficial similarity of the CTE fold to that of cytochrome P450, OleP (PDB ID: 5mnv), could be detected using PDBeFold[26] (https://www.ebi.ac.uk/msd-srv/ssm/ssmcite.html)). Based on this, the CTE region of RON13 bares little to no structural similarity to any other proteins of known structure. RON13 clusters with the ROPK family members but differs from the ROPKs characterized to date. It localizes to the neck instead of the bulb of the rhoptries and does not appear to be secreted, although we cannot formally exclude it. Moreover, its kinase activity is essential for parasite survival and with its insensitivity to the broad kinase inhibitor staurosporine, it offers great promises for the identification of highly selective inhibitors. This atypical kinase operates in the secretory pathway and phosphorylates predominantly RON proteins, but also other ROPs known to be involved in subversion of host cell function.

The premature destruction of the HFF monolayer observed under RON13-KD infection supports the hypothesis that this kinase modulates the function of an unidentified secreted ROP that controls host cell survival by an unknown mechanism. Furthermore, infection of mice with RON13-KD parasites failed to mount a resistance to reinfection. This phenomenon was previously observed only in parasites incompetent in invasion, resulting from defect in rhoptry discharge. Thus, RON13-dependent phosphorylation of effectors likely participates in modulation of host immune response. In contrast the impact of RON13 on the RON complex is more evident. The phosphorylation of the individual components of the RON complex is clearly dependent on RON13 and ensures proper MJ formation at

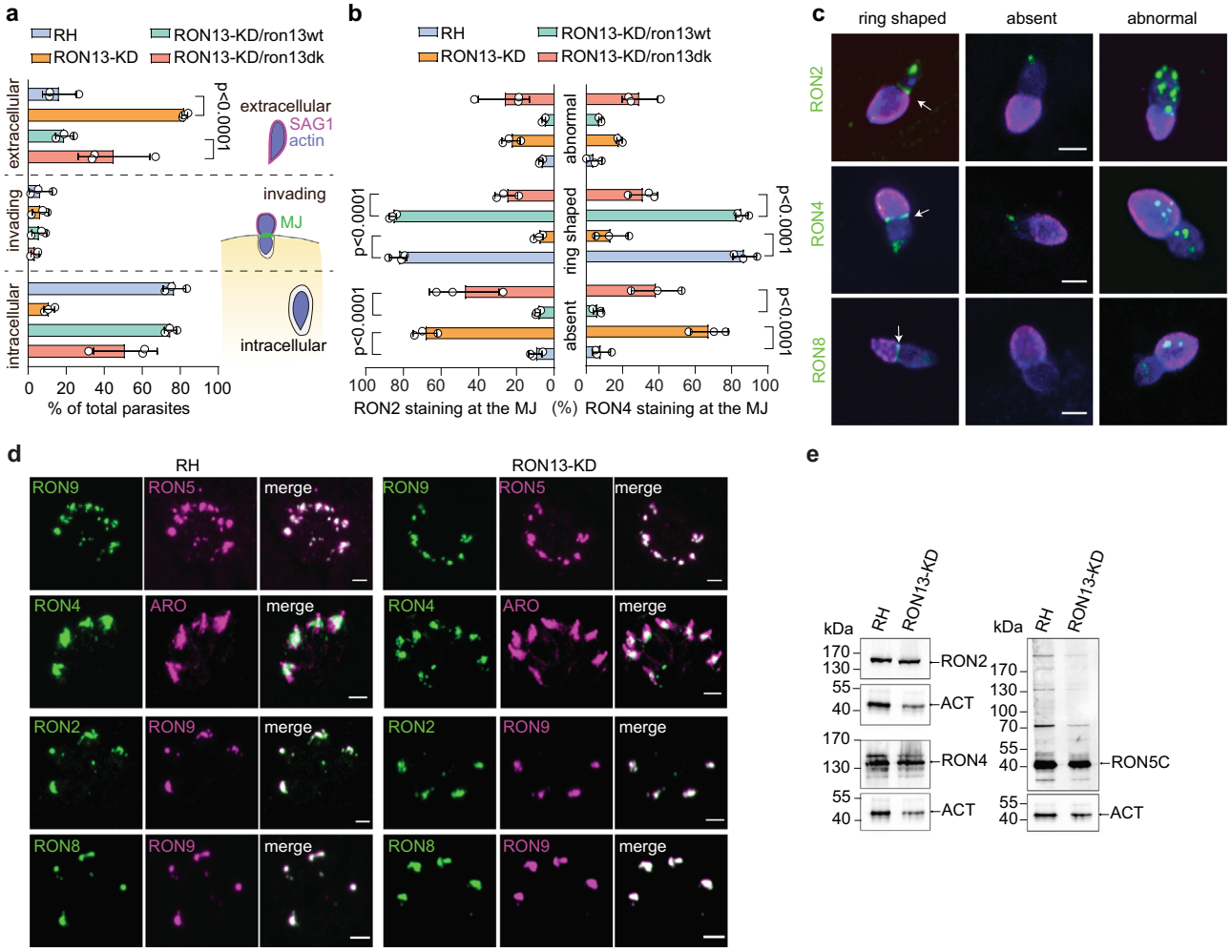

Fig. 8 RON13 kinase activity is important for moving junction formation during invasion. a Graph representing the proportion of extracellular, invading, and intracellular parasites observed in the pulse-invasion assay. The scheme depicts the three stages of the invasion process considered in this assay (mean ± SD; $n = 3$ biologically independent experiments). Statistical significance was assessed by a one-way ANOVA significance with Tukey's multiple comparison. **b** Quantification of the different types of RON2 and RON4 staining (absent, abnormal, and ring shaped) observed at the MJ of invading parasites. (Mean ± SD; $n = 3$ biologically independent experiments). Statistical significance was assessed by a one-way ANOVA significance with Tukey's multiple comparison. **c** IFAs showing a representative example of RON2, RON4 and RON8 staining (green) of invading RON13-KD parasites obtained from three biologically independent experiments. An arrow indicates the bona fide ring-shaped MJ. Anti-SAG1 (magenta) and anti-actin (blue) antibodies stain the extracellular part of the parasite and the parasite cytoplasm, respectively. For the last row, anti-GAP45 antibodies (blue) were used. Scale bar = 2 µm. **d** IFAs on RH and RON13-KD intracellular parasites showing that proteins of the RON complex are well expressed and addressed to the rhoptry in RON13-KD-treated parasites. For the first row, RON5 is in magenta and RON9 in green. RON4, RON2, and RON8 are in green. Anti-ARO (magenta) and anti-RON9 (magenta) antibodies are used as rhoptry compartment markers. Scale bar = 2 µm. Image representative of three biologically independent experiments. **e** WB showing a comparable level of expression of RON complex proteins between RH and RON13-KD parasites using anti-RON2, anti-RON4, and anti-RON5C antibodies. Actin (anti-ACT) is used as a loading control. Image representative of three biologically independent experiments. Source data are provided as a Source data file.

the parasite–host interface and host invasion (Fig. 10). Mutations in the known phosphorylated sites of RON4 were not sufficient to recapitulate the phenotype observed in absence of RON13. This result suggests a cooperative role of phorsporylation of RON2/4/5 and 8 for the proper assembly of the MJ at the host PM, as observed for the interaction between RON complex and host proteins[5]. This study unravels a new level of complexity in the mechanism that governs invasion highlighting the phosphorylation as a key posttranslational modification that arms the secreted virulence factors necessary for host cell invasion. RON13 is found and conserved in the coccidian subgroup of the Apicomplexa. Importantly, the components of the RON complex are also phosphorylated in the deadliest malaria parasite *Plasmodium falciparum*. In silico analysis identified a predicted atypical kinase (PF3D7_3121100) expressed in the invasive stages of *P. falciparum* that also displays some homology to *Tg*RON13, including a large CTE and a determinant to enter the secretory pathway (Supplementary Data 7). Such an atypical kinase is worthy of deeper investigations as it might unravel a potential candidate for targeting invasion in malaria parasites via chemotherapeutic intervention.

Methods

DNA vector constructs and transfections. The sequence of the oligonucleotide primers and the plasmids generated are listed in Supplementary Table 5. The *T. gondii ΔKU80* RH[27] and TaTi/*ΔKU80* (ref. [28]) strains were used to obtain all the transgenic strains generated in this study (Supplementary Table 5). *Escherichia coli* XL-10 Gold chemically competent bacteria were used for DNA amplification.

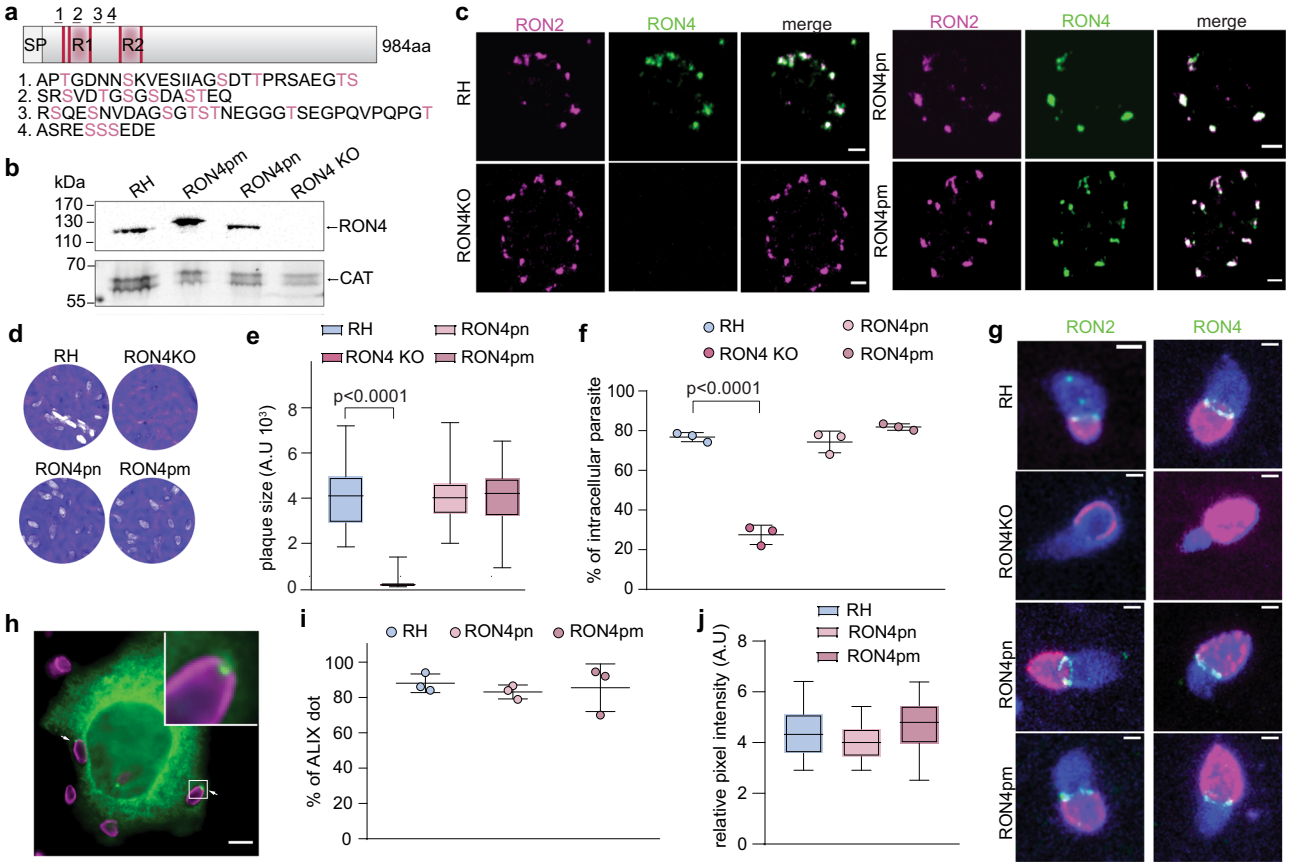

Fig. 9 Phosphorylation of RON4 is not required for MJ formation and ALIX recruitment. a Schematic representation of RON4 protein. Two repeats (R1 and R2) and five motifs (pink lines) known to be important for binding host cytoskeleton are present in the N-term of RON4. The number (1, 2, 3, and 4) indicate the regions of RON4 known to be phosphorylated. The corresponding amino acid sequences and phosphorylated residues are indicated below in pink. These amino acids have been mutated in alanine or negatively charged amino acid to generate RON4 phosphonull (ron4pn) and RON4 phosphomimetic (ron4pm) mutant parasites, respectively. **b** Western blot showing that RON4pn and RON4pm are properly expressed. RON4-KO parasites have undetectable amount of RON4. Image representative of three biologically independent experiments. **c** IFA showing that mutation of phosphorylated residues either in Ala (ron4pn) or in Asp (ron4pm) does not impact RON4 (green) targeting to the rhoptry neck. Scale bar = 2 µm. Image representative of three biologically independent experiments. RON2 (magenta). **d** Plaque assay comparing the ability parasites to accomplish the lytic cycle. Image representative of three independent experiments. **e** Quantification of the plaque assay experiment. Data are presented as box and whiskers plot (median with min to max, $n = 3$ biologically independent experiments). Statistical significance was assessed by a one-way ANOVA significance with Tukey's multiple comparison. **f** Invasion test showing the percentage of intracellular parasites reflecting their ability to invade. One-way ANOVA followed by Tukey's multiple comparison was used to test differences between groups. (Mean ± SD; $n = 3$ biologically independent experiments). **g** IFA of invading parasites with RON2 (green) and RON4 (green) seen at the MJ except for RON4-KO invading parasites. SAG1 (magenta) and GAP45 (blue) were used to discriminate invading parasites. Scale bar = 1 µm. Image representative of three biologically independent experiments. **h** ALIX-GFP (green) expressing HeLa cells infected by RH parasites (magenta). ALIX recruitment at the MJ closure is indicated by white arrowhead. The inset displays the white boxed area at higher magnification. Scale bar = 5 µm. Image representative of three biologically independent experiments. **i** Quantification of the proportion of intracellular parasites associated with an ALIX dot in an in/out assay. Data are presented as box and whiskers plot (median with min to max, $n = 3$ biologically independent experiments). Statistical significance was assessed by a one-way ANOVA significance with Tukey's multiple comparison. **j** Relative pixel intensity of ALIX dot recruited at the MJ in infected ALIX-GFP HeLa cells. When not stated two-way ANOVA followed by Tukey's multiple comparison was used to test differences between groups. (Mean ± SD; $n = 3$ biologically independent experiments). Source data are provided as a Source data file.

To generate RON13-3Ty transgenic parasites, 1763bp corresponding to the C-terminal part of RON13 (TGGT1_321650) were amplified using the primers 6765/6766, and cloned into the ApaI and SbfI sites of the vector Ct-ASP5-3Ty-DHFR[29]. A total of 40 µg of Ct-RON13-3Ty-DHFR plasmid were linearized by BstBI prior transfection.

For the YFP C-term tagging of ARO and RON11, we amplified the 3′ coding sequence of each gene using the primer pairs 8798/8799 (1043 bp) and 8800/8801 (1345 bp), respectively. PCR fragments were cloned into the LIC-YFP-DHFR vector[27] and the final vectors were digested with BclI for ARO-YFP-DHFR and with AflII for RON11-YFP-DHFR, respectively, prior to transfection.

For YFP C-term tagging of RON13, we amplified the 3′ coding sequence using two pairs of primers 8802/8803 and 8804/8805 (1135 bp) to introduce a silent mutation, and thus generate an EcoRV restriction site used for LIC-RON13-YFP-DHFR vector linearization.

To generate RON13-KD parasite line, we amplified a PCR fragment encoding the TaTi trans-activator, the HXGPRT selection cassette and the TetO7S1 promoter from the vector 5′COR-pT8TATi1-HXtetO7S1myc[30], using the primers 7013/7015 and KOD polymerase (Novagen, Merck). Primers 7013 and 7015 each share 30 and 32 bp of homology with the 5′ end of RON13. A specific gRNA vector generated by Q5 Hot Start site-directed mutagenesis kit (NEB) with the primers 4883/7012 on the vector template pSAG1::CAS9-GFPU6::sgUPRT[31] was used to direct the insertion of the PCR cassette by double homologous recombination at the 5′ of the *ron13* locus.

To generate RON4-KO parasites, a gRNA targeting the 5′ coding sequence of RON4 was used to introduce a frameshift, resulting in RON4-KO. RON4 protein ablation was verified by IFA and western blotting using anti-RON4 antibodies (Supplementary Table 6).

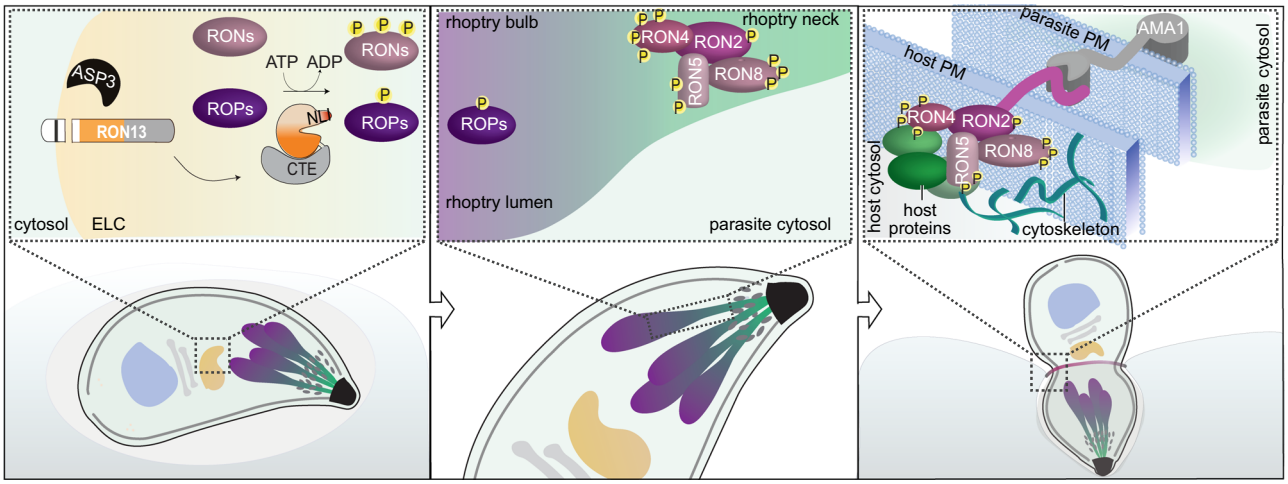

Fig. 10 Cartoon summarizing the main findings. Left: in the endosome-like compartment (ELC) where protein trafficking to secretory organelles is determined, Asp3 protease cleaves the N-terminal transmembrane segment of RON13. Rhoptry proteins, including RONs and ROPs (violet tones), are phosphorylated by RON13 within this compartment. Center: RON13-phosphorylated proteins assemble to form the RON complex within the rhoptry neck, prior to being secreted into the host. Right: the RON complex, localized to the cytosolic face of the host, contributes to parasite invasion by forming a moving junction by associating with adhesins at the parasite plasma membrane (blue). Phosphorylated proteins of the RON complex additionally recruit host proteins (green) to assist in parasite invasion and subvert host cellular functions.

RON4pm and RON4pn parasites were generated by modifying the *ron4* endogenous locus. Synthetic fragments corresponding to the bp 208 to bp 1104 of the RON4 cDNA flanked by 100 bp of ron4 gDNA homology region in 5′ and 3′ and EcoRV restriction sites were purchased from Genewiz®. In those fragments, the 23 phosphosites identified previously[13] and in this study were mutated either to alanine (ron4pn) or to acid aspartic (ron4pm). Following enzymatic restriction, each fragment was co-transfected with the vector 2gRNA CRISPR-Cas9 plasmid[32] containing 2gRNA targeting sequences located at 958 and 2519 bp from the start codon (Supplementary Table 5). Parasite clones were selected by FACS and screened by PCR for integration. The modified region was verified by sequencing.

To complement the RON13-KD line with a wild-type copy of *ron13* under a rhoptry promoter (p*ron5*), total RNA was extracted from RH tachyzoites using the RNeasy Minikit (Qiagen), and reverse transcribed in cDNA using the Superscript II kit (Invitrogen). The specific full-length cDNA of *ron13* gene was PCR-amplified in three parts using the primers 8178/7813 (part 1—2097 bp), 7814/7815 (part 2—960 bp), 7816/8179 (part 3—1152 bp), and the Pangea polymerase (Canvax).The three fragments were Gibson assembled with the vector pUPRT-promRON5-G13-4myc[5] digested by PacI/EcoRV. A total of 60 µg of the resulting vector pUPRT-pRON5-RON13-4myc was digested by KpnI/BamHI and co-transfected with 15 µg of the pU6-Cas9-Universal-gRNAUPRT vector[33]. Parasites for which the integration of the vector pUPRT-p*ron*5-RON13-4myc at the UPRT locus by double homologous recombination had occurred were selected by 5′-fluo-2′-deoxyuridine (FUDR) negative selection and designated as RON13-KD/ron13wt. Point mutagenesis introduced by Q5 site-directed mutagenesis (NEB) on p*ron*5-RON13-4myc were used to generate ron13dk, ron13cte, ron13pn, and ron13pm vectors (Supplementary Table 5).

To assess RON13 secretion into the host cell, we modified the vector SP3-toxofilin-BLA (kind gift from Dr. Lodoen MB.)[16] by cloning RON13 cDNA in frame with the beta-lactamase tag. The fragment p*ron*5-RON13-4myc (5565 bp) was PCR-amplified with the pair of primers 8263/8264 using the FastPangea polymerase (Canvax), and subconed in the SP3-toxofilin-BLA vector previously digested with SfoI and HindIII. The resulting construct was sequence verified and transfected in RH parasites. Transgenic parasites were selected by addition of hypoxanthine and mycophenolic acid.

Parasite culture. Tachyzoites from parental and modified strains were propagated in confluent human foreskin fibroblasts (HFFs) with Dulbecco modified Eagle's medium supplemented with 5% fetal bovine serum, 2 mM glutamine, and 25 µg/mL gentamicin. To generate transgenic parasites, 20 µg of linearized plasmid or of PCR product were transfected with a mix of 15 µg Cas9-sgRNA plasmid. Transgenic parasites were selected by addition of mycophenolic acid (25 µg/mL) and xanthine (50 µg/mL) exploiting the HXGPRT selection cassette, 1 µM of pyrimethamine for the DHFR selection cassette, and 5 µM of FUDR for the negative selection at the UPRT locus. Clones were isolated by limiting dilution or FACS and checked for proper integration by immunofluorescence (Supplementary Table 6), western blotting (Supplementary Table 6), and PCR on genomic DNA (Supplementary Table 5) using the GoTaq polymerase (Promega). ATc treatment were done for 48 h at 1 µg/mL. For treatment with 49c, infection was performed in the presence of 1 µM of 49c and parasites were collected 48 h post infection.

Western blotting. Freshly egressed tachyzoites were pelleted by centrifugation, washed with PBS, and resuspended in SDS–PAGE buffer (50 mM Tris-HCl, pH 6.8, 10% glycerol, 2 mM EDTA, 2% SDS, 0.05% bromophenol blue, and 100 mM dithiothreitol (DTT)). After boiling and sonication, samples were subjected to SDS–PAGE under reducing conditions. Proteins were transferred to nitrocellulose membrane and immunoblot analysis was performed. Primary antibodies (Supplementary Table 6) were diluted in 5% milk/0.05% Tween-20/PBS. Secondary antibodies coupled with HRP were purchased from Invitrogen® and were used according to manufacturer information. All western blots were done in triplicate. Uncropped and unprocessed western blot can be found in the Source data file of this manuscript.

Immunoprecipitation of RON4 and analysis by mass spectrometry. Freshly egressed parasites RH and RON13-KD from a 10 cm dish were centrifuged, rinsed in PBS, and lysed in PBS-1%Triton X-100 in the presence of protease and phosphatase inhibitors (PhosSTOP™, Roche®, and A32965, ThermoFisher®). Following five cycles of freeze/thaw, the lysate was sonicated, incubated 10 min on ice, and the soluble fraction was incubated with 10× concentrated supernatant containing RON4 mAb 4H1 overnight. The next day protein A-sepharose equilibrated in IP buffer was added and the incubation was continued for 1–2 h at 4 °C. Beads were then washed three times in IP buffer, two times in PBS, resuspended in SDS–PAGE sample buffer, and boiled. Sample were then loaded on a polyacrylamide gel and directly upon entry in the separating gel, migration was stopped and bands were cut, and submitted to the Proteomic Core Facility, Faculty of Medicine, Geneva.

To prepare the samples, bands of interest were digested as follow: gel pieces were destained by incubation in 100 µL of 50% acetonitrile (AcN) in 50 mM ammonium bicarbonate (AB) for 15 min at room temperature. Proteins were reduced by incubation of gel pieces for 30 min at 50 °C in 100 µL of 10 mM DTT in 50 mM AB. DTT solution was then replaced by 100 µL of 55 mM iodoacetamide in 50 mM AB, and protein were alkylated by incubation of the gel pieces for 30 min at 37 °C in the dark. Gel pieces were then washed for 15 min with 100 µL of 50 mM AB and for 15 min with 100 µL of 100% AcN. Gel pieces were then air dried for 15 min at room temperature. Dried pieces of gel were rehydrated for 45 min at 4 °C in 35 µL of a solution of 50 mM AB containing trypsin at 10 ng/µL and 0.01% of Protease Max Surfactant trypsin enhancer (Promega). Subsequently, 10 µL of 0.01% of Protease Max in 50 mM AB was added before incubating the samples for 1 h at 50 °C. Supernatant was transferred to a new polypropylene tube and an additional peptide extraction was performed with 70 µL of 20% FA for 15 min at room temperature with occasional shaking. Extractions were pooled, completely dried under speed vacuum, and stored at −20 °C.

For ESI-LC-MSMS, samples were diluted in 15 µL of loading buffer (5% CH_3CN and 0.1% FA) and 2 µL were injected on column. LC-ESI-MS/MS was performed on a Q-Exactive Plus Hybrid Quadrupole-Orbitrap Mass Spectrometer (Thermo Fisher Scientific) equipped with an Easy nLC 1000 liquid chromatography system (Thermo Fisher Scientific). Peptides were trapped on a Acclaim pepmap100, C18, 3 µm, 75 µm × 20 mm nano trap column (Thermo Fisher Scientific) and separated on a 75 µm × 250 mm, C18, 2 µm, 100 Å Easy-Spray column (Thermo Fisher Scientific). The analytical separation was run for 90 min using a gradient of H_2O/0.1% formic acid (solvent A) and CH_3CN/0.1% formic acid (solvent B). The gradient was run as follows: 0–5 min 95% A and 5% B,

then to 65% A and 35% B for 60 min, then to 10% A and 90% B for 10 min, and finally stay 15 min at 10% A and 90% B. Flow rate was of 250 nL/min for a total run time of 90 min. For MS survey scans, the resolution was set to 70,000 and the ion population was set to 3 × 106 with an *m/z* window from 400 to 2000. For data-dependant analysis, up to 15 precursor ions were isolated and fragmented by higher-energy collisional dissociation HCD at 27% normalized collision energy (NCE). For MS/MS detection, the resolution was set to 17,500, the ion population was set to 1 × 105 with an isolation width of 1.6 *m/z* units. Peak lists (MGF file format) were generated from raw data using the MSConvert conversion tool from ProteoWizard. The peaklist files were searched against the ToxoDB_Tgondii_GT1 database (http://ToxoDB.org, release 42, 8460 entries) combined with an in-house database of common contaminant using Mascot (Matrix Science, London, UK; version 2.5.1). Trypsin was selected as the enzyme, with one potential missed cleavage. Precursor ion tolerance was set to 10 p.p.m. and fragment ion tolerance to 0.02 Da. Carbamidomethyl of cysteine was specified as fixed modification. Deamidation of asparagine and glutamine, and oxidation of methionine were specified as variable modifications. The Mascot search was validated using Scaffold 4.9.0 (Proteome Software). Peptide identifications were accepted if they could be established at >5.0% probability to achieve an false discovery rate (FDR) < 0.1% by the Peptide Prophet algorithm[34] with Scaffold delta-mass correction. Protein identifications were accepted if they could be established at >26.0% probability to achieve an FDR < 1.0 % and contained at least two identified peptides. Protein probabilities were assigned by the Protein Prophet algorithm[35]. Proteins that contained similar peptides and could not be differentiated based on MS/MS analysis alone were grouped to satisfy the principles of parsimony. The mass spectrometry proteomics data have been deposited to the ProteomeXchange Consortium via the PRIDE[36] partner repository with the dataset identifier PXD021516.

Plaque assay. Confluent HFF monolayers were inoculated with freshly egressed parasites in absence or presence of ATc. Seven days post infection, the infected cells were fixed with 4% paraformaldehyde (PFA) and stained with a crystal violet (Sigma). Lysis plaque area were quantified using ImageJ software (NIH, version 1.53c). Ten lysis plaque were quantified for each strain in each replicate. Quantification represents the mean (±SD) from three independent experiments. Statistical significance was assessed by one-way ANOVA significance test with Tukey's multiple comparison on GraphPad Prism 8 software.

Intracellular growth assay. Freshly egressed parasites pretreated ±ATc for 24 h were used to infect new confluent HFF on glass coverslips. Cells were fixed 24 h post infection and parasite were visualized using anti-GAP45 antibodies by IFA. For each condition, at least 200 vacuoles were counted. Experiments were performed in three independent replicates. Results are presented as mean ± SD. Two-way ANOVA followed by Tukey's multiple comparison was used to test differences between groups on GraphPad Prism 8 software.

Egress assay. Freshly egressed parasites pretreated ±ATc for 12 h were used to infect new confluent HFF on glass coverslips. Cells were fixed 30 h post infection and parasite boundaries were visualized using anti-GAP45 antibodies by IFA. At least 200 vacuoles were counted. Results are presented as mean ± SD and the experiment performed in three independent replicates. Two-way ANOVA followed by Tukey's multiple comparison was used to test differences between groups on GraphPad Prism 8 software.

Microneme secretion. Freshly egressed RH and RON13-KD parasites were resuspend in harvested and resuspended in intracellular buffer (5 mM NaCl, 142 mM KCl, 1 mM $MgCl_2$, 2 mM EGTA, 5.6 mM glucose, and 25 mM HEPES, pH 7.5) ± ethanol 2%. After an incubation for 30 min at 37 °C, parasites were pelleted and washed once with PBS, while the supernatant was cleared again by a second centrifugation. Pellet and supernatant (excreted–secreted antigens—ESA) were resuspend in sample buffer before boiling and immunoblotting. MIC2 secretion and processing was assessed by western blotting. GRA1 is used as a marker for constitutive secretion and catalase as a positive control of parasite lysis. This experiment as done in triplicate.

Rhoptry secretion by e-vacuole assay. Freshly egressed parasites were washed once with PBS, resuspended in prechilled egress buffer containing 1 µM cytochalasin D, and incubated 10 min on ice. Then, the parasites were added to prechilled HFFs. After a short centrifugation and 20 min on ice to allow the parasites to settle, HFFs were washed with cold PBS. The PBS was replaced by warm media + cytochalasin D. Rhoptry secretion was triggered by incubating the infected coverslips at 37 °C for 20 min. The coverslips were then fixed with PFA 4%. Approximately 100 parasites were counted in duplicate in three independent experiments. Results are presented as mean ± SD and the statistical analysis was done using one-way ANOVA statistical test on GraphPad Prism 8 software.

Rhoptry secretion by phospho-STAT6. Freshly egressed parasites (5×10^5) pretreated ±ATc for 48 h were used to infect HFF-coated coverslips. Following a short centrifugation (30 s at 1100 × *g*) and an incubation on ice for 20 min, the cells were incubated at 37 °C for 20 min and fixed with ice-cold methanol. After blocking, immune-detection was performed using anti-phospho-STAT6 antibody (Cell signaling 9361; 1/400). The experiments were done in triplicate and >200 host cell nuclei were counted each time. *P* values were calculated using a two-way ANOVA test on GraphPad Prism 8 software. The line represents the median and the whiskers represent the min to max values from 30 fields.

Red/green invasion assay. Freshly egressed parasites were allowed to invade a HFF for 30 min before fixing with PAF/Glu for 7 min. A first immune-detection using anti-SAG1 antibodies on non-permeabilized cells was performed. Cells were then fixed with 1% formaldehyde/PBS for 7 min, washed with PBS, and permeabilized using 0.2% Triton X-100/PBS. Parasites were labeled using anti-GAP45 antibodies. At least 100 parasites were counted in duplicate for each strain in three independent experiments. Results are presented as mean ± SD, and the statistical analysis was done using one-way ANOVA followed by Tukey's multiple comparisons on GraphPad Prism 8 software.

In/out assay and moving junction formation. Freshly egressed parasites were resuspended in cold DMEM and added to prechilled HFF monolayer on a glass coverslip. Following a quick centrifugation (30 s at 500 × *g*) and an incubation of 20 min on ice, the culture was incubated at 38 °C for 3 min in a water bath and fixed with PFA for 15 min. A first indirect immuno-detection using anti-SAG1 antibodies, and secondary antibodies was done followed by another fixation step with 1% formaldehyde/PBS for 7 min and permeabilization with 0.025% saponin for 10 min. After blocking, a second immuno-detection with anti-RON2, or anti-RON4 or anti-RON8 antibodies was performed. Finally, cells were permeabilized with 0.2%Triton X-100/PBS and stained with anti-GAP45 or anti-actin antibodies. Extracellular parasites (SAG1+/GAP45+), in/out (half SAG1+/GAP45+; half GAP45+), and intracellular parasites (GAP45+) were quantified. RON2 and RON4 staining at the MJ was examined for at least 100 parasites. Values represent means ± SD, from three independent assays. *P* values reported are from two-way ANOVA statistical analysis followed by Tukey's multiple comparison on GraphPad Prism 8 software.

ALIX recruitment. The recruitment of ALIX at the MJ was assessed by quantifying ALIX-positive staining at the site of invasion[5]. HeLa cells (0.8×10^5) were seeded on glass coverslips and transfected after 24 h with 500 ng of ALIX-GFP plasmid (kind gift from Dr. M. Lebrun) using lipofectamine 2000® (ThermoFisher), according to the manufacturer's protocol. The following day, in/out assays were performed and cells were fixed with methanol and processed for IFA using anti-GFP and anti-GAP45 antibodies. ALIX recruitment was assessed over 50 invading parasites. Results are presented as mean ± SD of three independent replicates. *P* values reported are from two-way ANOVA statistical analysis followed by Tukey's multiple comparison. Pixel intensity at the site of ALIX recruitment was normalized to the background fluorescence in the HeLa cytoplasm. The pixel intensity of thirty ALIX dots were quantified per experiment and results are presented as mean ± SD of three independent replicates. *P* values reported are from two-way ANOVA statistical analysis followed by Tukey's multiple comparison on GraphPad Prism 8 software.

Topology. To assess RON13 topology, we used GFP nanobodies (kind gift from Clare Harding)[37]. Briefly, 2×10^6 RH (negative control), ARO-YFP, and RON11-YFP (positive controls) and RON13-YFP parasites were transiently transfected with 30 µg of mCherry-GFP nanobodies-DD plasmid and used to infect an HFF monolayer. The day after, 1 µM of Shield was added to the infected cells for 1 h prior to methanol fixation and immunofluorescence assay using anti-myc and anti-GFP antibodies. This experiment was done in triplicate.

Solubility test. To assess the solubility of RON13, extracellular parasites ASP3-iKD/RON13-3Ty from culture pretreated ±ATc for 48 h, were pelleted and resuspended in PBS or PBS-2% TX-100. Samples were lysed by freeze-thawing and incubated at 37 °C. The pellet and the soluble fraction were separated by centrifugation for 30 min at 4 °C max and 15,000 × *g*. Samples were finally resuspended with SDS–PAGE loading buffer (±10 mM DTT) and heated at 95 °C for 10 min prior to separation. This experiment was done in triplicate.

Beta-lactamase assay. The activity of the beta-lactamase fusion proteins was assessed on extracellular parasites. Extracellular parasites from RH, toxofilin-BLA, and RON13-BLA strains were washed twice in PBS and incubated with the BLA substrate CCF4-AM (Thermo Fisher Scientific) or DMSO (control) in DMEM, 5% FCS for 2 h in the dark at room temperature, according to manufacturer's protocol. Following two washes in PBS, extracellular parasites were distributed in a 96-well plate and the fluorescence at 450 and 550 nm (excitation 405 nm) was read on a SpectraMax Paradigm reader (Molecular Devices,LLC) at the READS platform of the University of Geneva. The experiment was performed in three independent experiments. The relative fluorescence was obtained by subtracting the background fluorescence (DMSO wells) to the absolute fluorescence (CCF4-AM wells).

Analysis of rhoptry protein secretion into the host cell was assessed by flow cytometry by detection of beta-lactamase activity in the host cell[16]. HFF monolayers were infected with extracellular parasites from RH, toxofilin-BLA, and RON13-BLA parasites at a MOI of 30. After 1 h, cells were washed and incubated with the BLA substrate CCF4-AM (Thermo Fisher Scientific) or DMSO (control) for 2 h in the dark at room temperature. Cells were washed three times with PBS, trypsinised and analyzed by flow cytometry on a Gallios flow cytometer (Beckman Coulter) at the flow cytometry platform (University of Geneva, Switzerland). Samples were excited at 405 nm and coumarin and fluorescein were detected with the 450/50 nm laser and the 550/40 nm laser, respectively. FlowJo (Becton, Dickinson & Company) and Kaluza (Beckman Coulter) softwares were used for analysis. Graphs were made using GaphPad Prism 8 and represent means ± SD from three independent assays. Statistical significance was assessed by a paired *t* test.

Kinetic assay measuring host cell impedance. Host cell damage following infection was assessed by the Live Cell Analysis System xCELLigence (OLS®) that measure cellular impedance in a kinetic assay and collected on the RTCA software (Agilent, version 1.0). HFF (5×10^4 cells) were seeded in an eight-well E-plate and cellular impedance was measured every 30 min during 24 h. The next day, medium was renewed 2 h prior infection. HFF were infected with 5×10^5 freshly egressed parasites, the plate was centrifuged 1 min at $2500 \times g$ and put back in the xCELLigence. Extracellular parasites were washed away 30 min post infection and cellular impedance was measured every 30 min during 60 h. Data were normalized according to the cellular impedance at the time of the last wash, and expressed as a percentage of the impedance measured for uninfected wells overtime. Three independent experiments were done in duplicate.

Animal experimentation. Virulence assays were performed by intraperitoneal injection of 100 freshly lysed tachyzoites (RH and mutant strains) in 7-week-old female CD1 mice (Charles River). Mice were monitored daily and sacrificed at the onset of signs of acute infection (ruffled fur, difficulty moving, and isolation). Surviving mice were assessed for seroconversion by Western blotting, as well as challenged with an inoculation with 1000 freshly lysed RH tachyzoites at 84 days post infection. Surviving mice were humanely sacrificed at the end of the experiment, ~40 days after the challenge infection.

Ethics statement. All animal experiments were conducted with the authorization numbers GE121-19, according to the guidelines and regulations issued by the Swiss Federal Veterinary Office. All animals were housed at the University of Geneva in room with day/night cycle of 12 h/12 h and constant ambient temperature of 22 °C and 35% humidity, respectively.

Transmission electron microscopy (TEM). Infected HFF cells grown on a round glass coverslips were fixed with 2.5% glutaraldehyde (Electron Microscopy Sciences) and 2% PFA (Electron Microscopy Sciences) in 0.1 M sodium cacodylate buffer at pH 7.4 for 1 h at room temperature. Traces of fixative were removed by extensive washing with 0.1 M sodium cacodylate buffer, pH 7.4, and postfixed with reduced 1% osmium tetroxide (Electron Microscopy Sciences) with 1.5% potassium ferrocyanide in 0.1 M sodium cacodylate buffer, pH 7.4 for 1 h and immediately followed by 1% osmium tetroxide alone (Electron Microscopy Sciences) in the same buffer for 1 h. After two washes in double-distilled water (ddH_20) for 5 min each wash samples were en bloc stained with aqueous 1% uranyl acetate (Electron Microscopy Sciences) for 1 h or overnight at 4 °C. After a 5 min wash in ddH_20, cells were dehydrated in graded ethanol series (2× 50, 70, 90, 95%, and 2× absolute ethanol) for 10 min each wash and infiltrated with graded series of Durcupan resin (Electron Microscopy Sciences) diluted with ethanol at 1:2, 1:1, and 2:1 for 30 min each. Next, cells were infiltrated twice with pure Durcupan for 30 min each and with fresh Durcupan resin for additional 2 h. Finally, coverslips with cells facing down, were placed on 1 mm thick teflon rings filled with resin and placed on glass slide coated with mold separating agent (Glorex) and polymerized in the oven at 65 °C for 24 h. The glass coverslip was removed from the cured resin disk by alternate immersion into hot (60 °C) water and liquid nitrogen, until the glass parted. Laser microdissection microscope (Leica Microsystems) was used to select suitable areas and to outline their positions on the resin surface to cut out from the disk using a single-edged razor blade and glued with superglue (Ted Pella) to a blank resin block. The cutting face was trimmed using a Leica Ultracut UCT microtome (Leica Microsystems) and a glass knife. A 70 nm ultrathin serial sections were cut with a diamond knife (DiATOME) and collected onto 2 mm single slot copper grids (Synaptec, Ted Pella) coated with Formvar plastic support film.

Sections were examined using a Tecnai 20 TEM (FEI) operating at an acceleration voltage of 80 kV and equipped with a side-mounted MegaView III CCD camera (Olympus Soft-Imaging Systems) controlled by iTEM acquisition software (Olympus Soft-Imaging Systems).

FIB-SEM and 3D reconstruction. Sample for FIB-SEM imaging were prepared in the same way as for the TEM. Selected parasitophorous vacuoles were marked on the surface of the resin block by laser microdissection microscope (Leica Microsystems). Either whole resin block or large cut out area containing the region of interest was glued onto a flat SEM stub with superglue, and silver conductive paste was applied on each side of the resin block to ensure the conductivity within SEM. Finally, the mounted sample was gold coated with 20 nm thick layer of gold.

The samples were imaged inside a FEI Helios NanoLab G3 UC DualBeam microscope (FEI). Ion beam was used in conjunction with a gas injection system to deposit a thick (~1.5 µm) layer of platinum on the top surface of the sample above the region of interest to reduce the FIB milling artefacts. The imaging surface was exposed by creating the front trench using 21 nA of focused ion beam current at 30 kV voltage and subsequently two side trenches were created using the same parameters. AutoSlice and View G3 software (FEI) was used to acquire the serial SEM images. Focused ion beam at current of 2.5 pA and 30 kV of acceleration voltage was applied to mill 10 nm layer from imaging face, and freshly exposed surface was imaged with back scattered electron beam at current of 400 pA and at acceleration voltage of 2 kV, the dwell time of 9 µs/pixel and at the resolution of 4 nm/pixel. Serial images were combined into single image stack, aligned, and scaled down to obtain imaged volume with isotropic pixel properties of the 10 nm/pixel in all *x*-, *y*-, and *z*-dimension using the FIJI program (fiji.sc/). Semiautomated approach using Ilastik software (ilastik.org) was used for segmentation and 3D reconstruction. Final 3D models were visualized using the Blender software (v.2.79; blender.org).

Image acquisition. Confocal images were acquired with a confocal laser scanning microscope LSM700 (Zeiss) and confocal expansion microscopy images were collected with a TCS SP8 STED ×3 microscope (Leica) at the Bioimaging Core Facility of the University of Geneva Medicine Faculty. Image processing for expansion microscopy was performed using LasX Software (Leica, version 3.7.0), while ImageJ (NIH; version 1.53c) was used otherwise. The antibodies used for immunofluorescence assay and their dilutions are listed in Supplementary Table 6. Secondary antibodies were purchased from Invitrogen® and used according to the manufacturer's protocol.

Ultrastructure expansion microscopy. U-ExM was performed on extracellular parasites[38]. Extracellular parasites were resuspended in PBS and settled on a poly-D-lysine (Gibco) coated 12 mm coverslip. Protein crosslinking was performed by incubating the coverslip in 1.4% formaldehyde/2% acrylamide/PBS solution for 5 h at 37 °C. The monomer solution (19% sodium acrylate (Sigma)/10% acrylamide (Sigma)/0.1% N, N′-methylenbisacrylamide (Sigma)/PBS), as well as the 10% TEMED and 10% APS solutions were thawed on ice. The gelation step was performed on ice as well with the coverslip incubated face down on a drop of 35uL of the gelation solution (90 µL monomer solution + 5 µL TEMED 10% + 5 µL APS 10%) in a humid chamber for 5 min followed by an incubation at 37 °C for 1 h. The gel and coverslip were then transferred to six-well plate filled with denaturation buffer (200 mM SDS, 200 mM NaCl, and 50 mM Tris pH 9.0) face up for 15 min at room temperature under agitation. When the gel detached from the coverslip, it was transferred into a Eppendorf filled with denaturation buffer and incubated at 95 °C for 1.5 h. A first round of expansion was performed by incubating the gel three times in ddH_20 for 30 min. Prior incubation with the primary antibodies diluted in Tween 0.1%/PBS for 3 h at 37 °C, two rounds of gel shrinkage were performed by replacing the ddH_2O with PBS for 15 min. Following three washes of 10 min each in Tween 0.1% / PBS, secondary antibody detection was performed. A last round of expansion was done by incubating the gel for 30 min twice in ddH_2O and then overnight. For imaging, pieces of gel were put on poly-D-lysine (Gibco) coated 24 mm coverslip with sample facing down clipped on 35 mm round adapters (Okolab). Images were acquired on a Leica Thunder inverted microscope using 63× 1.4 NA oil objective with Small Volume Computational Clearing mode to obtained deconvolved images. 3D stacks were acquired. Images were analyzed and merged using LasX software (Leica).

The antibodies used and the appropriate dilution are mentioned in Supplementary Table 6.

Phylogeny. Sequences of Apicomplexan kinases were procured from EuPathDB and aligned using MUSCLE sequence alignment software (version 3.8.31)[39]. The resulting sequence alignment was manually curated utilizing BioEdit (http://www.mbio.ncsu.edu/bioedit/bioedit.html) to edit out uninformative alignment positions. Phylogeny tree was generating utilizing PhyML (version 3.0)[40] on the curated MUSCLE alignment. The curated alignment of sequences used in the phylogenetic analysis can be found in Supplementary Data 8.

RON13 purification for antibody generation. The RON13 kinase domain (163–769) was inserted into a pGEX-modified vector to contain a N-terminal His10-tag followed by a tobacco etch virus (TEV) protease recognition site (Gibson; digested with NotI/KpnI). The plasmid was transformed into Rosetta DE3 pLysS cells and cultures were grown until reaching an OD600 of 0.6. Protein production was induced by adding IPTG to a final concentration of 0.5 mM and left to incubate for 4 h at 37 °C. Cells were then harvested by centrifugation at $4000 \times g$ for 15 min and the pellet was frozen at −80 °C. The pellet from 1 L of cells was resuspended in 25 mL of bacteria lysis buffer (50 mM Tris pH 8, 400 mM NaCl, 15 mM imidazole, 0.05 % Triton X-100, 8 M urea, and 3 mM beta-mercaptoethnol (2-ME)). Cells were lysed by two passages through a French

Pressure Cell at 1000 p.s.i. Cell membranes and debris were removed by centrifugation at 35,000 × *g* for 30 min at 4 °C. The supernatant containing soluble proteins was applied to a 5 mL His-trap FF column (GE healthcare), washed with 50 mL of lysis B buffer, followed by a second washing step using bacteria Ni-A buffer (15 mM Tris pH 8, 200 mM NaCl, 15 mM imidazole, 5 M urea, and 3 mM 2-ME). Protein was then eluted using bacteria Ni-A buffer supplemented with 430 mM imidazole. Eluted proteins were concentrated to 1 mg/mL using AMICON 30 MWCO concentrators and used as antigens for antibodies generation at the Geneva Antibody Facility (University of Geneva, Switzerland).

ASP3 purification from insect cells. Recombinant ASP3 protease was expressed in baculovirus-infected Sf9 insect cells. Baculovirus were generated using a modified pFastBac vector encoding a N-terminal Melittin secretion signal, followed by ASP3 protease (TGME49_ 246550, amino acids 38–643) and a C-terminal His6 tag. Cells infected for 68 h were harvested by centrifugation at 4000 × *g* for 15 min at 4 °C. The pellet was dissolved in Asp3 lysis buffer (50 mM Tris-HCl pH 8, 500 mM NaCl, 10 mM imidazole, 0.1% Triton X-100, and 3 mM 2-ME) and lysed by one passage through a French Pressure Cell at 1500 p.s.i. Cell membranes and debris were removed by centrifugation of the lysate at 35,000 × *g* for 35 min at 4 °C. The supernatant containing soluble protein was applied to a 5 mL His-trap column (GE healthcare), washed with 40 mL of Asp3 lysis buffer and with 40 mL of Asp3 Ni-A buffer (20 mM Tris pH 8, 150 mM NaCl, 15 mM imidazole, and 3 mM 2-ME). Protein was eluted with 15 mL of Asp3 Ni-B buffer (20 mM Tris pH 8, 150 mM NaCl, 350 mM imidazole, and 3 mM 2-ME). Eluted protein was diluted fivefold with Asp3 Q-A buffer (20 mM Tris pH 8, 10 mM NaCl, and 3 mM 2-ME) and loaded to a 5 mL Q-HP column (GE healthcare). The protein was eluted by applying a gradient from 10 to 30% Asp3 Q-B buffer (20 mM Tris pH 8, 1 M NaCl, and 3 mM 2-ME) in 40 mL. Fractions containing ASP3 protein were pooled, concentrated to 1 mL using AMICON 30 MWCO concentrators, and loaded on a size-exclusion Superdex 200 10/300 column at 4 °C equilibrated in Asp3 final buffer (50 mM Hepes pH 7.4/150 mM KCl, 5% glycerol, and 1 mM DTT). Fractions containing pure ASP3 were pooled, concentrated to 1 mg/mL and flash frozen in liquid nitrogen.

Recombinant RON13 purification. All RON13 constructs and mutants used for structural and biochemical studies were expressed in insect cells and purified, following the same procedure. RON13 coding sequence (amino acids 271–1375) was inserted into a modified pFastBac vector encoding a N-terminal Melittin secretion signal, a GST-tag and a TEV recognition site preceding RON13, and a C-terminal 10-His tag. Proteins were expressed in baculovirus-infected Sf9 cells for 66 h at 27 °C before cell harvesting and purification. The pellet from 1 L of cells was resuspended in 60 mL of Sf9 lysis buffer (50 mM Tris-HCl pH 7.5, 300 mM NaCl, 5 mM EDTA, and 3 mM 2-ME) containing protease inhibitors and lysed by one passage through a French Pressure Cell at 1500 p.s.i. Cell membranes and debris were removed by centrifugation at 35,000 × *g* for 30 min at 4 °C and soluble proteins were applied to 5 mL (bed volume) of gluthatione-agarose resin equilibrated in Sf9 lysis buffer. The sample was incubated for 4 h at 4 °C on a roller, then transferred to a gravity purification column to remove unbound material. The resin was washed with 50 mL of Sf9 lysis buffer followed by another 50 mL wash with Sf9 wash buffer (20 mM Tris pH 7.5, 100 mM NaCl, 0.5 mM EDTA, and 3 mM 2-ME). On-resin digestion was performed to elute the untagged RON13 protein from the resin. For this, 400 µg of pure TEV protease was diluted in 5 mL of Sf9 wash buffer and applied to the resin. After 2 h incubation at 22 °C, the digested protein was eluted by applying twice 7 mL of Sf9 wash buffer. The TEV protease was separated from RON13 using an anion-exchange column. Proteins eluted were concentrated to 3 mL using AMICON 30 MWCO concentrators, diluted fourfold with a 100 mM Tris-HCl pH 8 solution, and passed through a 1 mL Q-XL column (GE healthcare). The unbound material, containing RON13, was concentrated to 1 mL using AMICON 30 MWCO concentrator and loaded on a Superdex 200 10/300 size-exclusion chromatography column equilibrated in Sf9 final buffer (5 mM Tris-HCl pH 7.5/200 mM NaCl/0.5 mM EDTA/3 mM DTT). Fractions containing pure RON13 protein, eluting ~13 mL, were pooled, concentrated, and flash frozen in liquid nitrogen before storage at −80 °C.

Recombinant dephosphorylated RON4 purification. RON4 FL (gene TGGT1_229010 product, residues 27–984) purification was performed using Ni^{2+} metal affinity purification[5]. Sequence of RON4 (27–984) with a C-terminal His_6 tag was inserted into a modified pFastBac vector encoding a N-terminal gp67 secretion signal. Baculoviruses encoding RON4 protein were generated following standard procedures. Briefly, a pellet of Sf9 cells infected for 70 h was resuspended in lysis buffer 4 (50 mM Tris pH 8, 500 mM NaCl, 20 mM imidazole, and 3 mM 2-ME), lysed by shear forces at 15,000 p.s.i. using a Microfluidizer instrument. Cell membranes and debris were removed by centrifugation at 35,000 × *g* for 30 min at 4 °C, and soluble proteins were passed through a 5 mL His-trap FF column, washed with 50 mL of lysis buffer 4, and eluted with 15 mL of lysis buffer 4 supplemented with 350 mM imidazole. The protein was dephosphorylated using 400 units of alkaline phosphatase (CIAP, Promega # M1821A, 1 U/µL) in a buffer supplemented with 10 mM $MgCl_2$ prior to running a Superdex 200 size-exclusion chromatography step equilibrated in SEC buffer 4 (25 mM Tris pH 7.5, 150 mM NaCl, and 0.5 mM EDTA) to separate RON4 protein from the phosphatase.

Radioactive kinase assays. RON13 in vitro kinase activity was measured by looking at the transfer of γ-32P from ATP to substrate proteins. Reactions were run in 15 µL volume with a final RON13 concentration of 50 nM in kinase reaction buffer (20 mM Tris pH 7.5/50 mM NaCl/0.5 mM EDTA/0.5 mM EGTA). Reactions were supplemented with 6 mM of metal ion cofactor ($MgCl_2$ for Mg^{2+}, $CaCl_2$ for Ca^{2+}, and $MnCl_2$ for Mn^{2+}). Substrates were used at a final 1.5 µM concentration (MBP, dephosphorylated, Millipore #13-110). Reactions were initiated by the addition of tenfold concentrated ATP (100 µM final) containing 5 µCi of ATP-γ −32P. Reactions were run for 5 min at 37 °C. Phosphotransfer activity was monitored by analyzing 5 µL of reaction sample on a SDS–PAGE and the amount of protein phosphorylation was determined by exposing the gel to a X-ray sensitive plate. ATPase activity was measured by spotting 1 µL of reaction onto a TLC plate. ATP was separated from free phosphate by migrating the silica plate using a solution of 1 N formic acid/0.5 N LiCl as eluent. Exposure to an X-ray sensitive plate was used to measured radioactive 32P on a Typhoon instrument (GE healthcare). Experiments were done in triplicate.

Hydrogen/deuterium exchange coupled to mass spectrometry. HDX-MS experiments were performed at the UniGe Protein Platform (University of Geneva, Switzerland) following a well-established protocol with minimal modifications[41]. HDX reactions were done in 50 µL volumes using 60 pmol (1.3 µM) of rRON13dk and a threefold molar excess of recombinant RON4. Briefly, rRON13dk was pre-incubated with buffer (RON13-alone) or RON4 on ice in a final volume of 7.7 µL. The mix was then left to equilibrate at the room temperature for 10 min. Deuterium exchange reactions were initiated by adding 42.3 µL of D2O exchange buffer (96% D2O, 10 mM HEPES pH 7.5, 100 mM NaCl, and 0.5 mM EDTA) to the rRON13 protein mixture. Reactions were carried-out for 3, 30, and 300 s at room temperature, and terminated by the sequential addition of 20 µL of ice-cold quenching buffer 1 (6 M urea/0.1 M NaH_2PO_4 pH 2.5/1% formic acid). Samples were immediately frozen in liquid nitrogen and stored at −80 °C for up to 4 weeks. All experiments were repeated in triplicates.

To quantify deuterium uptake, protein samples were thawed and injected in UPLC system immersed in ice. The protein was digested via two immobilized pepsin columns (Thermo #23131), and peptides were collected onto a VanGuard pre-column trap (Waters). The trap was subsequently eluted and peptides separated with a C18, 300 Å, 1.7 µm particle size Fortis Bio column 100 × 2.1 mm over a gradient of 8–30% buffer B over 20 min at 150 µL/min (buffer A: 0.1% formic acid; buffer B: 100% AcN). Mass spectra were acquired on an Orbitrap Velos Pro (Thermoscientific), for ions from 400 to 2200 *m/z* using an electrospray ionization (ESI) source operated at 300 °C, 5 kV of ion spray voltage. Peptides identified by data-dependent acquisition after MS/MS and data were analyzed by Mascot. A 94% sequence coverage was obtained. Deuterium incorporation levels were quantified using HD examiner software version 1.4 (Sierra Analytics), and quality of every peptide was checked manually. Results are presented as percentage of theoretical maximal deuteration level and can be compared to a highly-deuterated sample that was prepared by incubating the protein for 1 h in 1 M guanidinium-HCl before incubation for 2 h in deuterated buffer. All experimental details and data of percentage deuterium incorporation for all peptides can be found in Supplementary Table 3 and Supplementary Data 6. The HDX-MS data have been deposited on the ProteomeXchange Consortium via the PRIDE[42] partner repository with the dataset identifier PXD023791.

Cryo-EM sample preparation and data collection. The purified RON13-KD was concentrated (15 mg/mL) and immediately used for cryo-EM grid preparation. For cryo-EM sample preparation, Quantifoil 1.2/1.3 200-mesh grids were glow discharged using a PELCO easiGlow (Ted Pella) for 30 s at 25 mA in air. An aliquot of the protein (3.5 µL) was deposited on the surface of the grid immediately before blotting for 3 s on a Vitrobot Mark IV (FEI) operating at 4 °C with 100% humidity (blot force 0) and plunging the grid into liquid ethane. The grids were transferred into liquid nitrogen for storage until the day of cryo-EM data collection. A cryo-EM dataset was collected at using Titan Krios microscope equipped with a Gatan K2 Summit detector and an energy filter at ETH Zurich (ScopeM). The dataset was collected in counting mode using EPU, at a magnification of 165,000×, corresponding to a pixel size 0.8544 Å/pix. The exposure was 8 s over 40 frames, with a total dose of 47 $e^{-}/Å^2$.

Cryo-EM data analysis. Motion correction and alignment of the cryo-EM movies was performed using MotionCor2 (UCSF; version 1.3.0)[43]; the defocus of the aligned micrographs was estimated using Gctf (version 1.06)[44]. The images with an estimated resolution higher than 4.5 Å (4782 micrographs) were used in the further processing steps; all subsequent steps were performed in relion-3.0 (refs. [45,46]). Manual particle picking and 2D classification of a small subset of particles (732) was used to generate four autopicking templates. In total 1,385,124 particles were autopicked and extracted from the selected micrographs (downsampled to 2.56 Å/pix in a 100 pix box). Two rounds of 2D classification produced 2D classes with clearly visible secondary structure elements (711,852 particles). An initial model

generated using this particle selection in relion-3.0 was used for 3D classification. A round of 3D classification with four classes ($T = 4$, $E = 8$, mask 190 Å) produced a single class (348,152 particles) was followed by a round of masked 3D classification without alignment ($T = 4$, $E = -1$) generating a 3D class used for further processing (320,723 particles). The particles constituting this 3D class were used in 3D refinement (3.4 Å resolution, FSC cutoff 0.143). Further CTF refinement and Bayesian particle polishing, followed by 3D refinement and a post-processing step (applying a *b*-factor of −85.7 estimated in relion-3.0), produced the final map 3.1 Å resolution. The local resolution of the map was estimated in relion-3.0. The anisotropy of the cryo-EM map was assessed using the 3DFSC server[47]. Slight anisotropy was detected (Supplementary Fig. 4i), without a substantial effect on the quality of the density map (global resolution reported by 3DFSC is 3.09 Å, consistent with the results of Relion processing). The complete cryo-EM data analysis procedure is illustrated in Supplementary Fig. 4.

Model building and validation. An initial round of autobuilding was performed using phenix.map_to_model (Phenix 1.16-3549)[48]. All subsequent model building steps were performed in Coot (version 0.9.5)[49] using the 3.1 Å post-processed map. The atomic model of RON13-KD was refined using phenix.real_space_refine in Phenix (version 1.16-3549). For model validation, the atom coordinates in the refined model were randomLy displaced by a 0.5 Å using the PDB tools in Phenix and the derived model was subjected to real space refinement using one of the refined half maps (half-map1). Map versus model FSC comparison was made for the model against the corresponding half-map1 used in the refinement job, and for the same model versus the half-map2 (not used during refinement)[50]. The geometry of the model was validated using MolProbity (version 4.5.1)[51]. Figure panels featuring the density maps and structural models were prepared using PyMol (DeLano Scientific LLC, version 4.2.4)[52] and UCSF Chimera[53] (UCSF; version 1.13.1).

Phosphoproteome sample preparation. *T. gondii* tachyzoites were cultured using HFFs as host cells. After 48 h, the supernatant was removed and syringe homogenized prior to differential centrifugation at 200 × *g* for 5 min to pellet host cells. The supernatant containing extracellular parasites was filtered to remove cell debris and the parasites were washed five times in PBS containing protease inhibitors. Samples were prepared for each strain from four independent experiments. Proteins were extracted from tachyzoites in 4% SDS/0.1 M DTT/100 mM Tris-Cl pH 8.2 first by boiling at 95 °C for 5–10 min and following by at least one round of exposure to high-intensity focused ultrasound for 1 min at 100% amplitude and 80% duty cycle. Insoluble material was pelleted by high-speed centrifugation and 190–300 µg of proteins in 60 µL of 4% SDS/0.1 M DTT/100 mM Tris-Cl pH 8.2 were further processed using a modified protocol for filter-aided sample preparation[54]. A total of 400 µL of 8 M urea/100 mM Tris-Cl pH 8.2 were added, and the sample was loaded onto a Microcon-30kDa Centrifugal Filter Unit (Merck) and centrifuged at 14,000 × *g* until ~10 µL remained. The sample was washed with 200 µL 8 M urea/100 mM Tris-Cl pH 8.2 and subsequently, 100 µL 50 mM iodoacetamide/8 M urea/100 mM Tris-Cl pH 8.2 was added. The solution was shaken at 600 r.p.m. for 1 min and incubated for 5 min at RT. The sample was spun at 14,000 × *g* and washed three times with 100 µL 8 M urea/100 mM Tris-Cl pH 8.2. The sample was then washed twice with 50 mM of triethylammoniumbicarbonate (TEAB) in H_2O and spun at 14,000 × *g*. A total of 120 µL of trypsin in 50 mM TEAB at 1/50 w/w was added to the sample, mixed at 600 r.p.m. for 1 min, and incubated in a wet chamber overnight. Peptides were collected by centrifugation at 14,000 × *g*, a 5 µL aliquot was removed as input sample and the peptides concentrated by vacuum centrifugation. For the following steps, all the incubation steps were done while shaking at 700 r.p.m. at RT and supernatants removed after bead attachment to a magnet. A 50 µL of Ti-IMAC beads (ReSyn Biosciences) per sample were washed twice with 200 µL 70% ethanol for 5 min, and subsequently once with 100 µL 1% NH_4OH 10 min. Beads were equilibrated three times for 1 min in 50 µL loading buffer (380 mg glycolic acid/5% trifluoroacetic acid (TFA)/80% AcN). Peptides were taken up in 100 µL loading buffer and incubated 20 min. Beads were washed in 100 µL loading buffer for 30 s and washed three times with 100 µL 1% TFA/80% AcN for 2 min, and then twice with 0.2% TFA/10% AcN for 2 min. Phosphopeptides were eluted three times in 80 µL 1% NH_4OH for 15 min. Samples were vacuum dried and resuspended in 15 µL 0.1% formic acid/3% AcN. To the input sample, 10 µL 0.1% formic acid/3% AcN was added.

Reverse phase chromatography and mass spectrometry. For peptide separation by reverse phase chromatography, a Waters ACQUITY UPLC M-Class was used with a 20 mm nanoEase M/Z Symmetry C18 trap column (180 µm inner diameter packed with 5 µm C_{18} silica particles), and a 25 cm nanoEase M/Z HSS C18 T3 column (75 µm inner diameter and packed with 1.8 µm C_{18} silica particles), and analytical column. Total separation time was 75 min over a linear gradient from 5 to 35% solvent B (solvent A: 0.1% formic acid in H_2O, solvent B: 0.1% formic acid in AcN) with a flow rate of 300 nL/min. Separated peptides were directly applied by ESI into an Orbitrap Q-Exactive HF mass spectrometer (Thermo Fisher Scientific). The mass spectrometry was set up in full MS/data-dependent-MS^2 mode. For the full scans, a scan range of 350–1500 *m/z* at a resolution of 120,000 was used with an automatic gain control (AGC) target at 3 × 10e6 and a maximum injection time of 50 ms. The top 20 most intense ions were isolated with a maximum injection time of 119 ms, fragmented with a NCE of 28 and detected at 60,000 resolution with a scan range of 200–2000 *m/z* and an AGC target of 1 × 10e5 (fixed first mass 130 *m/z*).

Phosphoproteome data analysis. Individual data analysis workflows have been used for global protein and phosphopeptide analysis. The statistical analysis was done in a two-group comparison, i.e., RON13-KD versus RH and RON13-KD complemented with WT RON13 versus RON13-KD complemented with inactive RON13. For proteome and phosphoproteome, the acquired raw MS data were processed by MaxQuant (version 1.6.2.3), followed by protein identification using the integrated Andromeda search engine[55]. Spectra were searched against the ToxoDB GT1 protein database (release 44), concatenated to its reversed decoyed fasta database and common protein contaminants. By default, carbamidomethylation of cysteine was set as fixed modification, while methionine oxidation and N-terminal protein acetylation were set as variable. In addition, Phospho(STY) was set as a variable modification. Enzyme specificity was set to trypsin/P allowing a minimal peptide length of seven amino acids and a maximum of two missed-cleavages. For the proteome data, MaxQuant default search settings for Orbitrap were used. The maximum FDR was set to 0.01 for peptides and 0.05 for proteins. Label-free quantification was enabled and a 2 min window for match between runs was applied. In the MaxQuant experimental design, each file is kept separate to obtain individual quantitative values. Protein fold changes were computed based on intensity values reported in the proteinGroups.txt file. A set of functions implemented in the R package SRMService[56,57] was used to filter for proteins with two or more peptides allowing for a maximum of four missing values, normalizing the data with a modified robust *z*-score transformation and computing *P* values using the moderated *t* test with pooled variance (as implemented in the limma package[58]). If all measurements of a protein are missing in one of the conditions, a pseudo fold change was computed replacing the missing group average by the mean of 10% smallest protein intensities in that condition. For the phosphoproteome data, each file was kept separate in the experimental design to obtain individual quantitative values. Precursor and fragment tolerance was set to 10 and 20 p.p.m., respectively for the initial search. The maximum FDR was set to 0.01 for peptides and 0.05 for proteins. Label-free quantification was enabled and a 2 min window for match between runs was applied. The re-quantify option was selected.

For the phosphosite analysis, a similar data analysis strategy as described by Sharma et al.[59] was implemented. In brief, the MaxQuant phospho_STY_site.txt file was used as the input file. The phosphosite table was expanded with respect to their multiplicity and filtered for a minimum localization site probability of 0.75. For each two-group comparison, all peptides with a maximum of four missing values were retained. The data (like for the total proteome) was normalized with a modified robust *z*-score transformation and *P* values were computed with a moderated *t* test with pooled variance (as implemented in the limma package[58]). If all measurements of a protein were missing in one of the conditions, a pseudo fold change was computed replacing the missing group average by the mean of 10% smallest protein intensities in that condition. Calculated *P* values are adjusted for multiple testing using the BH-method. The statistics of the phosphopeptide analysis and the total proteome analysis were merged. The mass spectrometry proteomics data have been deposited to the ProteomeXchange Consortium via the PRIDE[36] partner repository with the dataset identifier PXD018056.

Data parsing and analysis. For comparison to the existing phosphoproteome[13], phosphopeptide data from all strains in this study, and data from purified tachyzoites and infected host cells (phosphopeptide-enriched and -depleted) were pooled. The ToxoDB gene IDs, as well as phosphosites from each study were then intersected and plotted as a Venn diagram. To identify potential targets of RON13, the comparison of RON13-KD to RH (dataset 1), as well as of RON13-KD/ron13wt and RON13-KD/ron13dk (dataset 2) were used. Peptide contaminants and peptides mapping to reverse proteins were removed. Phosphopeptides with at least fourfold more abundance in either comparison ($\log_2FC < -2$) were selected for further analysis. Peptides with the posterior error probabilities (PEPs) > 0.05 and with *P* values (associated to the $\log_2FC$) were >0.05 were excluded. The common hits between both datasets were then considered high-confidence candidates of RON13. Differences in multiplicity of phosphorylation were not taken into account if position of the phosphorylated amino acid was identical. The polar plot was built by slightly modifying the R package funscoR (https://github.com/evocellnet/funscoR)[60]. The phosphoproteome data have been deposited on the ProteomeXchange Consortium via the PRIDE[42] partner repository with the dataset identifier PXD018056.

Determination of phosphoserine sequence logo. To determine the sequence logos for phosphoserine, the phosphopeptides corresponding to RON13 substrates (Supplementary Data 5) containing phosphoserines were used. The flanking 15 amino acids of the phosphoserines were extracted, and the resulting 31 amino acid sequences were used as an input for Sequence Logo Analysis tool at PhosphoSitePlus[61] (www.phosphosite.org, version 6.5.9.3). PSP production was used as an algorithm and "Phoshpo Ser" used as background. The consensus

sequence was computed using EMBOSS[62] (https://www.ebi.ac.uk/Tools/msa/emboss_cons/).

Reporting summary. Further information on research design is available in the Nature Research Reporting Summary linked to this article.

Data availability

All data are present in the main text and the supplementary materials. The mass spectrometry proteomics regarding RON4 immunoprecipitation have been deposited on the ProteomeXchange Consortium via the PRIDE[42] partner repository with the dataset identifier PXD021516. The phosphoproteomic data have been deposited on the ProteomeXchange Consortium via the PRIDE[42] partner repository with the dataset identifier PXD018056. The HDX-MS data have been deposited on the ProteomeXchange Consortium via the PRIDE[42] partner repository with the dataset identifier PXD023791. The coordinates and the cryo-EM map have been deposited to the Protein Data Bank (PDB ID: 7NUR) and Electron Microscopy Data Bank (accession code: EMD-12600). The public dataset used for mass spectrometry analysis of RON4 immunoprecipitation is the ToxoDB_Tgondii_GT1 database (http://ToxoDB.org, release 42) and the one used for the phosphoproteomics analysis is the ToxoDB_Tgondii_GT1 database (http://ToxoDB.org, release 44). All biological materials and data are available from the authors upon request. Source data are provided with this paper.

Received: 12 January 2021; Accepted: 31 May 2021;
Published online: 18 June 2021

References

1. Aquilini, E. et al. An Alveolata secretory machinery adapted to parasite host cell invasion. *Nat. Microbiol.* **6**, 425–434 (2021).
2. Kemp, L. E., Yamamoto, M. & Soldati-Favre, D. Subversion of host cellular functions by the apicomplexan parasites. *FEMS Microbiol. Rev.* **37**, 607–631 (2013).
3. Shen, B. & Sibley, L. D. The moving junction, a key portal to host cell invasion by apicomplexan parasites. *Curr. Opin. Microbiol.* **15**, 449–455 (2012).
4. Besteiro, S., Dubremetz, J. F. & Lebrun, M. The moving junction of apicomplexan parasites: a key structure for invasion. *Cell. Microbiol.* **13**, 797–805 (2011).
5. Guérin, A. et al. Efficient invasion by *Toxoplasma* depends on the subversion of host protein networks. *Nat. Microbiol.* **2**, 1358–1366 (2017).
6. Graindorge, A., Frénal, K., Jacot, D. & Salamun, J. The conoid associated motor MyoH Is indispensable for *Toxoplasma gondii* entry and exit from host cells. *PLoS Pathog.* **12**, e1005388 (2016).
7. Suss-Toby, E., Zimmerberg, J. & Ward, G. E. *Toxoplasma* invasion: the parasitophorous vacuole is formed from host cell plasma membrane and pinches off via a fission pore. *Proc. Natl Acad. Sci. USA* **93**, 8413–8418 (1996).
8. Pavlou, G. et al. *Toxoplasma* parasite twisting motion mechanically induces host cell membrane fission to complete invasion within a protective vacuole. *Cell Host Microbe* **24**, 81–96.e5 (2018).
9. Håkansson, S., Charron, A. J. & Sibley, L. D. *Toxoplasma* evacuoles: a two-step process of secretion and fusion forms the parasitophorous vacuole. *EMBO J.* **20**, 3132–3144 (2001).
10. Talevich, E. & Kannan, N. Structural and evolutionary adaptation of rhoptry kinases and pseudokinases, a family of coccidian virulence factors. *BMC Evol. Biol.* **13**, 117 (2013).
11. Peixoto, L. et al. Integrative genomic approaches highlight a family of parasite-specific kinases that regulate host responses. *Cell Host Microbe* **8**, 208–218 (2010).
12. Fox, B. A. et al. The *Toxoplasma gondii* rhoptry kinome is essential for chronic infection. *MBio* **7**, 193–216 (2016).
13. Treeck, M., Sanders, J. L., Elias, J. E. & Boothroyd, J. C. The phosphoproteomes of *Plasmodium falciparum* and *Toxoplasma gondii* reveal unusual adaptations within and beyond the parasites' boundaries. *Cell Host Microbe* **10**, 410–419 (2012).
14. Dogga, S. K. et al. A druggable secretory protein maturase of Toxoplasma essential for invasion and egress. *Elife* **6**, 1–35 (2017).
15. Sidik, S. M. et al. A genome-wide CRISPR screen in *Toxoplasma* identifies essential Apicomplexan genes. *Cell* **166**, 1423–1435 (2016).
16. Lodoen, M. B., Gerke, C. & Boothroyd, J. C. A highly sensitive FRET-based approach reveals secretion of the actin-binding protein toxofilin during *Toxoplasma gondii* infection. *Cell. Microbiol.* **12**, 55–66 (2010).
17. Tagliabracci, V. S. et al. Secreted kinase phosphorylates extracellular proteins that regulate biomineralization. *Science* **336**, 1150–1153 (2012).
18. Qiu, W. et al. Novel structural and regulatory features of rhoptry secretory kinases in *Toxoplasma gondii*. *EMBO J.* **28**, 969–979 (2009).
19. Beck, J. R., Chen, A. L., Kim, E. W. & Bradley, P. J. RON5 is critical for organization and function of the toxoplasma moving junction complex. *PLoS Pathog.* **10**, e1004025 (2014).
20. Mueller, C. et al. The toxoplasma protein ARO mediates the apical positioning of rhoptry organelles, a prerequisite for host cell invasion. *Cell Host Microbe* **13**, 289–301 (2013).
21. Butcher, B. A. et al. Toxoplasma gondii rhoptry kinase rop16 activates stat3 and stat6 resulting in cytokine inhibition and arginase-1-dependent growth control. *PLoS Pathog.* **7**, e1002236 (2011).
22. Sloves, P.-J. et al. Apical organelle secretion by *Toxoplasma* controls innate and adaptive immunity and mediates long-term protection. *J. Infect. Dis.* **212**, 1449–1458 (2015).
23. Barylyuk, K. et al. A comprehensive subcellular atlas of the *Toxoplasma* proteome via hyperlopit provides spatial context for protein functions. *Cell Host Microbe* **28**, 752–766.e9 (2020).
24. Behnke, M. S. et al. Coordinated progression through two subtranscriptomes underlies the tachyzoite cycle of *Toxoplasma gondii*. *PLoS ONE* **5**, e12354 (2010).
25. Harrison, R. A. & Engen, J. R. Conformational insight into multi-protein signaling assemblies by hydrogen-deuterium exchange mass spectrometry. *Curr. Opin. Struct. Biol.* **41**, 187–193 (2016).
26. Krissinel, E. & Henrick, K. Secondary-structure matching (SSM), a new tool for fast protein structure alignment in three dimensions. *Acta Crystallogr. Sect. D Biol. Crystallogr.* **60**, 2256–2268 (2004).
27. Huynh, M. H. & Carruthers, V. B. Tagging of endogenous genes in a *Toxoplasma gondii* strain lacking Ku80. *Eukaryot. Cell* **8**, 530–539 (2009).
28. Meissner, M., Schlüter, D. & Soldati, D. Role of *Toxoplasma gondii* myosin A in powering parasite gliding and host cell invasion. *Science* **298**, 837–840 (2002).
29. Hammoudi, P. M. et al. Fundamental roles of the golgi-associated *Toxoplasma* aspartyl protease, ASP5, at the host-parasite interface. *PLoS Pathog.* **11**, 1–32 (2015).
30. Salamun, J., Kallio, J. P., Daher, W., Soldati-favre, D. & Kursula, I. Structure of *Toxoplasma gondii* coronin, an actin-binding protein that relocalizes to the posterior pole of invasive parasites and contributes to invasion and egress. *FASEB J.* **28**, 4729–4747 (2014).
31. Shen, B., Brown, K. M., Lee, T. D. & Sibley, L. D. Efficient gene disruption in diverse strains of *Toxoplasma gondii* using CRISPR / CAS9. *MBio* **5**, 1–11 (2014).
32. Krishnan, A. et al. Functional and computational genomics reveal unprecedented flexibility in stage-specific *Toxoplasma* metabolism. *Cell Host Microbe* **27**, 290–306.e11 (2020).
33. Suarez, C. et al. A lipid-binding protein mediates rhoptry discharge and invasion in *Plasmodium falciparum* and Toxoplasma gondii parasites. *Nat. Commun.* **10**, 4041 (2019).
34. Keller, A., Nesvizhskii, A. I., Kolker, E. & Aebersold, R. Empirical statistical model to estimate the accuracy of peptide identifications made by MS/MS and database search. *Anal. Chem.* **74**, 5383–5392 (2002).
35. Nesvizhskii, A. I., Keller, A., Kolker, E. & Aebersold, R. A statistical model for identifying proteins by tandem mass spectrometry. *Anal. Chem.* **75**, 4646–4658 (2003).
36. Perez-Riverol, Y. et al. PRIDE inspector toolsuite: moving toward a universal visualization tool for proteomics data standard formats and quality assessment of proteomexchange datasets. *Mol. Cell. Proteom.* **15**, 305–317 (2016).
37. Harding, C. R. et al. Alveolar proteins stabilize cortical microtubules in *Toxoplasma gondii*. *Nat. Commun.* **10**, 401 (2019).
38. Tosetti, N. et al. Essential function of the alveolin network in the subpellicular microtubules and conoid assembly in *Toxoplasma gondii*. *Elife* **9**, 1–22 (2020).
39. Edgar, R. C. M. U. S. C. L. E. Multiple sequence alignment with high accuracy and high throughput. *Nucleic Acids Res.* **32**, 1792–1797 (2004).
40. Guindon, S. et al. New algorithms and methods to estimate maximum-likelihood phylogenies: assessing the performance of PhyML 3.0. *Syst. Biol.* **59**, 307–321 (2010).
41. Wang, H. et al. Autoregulation of class II alpha PI3K activity by its lipid-binding PX-C2 domain module. *Mol. Cell* **71**, 343–351.e4 (2018).
42. Perez-Riverol, Y. et al. The PRIDE database and related tools and resources in 2019: Improving support for quantification data. *Nucleic Acids Res.* **47**, D442–D450 (2019).
43. Zheng, S. Q. et al. MotionCor2: anisotropic correction of beam-induced motion for improved cryo-electron microscopy. *Nat. Methods* **14**, 331–332 (2017).
44. Zhang, K. Gctf: Real-time CTF determination and correction. *J. Struct. Biol.* **193**, 1–12 (2016).
45. Fernandez-Leiro, R. & Scheres, S. H. W. A pipeline approach to single-particle processing in RELION. *Acta Crystallogr. Sect. D Struct. Biol.* **73**, 496–502 (2017).
46. Zivanov, J. et al. RELION-3: new tools for automated high-resolution cryo-EM structure determination. *Elife* **7**, 1–22 (2018).

47. Tan, Y. Z. et al. Addressing preferred specimen orientation in single-particle cryo-EM through tilting. *Nat. Methods* **14**, 793–796 (2018).
48. Adams, P. D. et al. PHENIX: A comprehensive Python-based system for macromolecular structure solution. *Acta Crystallogr. Sect. D Biol. Crystallogr.* **66**, 213–221 (2010).
49. Emsley, P., Lohkamp, B., Scott, W. G. & Cowtan, K. Features and development of Coot. *Acta Crystallogr. Sect. D Biol. Crystallogr.* **66**, 486–501 (2010).
50. Amunts, A. et al. Structure of the yeast mitochondrial large ribosomal subunit. *Science* **343**, 1485–1489 (2014).
51. Chen, V. B. et al. MolProbity: All-atom structure validation for macromolecular crystallography. *Acta Crystallogr. Sect. D Biol. Crystallogr.* **66**, 12–21 (2010).
52. Lilkova, E. et al. *The PyMOL Molecular Graphics System, Version 2.0* (Schrödinger & LLC, 2015).
53. Pettersen, E. F. et al. UCSF Chimera - a visualization system for exploratory research and analysis. *J. Comput. Chem.* **25**, 1605–1612 (2004).
54. Wiśniewski, J. R., Zougman, A., Nagaraj, N. & Mann, M. Universal sample preparation method for proteome analysis. *Nat. Methods* **6**, 359–362 (2009).
55. Cox, J. & Mann, M. MaxQuant enables high peptide identification rates, individualized p.p.b.-range mass accuracies and proteome-wide protein quantification. *Nat. Biotechnol.* **26**, 1367–1372 (2008).
56. Wolski, W. & Panse, C. SRMService - R-package to report quantitative mass spectrometry data http://github.com/protViz/SRMService (2018).
57. Manes, N. P. & Nita-Lazar, A. Application of Targeted mass spectrometry in bottom-up proteomics for systems biology research. *J. Proteom.* **189**, 75–90 (2018).
58. Ritchie, M. E. et al. Limma powers differential expression analyses for RNA-sequencing and microarray studies. *Nucleic Acids Res.* **43**, e47 (2015).
59. Sharma, K. et al. Ultradeep human phosphoproteome reveals a distinct regulatory nature of Tyr and Ser/Thr-based signaling. *Cell Rep.* **8**, 1583–1594 (2014).
60. Ochoa, D. et al. The functional landscape of the human phosphoproteome. *Nat. Biotechnol.* **38**, 365–373 (2020).
61. Hornbeck, P. V. et al. PhosphoSitePlus, 2014: mutations, PTMs and recalibrations. *Nucleic Acids Res.* **43**, D512–D520 (2015).
62. Madeira, F. et al. The EMBL-EBI search and sequence analysis tools APIs in 2019. *Nucleic Acids Res.* **47**, W636–W641 (2019).

Acknowledgements

We thank Stephane Haussmann from the MIMOL department (University of Geneva) for assistance with kinase activity assays. We thank Dr. Alexandre Hainard and colleagues from the proteomic core facility (University of Geneva) for assistance with HDX-MS and MS data acquisition and analysis, Yves Cambet from the READS platform (University of Geneva) for his help in analyzing the xCELLigence data, and Dr. Iryna Nikonenko (PFMU, University of Geneva) for her expertise and help with Helios FIB-SEM image acquisition. We thank Dr. Tobias Kockmann from the FGCZ (University of Zurich) for his expertise and valuable help in the phosphoproteome acquisition and analysis. We thank Dr. Aarti Krishnan and Dr. Damien Jacot for helping to build the polar plot for generating the KD-RON13 and KO-RON4 parasite lines, respectively. Thanks to Dr. Lyer Aravind at the NLM/NCBI/NHI (Bethesda, USA) for his valuable input and discussion regarding the RON13 atypical structure. We also thank Dr. Martin Boulanger for kindly sharing the RON4 plasmid for insect cell expression, Dr. Maryse Lebrun for sharing antibodies and the GFP-ALIX plasmid, and Pr. Jean Gruenberg and Dr. Vincent Mercier for sharing the ALIX antibodies. O.V. were supported by Carigest SA. R.B.C., M.L., R.V., and G.L. were supported by the SNSF (310030B_166678 and 310030_185325). B.M. was supported by the European Research Council (ERC) under the European Union's Horizon 2020 research and innovation program under grant agreement no. 695596. Work in the laboratory of AH was supported by the SNSF (310030_184706). G.L. is supported by the Faculty of Medicine, University of Geneva.

Author contributions

R.V. and O.V. expressed and purified the proteins. V.M.K. and V.M. collected and processed the cryo-EM data, built, and refined the atomic model. G.L. and R.B.C. performed all the functional experiments. B. Mu. performed initial experiments, related analysis, and conceptualization. C.R., J.G., and A.B.H. generated and analyzed the phosphoproteomes. M.L. performed the mouse experiments. B. Ma. generated and documented the electron microscopy images. G.L. and D.S.-F. wrote the manuscript with input from all authors. G.L. create the images used for Figs. 1e, 2b, 6a and 10. G.L, R.B.C., O.V., and D.S.-F. conceived and directed the project with input from all the authors.

Competing interests

The authors declare no competing interests.

Additional information

Supplementary information The online version contains supplementary material available at https://doi.org/10.1038/s41467-021-24083-y.

Correspondence and requests for materials should be addressed to V.M.K. or D.S.-F.

Peer review information *Nature Communications* thanks the anonymous reviewers for their contribution to the peer review of this work.

Reprints and permission information is available at http://www.nature.com/reprints

Publisher's note Springer Nature remains neutral with regard to jurisdictional claims in published maps and institutional affiliations.

Supplementary Information for

Structural insights into an atypical secretory pathway kinase crucial for *Toxoplasma gondii* invasion

Gaëlle Lentini1†, Rouaa Ben Chaabene1†, Oscar Vadas1†, Chandra Ramakrishnan2, Budhaditya Mukherjee1,3, Ved Mehta4, Matteo Lunghi1, Jonas Grossmann5,6, Bohumil Maco1, Rémy Visentin1, Adrian B. Hehl2, Volodymyr M. Korkhov4,7,* and Dominique Soldati-Favre1,*

Correspondence to: dominique.soldati-favre@unige.ch, volodymyr.korkhov@psi.ch

†These authors contributed equally to the work

This PDF file includes:

Supplementary Figures 1 to 10
Supplementary Tables 1 to 6
Supplementary references

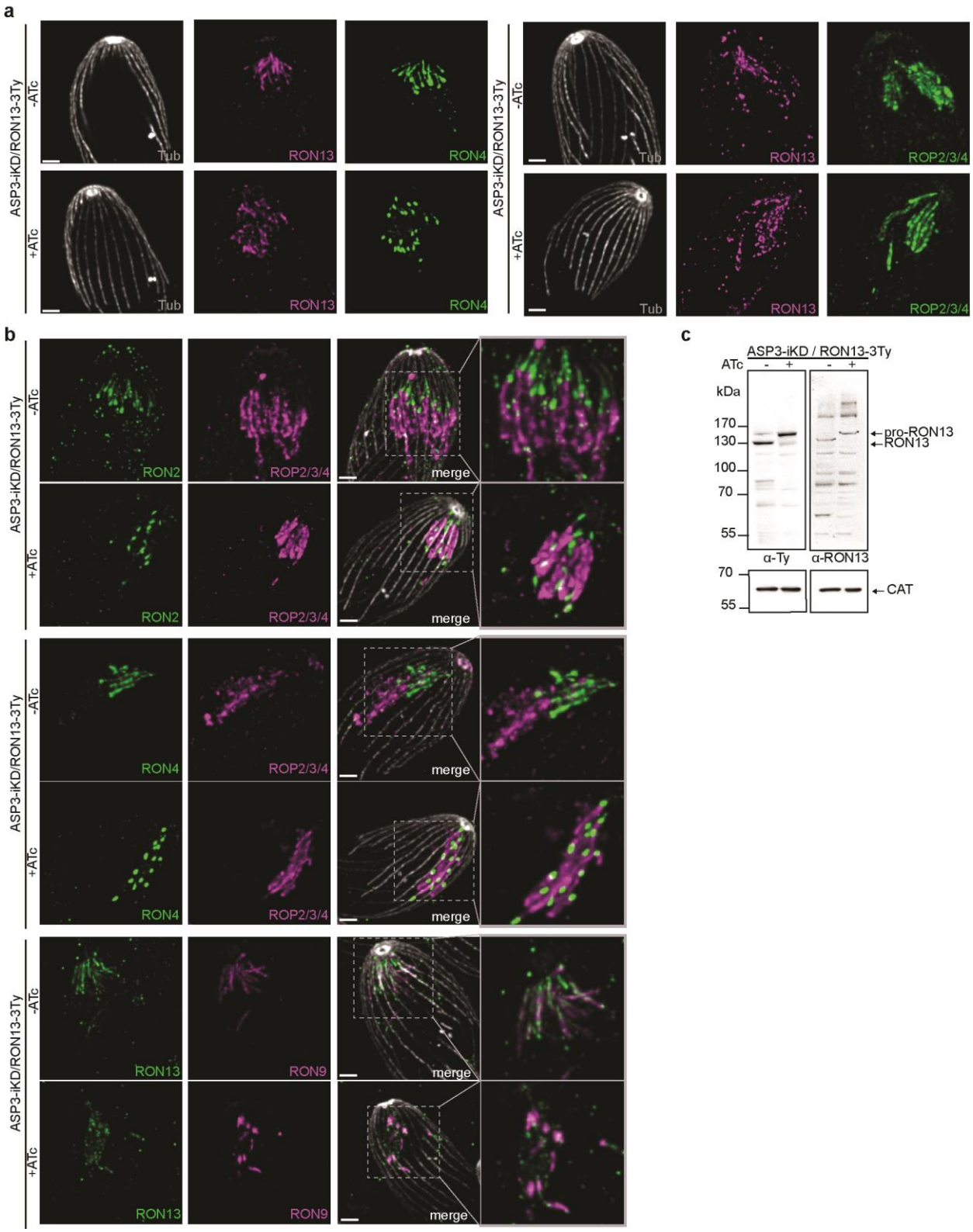
a
ASP3-iKD/RON13-3Ty
-ATc
+ATc
Tub
RON13
RON4
ROP2/3/4
b
RON2
ROP2/3/4
merge
RON4
RON13
RON9
c
ASP3-iKD / RON13-3Ty
ATc
kDa
170
130
100
70
55
pro-RON13
RON13
α-Ty
α-RON13
CAT

1

2

Supplementary Fig. 1. ASP3 depletion impacts rhoptry morphology and content localization. a. U-ExM images of parasites from ASP3-iKD/RON13-3Ty extracellular parasites ± anhydrotetracycline (ATc). The images presented here correspond to the individual channel merged in Figure 1a. ROP2/3/4 (green) antibodies are used to visualize the bulb of the rhoptries while RON4 (green) stains the neck of the rhoptries. RON13 (magenta) is detected using anti-Ty antibodies and parasite subpellicular microtubules are detected with anti-α/β tubulin antibodies (grey). Scale bar = 2 µm. Images representative of three biologically independent experiments. **b.** U-ExM images of rhoptries from ASP3-iKD/RON13-3Ty extracellular parasites ±ATc. ROP2/3/4 (magenta) antibodies are used to visualize the bulb of the rhoptries while RON2 (green), RON4 (green), RON9 (magenta) antibodies stain the neck of the rhoptries. RON13 (green) is detected using anti-Ty antibodies. Scale bar = 2 µm. Images representative of three biologically independent experiments. **c.** Immunoblot on ASP3-iKD/RON13-3Ty parasite lysates ±ATc demonstrating that the RON13 antibodies generated recognize both pro and mature RON13. Catalase (anti-CAT) is used as a loading control. Image representative of three biologically independent experiments. Source data are provided as a Source data file.

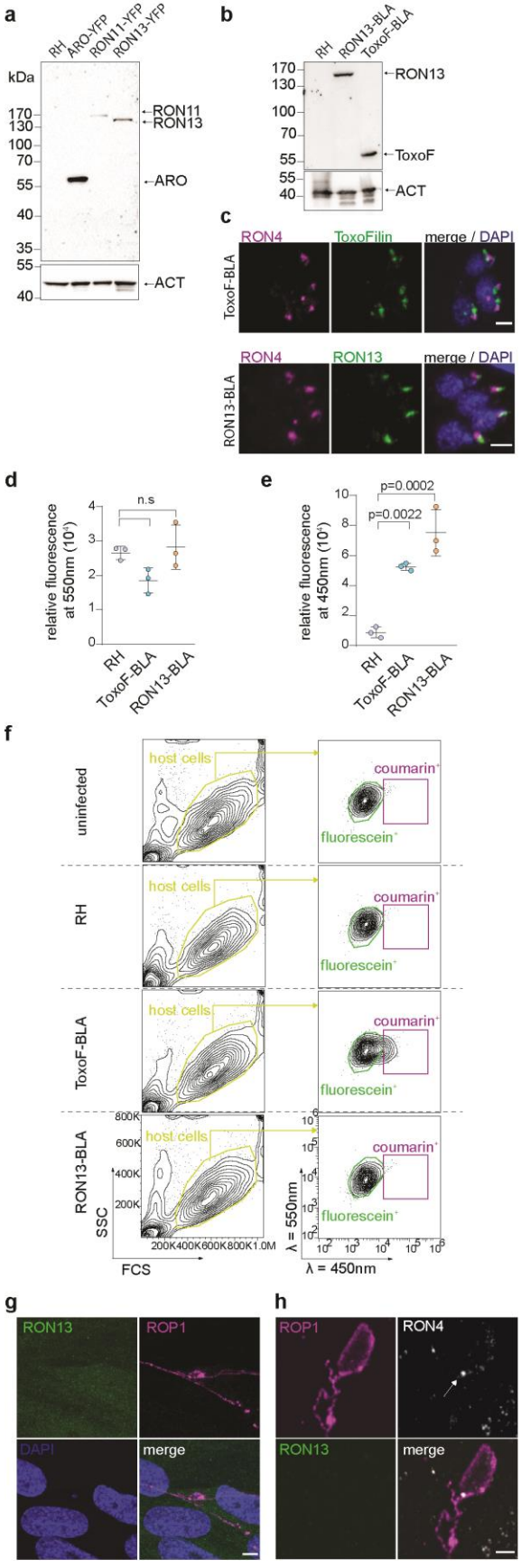
a
RH
ARO-YFP
RON11-YFP
RON13-YFP
kDa
170
130
100
70
55
40
35
55
40
←RON11
←RON13
←ARO
←ACT
b
RH
RON13-BLA
ToxoF-BLA
170
130
100
70
55
55
40
←RON13
←ToxoF
←ACT
c
RON4
ToxoFilin
merge / DAPI
ToxoF-BLA
RON4
RON13
merge / DAPI
RON13-BLA
d
n.s
relative fluorescence at 550nm (10⁴)
RH
ToxoF-BLA
RON13-BLA
e
p=0.0002
p=0.0022
relative fluorescence at 450nm (10⁴)
RH
ToxoF-BLA
RON13-BLA
f
uninfected
RH
ToxoF-BLA
RON13-BLA
host cells
coumarin⁺
fluorescein⁺
SSC
FCS
λ = 550nm
λ = 450nm
g
RON13
ROP1
DAPI
merge
h
ROP1
RON4
RON13
merge

19

Supplementary Fig. 2. RON13 is not secreted during invasion. a. Immunoblot on RH and ARO-YFP, RON11-YFP and RON13-YFP transgenic parasites showing proper expression of the fusion protein used in the topology assay. Actin (ACT) is used as a loading control. Image representative of three biologically independent experiments. **b.** Immunoblot showing the fusion of ToxoFilin and RON13 with the beta-lactamase protein (BLA). Anti-HA antibodies were to detected the fusion protein ToxoFilin-HA-BLA (ToxoF-BLA) and anti-myc antibodies were used to detect the fusion protein RON13-4myc-BLA (RON13-BLA). Image representative of three biologically independent experiments. **c**. ToxoF-BLA (green) and RON13-BLA (green) fusion proteins are properly targeted to the rhoptries as shown by IFA on intracellular parasites using anti-HA antibodies. Anti-HA antibodies were used to detect the fusion protein ToxoF-BLA and anti-myc antibodies to detect the fusion protein RON13-BLA. Scale bar = 2µm. Images representative of three biologically independent experiments. RON4 (magenta). DAPI (blue). **d and e**. Lactamase activity assessed on extracellular parasites demonstrating that the beta-lactamase is active when fused to ToxoFilin or RON13. The relative fluorescence of extracellular parasites incubated with the beta-lactamase substrate at 550nm (**d**) and 450nm (**e**) is shown for RH, ToxoF-BLA and RON13-BLA strains. This experiment was performed in triplicate. One ANOVA followed by Tukey's multiple comparison was used to test differences between groups (mean ± SD; n=3 biologically independent experiments). **f**. Gating strategy for quantification of fluorescein^{+} cell (λ=550nm; green gate) and coumarin^{+} cell (λ=450nm; violet gate) frequency for uninfected cell monolayer, RH, RON13-BLA and ToxoFilin-BLA infected cell monolayer (yellow gate) analyzed by flow cytometry. The gating strategy for RON13-BLA and ToxoFilin-BLA is also shown in Figure 2c.The frenquencies of fluorescein^{+} cell

(λ=550nm; green gate) and coumarin^{+} cell (λ=450nm; violet gate) were used to generate the graph shown in Figure 2d and 2e respectively. This experiment was performed in triplicate (n=3 biologically independent experiments). **g.** IFAs of extracellular parasites treated with cytochalasin D to block invasion but not rhoptry secretion. E-vacuoles are visualized with anti-ROP1 antibodies (magenta) and DAPI (blue) is used to stain DNA. Anti-Ty antibodies failed to detect RON13 (green) post-secretion. Scale bar = 5 μm. Images representative of three biologically independent experiments. **h.** IFAs of e-vacuole rhoptry secretion assay on RON13-3Ty parasites. ROP1 (magenta) is detected in the e-vacuoles post-secretion using anti-ROP1 antibodies and RON4 (white) is detected as a dot post-secretion using anti RON4 antibodies (arrow). RON13 (green) is not detected in the host cell post-secretion using anti-Ty antibodies. Scale bar = 2 μm. Images representative of three biologically independent experiments. Source data are provided as a Source data file.

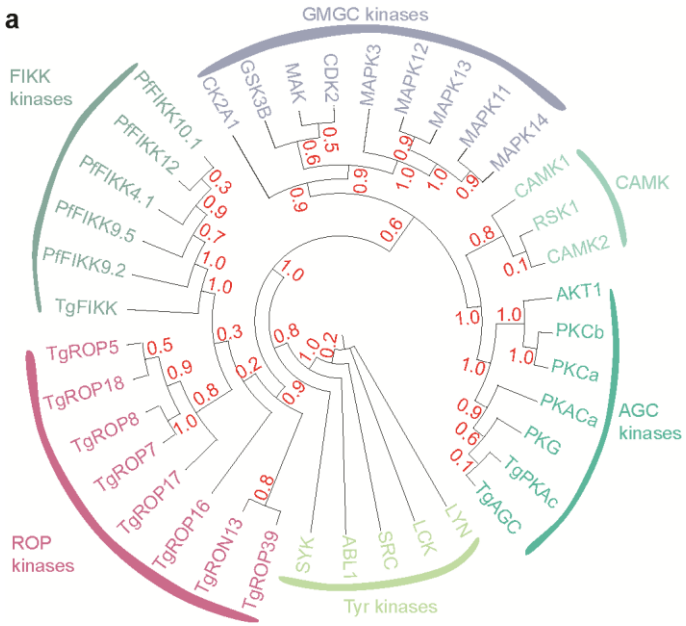

Supplementary Figure 3. RON13 belongs to the ROPK clade. Maximum-likelihood phylogenetic tree estimated from the multiple sequence alignment of the indicated kinases from different families (Supplementary Data 8). Bootstrap values are indicated in red.

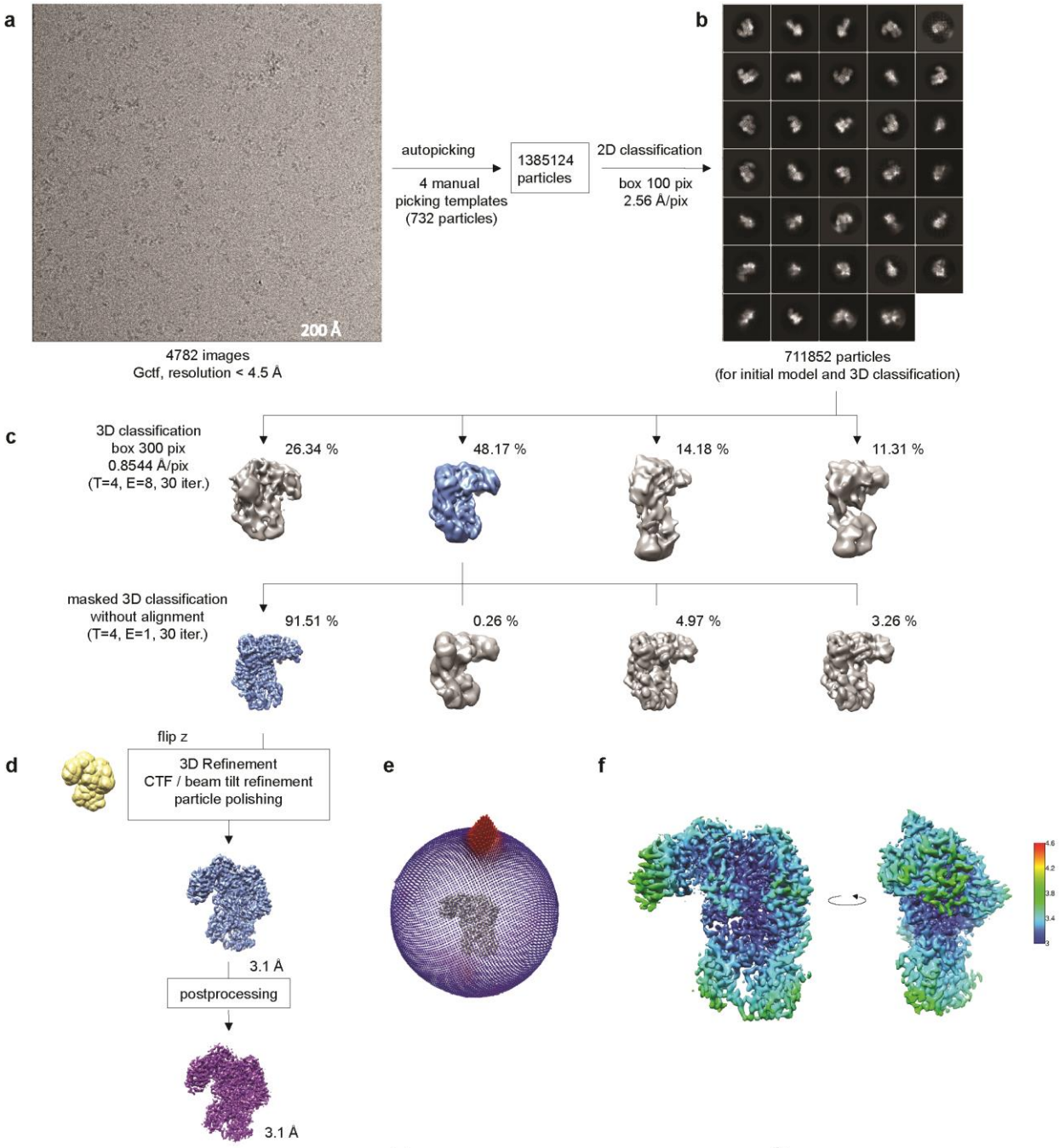
a
200 Å
4782 images
Gctf, resolution < 4.5 Å
autopicking
4 manual
picking templates
(732 particles)
1385124
particles
2D classification
box 100 pix
2.56 Å/pix
b
711852 particles
(for initial model and 3D classification)
c
3D classification
box 300 pix
0.8544 Å/pix
(T=4, E=8, 30 iter.)
26.34 %
48.17 %
14.18 %
11.31 %
masked 3D classification
without alignment
(T=4, E=1, 30 iter.)
91.51 %
0.26 %
4.97 %
3.26 %
d
flip z
3D Refinement
CTF / beam tilt refinement
particle polishing
3.1 Å
postprocessing
3.1 Å
e
f

60

61

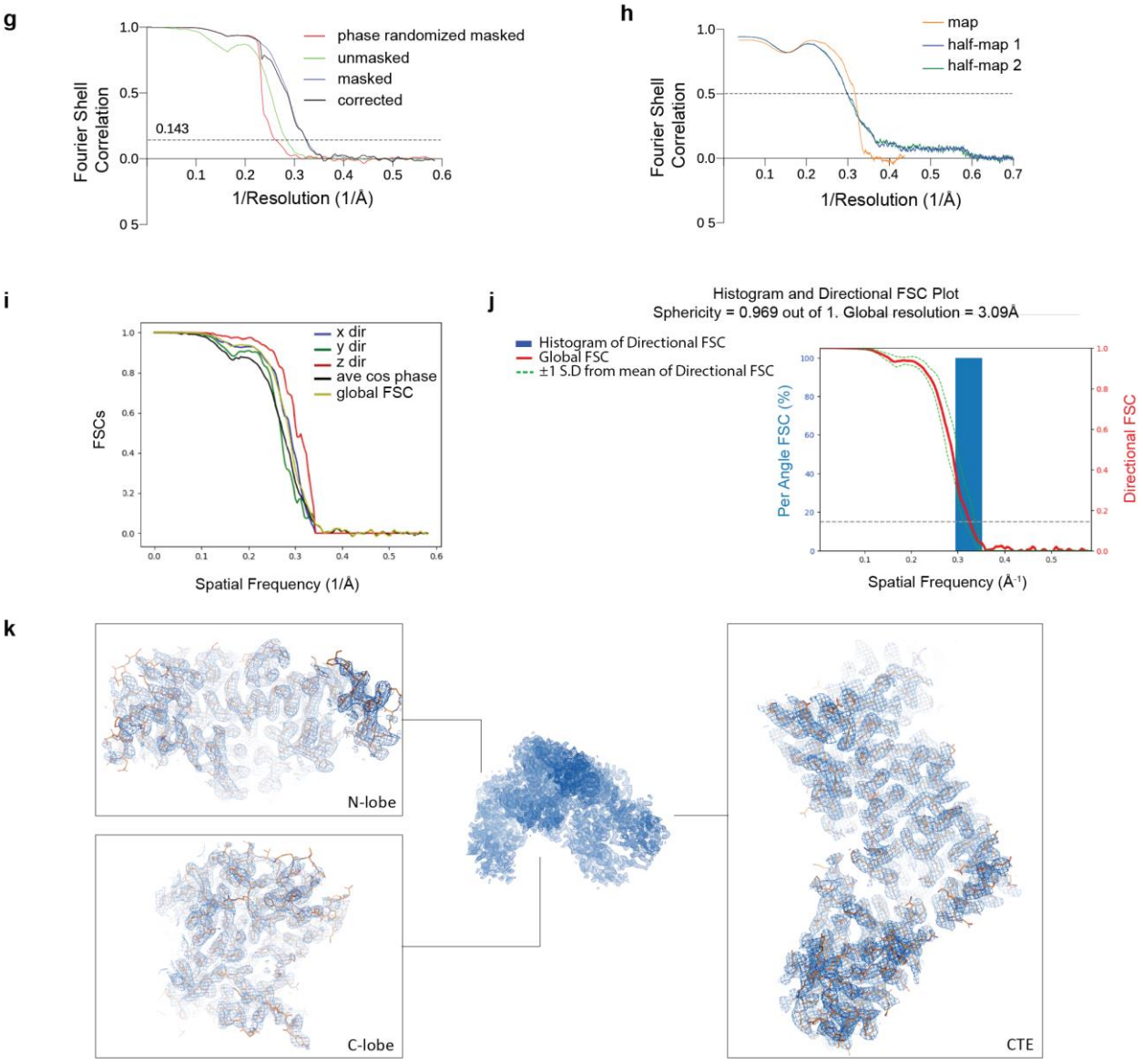

Supplementary Fig. 4. Cryo-EM and single particle analysis of rRON13dk. a. A representative motion-corrected micrograph of rRON13dk (scale bar corresponds to 200Å). **b.** A selection of the best 2D classes (bottom; box edge corresponds to 256 Å). **c.** Several rounds of 3D classification resulted in the final selection of particles for 3D refinement (blue). **d**. The z-flipped 3D class and mask were used for 3D refinement, followed by CTF refinement and Bayesian particle polishing, as described in "Methods". The final postprocessed density map at 3.1 Å resolution is shown in magenta. **e.** Angular distribution

histogram of the rRON13dk dataset used in the final refinement. **f**. Local resolution estimate for the refined density map, calculated in relion-3.0. **g.** Fourier shell correlation (FSC) plot for the 3D map shown in d, refined and postprocessed to a resolution of 3.1 Å (FSC 0.143). **h.** Model to map FSC curve. **i** and **j.** Output of the 3DFSC server, reporting the directional (**i**) and global FSC (**j**) of the cryo-EM reconstruction. The sphericity and global resolution are indicated in (**j**). **k.** The postprocessed density map of RON13-KD, contoured at 8σ. The views of the map in boxes corresponding to the kinase N-lobe, C-lobe and CTD are overlayed with the model of the protein in stick representation.

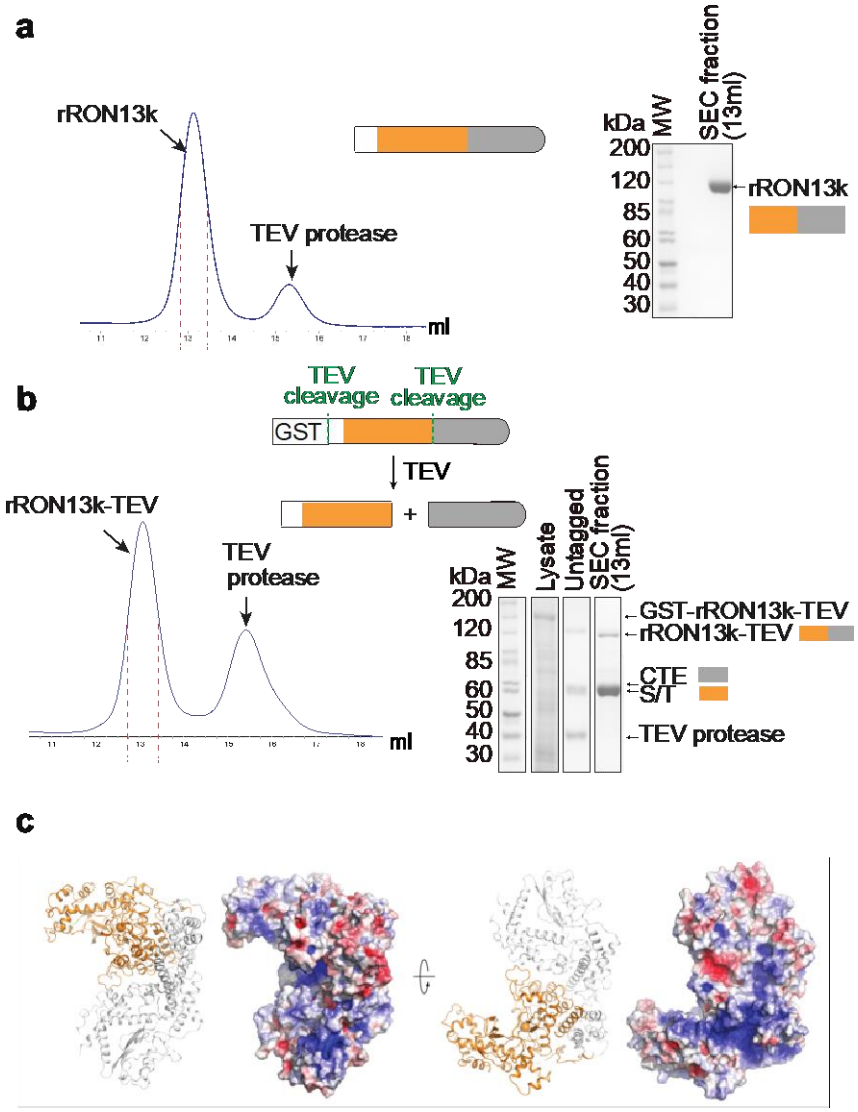

Supplementary Figure 5. RON13 CTE is essential for its folding and stability. a and **b.** Size-exclusion chromatography elution profiles of rRON13k protein (**a**) and a RON13 protein composed of individual kinase domain (orange) + CTE fragment (grey) (rRON13k-TEV) (**b**). The two fragments (kinase and CTE) were generated by cloning a TEV protease recognition site between the two domains, yielding the two expected fragments after purification and TEV proteolytic cleavage (SDS-PAGE analysis). Both rRON13wt and rRON13k-TEV behave identically on a Superdex 200 size-exclusion column. **c.** Cartoon and surface representation of RON13 from two opposite points of views; the sphere in the

cartoon representation indicates the position of the active site (residue 595). The protein surface is colored according to electrostatic potential, calculated using APBS (from red, -5 kT/e, to blue, +5 kT/e). Source data are provided as a Source data file.

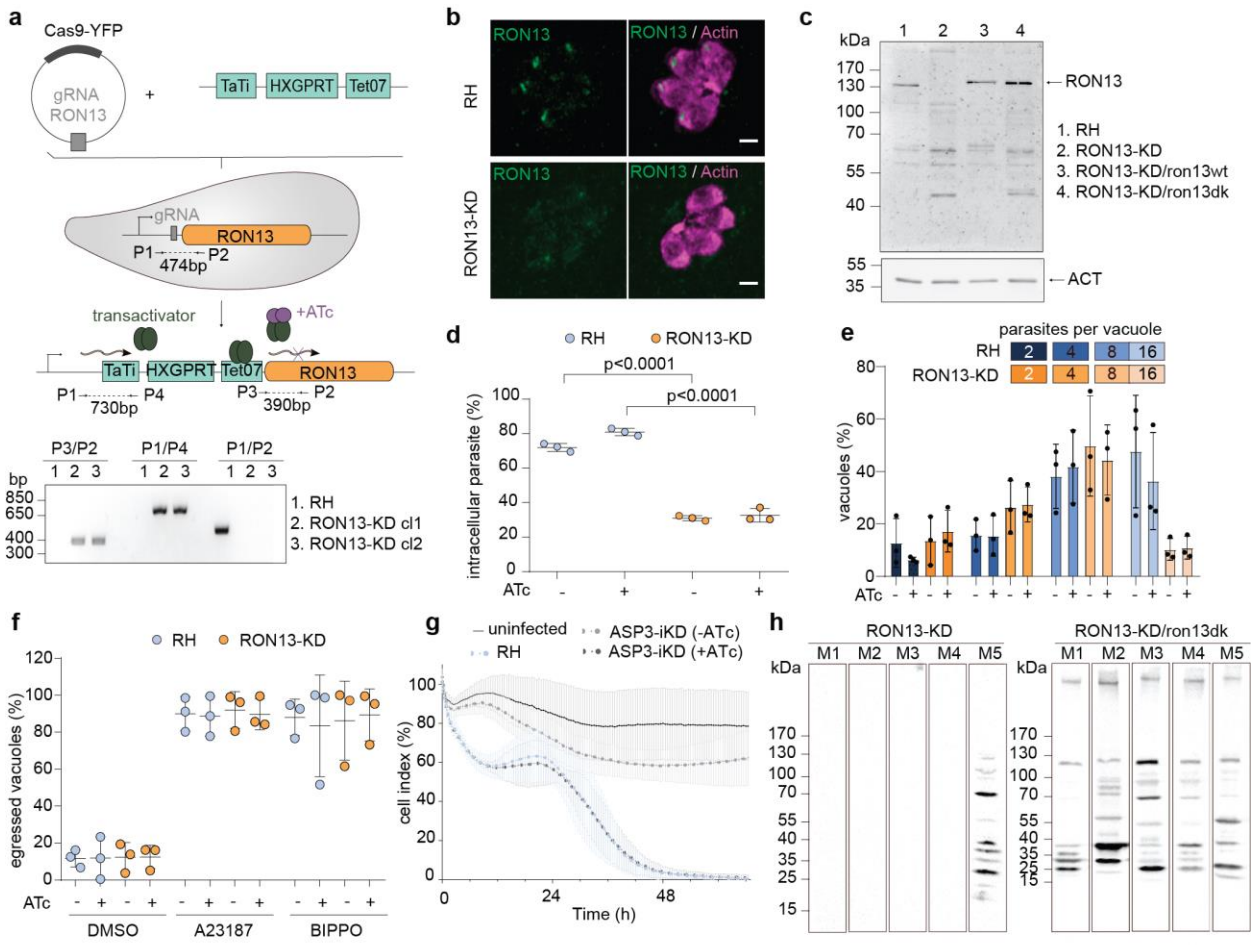

94

95 **Supplementary Fig. 6. RON13 is an important invasion and virulence factor. a.** Genetic
96 strategy used to generate RON13-KD and integration PCRs on the RON13-KD clonal lines
97 and RH parental line performed with primers P1/P4 (5' integration), P3/P2 (3' integration)
98 and P1/P2 to control the locus (wt = 474 bp; modified locus = 4429 bp). **b.** IFAs of
99 intracellular RH and RON13-KD parasites using anti-RON13 antibodies (green). An anti-
100 actin antibody (magenta) stained the parasite cytoplasm. Scale bar = 2µm. Images
101 representative of three biologically independent experiments. **c.** Western blot using anti-
102 RON13 antibodies showing the downregulation of RON13 in RON13-KD parasites
103 compared to the parental line RH or the complemented lines RON13-KD/ron13wt

(complemented wild-type) and RON13-DK/ron13dk (complemented dead kinase). Actin (anti-ACT) is used as a loading control. Image representative of three biologically independent experiments. **d.** Graph showing the percentage of intracellular parasites following 30 min of incubation with host cells reflecting the ability of extracellular parasites (±ATc) to invade. One ANOVA followed by Tukey's multiple comparison was used to test differences between groups (mean ± SD; n=3 biologically independent experiments). **e.** Intracellular replication assay. Graph representing the number of parasite per vacuole observed at 36 h post-invasion. Two-way ANOVA followed by Tukey's multiple comparison was used to test differences between groups (mean ± SD; n=3 biologically independent experiments). **f.** Induced egress assay. Graph representing the percentage of ruptured vacuoles following treatment with the egress inducers A23187 or BIPPO for RH and RON13-KD parasites (±ATc). Two-way ANOVA followed by Tukey's multiple comparison was used to test differences between groups (mean ± SD; n=3 biologically independent experiments). **g.** Kinetic assay representing the cell index of HFF infected with different parasite strains (mean ± SD; n=3 biologically independent experiments). **h.** Immunoblots showing the serology of infected mice at 84 days post-infection with RON13-KD and RON13-KD/ron13dk parasites (prior challenge). M1= mouse 1. Samples derive from the same experiment and gels were processed in parallel. The experiment was done once simultaneously with five mice for each strains tested (n=5 biologically independent animals). Source data are provided as a Source data file.

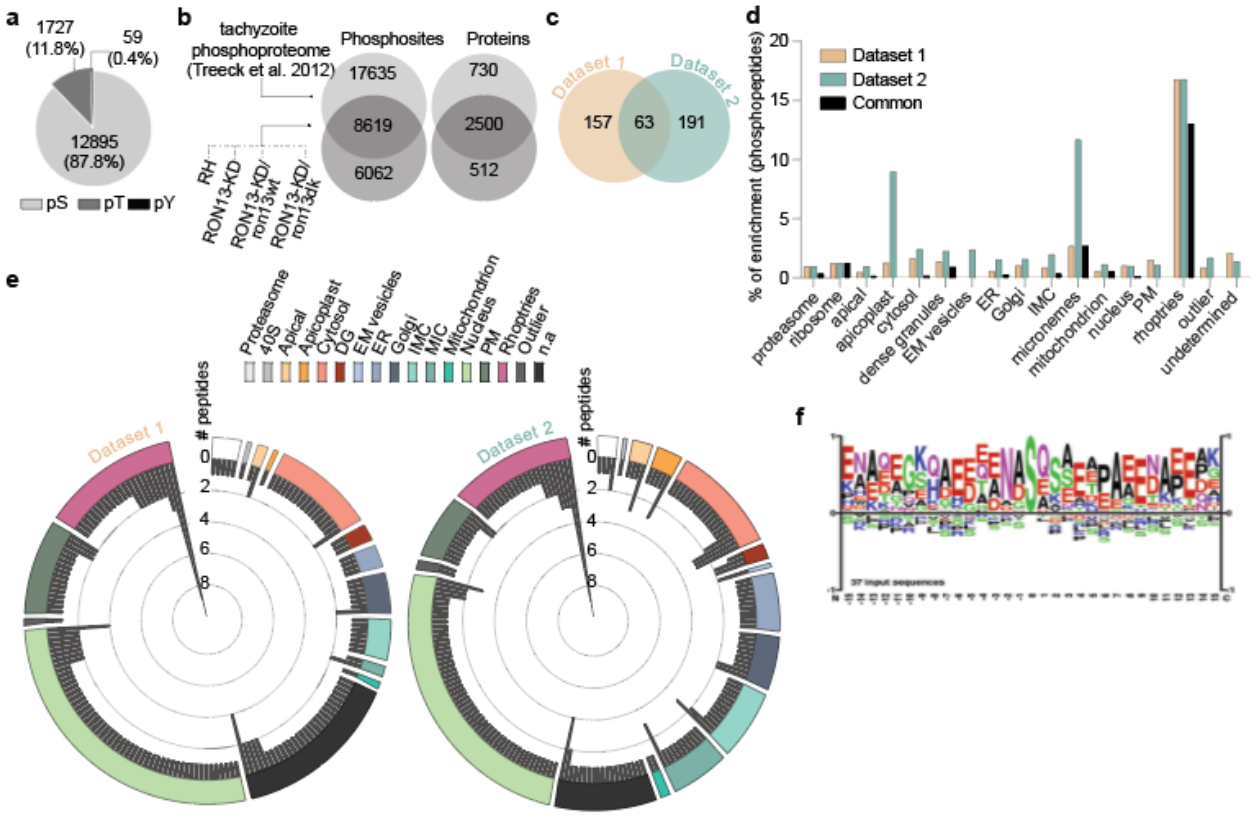

Supplementary Fig. 7. Rhoptry proteins are the major substrate of RON13. a. Pie chart showing the repartition of phospho-Ser (pS), phosphor-Thr (pT) and phosphor-Tyr (pY) among the identified phosphopeptides in the total phosphoproteome. Phosphoproteome analysis combined results obtained from four independent experiments. **b.** Venn diagrams showing the overlapping data in terms of proteins and phosphosites between the already published phosphoproteome [20] and the total phosphoproteome of this study. **c.** Venn diagram of the phosphosites found in Dataset 1 and Dataset 2. **d.** Bar graph showing the percentage of phosphopeptides for Datasets 1, Dataset 2 and common to both datasets relative to the total number of phosphopeptides according to their predicted localization[1]. **e.** Polar plots of the number of phosphopeptides found in Dataset 1 (left) and Dataset 2 (right) binned by gene IDs and clustered according to their predicted subcellular localization[1]. **f.**

137 Sequence logo for phosphoserine of RON13 substrates (37 input sequences). Position 0
138 indicates the serine that is phosphorylated. Source data are provided as a Source data file.

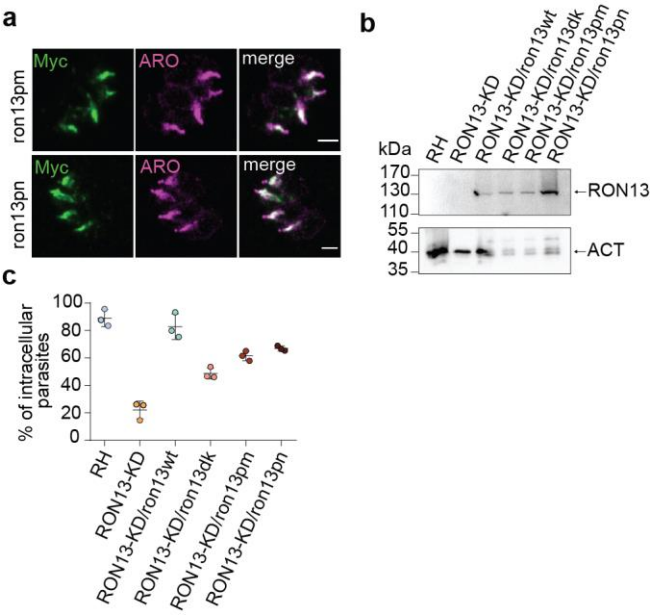

Supplementary Fig. 8. Phosphorylation of RON13 slightly influence its function. a. IFA on RON13-KD parasites expressing RON13 phospho-mimetic (ron13pm) or RON13 phospho-null (ron13pn) mutants. Anti-myc antibodies (green) were used to visualize the mutant copy of RON13 and anti-ARO antibodies (magenta) marked the rhoptries. Scale bar = 2µm. Images representative of three biologically independent experiments. **b.** Immunoblot of lysates from RON13-KD parasite complemented with either RON13pm or RON13pn. Anti-myc antibodies were used to visualize the mutant copy of RON13. Image representative of three biologically independent experiments. **c.** Invasion test showing the percentage of intracellular parasites reflecting their ability to invade. One-way ANOVA followed by Tukey's multiple comparison was used to test differences between groups (mean ± SD; n=3 biologically independent experiments). Source data are provided as a Source data file.

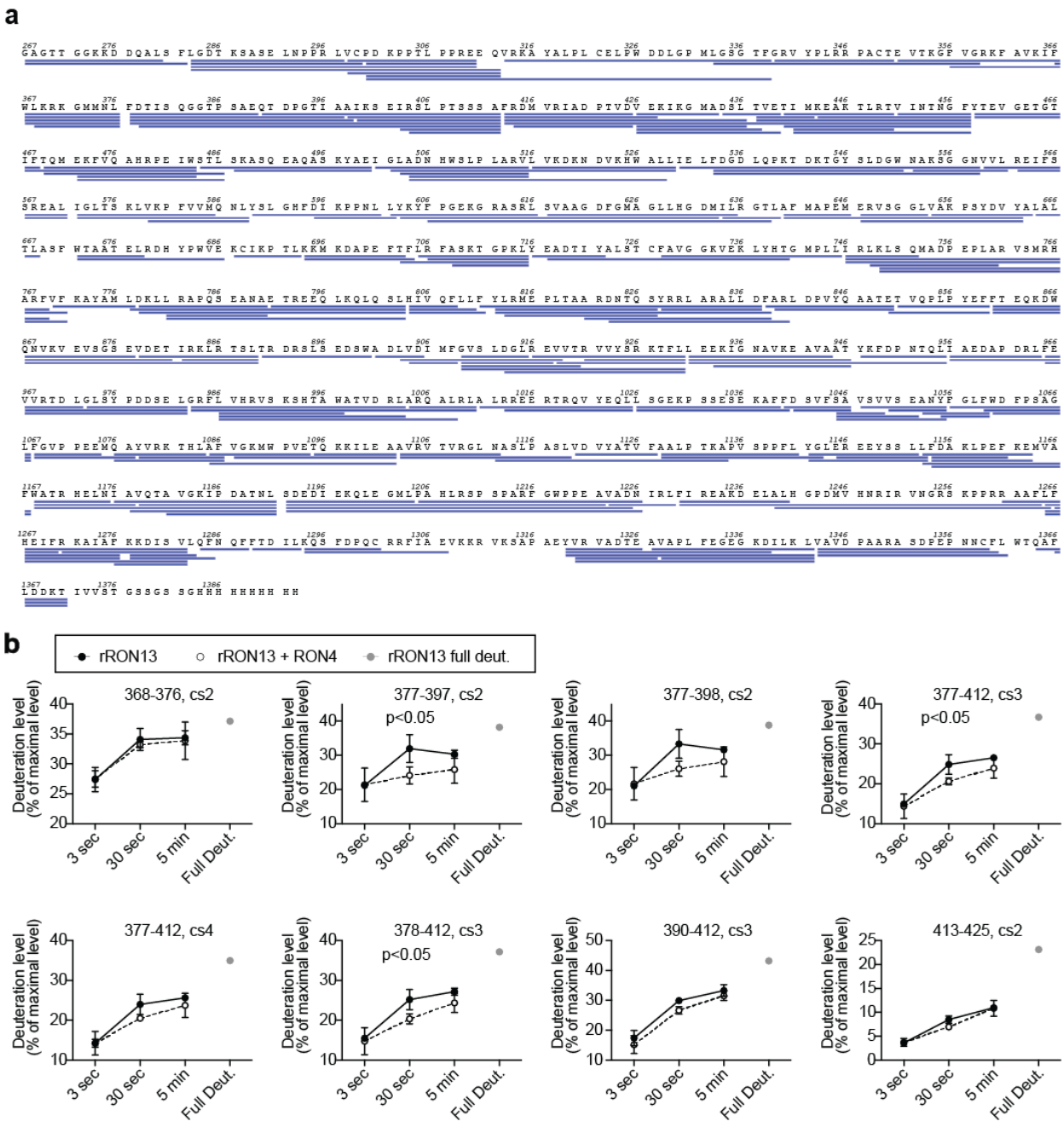

Supplementary Fig. 9. HDX-MS analysis of RON4 interaction with rRON13dk. a. Peptide map showing the peptides selected for HDX-MS analysis **b.** Uptake plots of a selection of peptides used in the HDX-MS analysis. cs: charge state. Indicated p values were determined using a two-tailed paired t-test; n=3 biologically independent experiments. Source data are provided in Supplementary Data 6.

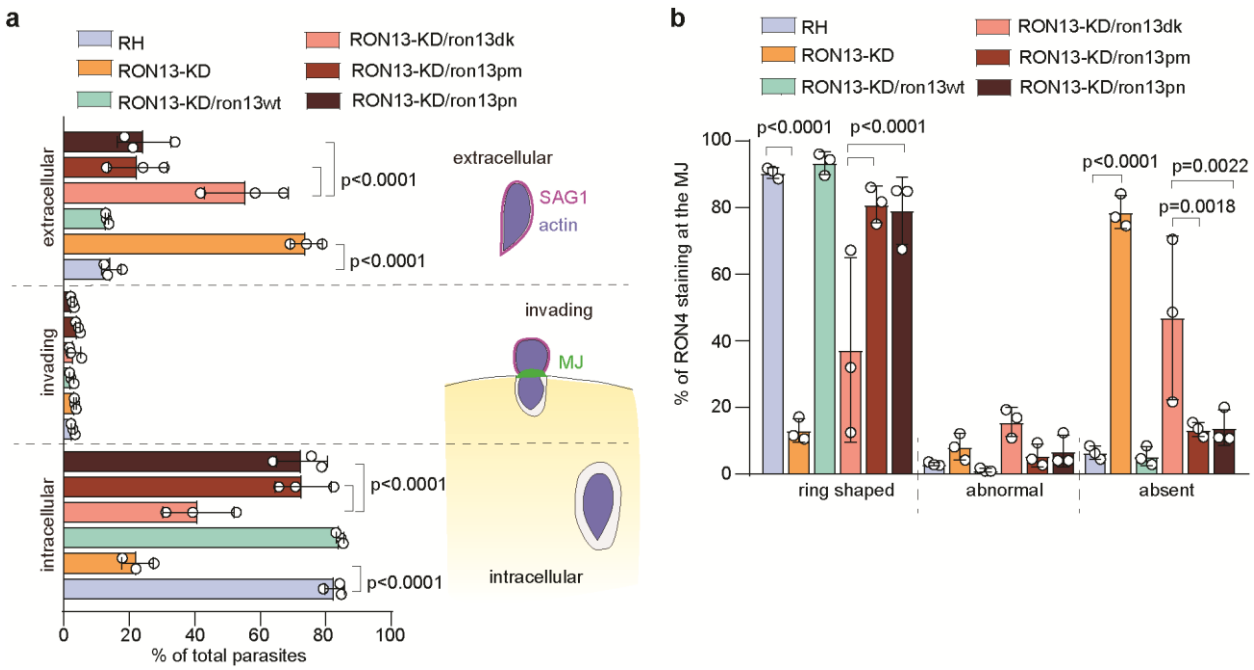

158

159 **Supplementary Fig. 10. RON13 auto phosphorylation does not impact MJ formation.**

160 **a.** Graph representing the proportion of extracellular, invading and intracellular parasites

161 observed in the pulse-invasion assay of RH, RON13-KD, RON13-KD/ron13t, RON13-

162 KD/ron13dk as well as the RON13-KD parasites expressing RON13 phospho-mimetic

163 (ron13pm) or RON13 phospho-null (ron13pn) mutants. A scheme representing the three

164 steps of the invasion processed is depicted. Two-way ANOVA followed by Tukey's multiple

165 comparison were used to test differences between groups in the panel of this figure (mean ±

166 SD; n=3 biologically independent experiments). **b.** Quantification of the different types of

167 RON4 staining (absent, abnormal, ring shaped) observed at the MJ of invading parasites.

168 Two-way ANOVA followed by Tukey's multiple comparison were used to test differences

169 between groups in the panel of this figure (mean ± SD; n=3 biologically independent

170 experiments). Source data are provided as a Source data file.

171

Data collection	
Instrument	FEI Titan Krios / Gatan K2 Summit / Quantum GIF
Magnification	61425 (165kx)
Voltage (kV)	300
Electron exposure ($e^-/Å^2$)	47
Defocus range (um)	-0.6 to -2.4
Pixel size (Å)	0.8544
Resolution, Å (FSC 0.143)	3.125
Number of particles	320723
Model refinement	
FSC 0.5 (masked), Å	3.15
Map sharpening b-factor (Å)	-85.7
Map CC (mask)	0.86
Model composition	
protein residues/ligands	1044 / 0
B factor min / max / mean ($Å^2$)	19.84 / 110.98 / 49.14
Bond length RMSD (Å)	0.007
Bond angle RMSD (°)	0.756
Validation	
MolProbity score	1.76
Clash score	5.20
Rotamer outliers (%)	0.11
Ramachandran plot	
Favored (%)	92.02
Allowed (%)	7.68
Disallowed (%)	0.29

Supplementary Table 1. Cryo-EM data collection, single particle analysis and model building statistics.

177 Infection 19.02.2020

178 Challenge 13.05.2020

179 End of the experiment 19.06.2020

180 Number of mice infected by each strain n =5 biologically independent animals

181

		RH		RON13-KD		RON13-KD/ron13wt		RON13-KD/ron13dk	
	days p.i	n sacrifices	Date	n sacrifices	Date	n sacrifices	Date	n sacrifice	Date
	8	1	27.02			1	27.02		
	9	1	28.02			3	28.02		
	10	3	29.02			1	29.02		
Survived	84	0		5		0		5	
challenge	84	n.a		5		n.a		5	
	93			2	22.05				
	94			2	23.05				
end	121			1	19.06			5	19.06
Survived challenge		0		1		0		5	
n seroconverted		n.a		1		n.a		5	

182 **Supplementary Table 2. Virulence of RON13 mutant strains.** Table representing the
183 number of CD1 mice infected with the specified parasite strains (top row), their survival and
184 seroconversion to the infection (penultimate and ultimate rows respectively). At day 84 post-
185 infection (p.i) surviving mice were challenged with RH parasites (turquoise row). The blue
186 row indicates the number surviving the challenge infection. Abbreviations: n, number of
187 biologically independent mouse; n.a, not applicable.

188

Dataset :	RON13	RON13 + RON4	RON13 FD
Description :	**RON13**	**RON13 + RON4**	**RON13 FD**
Reaction volume :	50 ul	50 ul	50 ul
% D2O in the reaction :	81.0%	81.0%	81.0%
temperature :	22 °C	22 °C	22 °C
D2O incubation times (sec) :	3 sec, 30 sec, 5 min	3 sec, 30 sec, 5 min	90 min
Control sample :	Non-deuterated (ND) and fully deuterated (FD) RON13		
Quench buffer :	6 M Urea / 0.1 M NaH2PO4 pH 2.4 / 1% Formic acid		
Quench buffer volume :	20 ul	20 ul	20 ul
Number of peptides analysed :	205	205	205
Sequence coverage :	94.0%	94.0%	94.0%
Replicates :	3, 3, 3	3, 3, 3	1
Standard deviation average (RON13, all time points, %D) :	1.03	1.55	-
Criteria for HDX rate difference :	Difference of HDX level at a given timepoint is > 5 % and > 1 Da and p values of two-tailed paired student t-test is < 0.05		

189 **Supplementary Table 3. HDX-MS experimental details.**

190

191

			RH/RON4-3Ty			RON13-KD/RON4-3Ty		
Protein	Gene ID	MW (kDa)	TSC IP	TSC input	**Enrichment**	TSC IP	TSC input	**Enrichment**
RON8	TGGT1_306060	329	66	5	**13.2**	30	4	**7.5**
RON2	TGGT1_300100	166	82	16	**5.125**	67	3	**22.33333333**
RON4	TGGT1_229010	107	64	20	**3.2**	49	11	**4.454545455**
RON5	TGGT1_311470	187	82	26	**3.153846154**	78	25	**3.12**
AMA1	TGGT1_255260	63	26	15	**1.733333333**	26	17	**1.529411765**

Supplementary Table 4. The MJ complex is form in absence of RON13. Table depicting the MJ proteins identified by mass spectrometry in the co-immunoprecipitation of RON4 samples from RH and RON13-KD parasites. The table include information regarding the total spectrum count (TCS) in the input (total lysate) and in the IP samples as well as the ratio of enrichment for each of the proteins. Anti-Ty antibodies have been used to immunoprecipitate RON4.

Primer #	Orientation	Sequence 3'->5'	Construct	Strain
6765	F	GATGGGCCCTCACCGACATCCTCAAACAGAG	KI-3TY-DHFR	ASP3-iKD/RON13-3Ty[2]
6766	R	ACGCCTGCAGGGCTCACGACGATTGTTTTATCG	KI-3TY-DHFR	ASP3-iKD/RON13-3Ty[2]
4883	R	AACTTGACATCCCCATTTAC	gRNA 5'ron13 locus	RON13-KD
7012	F	GGAGTTCACAGGTTCTCTTGGTTTTAGAGCTAGAAATAGC	gRNA 5'ron13 locus	RON13-KD
7013	F	CCTCTATGTTTGTCTCTAGCAACGAATCGGCATGTTTGCGGATCCGGGG	PCR cassette TaTi-HXGPRT-TetO7S1	RON13-KD
7015	R	CACGCTTCGTTCGCTTTGCATGCGAGGCAACATTTTGATATCCCTAGGAATTC	PCR cassette TaTi-HXGPRT-TetO7S1	RON13-KD
P1-7069	F	CTTAGGTCCCTCGTTCCGTAG	Check 5’ integration RON13-KD	-
P4-2903	R	GAGCGAGTTTCCTTGTCGTCAGGCC	Check 5’ integration RON13-KD	-
P3-1935	F	CGCTGCACCACTTCATTATTTCTTCTGG	Check 3’ integration RON13-KD	-
P2-7070	R	CTCTGCATTCAGGTGCCTG	Check 3’ integration RON13-KD	-
8178	F	GTCTTCAGAGGCGCCTTAATGACAAAATGTTGCCTCGC	pRON5-RON13-4myc (part 1)	RON13-KD/ron13wt
7813	R	GCTTGATGCATTTCTCCACCCACGGATAGT	pRON5-RON13-4myc (part 1)	RON13-KD/ron13wt
7814	F	GGTGGAGAAATGCATCAAGCCGACGCTGAAGA	pRON5-RON13-4myc (part 2)	RON13-KD/ron13wt
7815	R	CCAGACGATCCACGGTCGCCCAGGCAGT	pRON5-RON13-4myc (part 2)	RON13-KD/ron13wt
7816	F	GACCGTGGATCGTCTGGCGCGTCAG	pRON5-RON13-4myc (part 3)	RON13-KD/ron13wt
8179	R	GAGATGAGTTTTTGTTCGATGCTCACGACGATTGTTTTATC	pRON5-RON13-4myc (part 3)	RON13-KD/ron13wt
8548	F	GGGTCACTTTGCGATCAAGCCGC	pRON5-RON13dk-4myc	RON13-KD/ron13dk
8549	R	AAGCTGTAGAGGTTCTGC	pRON5-RON13dk-4myc	RON13-KD/ron13dk
9757	F	CGCTGAACTCGACCCCGTGTACCAG	pRON5-RON13cte(R840E)-4myc	RON13-KD/ron13cte
9026	F	GGGCGCCggtaccACAGGAGGAAAGAAGGATGACCAAG	pFastBac-Melittin-GST-RON13 (271-1371)-His6	Insect cell expression vector
9027	R	CCGAGGAaccggtGCTCACGACGATTGTTTTATCGTCG	pFastBac-Melittin-GST-RON13 (271-1371)-His6	Insect cell expression vector
9595	F	GAgAAtttGTAcTTcCAaGCCGCGCGAGACAACACACAG	pFastBac-RON13 kinase domain-TEV-CTE	Insect cell expression vector
9596	R	tTGgAAgTACaaaTTcTCAGTGAGAGGCTCCATTCGAAGATAAAAC	pFastBac-RON13 kinase domain-TEV-CTE	Insect cell expression vector
9758	R	GTCGAGTTCAGCGAAGTCGAGTAAAGCGC	pRON5-RON13cte(R840E)-4myc	RON13-KD/ron13cte
9759	F	GTCACGGCAGTCGTCTATTCGAGAAAAACGTTTTTG	pRON5-RON13cte(R921E)-4myc	RON13-KD/ron13cte
9760	R	GACGACTGCCGTGACGACCTCACGCAG	pRON5-RON13cte(R921E)-4myc	RON13-KD/ron13cte
9761	F	GTTCACGAAGTTTCCGCAAGCCACACTGCCTGGGC	pRON5-RON13cte(R989E+K992A)-4myc	RON13-KD/ron13cte

9762	R	TGGCTTGCGGAAACTTCGTGAACCAAAAACCTCCCCAG	pRON5-RON13cte(R989E+K992A)-4myc	RON13-KD/ron13cte
9590	F	GCCATCGCCCAGGGCGGAACAC	pRON5-RON13pn(T379A+S381A)-4myc	RON13-KD/ron13pn
9763	F	ggtggatccggtggcGAgAAtttGTAcTTcCAaGCCGCGC	pFastBac-RON13 kinase domain-linker-TEV-linker-CTE	Insect cell expression vector
9764	R	gccaccggatccaccAGTGAGAGGCTCCATTCGAAGATAAAAAC	pFastBac-RON13 kinase domain-linker-TEV-linker-CTE	Insect cell expression vector
9765	F	ggaagcggtggatccGCCGCGCGAGACAACACACAG	pFastBac-RON13 kinase domain-linker-TEV-linker-CTE	Insect cell expression vector
9766	R	ggatccaccgcttcctTGgAAgTACaaaTTcTCgccaccg	pFastBac-RON13 kinase domain-linker-TEV-linker-CTE	Insect cell expression vector
9591	R	GGCGATGGCGTCGAACAGATTCATC	pRON5-RON13pn(T379A+S381A)-4myc	RON13-KD/ron13pn
9946	F	GCCAGAGTTCGCCTTCCTGCGGT	pRON5-RON13pn(T379A+S381A+T703A)-4myc	RON13-KD/ron13pn
9947	R	GCGTCCTTCATCTTCTTCAGCG	pRON5- RON13pn(T379A+S381A+T703A)-4Myc pRON5- RON13pm(T379D+S381D+T703D)-4Myc	RON13-KD/ron13pn RON13-KD/ron13pm
9806	F	GATATCGACCAGGGCGGAACAC	pRON5-RON13pm(T379D+S381D)-4myc	RON13-KD/ron13pm
9807	R	GTCGATATCGTCGAACAGATTCAT	pRON5-RON13pm(T379D+S381D)-4myc	RON13-KD/ron13pm
9948	F	GCCAGAGTTCGACTTCCTGCGGT	pRON5- RON13pm(T379D+S381D+T703D)-4Myc	RON13-KD/ron13pm
8263	F	GCAAGGTTTCGTGCTGATCAGCGCTTCTTATCGTAGGG	pRON5-RON13-4myc-BLA	RON13-BLA
8264	R	ACCAGCGTTTCTGGGTGGGCCAGATCTTCTTCAGAAATAAGTTTTTG	pRON5-RON13-4myc-BLA	RON13-BLA
8798	F	TACTTCCAATCCAATTTAATGCCCTGTCTCAGAGATGATTACGAC	LIC-ARO-YFP	ARO-YFP
8799	R	TCCTCCACTTCCAATTTTAGCCTCCGACAGCCGGACCAAGA	LIC-ARO-YFP	ARO-YFP
8800	F	TACTTCCAATCCAATTTAATGCTTGTGGAAGCAGAGAATTTGAGG	LIC-RON11-YFP	RON11-YFP
8801	R	TCCTCCACTTCCAATTTTAGCCACTCGCTCTCCAGGAATTGG	LIC-RON11-YFP	RON11-YFP
8802	F	TACTTCCAATCCAATTTAATGCTTTCGTCCTTTTCTTGGAGAAGATCCG	LIC-RON13-YFP (part 1)	RON13-YFP
8803	R	GAAGGATATCGAATGCTTTCATGAAAAC	LIC-RON13-YFP (part 1)	RON13-YFP
8804	F	CATTCGATATCCTTCGATTGCATGCAGT	LIC-RON13-YFP (part 2)	RON13-YFP
8805	R	TCCTCCACTTCCAATTTTAGCGCTCACGACGATTGTTTT	LIC-RON13-YFP (part 2)	RON13-YFP
10019	F	GGATGAACTTCGACAAACTCGTTTTAGAGCTAGAAATAGC	gRNA RON4 frame shift	RON4 KO
10116	F	gtaaatggggatgtcaagttGCAAAGTGGAGAGCATCATTGCgtttta gagctagaaatagc	gRNA RON4 locus editing RON4pn and RON4pm	RON4pn and RON4pm

10117	R	gctatttctagctctaaaacGAGTTTGTCGAAGTTCATCCaacttgacatc cccattta	gRNA RON4 locus editing RON4pn and RON4pm	RON4pn and RON4pm
10094	F	gctctcagGGATGTATCCGAACATG	Sequencing RON4 frameshift	RON4 KO
10097	R	GCAACCGGTTCCTCAGCACT	Sequencing RON4 frameshift	RON4 KO

Supplementary Table 5. List of oligonucleotide primers and constructs used in this study.

		Dilution	
Antibody	Reference	IFA	WB
RON2 (rb)	[3] kind gift from Dr. M. Lebrun	1/250 (U-ExM); 1/500 (IFA)	1/1000
RON4 (rb)	[3] kind gift from Dr. M. Lebrun	1/1500 (U-ExM); 1/3000 (IFA)	1/1000
RON4 (ms) hybridoma T5 4H1	[4] kind gift from Dr. JF. Dubremetz	1/10	-
RON5C (ms)	[5] kind gift from Dr. P. Bradley	1/1000	1/1000
RON8 (rat)	[5] kind gift from Dr. M. Lebrun	1/400	-
RON9 (ms) hybridoma	[4] kind gift from Dr. JF. Dubremetz	1/2.5 (U-ExM); 1/10 (IFA)	-
RON13 (rb)	this study	1/1000	1/500
ROP2/3/4 (ms) hybridoma	[6] kind gift from Dr. JF. Dubremetz	1/2.5 (U-ExM)	
ROP1 (ms) hybridoma	kind gift from Dr. JF. Dubremetz	1/10	-
ARO (rb)	[7]	1/1000	-
GAP45 (rb)	[8]	1/10000	-
SAG1 (ms) hybridoma T4 1E5	[9]	1/10	-
SAG1 (ascite)	[10]	1/3000	-
Actin (ms) hybridoma	[11]	1/10	1/10
Catalase (rb)	[12]	-	1/2000
α + β tubulin (gp)	[13]	1/250 (U-ExM)	
Phospho-STAT6 (rb)	Cell signalling (9361)	1/400	-
Myc (ms) hybridoma 9E10	from DSHB by Bishop, J.M. (DSHB Hybridoma Product 9E 10)	1/10	1/10
Myc (rb)	Sigma (3956)	1/1000	-
Ty (ms) hybridoma BB2	[14]	1/2.5 (U-ExM); 1/10 (IFA)	1/10
Ty (rb)	kind gift from Dr. CJ. Tonkin[15]	1/1000 (U-ExM)	-
GFP (ms)	Roche	1/2000	1/1000
MIC2 (ms)	kind gift from Dr. V. Carruthers	-	1/10
GRA1 (rb)	Anawa	-	1/3000
HA (rat)	Roche (clone 3F10)	1/1000	
HA (ms) hybridoma	Clone 12CA5		1/10

Supplementary Table 6. List of antibodies used in this study. The species in which the antibodies were produced are mentioned between parentheses. Rabbit (rb); mouse (ms) ; guinea pig (gp).

Supplementary references

1. Barylyuk, K. *et al.* A Comprehensive Subcellular Atlas of the Toxoplasma Proteome via hyperLOPIT Provides Spatial Context for Protein Functions. *Cell Host Microbe* **28**, 752-766.e9 (2020).
2. Dogga, S. K. *et al.* A druggable secretory protein maturase of Toxoplasma essential for invasion and egress. *Elife* **6**, 1–35 (2017).
3. Besteiro, S., Dubremetz, J. F. & Lebrun, M. The moving junction of apicomplexan parasites: A key structure for invasion. *Cell. Microbiol.* **13**, 797–805 (2011).
4. Leriche, M. A. & Dubremetz, J. F. Characterization of the protein contents of rhoptries and dense granules of Toxoplasma gondii tachyzoites by subcellular fractionation and monoclonal antibodies. *Mol. Biochem. Parasitol.* **45**, 249–259 (1991).
5. Straub, K. W., Cheng, S. J., Sohn, C. S. & Bradley, P. J. Novel components of the Apicomplexan moving junction reveal conserved and coccidia-restricted elements. *cell Microbiol.* **11**, 590–603 (2009).
6. Sadak, A., Taghy, Z., Fortier, B. & Dubremetz, J. Characterization of a family of rhoptry proteins of Toxoplasma gondii. *Mol. Biochem. Parasitol.* **29**, 203–211 (1988).
7. Mueller, C. *et al.* The toxoplasma protein ARO mediates the apical positioning of rhoptry organelles, a prerequisite for host cell invasion. *Cell Host Microbe* **13**, 289–301 (2013).
8. Frenal, K., Polonais, V., Marq, J., Stratmann, R. & Limenitakis, J. Functional Dissection of the Apicomplexan Glideosome Molecular Architecture. *Cell Host Microbe* 343–357 (2010) doi:10.1016/j.chom.2010.09.002.
9. Couvreur, G., Sadak, A., Fortier, B. & Dubremetz, J. F. Surface antigens of Toxoplasma gondii. *Parasites and Vectors* **97**, 1–10 (1988).
10. Kim, K., Soldati, D. & Boothroyd, J. Gene replacement in Toxoplasma gondii with chloramphenicol acetyltransferase as selectable marker. *Science (80-.).* **262**, 911–914 (1993).
11. Herm-gotz, A. *et al.* Toxoplasma gondii myosin A and its light chain : a fast , single-headed , plus-end-directed motor. *EMBO J.* **21**, 2149–2158 (2002).
12. Ding, M., Clayton, C., Soldati, D., Biologie, M. & Feld, I. N. Toxoplasma gondii catalase : are there peroxisomes in Toxoplasma ? *J. Cell Sci.* **2419**, 2409–2419 (2000).
13. Tosetti, N. *et al.* Essential function of the alveolin network in the subpellicular microtubules and conoid assembly in Toxoplasma gondii. *Elife* **9**, 1–22 (2020).
14. Bastin, P., Bagherzadeh, A., Matthews, K. R. & Gull, K. A novel epitope tag system to study protein targeting and organelle biogenesis in Trypanosoma brucei. *Mol. Biochem. Parasitol.* **77**, (1996).
15. Uboldi, A. D. *et al.* Regulation of Starch Stores by a Ca2+-Dependent Protein Kinase Is Essential for Viable Cyst Development in Toxoplasma gondii. *Cell Host Microbe* **18**, 670–681 (2015).

3.2. Dissecting the trafficking and processing of RON13

In this sub-chapter, I'm presenting some results and data on RON13 that were conducted during my PhD but not included in the manuscript.

My journey with RON13 started by trying to map the ASP3-dependent cleavage site. First, we assessed the proteolytic activity of ASP3 on RON13 *in vitro.* The putative ASP3-dependent cleavage site is located in the region between the TMD and the kinase domain (peptide detected [F]^{257}AEHKSGGEKASR^{268}[E]) (Dogga *et al.*, 2017). The cleavage assay was done using a bacterial recombinant RON13 fragment (r-RON13) **(Fig 3.1 A)** and a recombinant r-ASP3. r-RON13 fragment was efficiently processed by r-ASP3 *in vitro* while the addition of 49c, an ASP3 inhibitor, prevent this cleavage **(Fig 3.1 A)**. This confirmed that RON13 is a direct substrate of ASP3. Using different mutated constructs, we were able to map the cleavage site of RON13 to the 6 amino acids ^{254}IAFAEH^{259} and we demonstrated that their mutation to alanine abrogated the cleavage *in vitro* **(Fig 3.1 A)**. Importantly, mutations in alanine of the amino acids surrounding this cleavage site (^{246}DRVI^{249} or ^{261}SGGE^{264}) did not inhibit RON13 cleavage by ASP3 (data not shown). However, while the mutation of IAFAEH motif abrogates the cleavage *in vitro*, ectopically expressed RON13$^{IAFAEH/AAAAAA}$-4myc was still processed *in vivo* **(Fig 3.1 B)**. Interestingly, the processed form of RON13$^{IAFAEH/AAAAAA}$-4myc **(Fig 3.1 B)** migrates at a higher molecular weight than the mature RON13^{WT}-4myc form suggesting the existence of an alternative cleavage site. This alternative cleavage is likely also mediated by ASP3 as it is inhibited by the addition of 49c. The cleavage of RON13 also affects its localization as the unprocessed form localizes to the whole organelle rather than just in the rhoptry neck probably due to the retention of the TMD **(Fig 3.1 C)**. The sorting between RONs and ROPs is still enigmatic and as the localization of RON13 changes upon cleavage by ASP3 **(Fig 3.1 C)**, studying the trafficking determinants of RON13 from the ER to the rhoptry neck represents a good opportunity to shed light on the mechanism of protein targeting to the rhoptries.

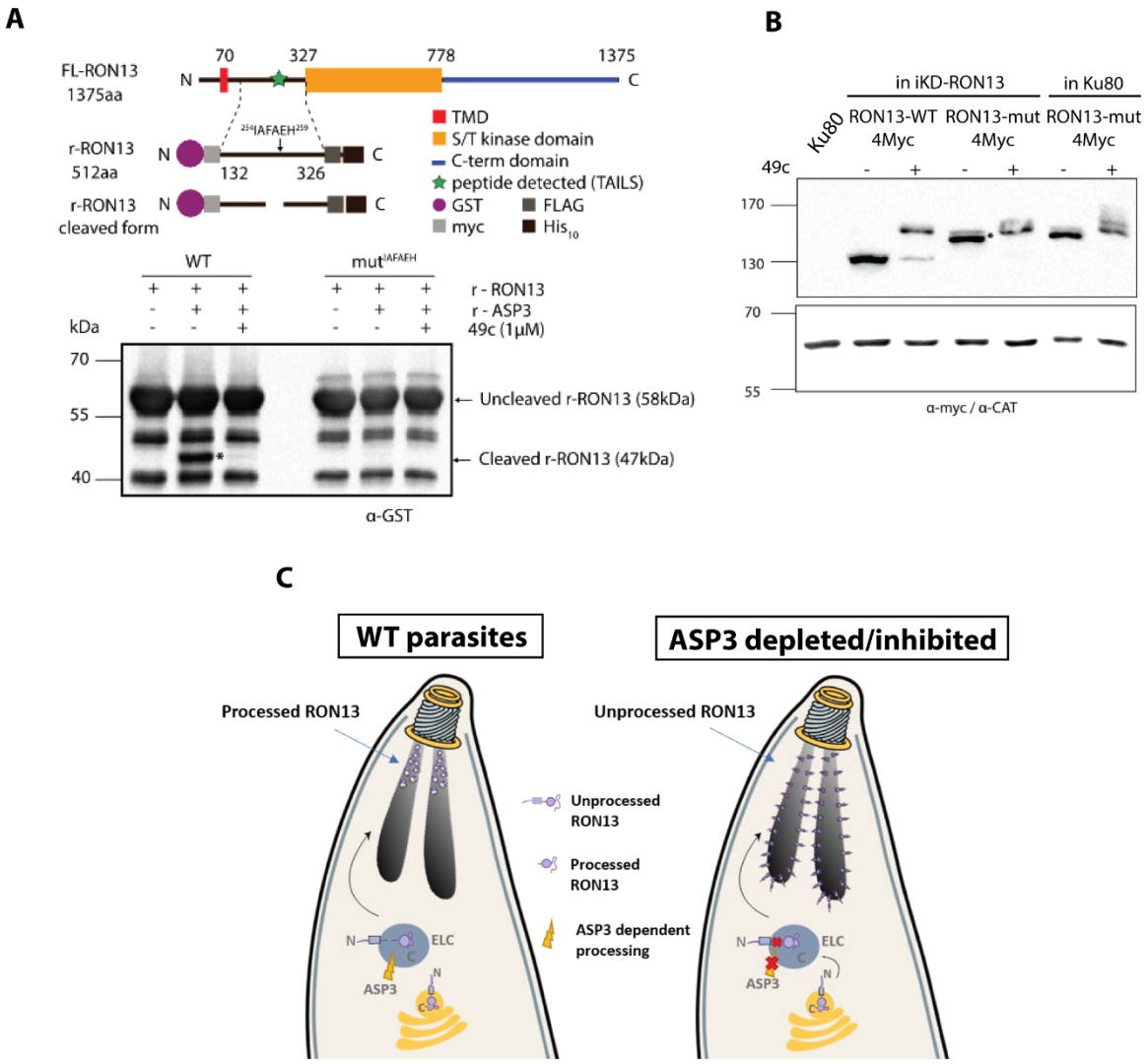

Figure 3.1 R**ON13 is a substrate of ASP3. A.** Scheme of full length RON13 (FL-RON13), the recombinant RON13 (r-RON13), and the recombinant cleaved form (r-RON13 cleaved form). Western blot shows the cleavage of r-RON13 using a recombinant ASP3 protease (r-ASP3). The cleavage is abrogated by using 49c that inhibits ASP3 activity. The mutated r-RON13 was not cleaved by r-ASP3 in absence of 49c. **B.** Western blot of the processing of the mutation in vivo. **C.** Schematic representation of RON13 and its processing by ASP3 and its fate in presence or in absence of cleavage. Without processing, RON13 is insoluble and is mistargeted to the whole rhoptry membrane.

We know from the cleavage test that RON13 loses its TMD, cleaved in the ELC by ASP3, and becomes soluble in the rhoptry neck. Does RON13 possess a rhoptry neck targeting signal or, associates with other proteins in the ELC that traffic to the rhoptry neck? In pursuance of these

questions, we first designed several RON13 truncated constructs that are devoid from the C-terminal domain and fused them with m-Cherry at their C-terminal ends. Our speculation was that if none of these constructs are sufficient to target RON13 to the rhoptries it hints at the C-terminal region downstream of kinase domain being indispensable for its correct localization. None of these truncations were sufficient to address the protein to the right localization **(Figure 3.2)**, but interestingly, construction 2 that stops just before the cleavage site (27 kDa) was sufficient to address it to the rhoptries but it was observed at the bulb and not the neck, probably through interaction with other rhoptry bulb proteins **(Figure 3.2 B).** These results emphase the important role of the C-terminal domain in RON13 trafficking to the rhoptry neck. This domain might be a targeting signal sequence or can play a role in the proper folding of the protein.

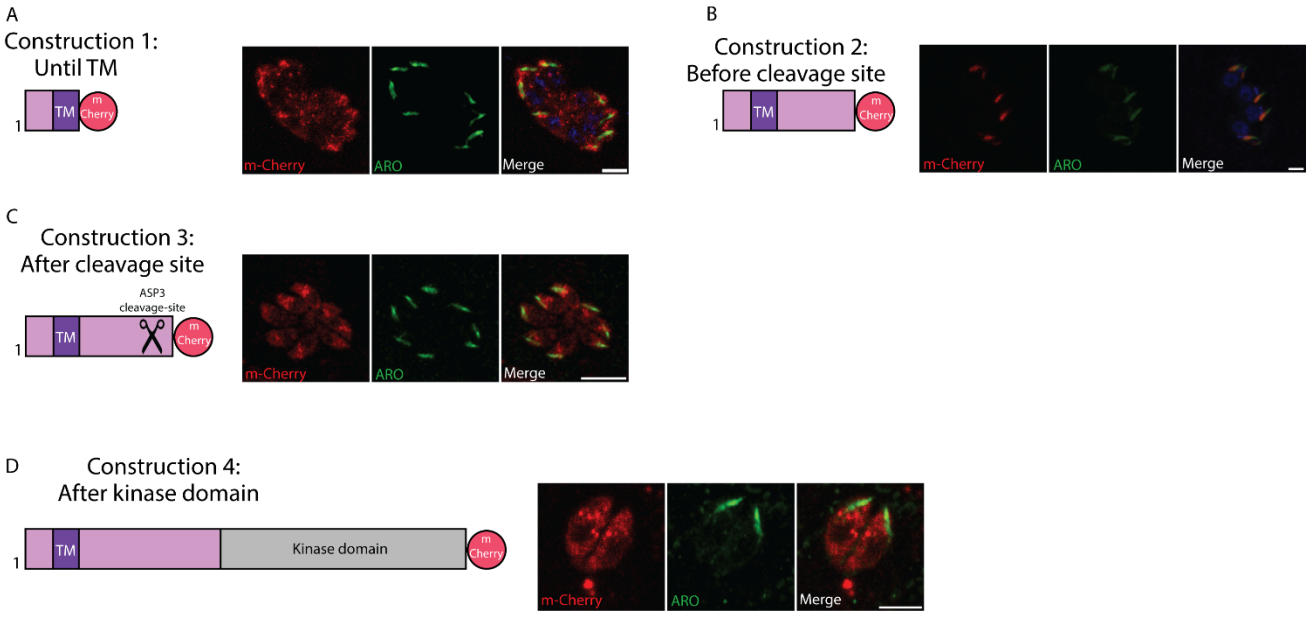

Figure 3.2 **Assessing RON13 trafficking *in vivo*. (A).** Construction 1 starts from ATG and stops just after the TMD. **(B).** Construction 2 starts from ATG and stops just before the cleavage site. **(C).** Construction 3 starts from ATG and stops just after the cleavage site. **(D).** Construction 1 starts from ATG and stops just after the kinase domain. For IFAs, we used anti.ARO antibodies to stain rhoptries (Green). mCherry staining for RON13 constructs in red. DAPI is used to stain DNA (Blue). Scale bar for all IFAs = 2µM.

The C-terminal extension (CTE) of RON13 is a unique feature located downstream the kinase domain. It is composed of 550 amino acids mainly arranged in α-helices clamping the kinase domain C-lobe **(Figure 3.3 A)**.

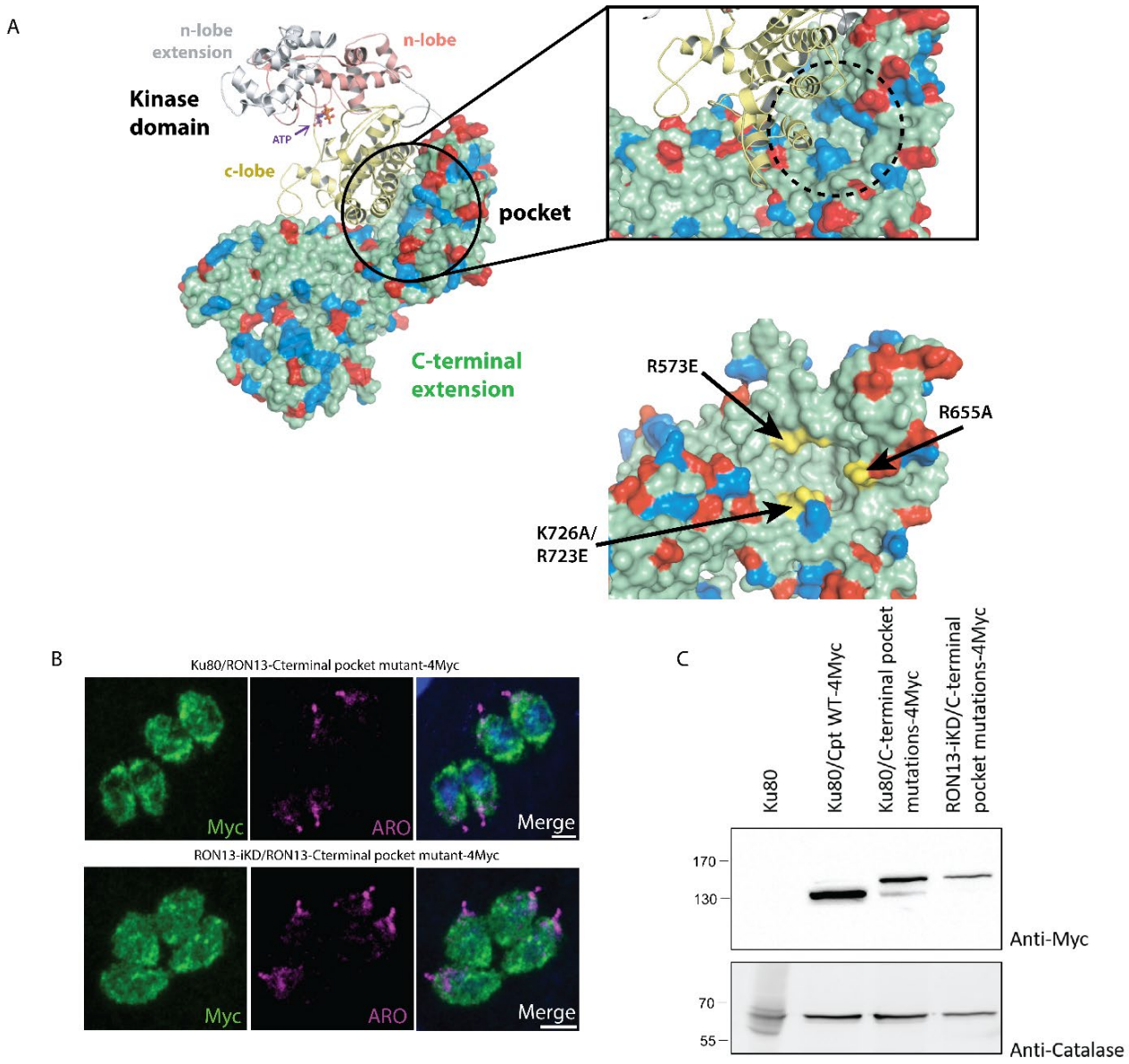

Figure 3.3 **The C-terminal extension of RON13. A.** Structure of RON13 kinase domain and surface representation of the C-terminal extension. In yellow are the four mutations introduced to the C-terminal pocket. **B.** IFAs showing the mislocalisation of RON13-Cterminal pocket mutant introduced as a second copy in WT (Ku80) or in RON13-iKD. Scale bar = 2µM. **C.** Western blot showing that the mutated protein is not processed *in vivo*.

We demonstrated that the CTE is important for RON13 stability and folding *in vitro* since the expression of the kinase domain alone and separating the kinase domain from the CTE by proteolytic cleavage led to a non-functional RON13 kinase. This was confirmed *in vivo,* since RON13 with four basic residues mutated in the CTE pocket **(Figure 3.3 A)** accumulated in vesicular structures **(Figure 3.3B)** and we also observed accumulation of pro-RON13 by western blot **(Figure 3.3 C)** suggesting that RON13 is not trafficked to the ELC anymore where ASP3 is active. This data speaks for a critical role of the CTE to ensure proper folding and trafficking through the secretory pathway probably through interaction with other rhoptry proteins.

3.3. Identification of novel rhoptry proteins in *T. gondii*

In the past years, the invasion and rhoptry secretion has been under the spotlight and many key molecular players and structures were identified. However, the mechanism that triggers rhoptry discharge is still unknown and proteins that play a role in this step are yet to be identified. Lately, genome-wide experimental datasets including the CRISPR/Cas9 screen (Sidik *et al.*, 2016) and the localization of organelle proteins by isotope tagging (LOPIT) (Barylyuk *et al.*, 2020), contributed to a better comprehension of Apicomplexa biology, especially for *T. gondii*, *P. falciparum* and *P. berghei*.

In this chapter, using these datasets, I describe our preliminary data to identify and characterize novel rhoptry proteins.

The main findings of this work are summarized as follow:

- We selected 9 proteins, predicted to be essential and to localize to rhoptries.
- We localized 7 of these proteins to the rhoptry organelle.
- Among the 7 proteins characterized, only LOPIT-1 was essential for parasite survival.

Author contributions for this work:

R.B.C conceptualized and designed the study. Alessandro Bonavoglia generated and performed some of the experiments concerning the characterization of LOPIT 6-9 under the supervision of **R.B.C**. **R.B.C.** generated all the other strains and performed all the other experiments.

3.3.1. Selection of candidates

To discover novel essential rhoptry proteins, we selected candidates using four criteria:

(1) Genes coding for uncharacterized or hypothetical proteins predicted to localize to the rhoptries, based on localization prediction LOPIT (Barylyuk *et al.*, 2020).

(2) Genes coding for proteins predicted to contain a transmembrane domain or a signal peptide.

(3) Genes exhibiting a negative fitness score from global CRISPR/Cas9 screen (≤ −2) (Sidik *et al.*, 2016).

(4) The cell cycle transcriptome profile (Behnke *et al.*, 2010).

We prioritized 9 genes that met the criteria **(Table 2)**.

Name	Gene ID	CRISPR score *Tg*	LOPIT Localisation	Signal Peptide	Transmembrane Domain (TM)	Molecular Weight (kDa)	Tg	Hh	Nc	Sn	Et	Ta	Bb	Pf	Pb	Cp	G
LOPIT 1	TGGT1_242820	-5.03	rhoptries 1	Yes	0	21.21	●	●	●	○	○	○	○	○	○	○	○
LOPIT 2	TGGT1_223920	-4.41	rhoptries 1	YES	1	229.92	●	●	●	●	●	○	○	●	●	○	○
LOPIT 3	TGGT1_297960	-3.48	rhoptries 1	YES	1	238.66	●	●	●	●	●	○	●	●	●	●	○
LOPIT 4	TGGT1_305590	-3.05	rhoptries 2	NO	9	206.11	●	●	●	●	●	●	○	●	●	●	○
LOPIT 5	TGGT1_276210	-2.94	rhoptries 1	YES	0	94.51	●	●	●	●	●	○	○	○	○	○	○
LOPIT 6	TGGT1_315470	-2.83	rhoptries 2	YES	2	135.83	●	●	●	○	○	○	○	○	○	○	○
LOPIT 7	TGGT1_210820	-2.68	rhoptries 2	NO	10	113	●	●	●	○	●	○	○	○	○	○	○
LOPIT 8	TGGT1_225200	-2.54	rhoptries 1	YES	0	160.96	●	●	●	●	●	○	○	○	○	○	○
LOPIT 9	TGGT1_246710	-2.18	rhoptries 2	NO	3	50	●	●	●	●	●	○	○	○	○	○	○

Table 2 **List ID of the investigated candidates.** Table includes the predicted localization (LOPIT) (Barylyuk et al., 2020), the conferred fitness score (Sidik et al., 2016), number of predicted TM, the molecular weight and conservation across Apicomplexa.

LOPIT-2 was initially described in *T. gondii* proteome analysis of rhoptry organelles (Bradley *et al.*, 2005) and annotated as RON3. In *P. falciparum,* PfRON3 was re-assigned as a rhoptry bulb protein, interacting with PfRON2, PfRON4 and PfRAMA during invasion (Ito *et al.*, 2011, 2021). LOPIT-3 is annotated as RON6 in *P. falciparum,* but its function is still unknown (Proellocks *et al.*, 2010). LOPIT-4 is described as an ABC transporter (https://toxodb.org). LOPIT-5 was assigned to a family of phosphoglycerate mutase proteins (McPhillie *et al.*, 2016). The remaining LOPITs were annotated as hypothetical proteins. LOPIT-5, LOPIT-8 and LOPIT-9 are coccidian specific whereas LOPIT-1, LOPIT-6 and LOPIT-7 are conserved in some of the coccidian species. LOPIT-2 is conserved across coccidian and hemosporidia parasites. LOPIT-3 is conserved across Apicomplexa but absent in gregarines and *Theileria* and LOPIT-4 is missing in *Babesia* and gregarines. Only LOPIT-2 and LOPIT-3 were identified as ASP3 substrates in the N-terminome analysis (Dogga *et al.*, 2017). All LOPITs showed a cell cycle similar to rhoptry proteins (RON4 and ROP18 as examples) except for LOPIT 1 that showed a different cell cycle that differed from rhoptry proteins **(Figure 3.4)**.

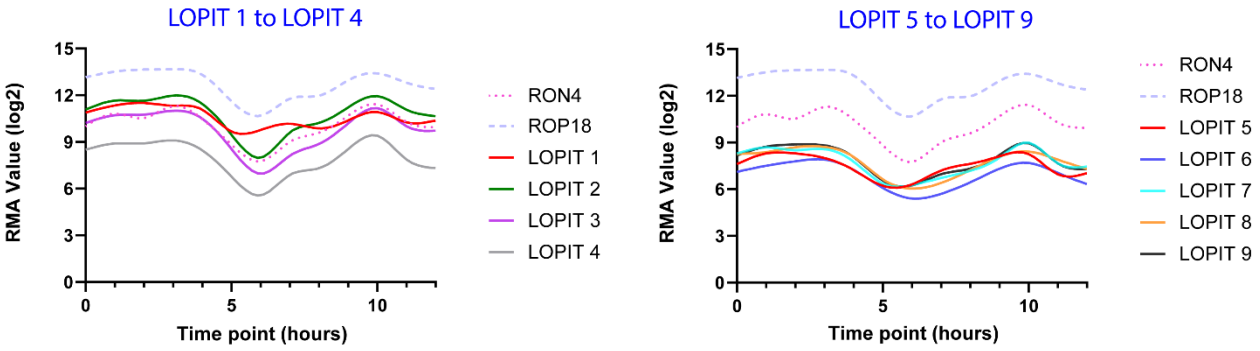

Figure 3.4 **Cell cycle transcriptomic profile of candidate genes.** Cell cycles were compared to RON4 and ROP18 for control.

3.3.2. Tagging and phenotyping of the candidates

Candidate genes were tagged by 3-Ty tags at the 3' end of the coding sequence to assess their localization, and we opted for the U1 mediated downregulation approach for functional

characterization **(Figure 3.5 A)**. The U1 small nuclear ribonucleoprotein (snRNA), are part of the spliceosome and are important for RNA splicing and maturation (Will and Lührmann, 2011). The RNA level of a gene of interest can be regulated by inserting a U1 recognition sequence at the 3'UTR (Pieperhoff *et al.*, 2015). This approach was used in parasites carrying a dimerizable Cre (DiCre). Addition of rapamycin induces the Cre dimerization and excision of the sequence between the LoxP sites (Hunt *et al.*, 2019). The U1 snRNA binds to the U1 recognition sequence and induces the destabilization of the RNA and the inhibition of protein translation.

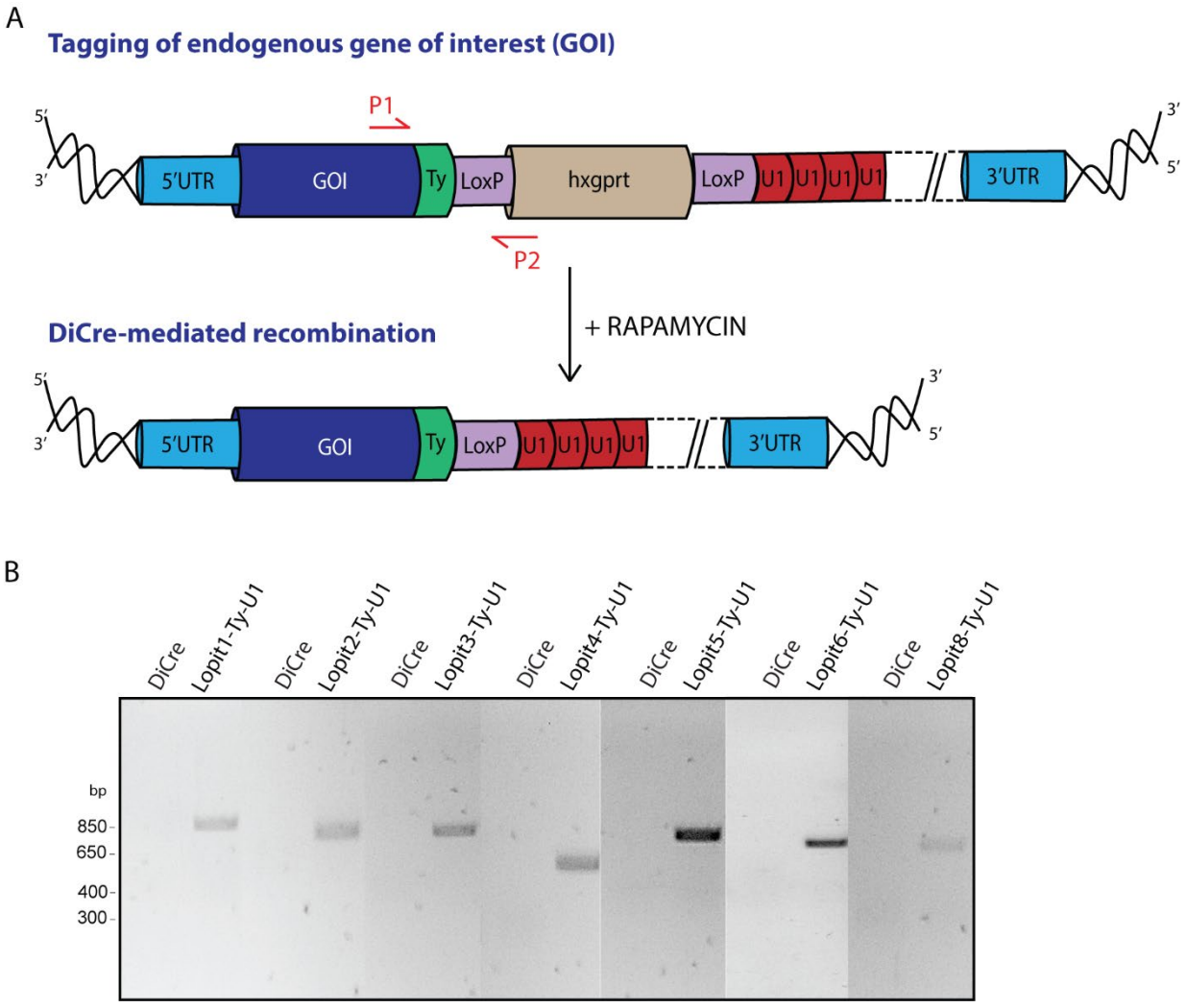

Figure 3.5 **Tagging and down-regulation of the candidate proteins using the U1 down-regulation strategy. A.** Genetic strategy used to tag the genes of interest. **B.** Integration PCR on the LOPITs clonal lines and DiCre parental line.

A CRISPR-Cas9 mediated tagging was performed at the endogenous locus for all candidates with the 3xTy-U1 cassette. Tagging was successful for all LOPITs except for LOPIT-7 and LOPIT-9. This failure of finding live parasites after transfections of LOPIT-7 and LOPIT-9 can indicates that the C-terminal tagging is not tolerated. Integrations of the constructs were confirmed by PCR **(Figure 3.5 B)**. The efficient downregulation of protein expression and levels by addition of rapamycin was monitored by western blot **(Figure 3.6)**. The western blots showed that almost all the tagged proteins migrated close to the expected molecular weight (MW) shown in **Table 2**. LOPIT-3 migrated at a MW between 70 kDa and 100 kDa instead of 238 kDa **(Figure 3.6 C)**.

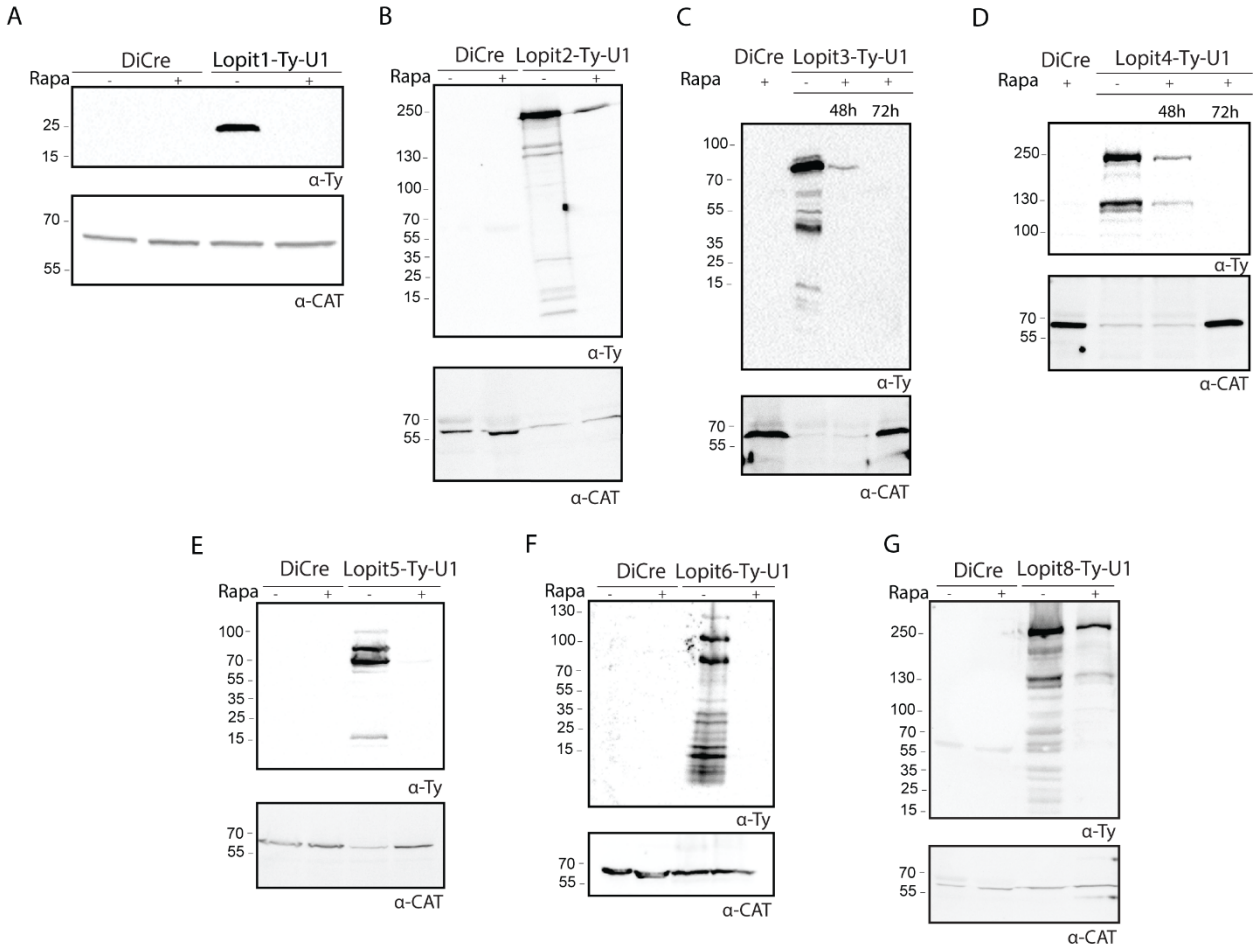

Figure 3.6 **Assessing the down-regulation of the candidate proteins using western blot A-G.** Western blot using anti-Ty antibodies showing the downregulation of the tagged proteins compared to the parental line DiCre. Catalase (anti-CAT) is used as a loading control. Images representative of three biologically independent experiments.

This can be the product of the processing by ASP3. However, LOPIT-6 (expected at 135 kDa) and LOPIT-8 (expected at 160 kDa) show processed products **(Figure 3.6 F and G)**. This can be due to an ASP3-independent processing or degradation products. Downregulation of LOPIT-2 and LOPIT-8 was not efficient as a band was still observed even after 48h of rapamycin treatment **(Figure 3.6 B and G)**.

Immunofluorescence showed that all selected proteins are localizing to the rhoptries **(Figure 3.7 A-G)** as they partially co-localize with ARO, a marker of the entire rhoptry surface. LOPIT-1 **(Figure 3.7 A)**, LOPIT-2 **(Figure 3.7 B)** and LOPIT-5 **(Figure 3.7 E)** localized to the rhoptry bulb confirming that RON3 (LOPIT-2) is indeed a bulb protein in *T. gondii* as well. LOPIT-3 and LOPIT-6 **(Figure 3.7 C and G)** localizes to the tip of the rhoptry organelle. LOPIT-4 localized to the entire organelle **(Figure 3.7 D)** whereases LOPIT-8 showed a vesicular staining around the rhoptry organelle (**Figure 3.7 G)**.

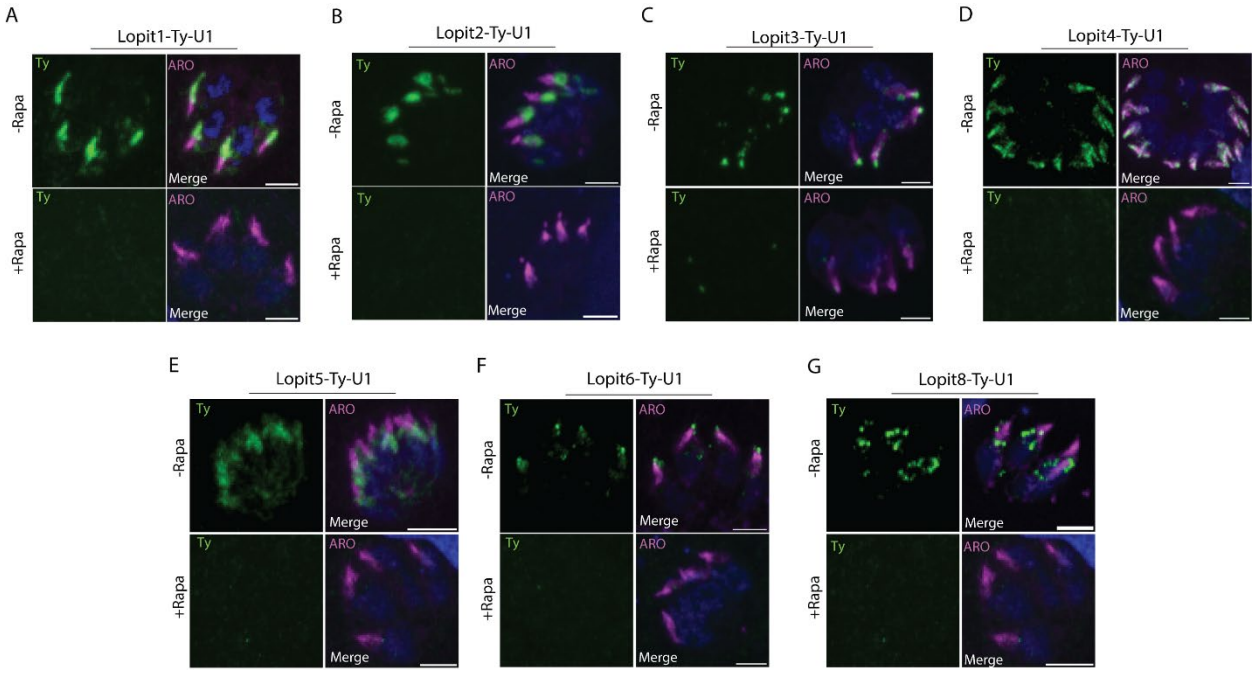

Figure 3.7 **Localization of the selected candidates. A-G.** IFAs of intracellular DiCre and LOPITs-Ty-U1 parasites using anti -Ty antibodies (green). An anti-ARO antibody was used to stain the rhoptry organelles. Scale bar = 2µm. Images representative of three biologically independent experiments.

To assess the overall impact of these protein depletion on the parasite lytic cycle, plaque assays were performed on DiCre parasites (parental strain) and the mutant parasites, incubated with or without rapamycin for 7 days. The fitness of the parasites was assessed by the size of the lysis plaques rather than the number.

All LOPITs depleted parasites showed a normal plaque formation as compared to the parental strain **(Figure 3.8 A-G)**, except for LOPIT-2 and LOPIT-3 that showed a partial reduction in size **(Figure 3.8 B and C)** and LOPIT-1 that led to a dramatic loss of parasite fitness **(Figure 3.8 A)** confirming the essential role of LOPIT-1 for the lytic cycle of *T. gondii.* These results will be discussed in more detail in the discussion section.

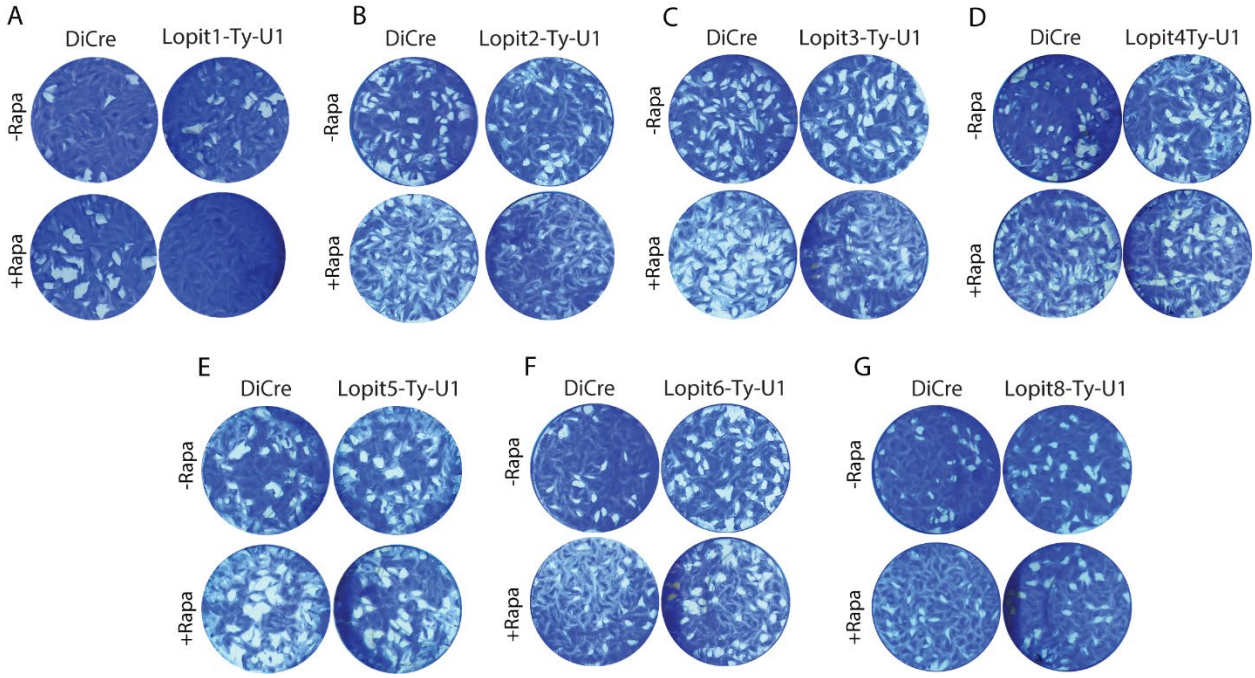

Figure 3.8 **Essentiality assessment for the selected candidates. A-G.** Plaque assays to assess the overall fitness cost of depletion of the selected candidates. DiCre was used as a control (n=3).

3.4. *Toxoplasma gondii* RAP1 is critical for rhoptry discharge and invasion

In the previous chapter, we identified TGGT1_242820 (LOPIT-1) as a rhoptry bulb protein essential for parasite survival. In this chapter, we functionally characterized this protein.

The main findings of this work are summarized as follow:

- TGGT1_242820 codes for a rhoptry protein that localizes to the bulb and the tip of rhoptries.
- TGGT1_242820 product is important for parasite survival.
- Depletion of TGGT1_242820 lead to a severe defect in invasion.
- Parasite depleted in TGGT1_242820 are unable to discharge the rhoptries.
- TGGT1_242820 protein has a dynamic localization.
- TGGT1_242820 protein colocalizes with other molecular players of rhoptry secretion.

Author contributions for this work:

R.B.C. and Gaëlle Lentini conceptualized and designed the study. Alessandro Bonavoglia performed the microneme secretion and the intracellular growth under the supervision of **R.B.C**. Bohumil Maco performed the EM experiment. Cryofixation was performed by Marine Laporte in Paul Guichard lab at the faculty of sciences. **R.B.C.** generated all the other strains and performed all the other experiments.

3.4.1. TgRAP1 is a novel rhoptry protein important for *T. gondii* lytic cycle

TGGT1_242820 (here referred to as *rap1* for **R**hoptry **A**ssociated **P**rotein **1)** is reported to be a fitness conferring gene, coding for a protein of 22 kDa with a predicted signal peptide and no identifiable domains **(Figure 3.9 A)**. Interestingly, RAP1 shows an atypical amino acids composition made of alternative stretches of acidic and basic residues **(Figure 3.9 A)**. Though RAP1 has no homolog in *Plasmodium spp.* **(Table 2)**, the *Plasmodium* Apical Sushi protein (PfASP) which is also known as PfRON1 also contains repetition of acidic and basic residues **(Figure 3.9 B)** (O'Keeffe *et al.*, 2005).

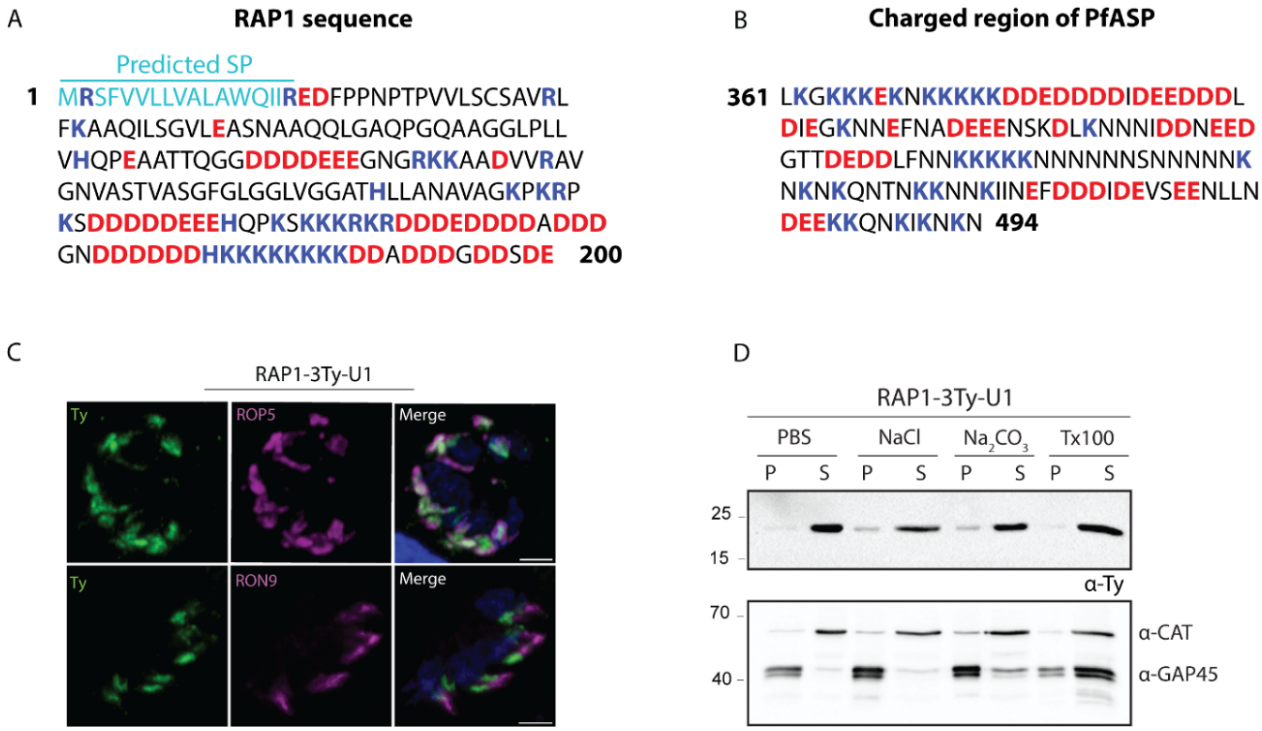

Figure 3.9 **RAP1 is an essential novel rhoptry protein A.** Amino-acids composition of RAP1. Predicted signal peptide is highlighted in light blue. In dark blue are highlighted the positively charged residues and in red the negatively charged ones **B.** Amino-acids sequence of the charged region of PfASP. **C.** IFA of intracellular RAP1-3Ty-U1 parasites using anti-Ty antibodies (green), anti-ROP5 and anti-RON9 antibodies (magenta) stained the rhoptry bulb and rhoptry neck, respectively. DAPI in showed in blue. Scale bar = 2µm. **D.** Solubility assay of RAP1-3Ty-U1. P = pellet. S = supernatant. Catalase (cytoplasmic protein) is used as a control soluble in all conditions. GAP45 (anchored to IMC and PM) is used as a control only soluble by Tx-100.

Epitope tagging and fusion with the DiCre-mediated conditional U1 gene silencing system confirmed that the protein localized to the bulb of the rhoptries (**Figure 3.9 C**) and essential for parasite survival (**Figure 3.8 A**). To investigate the solubility of RAP1, we performed a solubility assay. The pellets were resuspended with PBS, PBS+NaCl, PBS+Na_2CO_3 and PBS triton X-100 (1% Triton X-100). In all conditions, we observed an enrichment in the supernatant (**Figure 3.9 D**). This demonstrates that RAP1 is a soluble rhoptry protein.

As shown previously in **Figure 3.8 A**, depletion of RAP1 (LOPIT-1) have a negative impact on the parasite lytic cycle. Complementation of RAP1-3Ty-U1 at the UPRT locus with a second copy of RAP1-4Myc (RAP1-3Ty-U1 + CptWT-RAP1-4Myc) **(Figure 3.10 A)** fully rescued the phenotype in the presence of rapamycin **(Figure 3.10 B)**. However, the second copy of RAP1 (RAP1-iKD/RAP1wt), showed an additional localization of the protein at the tip of the rhoptry as observed by immunofluorescence **(Figure 3.10 C)**. To investigate this, we first checked the solubility of the RAP1 extra copy. No difference in the solubility was observed **(Figure 3.10 D)**. Then we tagged the endogenous RAP1 in the RHΔKu80 strain with either 2xTy or 3xMyc tags. Immunofluorescence on intracellular parasites confirmed the double localization of RAP1 **(Figure 3.10 E)**. This difference in localization between both strains can be explained by the fact that in the conditional U1 gene silencing system, the LoxP sequences within the 3'UTR seems to affect the gene expression and a decrease in mRNA and protein level was observed (Pieperhoff *et al.*, 2015). This can also highlight the fact that, in intracellular parasites, we might have a higher level of protein expression in the bulb compared to the rhoptry tip. Finally, RAP1 was expressed in forming daughter cells as shown with the IMC1 staining **(Figure 3.10 F)**.

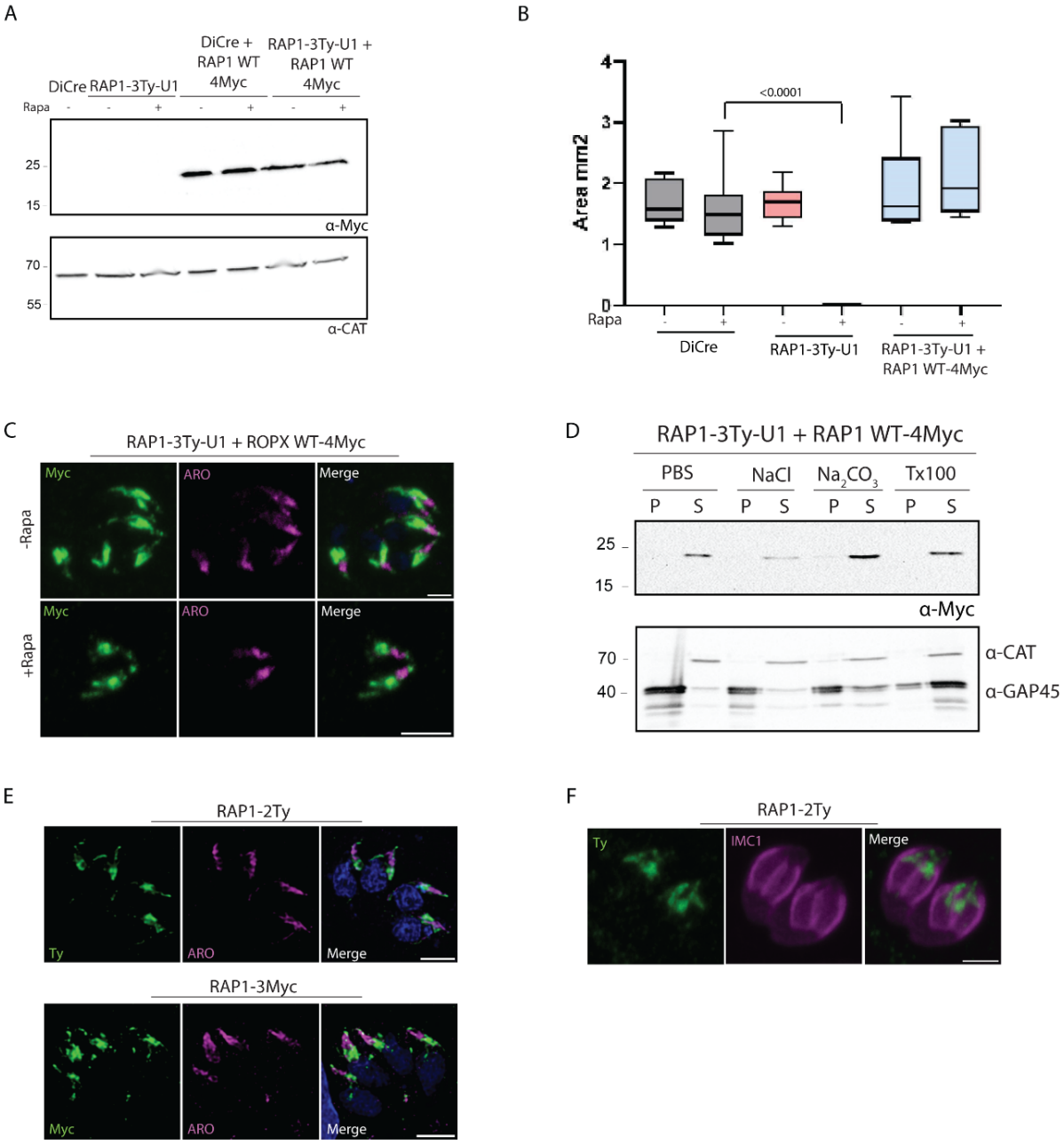

Figure 3.10 **Functional complementation of RAP1. A.** Western blot using anti-Myc antibodies showing the regulation of the complemented strain compared to the parental line DiCre, RAP1-3Ty-U1 and the parental strain complemented with a second copy of RAP1 as a control. Catalase (anti-CAT) is used as a loading control. **B.** Quantification of plaque assays for DiCre, RAP1-3Ty-U1 and complemented RAP1 strain. (n=3) **C.** IFA using anti-Myc antibody (green) showing the additional localization of RAP1 at the rhoptry tip. Anti-ARO antibody is used to stain the rhoptry organelle (magenta). Scale bar = 2µm. **D.** Solubility assay of the complemented RAP1-3Ty-U1. P = pellet. S = supernatant. **E.** IFAs of RAP1-2Ty and

RAP1-3Myc showing the double localization of RAP1 in intracellular parasites. Scale bar = 2µm. **F.** IFA of RAP1-2Ty intracellular parasites using anti-Ty antibody (green) and anti-IMC1 antibody (magenta). RAP1 is observed in daughter cells. Scale bar = 2µm.

To produce specific RAP1 antibodies, rabbits were injected with RAP1 recombinant protein (r-RAP1) produced in insect cells. Purification of the r-RAP1 is shown by the Coomassie gel and western blot **(Figure 3.11 A-B)**. r-RAP1 was further loaded on a Superdex size exclusion chromatography column **(Figure 3.11 C)** and fractions enriched in r-RAP1 **(Figure 3.11 D)** were eluted, pulled and concentrated to 1mg/mL.

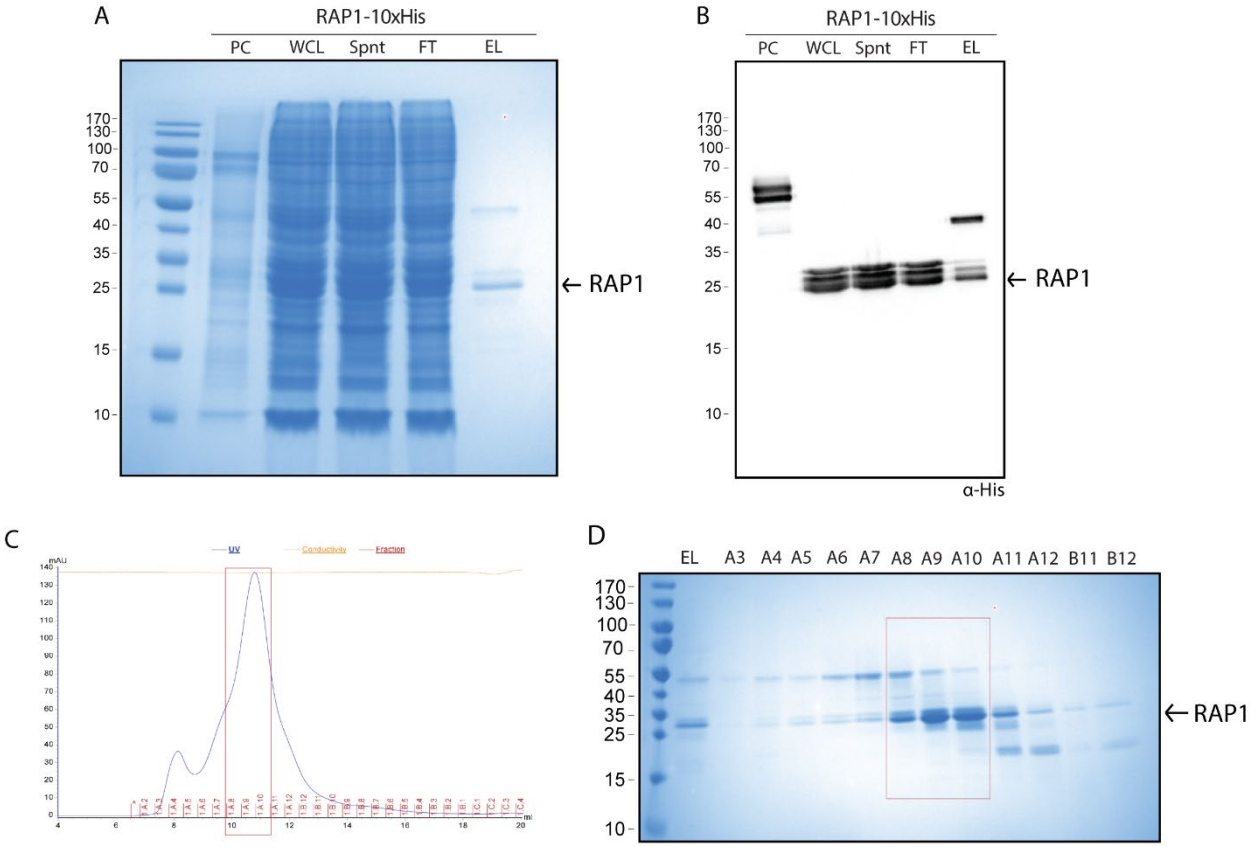

Figure 3.11 **Purification of RAP1 specific antibodies. A.** Coomassie gel of r-RAP1 purification. PC. Positive control for the His tag. WCL. Whole cell lysate. Spnt. Supernatant (soluble fraction). FT. Flowthrough EL. Elution. **B.** Western blot od r-RAP1 purification using anti-His antibody to detect r-RAP. **C.** Size-exclusion chromatography elution profile of r-RAP1. **D.** Coomassie gel of the eluted r-RAP1. Highlighted in the red box are the fractions pooled and used to generate the antibody.

However, western blot showed that both antibodies were not specific to RAP1 comparing to anti-Ty antibodies used to detect the tagged protein **(Figure 3.12 A-C)**. Immunofluorescence showed that these antibodies did not recognize RAP1 and displayed a high background. Therefore, these antibodies were not used in the study **(Figure 3.12 D)**.

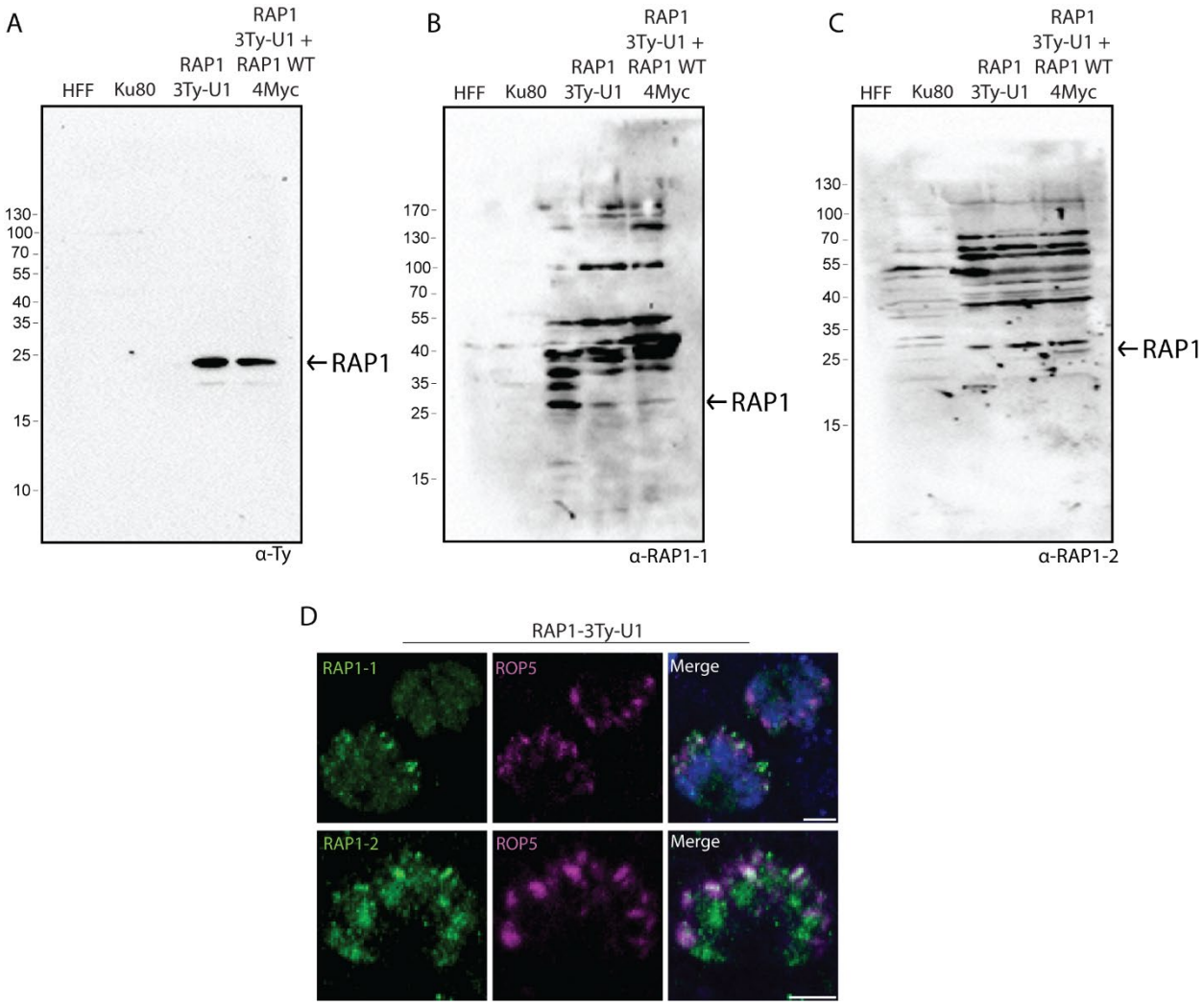

Figure 3.12 **Assessing the specificity of produced RAP1 antibodies. A.** Western blot used as control to for the specificity of RAP1 antibodies. Anti-Ty antibody was used to detect RAP1 in RAP1-3Ty-U1 and RAP1-3Ty-U1 + RAP1 WT-4Myc parasites. **B.** Western blot using anti-RAP1-1 antibodies. **C.** Western blot using anti-RAP1-2 antibodies. **D.** Immunofluorescence using RAP1-1 and RAP1-2 antibodies. Scale bar = 2µm.

3.4.2. RAP1 depletion leads to rhoptry discharge and invasion defects

This severe impairment in plaque formation indicates a severe defect in one or several steps of the lytic cycle. To point out which step is impacted by the absence of RAP1, specific assays assessing invasion, replication and egress of the parasites were performed. While host cell invasion was severely impaired upon depletion of RAP1 **(Figure 3.13 A)**, intracellular growth and induced egress from host cells were not affected **(Figure 3.13 B-C)**. ASP3 is a protein essential for invasion and rhoptry discharge and was used as a control in some of these experiments (Dogga *et al.*, 2017).

As previously mentioned, rhoptry and microneme proteins are key players in the invasion process. RAP1 depleted parasites are not impaired in microneme secretion **(Figure 3.13 F)** and showed proper positioning of rhoptry organelles at the apical end in intracellular parasites by EM **(Figure 3.13 G)**. Moreover, the rhoptry proteins seems to be properly expressed and targeted to the organelles in absence of RAP1, as observed for example with RON9 and ROP5 which seem to exhibit normal localization **(Figure 3.13 D)** and level of expression **(Figure 3.13 E)** in the absence of RAP1.

The severe defect in invasion, thus, might be the consequence of a defect in the discharge of rhoptry content. This was tested by assessing rhoptry organelle discharge by analyzing the empty vacuoles (e-vacuoles) formation in the host cells at the time of invasion upon treatment of parasites with cytochalasin D (CytD) (Hakansson *et al.*, 2001) **(See section 5.3.2)**. CytD is an inhibitor of actin polymerization, which blocks the motility and the invasion of the parasite without impairing rhoptry and microneme secretion (Hakansson *et al.*, 2001; Kessler *et al.*, 2008). RAP1 depleted parasites were severely impaired in rhoptry discharge to a similar extend as reported for ASP3-iKD (Dogga *et al.*, 2017) **(Figure 3.13 H)**.

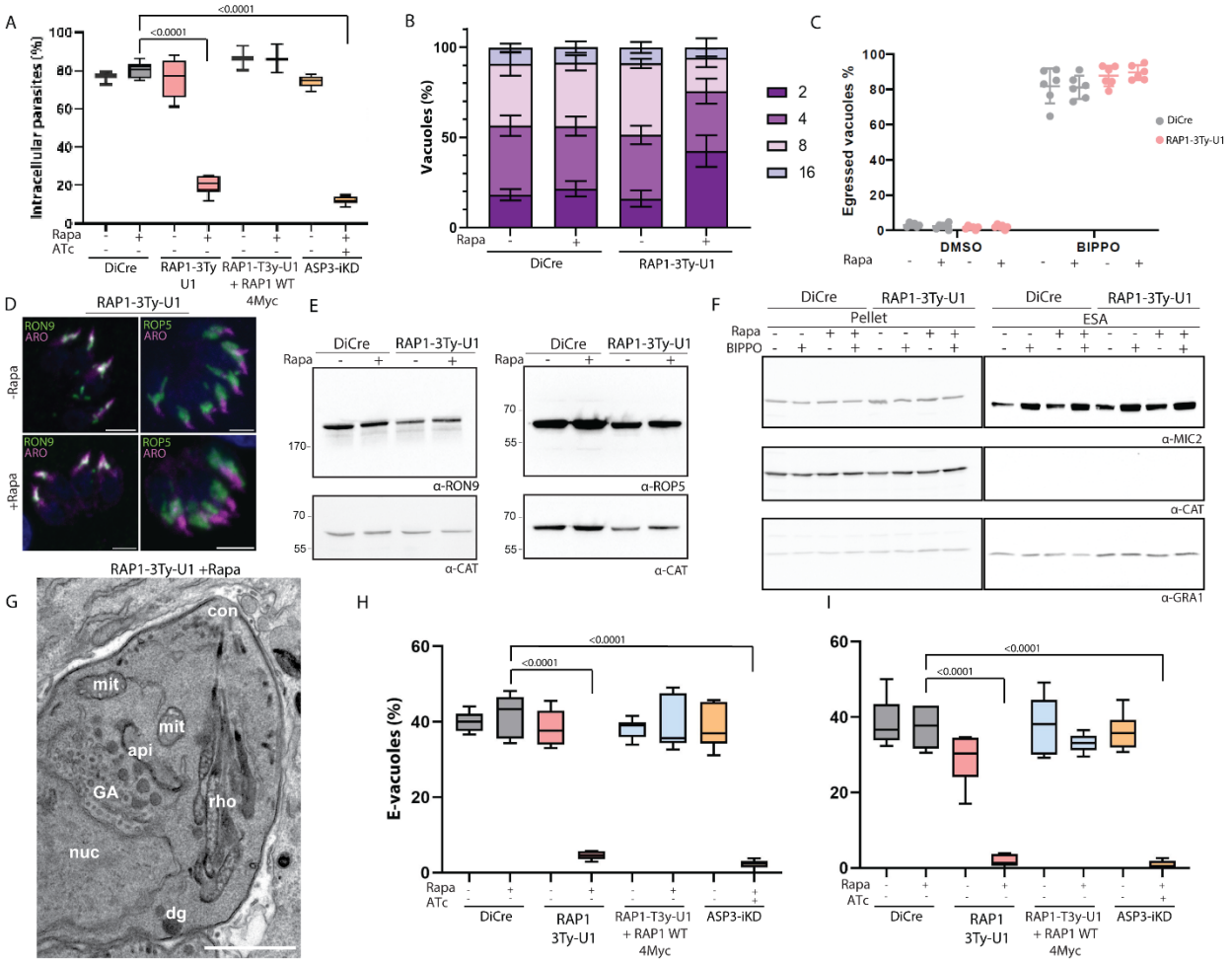

Figure 3.13 **RAP1 is important for invasion and rhoptry secretion. A.** Red/Green invasion assay showing that depletion of RAP1 impairs the invasion of the parasite (n=3). **B.** Intracellular replication assay. Graph representing the number of parasites per vacuole observed at 36h post-invasion (n=3). **C.** Induced egress assay. Graph representing the percentage of ruptured vacuoles following treatment with the egress inducer BIPPO for DiCre and RAP1-3Ty-U1 (n=3). **D.** IFA using anti-ARO (magenta), anti-ROP5 and anti-RON9 antibodies (green) that shown a normal localization of rhoptry proteins in absence of RAP1. DAPI in showed in blue. Scale bar = 2µm **E.** Western blots showing a normal expression of ROP5 and RON9 in absence of RAP1. **F.** Microneme secretion of extracellular parasites induced by BIPPO. ESA = supernatant. Catalase is used as a lysis control (should not be present in ESA) and GRA1 is used as a loading control. MIC2 secretion (ESA) is identical with or without rapamycin (n=3). **G.** Electron microscopy of parasites treated 48h with rapamycin and showing a normal localization of rhoptry organelles. Scale bar= 1µm. **H.** E-vacuole assay to assess the ability of the parasite to discharge ROP1 into the host cell (n=3). ASP3 is used as a negative control. ASP3 is conditionally depleted in presence of anhydrotetracycline (ATc). **I.** Phospho-STAT6 assays to assess the ability of the parasite to discharge ROP16 into the host cell, phosphorylating host STAT6 in the nucleus (n=3).

Because e-vacuole formation likely requires proper discharge of the membranous as well as proteinaceous materials from the rhoptry, we performed another rhoptry secretion assay based on the ROP16-dependent phosphorylation of host STAT6. Upon invasion, parasites inject their rhoptries content into the host cells. ROP16 is a rhoptry kinase secreted during invasion that modulates the host cell transcription by activating a signal transducer and activator of transcription (STAT) signaling pathway. Specifically, ROP16 phosphorylates and activates STAT6, which then translocate to the nucleus and activates the transcription of a key host cytokine, interleukin-12 (Ong *et al.*, 2010). Cells infected with depleted RAP1 parasites showed less phosphorylated STAT-6 positive nucleus than cells infected with wild-type parasites **(Figure 3.13 I)**, strengthening the claim that upon RAP1 disruption, injection of rhoptries is impaired.

In conclusion, these results strongly support that depletion of RAP1 compromises the ability of the parasites to discharge their rhoptry content, explaining the severe block in invasion.

3.4.3. RAP1 localization during invasion

As described before, rhoptry secretion relies on an arsenal of proteins located to the rhoptry secretion apparatus at the tip of the parasite (ben Chaabene *et al.*, 2021; Cova *et al.*, 2022; Sparvoli and Lebrun, 2021). Given the intriguing dual localization of RAP1 observed in intracellular parasites we sought to investigate this localization in extracellular parasite during and after invasion.

To assess RAP1 localization during host cell invasion, we used the RAP1-2Ty strain. Invasion was blocked in presence of cytochalasin D (CytD) a drug that prevent actin polymerization and we looked at the staining of RAP1 in these extracellular parasites. Interestingly, the staining of RAP1 at the tip of the rhoptry seems more intense and more distinct in extracellular parasites comparing to intracellular parasites **(Figure 3.14 E and Figure 3.10 E)**. Surprisingly, even though no staining was observed at the rhoptry tip in RAP1-3Ty-U1 intracellular strains, extracellular

parasites treated with CytD shows an accumulation similar to the one observed with RAP1-2Ty **(Figure 3.14 A)**. This suggests a higher accumulation or expression of RAP1 at the tip of the rhoptries at the time of invasion. In some parasites, RAP1 staining was observed at the rhoptry neck **(Figure 3.14 A)**. To further analyze this dynamic localization, we first checked the protein localization in the absence of host cells. Parasites were incubated on gelatin-coated coverslips and fixed after a 30s centrifugation. We observed the same localization, with a staining at the bulb and at the tip of the rhoptry with a colocalization with the rhoptry neck **(Figure 3.14 B)**. We then performed a time course infection, by synchronizing the invasion with cold (incubation on ice) and fixing the parasites at different time points post-invasion **(Figure 3.14 C-E).** The percentage on intracellular parasites at each time point was also quantified **(Figure 3.14 F)**. We can interestingly observe a highly dynamic change in the localization of RAP1, with the absence of RAP1 signal at 15 minutes to 1-hour post-invasion **(Figure 3.14 C and E)**.

After 4 hours, the signal of RAP1 is back as a vesicular staining observed around the rhoptry in 60% of the parasites whereas in almost 35% the staining was observed scattered at the bulb **(Figure 3.14 C and E)**. At that time, the parasite is not yet replicating and therefore these vesicles are distinct from the immature rhoptries that are present in dividing parasites. 6 hours post-invasion, a staining around the bulb is observed in almost 70% of the parasites with a vesicular staining still observed in around 25% of parasites **(Figure 3.14 C and E)**. Finally, 24 hours post-invasion, at the time where the parasites have gone through several replication cycle, a staining is observed at the tip and at the rhoptry bulb **(Figure 3.14 D)**. All these observations confirm a highly dynamic localization of RAP1, maybe, via a degradation of the vesicles just after invasion and the start of a new cycle of RAP1 expression when the parasite is inside. This also raised the question about the localization of RAP1 and whether it is inside the lumen or it is localized to the rhoptry surface (in vesicles or exposed in the cytoplasm). Additionally, the expression profile of RAP1 was different from other luminal rhoptry proteins **(Figure 3.4)**.

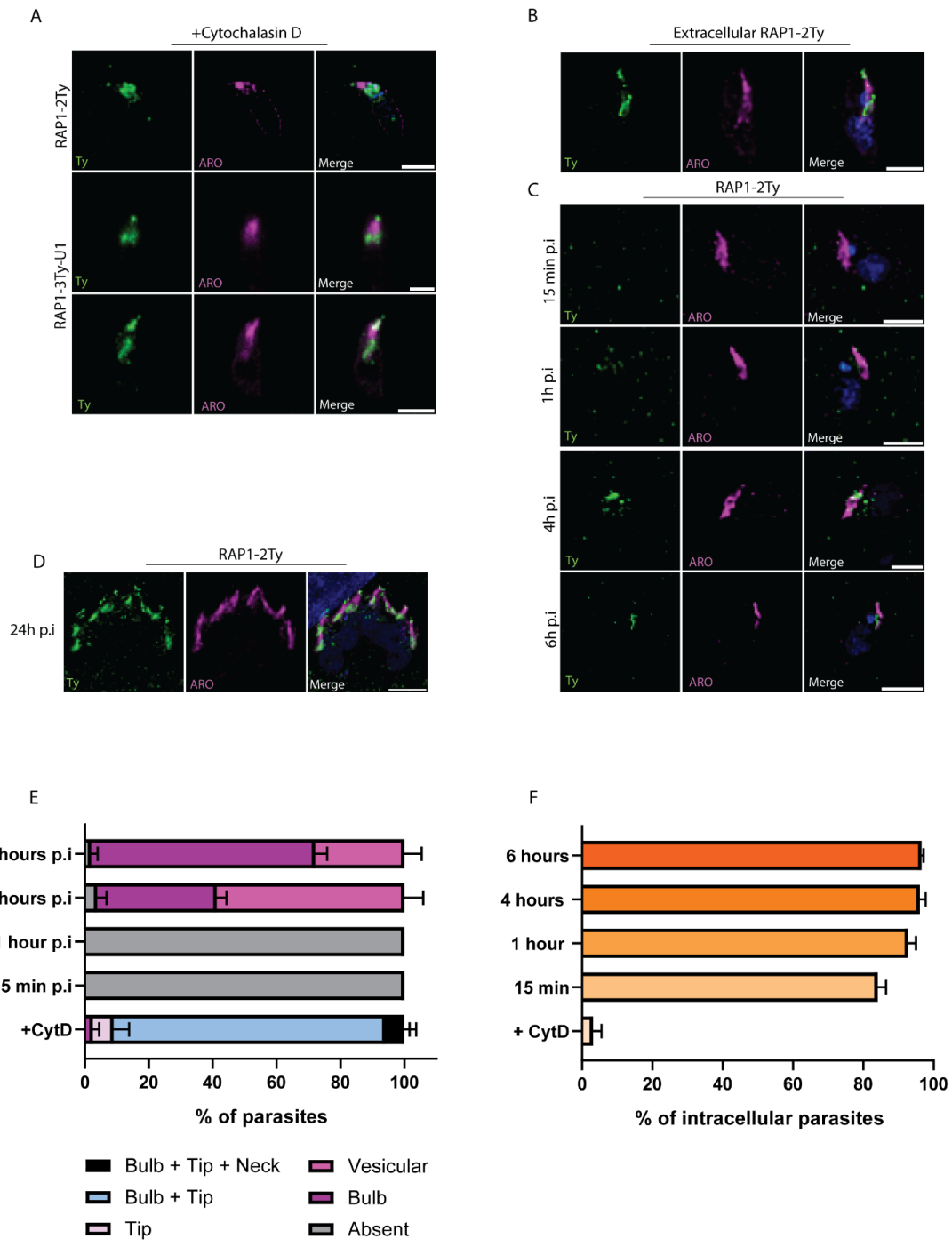

Figure 3.14 **RAP1 shows a highly dynamic localization at the time of invasion. A.** IFAs of extracellular RAP1-2Ty or RAP1-3Ty-U1 parasites in presence of cytochalasin D. **B.** IFAs of extracellular parasites incubated or not on gelatin-coated coverslips. **C.** IFAs of RAP1-2Ty parasites fixed at different time points post-infection. Anti-Ty antibody (green) is used to stain RAP1. Anti-ARO antibody is staining the rhoptry organelle. Counter-staining of DNA with DAPI (blue). Scale bar = 2µm. **D.** IFA of RAP1 24h post-invasion.

Scale bar = 2µm. **E.** Quantification of RAP1 staining at different time points post-invasion (n=3). **E.** Quantification of invasion of parasites at different time points post-invasion (n=3).

To further scrutinize RAP1 localization, RAP1 was tagged with a "mini auxin-induced degron" cassette followed by 3xTy tags (RAP1-mAID-3Ty) at the C-terminus locus in a TiR1 parental strain. Addition of auxin (indole-3-acetic acid or IAA) leads to a rapid ubiquitination of the mAID fused protein by the TiR1 complex and the degradation by the proteasome. Consequently, if the C-terminus of RAP1 is exposed to the cytosol, the protein would be degraded by the addition of auxin. Western blot confirmed that the protein is not downregulated upon addition of auxin **(Figure 3.15 A)**. The band migrated to the right size as observed with or without IAA. By immunofluorescence, the protein was still detected in the rhoptry bulb in presence of IAA, and like the RAP1-Ty-U1, no dot was observed at the rhoptry tip in intracellular parasites **(Figure 3.15 B)**. Finally, the parasite still formed lysis plaques comparable to the parental strain after 7 days of auxin treatment **(Figure 3.15 C)**. This imply that RAP1 C-terminal is not exposed to the parasite cytosol. U-ExM offers an opportunity to study in detail, the localization of a gene product at a high resolution (Ddos Santos Pacheco and Soldati-Favre, 2021). U-ExM on extracellular RAP1-3Ty-U1 revealed that RAP1 is indeed localizing to the bulb but we can observe that the staining is rather vesicular and dispersed comparing to the homogeneous ROP5 staining **(Figure 3.15 D)**. We can also observe a vesicular staining colocalizing with RON9 at the rhoptry neck **(Figure 3.15 D)**, confirming the dual localization of RAP1.

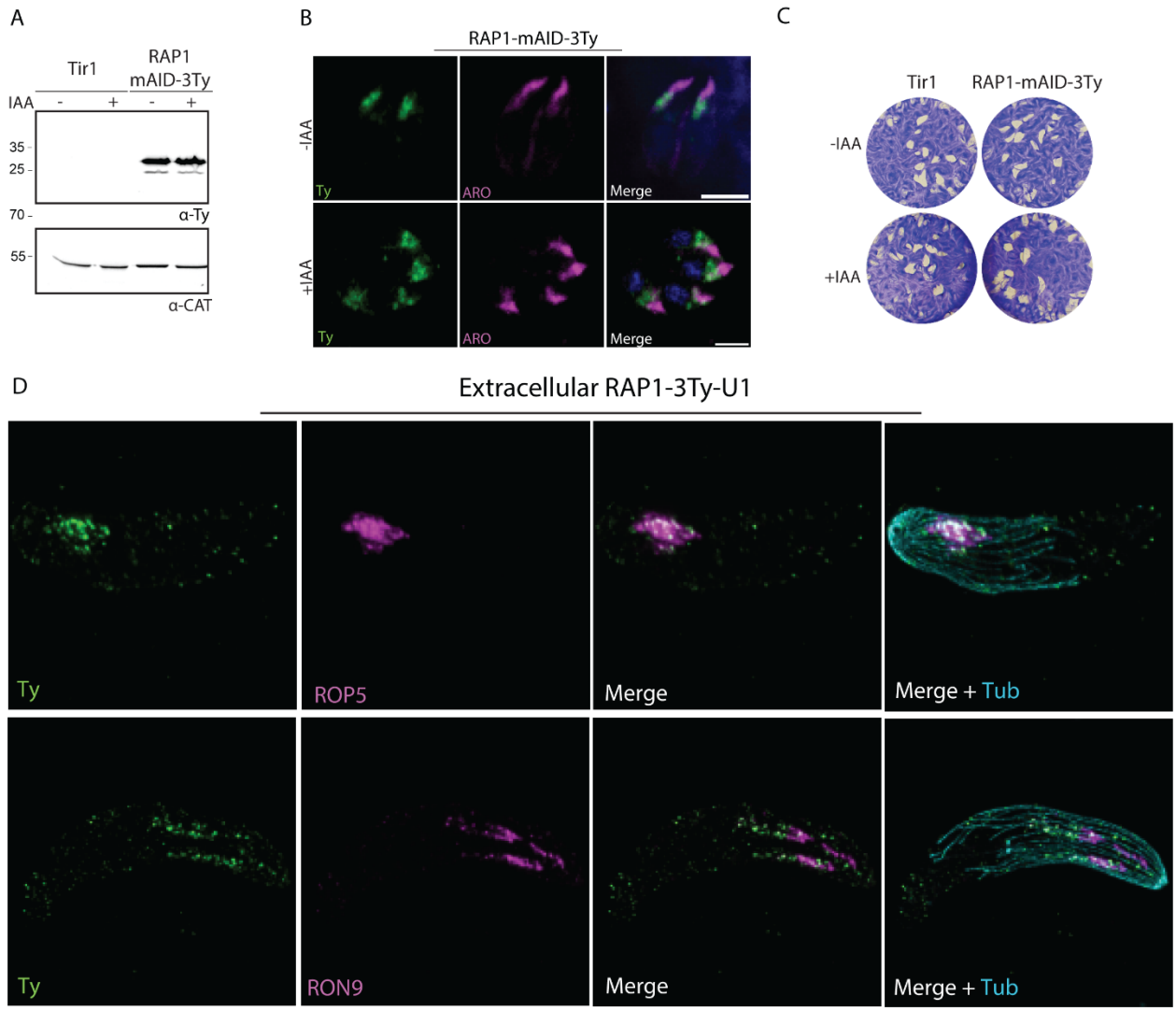

Figure 3.15 **Refining RAP1 localization**. **A.** Plaque assay showing that depletion of RAP1 using the mAID system does not affect parasite survival. Parental strain TiR1 was used as a control (n=3). **B.** Western blot showing the absence of downregulation of RAP1 in presence of IAA. Catalase (CAT) is used as a loading control. **D.** U-ExM pictures for localization of RAP1 in extracellular parasites. Expansion factor = 4. Scale bar = 1µm.

3.4.4. RAP1 mutagenesis

No specific domains were identified in RAP1, complicating the investigation of its function. To identify some functional domains, we generated three constructs with three different mutations

and tested them for functional complementation in the RAP1-3Ty-U1 strain at the UPRT locus. The three mutations are described in the predicted AplhaFold model of RAP1 **(Figure 3.16 A).** The first mutation, Mut1, (RAP1-3Ty-U1 + RAP1 Mut1-4Myc) was generated in the N-terminal part of RAP1 by mutating C31A, R35A and K38A. This mutation affected the localization of RAP1 **(Figure 3.16 B)**. Western blot showed a band detected with Myc antibodies in absence or presence of rapamycin (+Rapa), confirming the complementation by the second copy **(Figure 3.16 C).** However, we observed the presence of an additional band migrating a few kDa above the RAP1 signal.

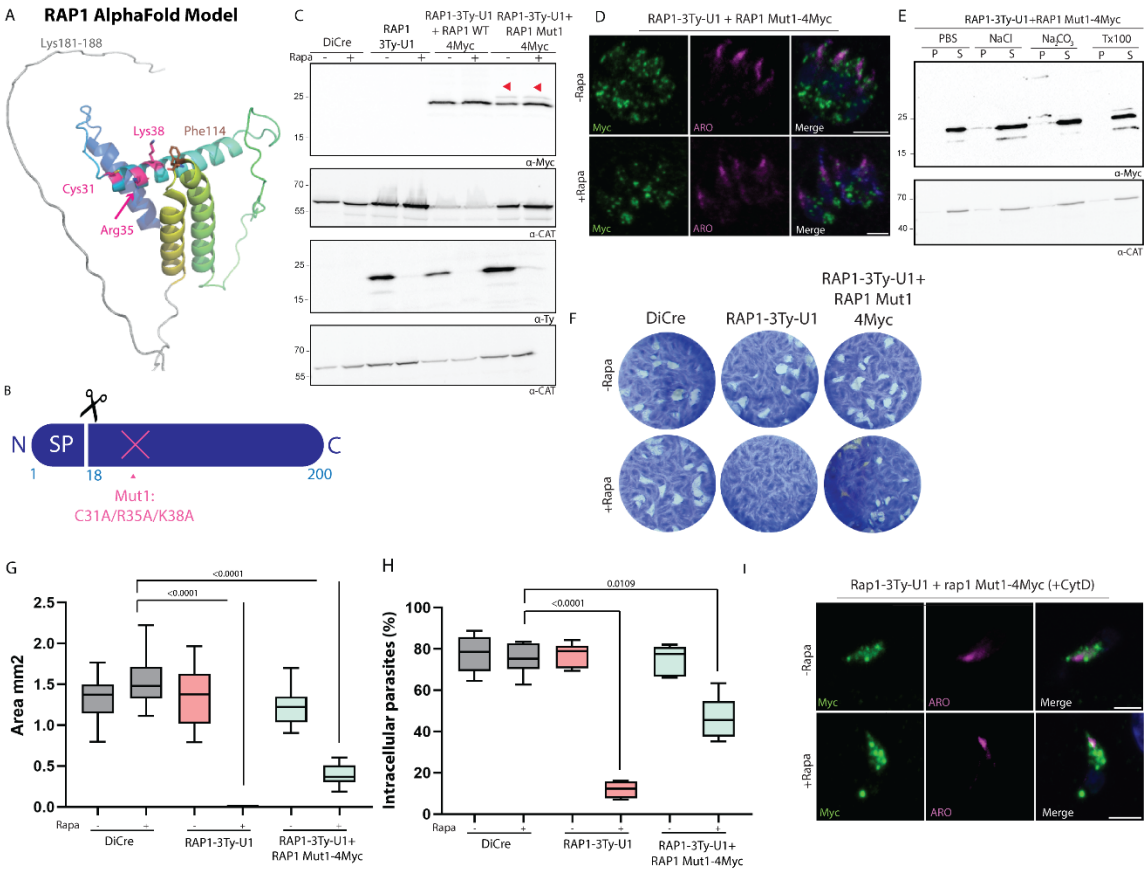

Figure 3.16 **Complementation of RAP1-3Ty-U1 with Mutation 1. A.** RAP1 AlphaFold Model. N-terminal part is colored from blue to yellow. The portion in grey represents the unfolded region (133-200). Three residues in pink, located in the second helix (C31, R35, K38) are mutated to alanine (Mut1). Phenylalanine residue shown in brown, at the turn between helices 3-4 (F114) is also mutated to alanine (Mut2). The acidic patch (K 181-188) is mutated to alanine (Mut3) **B.** Schematic presentation of Mutation 1. **C.** Western blot showing the regulation of the complemented RAP1-3Ty-U1 strain in presence or absence of

rapamycin (Rapa). Catalase (CAT) is used as a loading control. **D.** IFA using anti-Myc antibody (green) showing the localization of the complemented RAP1 strain. Anti-ARO antibody is used to stain the rhoptry organelle (magenta). DAPI (blue). Scale bar = 2µm. **E.** Solubility assay of the complemented RAP1-Ty-U1. P = pellet. S = supernatant. **F.** Plaque assay to test the fitness the complemented strain (n=3). **G.** Quantification of plaque assays for Dicre, RAP1-3Ty-U1 and complemented RAP1 strain (n=3). **H.** Red/Green invasion assay showing that depletion of the complemented RAP1 partially rescued the invasion of the parasite (n=3). **I.** IFAs of extracellular RAP1-3Ty-U1 + RAP1 Mut1-4Myc parasites in presence of cytochalasin D. DAPI (blue). Scale bar = 2µm.

Immunofluorescence showed that the signal of RAP1 in this mutant is vesicular and scattered throughout the parasite and mostly accumulated at its basal pole **(Figure 3.16 D)**. This did not impact on the protein solubility since in all conditions, we observe an enrichment of the mutated RAP1 in the supernatant (**Figure 3.16 E)**. By plaque assay, the mistargeted Mut1 parasite was able to form small plaques meaning that these parasites are still able to survive despite the mutation and mis-localization of RAP1 **(Figure 3.16 F-G)**. Surprisingly, even though the protein did not traffic to accurate destination, the Mut1 parasite was able to rescue almost 50% of the invasion defect compared to RAP1-3Ty-U1, in presence of rapamycin **(Figure 3.16 H)**. Finally, we checked the localization of the mistargeted RAP1 in extracellular parasites in presence of cytochalasin D. We observed that the protein still accumulated at the tip of the rhoptries and the scattered vesicles of RAP1 seems to move towards the apical pole of the parasite, potentially explaining why these parasites were able to invade host cells **(Figure 3.16 I)**.

The second mutation (RAP1-3Ty-U1 + RAP1 Mut2-4Myc) was generated by mutating the F114 to A114 **(Figure 3.17 A)**. This phenylalanine residue is located at the turn between helices 3 and 4 as predicted by the Alpha Fold model **(Figure 3.16 A)**. Western blot showed a band with the right molecular size detected in absence or presence of rapamycin (+Rapa), confirming the complementation by the second copy **(Figure 3.17 B).** The protein is trafficked to the right place **(Figure 3.17 C)** and this mutant can fully rescue the phenotype observed under RAP1 depletion **(Figure 3.17 D)**. The last mutation (RAP1-3Ty-U1 + RAP1 Mut3-4Myc), was the most drastic, were we changed the C-terminal acidic patch K111 - K118 to alanine **(Figure 3.17 E)**. Western blot showed that this mutation did not affect the expression of the protein in absence or presence of

rapamycin (+Rapa) **(Figure 5.17 F)**. The protein trafficked to the correct localization **(Figure 3.17 G)** and this mutation was not detrimental for the parasite lytic cycle as shown by the plaque assay **(Figure 3.17 H)**. This suggest that even if atypical, the acidic patch at the C-terminal end of RAP1 is not required for its function.

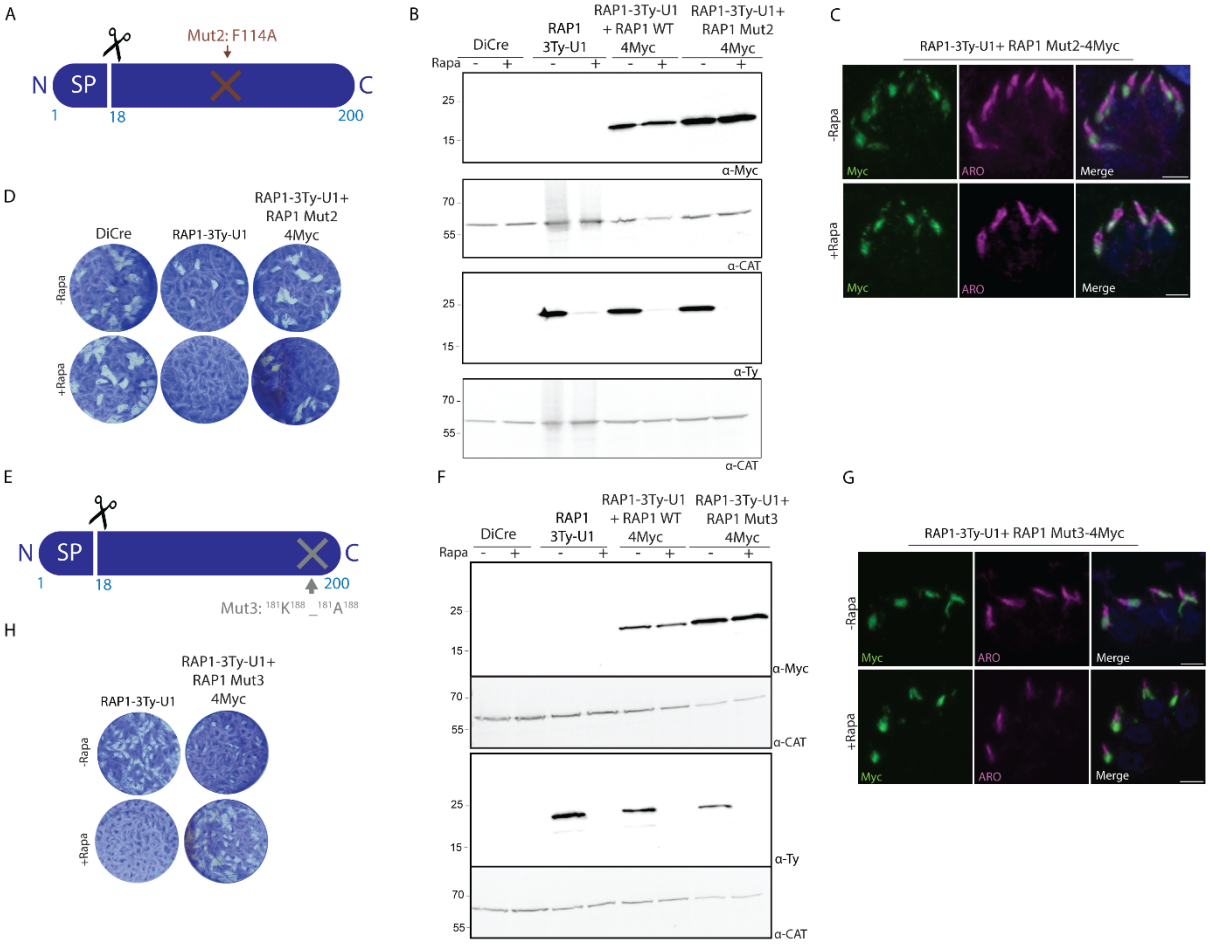

Figure 3.17 **Complementation of RAP1-3Ty-U1 with Mutation 2 and Mutation 3. A.** Schematic presentation of Mutation 2. **B.** Western blot showing the regulation of the complemented RAP1-3Ty-U1 strain in presence or absence of rapamycin (Rapa). Catalase (CAT) is used as a loading control. **C.** IFA using anti-Myc antibody (green) showing the localization of the complemented RAP1 strain. Anti-ARO antibody is used to stain the rhoptry organelle (magenta). DAPI (blue). Scale bar = 2µm. **D.** Plaque assay to assess the fitness the complemented strain (n=3). **E.** Schematic presentation of Mutation 3. **F.** Western blot showing the regulation of the complemented RAP1-3Ty-U1 strain in presence or absence of rapamycin (Rapa). Catalase (CAT) is used as a loading control. **G.** IFA using anti-Myc antibody (green) showing the localization of the complemented RAP1 strain. Anti-ARO antibody is used to stain the rhoptry organelle (magenta). DAPI (blue). Scale bar = 2µm. **H.** Plaque assay to test the fitness the complemented strain (n=3).

3.4.5. RAP1 colocalizes with RASP2 and CSCHAP at the rhoptry tip

Several proteins were recently described as key players in rhoptry discharge and they all localize to the tip of the parasite: Nd6, a marker of the apical vesicle which is anchored to the rosette at the PM (Aquilini *et al.*, 2021), RASP2 that caps the extremity of the rhoptry neck and is important for rhoptry secretion (Suarez *et al.*, 2019) and CSCHAP that plays a central role in the apical positioning of the rhoptries and decorates the tip of the rhoptries **(Figure 3.18 A)** (Morlon-Guyot, Berry, *et al.*, 2018). We first tagged RAP1 in Nd6-mAID-HA strain.

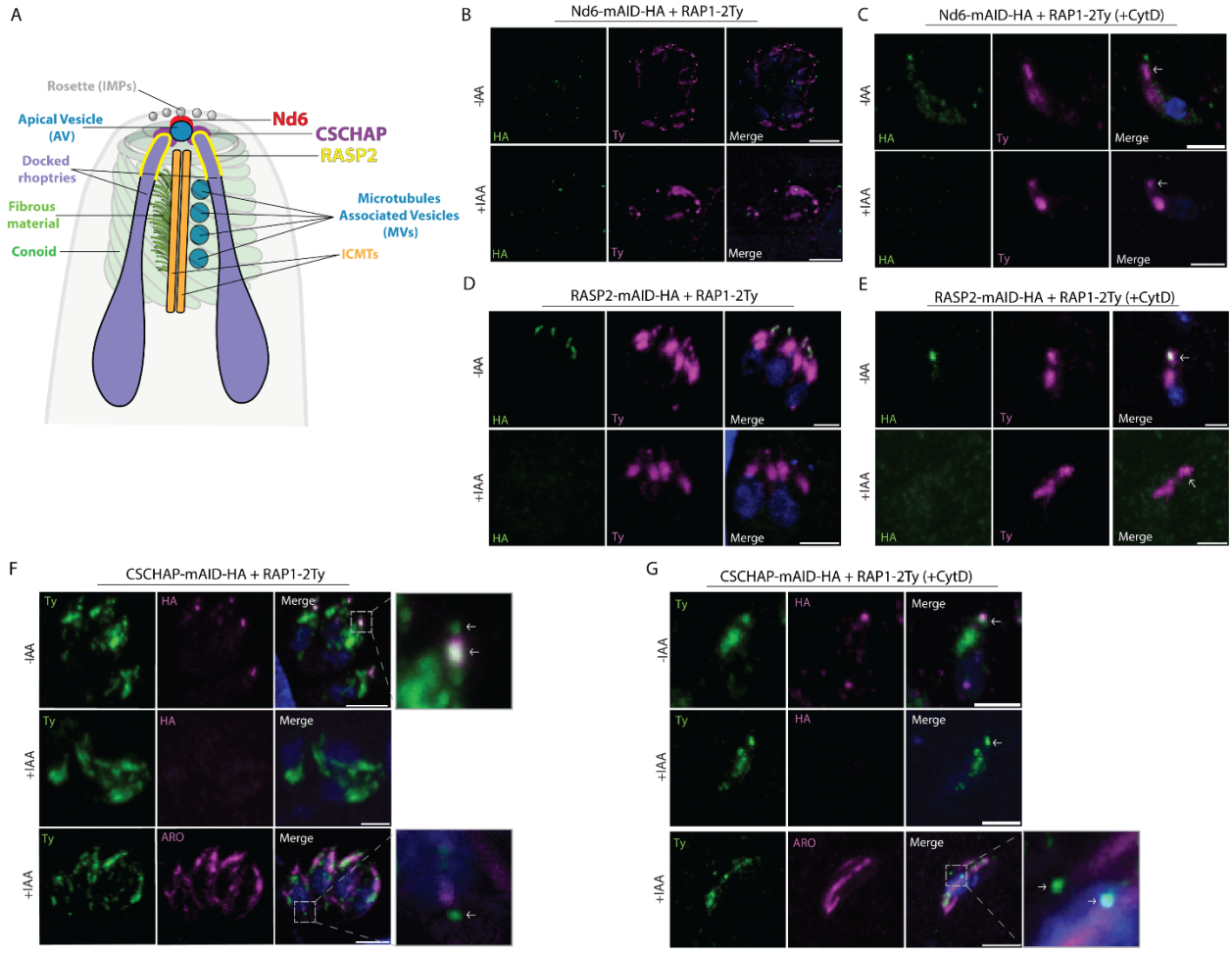

Figure 3.18 **RAP1 interaction and colocalization with other proteins. A.** Schematic representation of the apical complex of *T. gondii* highlighting the main structures and molecular players required for rhoptry secretion. **B.** Immunofluorescence to assess RAP1 and Nd6 localization in presence or absence of auxin (IAA). DAPI (blue). Scale bar = 2µm. **C.** IFAs on extracellular parasites in presence of cytochalasin D. DAPI

(blue). Scale bar = 2µm **D.** IFAs to assess RAP1 and RASP2 colocalization in presence or absence of auxin (IAA). DAPI (blue). Scale bar = 2µm. **E.** IFAs on extracellular parasites in presence of cytochalasin D. DAPI (blue). Scale bar = 2µm. **F.** Immunofluorescence to assess RAP1 and CSCHAP colocalization in presence or absence of auxin (IAA). DAPI (blue). Scale bar = 2µm. **G.** IFAs on extracellular parasites in presence of cytochalasin D. DAPI (blue). Scale bar = 2µm. **White arrows** point to RAP1 localization at the tip of the rhoptries.

Immunofluorescence confirmed the correct localization of RAP1 in intracellular parasites, with a bulb as well as a rhoptry tip staining **(Figure 3.18 B)**. It also appeared that the dot of RAP1 did not colocalize with Nd6 in intracellular parasites and it is found more basal **(Figure 3.18 B)**. Upon Nd6 depletion using IAA, RAP1 signal remains unchanged **(Figure 3.18 B)**. We also checked the colocalization of both proteins in extracellular parasites in presence of CytD **(Figure 3.18 C).** This confirmed that RAP1 do not colocalize with Nd6 at the tip of the parasite. RAP1 staining seems to be below the dot of Nd6, and even in absence of Nd6, RAP1 was still able to accumulate at the rhoptry tip **(Figure 3.18 C)**. This suggests that RAP1 accumulation does not require the presence of Nd6 and that RAP1 accumulation is more basal than the AV and the rosette-PM.

We then tagged RAP1 in RASP2-mAID-HA parasites. In intracellular parasites, RAP1 partially colocalizes with RASP2 at the rhoptry tip **(Figure 3.18 D)**. In the absence of RASP2, RAP1 signal and expression seems normal **(Figure 3.18 D)**. Interestingly, in extracellular parasites, the RASP2 signal seems different compared to intracellular parasites. The protein accumulates at the rhoptry tip in the same manner as RAP1, and both colocalizes **(Figure 3.18 E)**. However, depletion of RASP2 does not affect the localization or expression of RAP1 **(Figure 3.18 E)**.

Finally, we tagged RAP1 in CSCHAP-mAID-HA strain. In intracellular parasites, RAP1 signal at the rhoptry tip seems to colocalize with CSCHAP **(Figure 3.18 F)**. In some cases, we can observe an additional RAP1 signal above CSCHAP **(Zoom Figure 3.18 F)**. CSCHAP possesses two microtubules binding domains and it is suggested to anchor the rhoptries apically to the ICMTs. Depletion of CSCHAP leads to a defect in rhoptry organelle positioning (Morlon-Guyot, Berry, *et al.*, 2018), and this condition does not abrogate RAP1 localization or signal **(Figure 3.18 F)**. Interestingly, when

rhoptry organelles are disorganized and scattered throughout the parasite, RAP1 dot signal seems to always localize with the rhoptry tip even when they are not apical **(Zoom Figure 3.18 F)**. This suggests that the RAP1 localization is tightly associated to the rhoptry organelle. Additionally, in extracellular parasites treated with CytD, CSCHAP signal partially colocalized with RAP1 at the tip, and its depletion does not affect RAP1 expression and positioning **(Figure 3.18 G)**. RAP1 signal is still at the rhoptry tip in mispositioned organelles **(Zoom Figure 3.18 G)**, confirming the association of RAP1 with the rhoptries regardless of its position. Collectively this suggests that RAP1 is in the same vicinity as RASP2 and CSCHAP at the rhoptry tip.

To further confirm this, we tagged RASP2 and CSCHAP in RAP1-3Ty-U1. Depletion of RAP1 does not affect their expression or trafficking in intracellular parasites confirming that the function of RAP1 is independent of theirs **(Figure 3.19 A-B)**. We also tagged RASP2 in CSCHAP-mAID-3HA and CSCHAP in RASP2-mAID-3HA and investigated their localization and expression. Both proteins colocalized as expected and the depletion of one does not affect the expression of the other **(Figure 3.19 C-D)** confirming that these two proteins do not form a complex as well and they function independently of each other. Additionally, when depleting CSCHAP, RASP2 seems to also localize normally to the rhoptry tip even when the organelle is not apically positioned **(Figure 3.19 D)**.

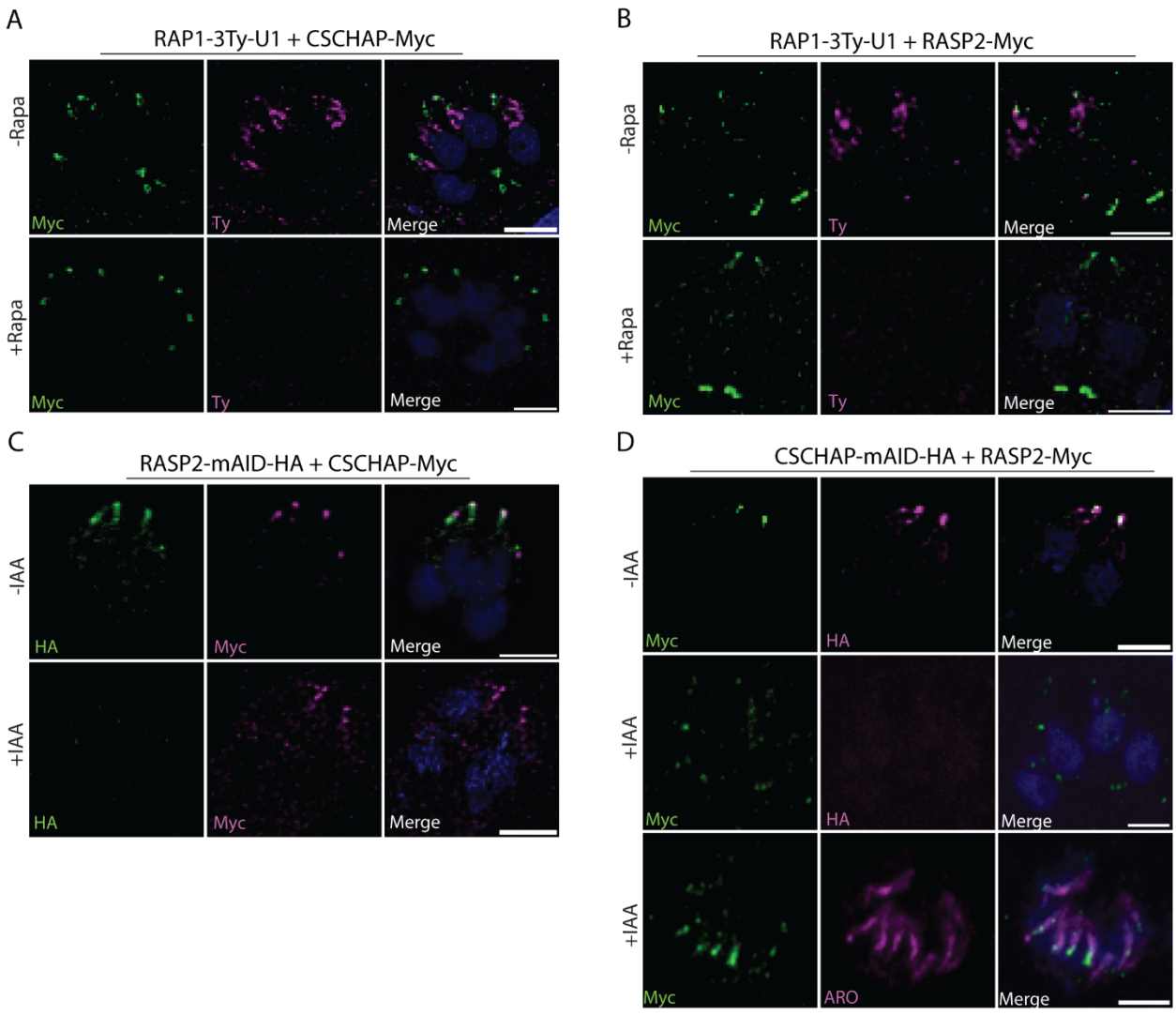

Figure 3.19 **Assessing RAP1 colocalization with other proteins and impact of microneme secretion on its function A.** IFAs to assess CSCHAP localization in RAP1 depleted parasites (+Rapa). DAPI (blue). Scale bar = 2µm **B.** IFAs to assess RASP2 localization in RAP1 depleted parasites (+Rapa). DAPI (blue). Scale bar = 2µm. **C.** IFAs to assess CSCHAP localization in RASP2 depleted parasites (+IAA). DAPI (blue). Scale bar = 2µm. **D.** IFAs to assess RASP2 localization in CSCHAP depleted parasites (+IAA). DAPI (blue). Scale bar = 2µm.

TFP1 is a transporter protein associated with micronemes. Depletion of TFP1 leads to an aberrant morphology of the organelle and a severe defect in microneme secretion (Hammoudi *et al.*, 2018). To investigate the localization and expression of RAP1 in absence of microneme secretion,

we tagged it in TFP1-iKD-3Ty. Immunofluorescence showed that RAP1 signal and localization were not affected in the absence of TFP1 in intracellular parasites **(Figure 3.20 E)**. Additionally, absence of microneme secretion does not affect the accumulation of RAP1 at the rhoptry tip in extracellular parasites suggesting that the localization of RAP1 at the tip of the rhoptry is independent from microneme exocytosis **(Figure 3.20 F)**.

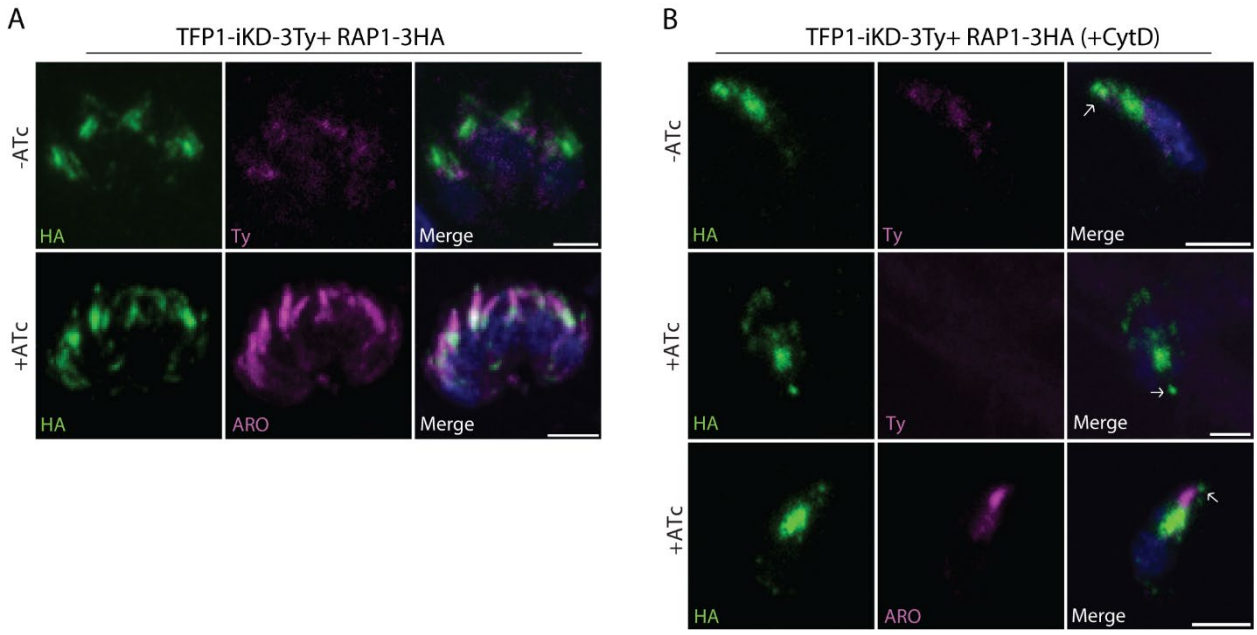

Figure 3.20 **Assessing RAP1 localization in absence of microneme secretion. A.** IFAs to assess RAP1 localization in TFP1 depleted parasites (+ATc). DAPI (blue). Scale bar = 2µm. **B.** IFAs on extracellular parasites in presence of cytochalasin D. DAPI (blue). Scale bar = 2µm. **White arrows** point to RAP1 localization at the tip of the rhoptries.

4. Materials and Methods

- ***Toxoplasma and host cell culture***

T. gondii tachyzoites RH strain, parental and modified strains, were grown on confluent monolayers of human foreskin fibroblasts (HFFs) in Dulbecco's Modified Eagle's Medium (DMEM, Gibco) with 5% fetal calf serum (FCS), 25 mg/ml gentamicin and 2 mM glutamine and. Parasites were grown 48h in presence or in absence of either Rapamycin (50nM), auxin (IAA) (500uM) or ATc (1ug/mL) prior analysis.

- ***Generation of parasite transgenic lines***

For generation of all transgenic parasites, a specific guide RNA was designed to target the 3'UTR of the gene of interest. Two universal primers containing the homology regions for the gene of interest were used to amplify by PCR the desired cassette. The *T. gondii* DiCre parental strain was used to generate RAP1-3Ty-U1 parasites. ΔKu80 RH strain was used to generate RAP1-2Ty and RAP1-3Myc strains. TiR1 strain was used to generate RAP1-mAID-Ty parasites. To generate RAP1-3Ty-U1 we used the pG152-KI-3Ty-lox-SAG1-HXGPRT-U1 cassette. For the generation of RAP1-mAID-Ty strain we used the mAID-3Ty-HXGPRT plasmid. To generate both RAP1-2Ty and RAP1-3Myc we used pLinker-2xTy-HXGPRT and Myc3-LIC-DHFR plasmids, respectively. To tag RAP1 in Nd6-mAID-3HA, RASP2-mAID-3HA and CSCHAP-mAID-3HA we used the pLinker-2xTy-DHFR cassette. To tag RASP2 and CSCHAP in RAP1-3Ty-U1 parasites, we used the Myc3-LIC-DHFR plasmid. To tag RASP2 in CSCHAP-mAID-3HA and CSCHAP in RASP2-mAID-3HA, we used the Myc3-LIC-DHFR plasmid. To tag RAP1 in TFP1-iKD-3Ty parasites we used 3xHA-LIC-DHFR. To complement the RAP1-3Ty-U1 line with a wild-type copy of RAP1, a pRAP1-RAP1-4Myc sequence was cloned in the pUPRT-4Myc plasmid. A total of 60 µg of the resulting vector pUPRT-pRAP1-RAP1-4Myc was digested and co-transfected using 15 µg of the pU6-Cas9-Universal-gRNAuprt vector (Shen *et al.*, 2014). Parasites that integrated pUPRT-pRAP1-RAP1-4Myc vector were selected using 5'-fluo-2'-deoxyuridine (FUDR) negative selection. Point mutagenesis introduced

by Q5 site-directed mutagenesis (NEB) on pRAP1-RAP1-4myc were used to generate RAP1-Mut1, RAP1-Mut2, and RAP1-Mut3 vectors.

To transfect parasites with the corresponding plasmid, freshly egressed parasites were resuspended in Cytomix (10mM KPO4, 120mM KCl, 0.15mM CaCl2, 5mM MgCl2, 25mM Hepes, 2mM EDTA), supplemented with 3 mM ATP and 3 mM GSH and then mixed with the plasmid to be transfected and the corresponding gRNA. The DNA-parasite mixture is then subjected to an electric pulse (2000V, 50 ohms and 25uF) and transfected parasites were then incubated with a culture dish containing HFF in CO2 incubator at 37 °C for maintenance and selection. Transgenic parasites were selected in the presence of mycophenolic acid (25µg/mL) and xanthine (50µg/mL) for the hypoxanthine-xanthine guanine- phosphoribosyl-transferase (HXGPRT) resistance cassette and in the presence of 1ug/ml of pyrimethamine for the DHFR resistance. Stable strains were cloned by limiting dilution in 96-well plates and checked by PCR for genomic integration and analyzed by IFA and/or WB for protein expression.

- ***Western blot analysis***

Freshly egressed parasites were pelleted by centrifugation at 1100g for 10 min. The pellet was washed in PBS and resuspended with SDS- PAGE loading buffer (+/- 10 mM DTT) and heated at 95°C for 10 min (for transmembrane proteins, the heating step was skipped). Proteins separated by SDS-PAGE (sodium dodecyl sulfate – polyacrylamide gel electrophoresis) were transferred to nitrocellulose membrane and immuno-blot analysis was performed. Primary and secondary antibodies are diluted in 5%milk/0.05% Tween/PBS and washes are performed in 0.05%Tween/PBS. Proteins were visualized with Pierce ECL Western blotting substrate, according to the manufacturer's protocol.

- ***Immunofluorescence analysis***

Freshly egressed *T. gondii* tachyzoites were used to infect HFF monolayers on coverslips and incubated at 37°C for 24h prior fixation. 4% paraformaldehyde (PFA)/0.05% glutaraldehyde (GA)

was used to fix the infected cells prior quenching with 0.1 M glycine/PBS. First, cells were permeabilized and blocked with 2%BSA/0.2%Triton/PBS for 1h (in the case of methanol fixation, only blocking with 2%BSA/PBS for 1h was performed). After blocking, cells were probed with primary antibodies diluted in 2%BSA/0.2%Triton/PBS for 1 hour followed by 3 washes with 0.2%Triton/PBS. Then, cells were incubated with secondary antibodies diluted in 2%BSA/0.2% Triton/PBS for 1 hr. DAPI (4',6-diamidino-2-phenylindole; 50 mg/ml in PBS) was used to stain the parasites and HFF nuclei and coverslips were mounted on Fluoromount G (Southern Biotech) on glass slides. Images were taking by LSM700 confocal microscope (Zeiss) at the Bioimaging core facility of the Faculty of Medicine at the University of Geneva. Images were processed and analyzed using ImageJ software.

- ***Plaque assay***

Confluent monolayer of HFF were infected with freshly egressed parasites and incubated for 7 days in presence or absence of the drug. 4% PFA / 0,05% Glutaraldehyde was used to fix the parasites for 10-15 minutes. After neutralization with 0,1M glycine/PBS, cells were stained using crystal violet.

- ***Invasion assay***

Freshly egressed parasites, pre-treated for 48 hours +/-rapamycin, were diluted 1:10, inoculated on HFF coverslips and centrifuged for 1 min at 1200 g to let them settle down on the host cell layer. Parasites were incubated for 30 min at 37°C to allow them to invade prior fixation using PFA/Glu for 7 minutes. Parasites were first incubated with anti-SAG1 antibody in non-permeabilized conditions (2%PBS-BSA) to stain extracellular parasites only. After several washes with PBS (3 or more), cells were fixed using 1% formaldehyde/PBS for 7 min under fume hood followed by a wash with PBS. Next, cells were permeabilized with 0.2%Triton/PBS and stained with anti-GAP45 antibody (staining both intracellular and extracellular parasites). Secondary antibodies were used as previously described. 100 parasites were counted for each experiment,

and % of intracellular parasite (GAP45 positive only) relative to the total number of parasites ($GAP45^+$ + $GAP45^+/SAG1^+$ parasites) is presented. Results are mean ± standard deviation of three independent biological replicate experiments.

- ***Induced egress assay***

Freshly egressed parasites pre-treated 24 hours +/- rapamycin, were used to infect HFF monolayers. The coverslips were washed two hours post infection to remove non-invading extracellular parasites and then left to grow for 36 hours at 37°C. Prior to inducing egress, the wells were washed three times with egress buffer (serum-free DMEM) to remove the serum. The infected HFF cells were then incubated for 7 min at 37°C with serum-free DMEM containing either BIPPO (Howard *et al.*, 2015) or DMSO as a control. Prior to fixing with PFA/GLU, the monolayers of the WT positive control were observed under the microscope to check if the parasites have egressed. IFA was performed as previously described using anti-GAP45 antibody to stain the parasites and anti-GRA3 antibody to stain the PV. 100 vacuoles were counted per condition and scored as egressed or non-egressed for quantification of the percentage of egress. Results are mean ± standard deviation of three independent biological replicates. Control experiment with DMSO showed no egress.

- ***Intracellular growth***

Freshly egressed parasites pre-treated 48 hours +/- rapamycin, were used to infect HFF monolayers cells and the coverslips were washed two hours post infection. Infected cells were fixed 24h post-infection with PFA/Glutaraldehyde. IFAs were performed using anti-GAP45 antibodies to detect parasites. The number of parasites per vacuole was scored, counting 100 vacuoles for each condition. Results are mean ± standard deviation of three independent biological replicates.

- ***E-vacuole secretion assay***

Rhoptry secretion was assessed using e-vacuole detection assay (Hakansson *et al.*, 2001). Freshly egressed parasites pre-treated 48 hours +/- rapamycin, were first counted (number of parasites/mL), washed in PBS and resuspended in pre-chilled DMEM medium containing ±1 uM Cytochalasin D (use to inhibit parasite entry without impacting on rhoptry secretion) followed by incubation on ice for 10 min. The parasites were then added to pre-chilled HFF-coated coverslips and incubated for 20 min on ice. The coverslips are then washed with cold PBS before adding complete DMEM medium containing ±1 uM Cytochalasin D or DMSO, for controls, and further incubated for 20 min at 37°C in the water bath. 4% paraformaldehyde was used to fix the parasites for 15 min. IFA was performed as described before. For this assay, ROP1 was used as a marker for rhoptry secretion (visualization of the e-vacuoles) while GAP45 was used to stain the parasites' pellicles. 100 parasites were analyzed per experiment for rhoptries secretion and quantified for the presence of the apical tip staining. The results are shown as mean ± standard deviation of three independent biological replicate experiments.

- ***STAT6-P as marker for rhoptry secretion***

Freshly egressed parasites were incubated with HFFs for 15 min at 37°C in Endo Buffer (106 mM sucrose, 10 mM Mg2SO4, 44.7 mM K_2SO_4, 20 mM Tris (pH 8.2), 5mM glucose, 3.5mg/mL BSA) known to inhibit invasion. Next, parasites were incubated in pre-warmed serum free DMEM for 5 minutes at 37°C to initiate parasites invasion prior to fixation with 100% ice-cold methanol for 10 minutes. DiCre and RAP1 parasites were pre-treated 48 hours +/- rapamycin for this experiment. Parasites from the tet-inducible knockdown strain of ASP3 (iKD-ASP3), pre-treated 48 hours with ATc, were used as negative control as they are defective in rhoptry secretion following ATc treatment (Dogga *et al.*, 2017). IFA was done using anti-STAT6-P antibody and the number of STAT6-P positive host cell nuclei were counted compared to the total number of cells for all conditions. 100 nuclei were counted for each condition and the experiment was done in two independent biological replicates.

- ***Cytochalasin D treatment on extracellular parasites***

Freshly egressed parasites pre-treated 48 hours +/- rapamycin or IAA or ATc, were first washed in PBS and resuspended in warm PBS containing ±1 uM Cytochalasin D followed by incubation on ice for 10 min. The parasites were incubated for 30 min at 37°C in the water bath. 4% paraformaldehyde was used to fix the parasites for 7 min. IFA was performed as described before.

- ***Solubility assay***

Freshly egressed parasites, pre-treated for 48 hours +/-rapamycin, were pelleted and resuspended in PBS, PBS containing NaCl, PBS triton (1% Tx) or PBS containing Na_2CO_3. These samples are then freeze and thawed using liquid nitrogen and 37°C water bath. The pellet and the soluble fraction are separated by centrifugation for 30 minutes at 4°C max speed. Samples were finally resuspended with SDS- PAGE loading buffer (+/- 10 mM DTT) and heated at 95°C for 10 min.

- ***Cryo-Expansion microscopy***

Cryo-expansion microscopy preparation was performed as previously described with few time-saving modifications (Laporte *et al.*, 2022; dos Santos Pacheco and Soldati-Favre, 2021). Briefly, extracellular parasites (in PBS supplemented with BIPPO to induce conoid extrusion) seeded on Poly-D-Lysin coated coverslips were fixed using cryofixation using conventional rapid plunging in liquid ethane-propane then incubated in acetone pre-cooled with liquid nitrogen and placed on dry ice overnight. This allows the dry ice evaporation and a gradual increase in the sample temperature from -180°C to 0°C. The water of the sample is replaced by acetone that preserves the sample architecture. We then rehydrate the sample using ethanol mixed with water and proceed to the U-ExM protocol.

Cells were embedded in an Temed/APS/Monomer solution (19% Sodium Acrylate, 0,1% BIS-AA and 10% AA in PBS 10X) gel on ice, prior incubation at 37°C during 30 min. Gels were then

denatured at 95°C during 1h30 with denaturation buffer (200mM SDS; 200mM NaCl; 50mM Tris-Base, pH 9). Gels were then expanded two times 30 minutes minimum in water. Gels were then measured before shrinking (2 washes of 15 min in PBS) and cutting in small piece of gel (roughly 1cmx1cm). The piece of gel was then incubated with primary antibodies in 2% BSA/PBS for 3 hours. Gels were then washed three times in PBS during 10 min. Then followed the incubation with secondary antibodies in 2% BSA/PBS for 3 hours. Gels were then washed three times in PBS during 10 min before final expansion (2 times 30 minutes in water). Imaging was performed using a Leica TCS SP8 inverted microscope, equipped with an HC PL Apo 100x/ 1.40 Oil CS2 objective and with HyD detectors. Pieces of gels were cut and placed on a 24mm poly-lysine coated coverslip (to avoid gel drifting during acquisition) fitted in a metallic O-ring 35mm imaging chamber (Okolab). Z-stack were acquired with the Leica LAS X software and deconvolved with the built-in "Lightning" mode. Images were then processed with the ImageJ software.

- ***Serial section transmission electron microscopy (ssTEM)***

HFF cells were infected with *T. gondii* parasites and let to grow for 24 hours before fixing with 2% paraformaldehyde and 2.5% glutaraldehyde in 0.1 M sodium cacodylate buffer (pH 7.4) for 1 hour at room temperature. The infected cells were then washed with 0.1 M sodium cacodylate buffer (pH 7.4) and fixed with 1.5% potassium ferrocyanide and 1% osmium tetroxide in 0.1 M sodium cacodylate buffer (pH 7.4) for 1 hour followed by 1% osmium tetroxide in 0.1 M sodium cacodylate buffer (pH 7.4) for another hour. Cells are then washed in double-distilled water twice and stained with aqueous 1% uranyl acetate for 1 h. Cells are washed with double-distilled water twice, and then dehydrated in graded ethanol series (2 x 50%, 70%, 90%, 95% and 2 x absolute ethanol) for 10 minutes. Cells are infiltrated twice after dehydration with a graded series of Durcupan resin diluted with ethanol at 1:2, 1:1, and 2:1 for 30 minutes each and then twice with pure Durcupan for 30 minutes each. Cells were infiltrated with fresh Durcupan resin for 2 hours. A coverslip with cells was placed on a 1-mm-high silicone ring filled with fresh resin and placed on a glass slide coated with mold-separating agent. It was then polymerized for 24 hours at 65°C.

Afterwards, the coverslip was removed from the resin disk by putting it in hot water (60°C) and then liquid nitrogen. A laser microdissection microscope was used to outline the position of the PV on the exposed surface of the resin. The area is then cut out from the disk and glued with to a blank resin block. Using a Leica Ultracut UCT microtome (Leica Microsystems) and a glass knife the cutting face was trimmed. Then, we cut a 70-nm ultrathin serial sections with a diamond knife (DiATOME) and collected onto 2-mm single-slot copper grids (Electron Microscopy Sciences) coated with Formvar plastic support film. Sections were examined using a Tecnai 20 TEM operating at an acceleration voltage of 80 kV and equipped with a side-mounted MegaView III CCD camera (Olympus Soft-Imaging Systems) controlled by iTEM acquisition software (Olympus Soft-Imaging Systems).

- ***RAP1 purification for antibody generation***

Recombinant RAP1 (without signal peptide) was expressed in baculovirus-infected Sf9 insect cells. Cells were harvested by centrifugation at 4000 x g for 20 min and the pellet was resuspended in 30mL of lysis buffer (50mM Tris pH 8, 450mM NaCl, 3mM β-mercaptoethanol, 15mM imidazole and 8M urea). Cell s were lysed using the microfluidizer. Cell debris and membrane were removed by centrifugation at 35,000 x g for 30 min at 4°C. A 5 mL His-trap FF column (GE healthcare) was washed with 40 mL 0.5M imidazole and 2.5M NaCl followed by an equilibration using 40 mL of the lysis buffer to which we add 10mM imidazole. The supernatant containing the soluble protein was applied to the column. Column was then washed using 100 mL of the lysis buffer to which we add 15mM imidazole. W second wash is done with 30 mL of lysis buffer. Protein was then eluted using 20 mL of lysis buffer supplemented with 450mM imidazole. Eluted protein was concentrated to 1 mL using AMICON concentrators and loaded on a size-exclusion Superdex 75 column at 4°C equilibrated using 20mM Tris pH 8, 150mM NaCl, 6M Urea and 3mM β-mercaptoethanol. Fractions containing pure RAP1 were pooled, concentrated to 1mg/mL and used as antigens for antibodies generation.

5. Discussion

5.1. Discussion of chapter 1 on RON13

The story of RON13 is a hallmark of my PhD. The project started with a clear hypothesis to be tested and ended up with a completely different conclusion. It was as challenging as it was fascinating for me and I learned all my basics with it and especially, I figured how tricky science can be. When we started this work, our aim was to find the ASP3 substrate(s) responsible for the rhoptry secretion defect observed in ASP3-depleted parasites. Among the list of hypothetical proteins identified as ASP3 substrates in the N-terminome analysis (Dogga *et al.*, 2017), RON13 (called TAILS6 at that time, then changed to TAILS8 then to RON13) showed compelling features: i) a negative fitness score (-2.57) (Sidik *et al.*, 2016), ii) a localization in the neck of rhoptry and iii) a putative catalytic kinase domain that can be involved in the signaling cascade leading the rhoptry secretion. We embarked in the study and characterization of this protein, hoping that we hit the jackpot.

The story of RON13 is the best example of serendipity.

5.1.1 RON13 is not a canonical protein kinase

Scrutinizing RON13 kinase activity took a big chunk of our time during this study. We implemented different kinase assays such as radioactivity, and PepTag® kit, under many different conditions. Our first surprise was that RON13 seems to be insensitive to the broad-spectrum kinase inhibitor staurosporine (STS). This inhibitor is known for its potent inhibition of many kinases, including protein kinase C, protein kinase A and protein kinase G by binding with high affinity to the ATP binding site. This absence of inhibition by STS can indicate that RON13 ATP pocket might be specific and different in its composition or folding, from the other classical kinases. Then we tried to evaluate the activity of RON13 using enzymatic methods like the measurement of ATP to ADP conversion that accompanied phosphorylation events using the

ATP-Lite luminescence assay. We measured ATPase activity without adding a substrate and we observed an important ATP consumption suggesting an autophosphorylation process. Our *in vitro* and comparative phosphoproteomic data comparing RON13wt and RON13deadkinase suggest that the ATP consumption observed *in vitro* likely results from a strong intrinsic ATPase activity of this kinase rather than efficient site phosphorylation in the tested conditions, catalysed at the enzyme active site. Taking advantage of this measurable intrinsic ATPase activity that does not require a substrate, we screened two sets of compounds, the 400 compounds of the pathogen box (MMV) as well as a small a set of 80 kinase inhibitors. None of these inhibitors appears to interfere with RON13 ATPase activity.

The autophosphorylation of RON13 was confirmed after the identification of three autophosphorylation sites. Mutation of these residues to alanine inhibit the autophosphorylation *in vitro* but we observed only a mild defect in invasion in mutated parasites suggesting that RON13 autophosphorylation is not strictly required for its activity.

5.1.2. The peculiar structure of RON13

The structures obtained for some rhoptry kinases, including ROP2, ROP5 and ROP18 showed an extended N-termini composed of helical arrangements present upstream the ATP- interacting beta-sheet of the N-lobe (Qiu *et al.*, 2009; Reese and Boothroyd, 2011). This extension is thought to contribute to the regulation of kinase activity by autophosphorylation. Interestingly, this extension is absent in RON13. In contrast, the N-lobe structure shows a unique insertion composed of four alpha helices between strand β3 and the helix equivalent to helix α3 in PKA. This N-terminal insertion (NTI) extends to the ATP binding pocket without occluding the access to nucleotides. The NTI is present in some RON13 coccidian homologues like *Eimeria tenella* and *Neospora caninum* but is absent in other known kinases. Another unique feature of RON13 is the C-terminal extension that shares no sequence homology with any kinase or other proteins apart from some coccidian homologues. It is mainly composed of alpha-helices with a large portion

that clamps over the kinase domain C-lobe. When searching for structural similarity of the C-terminal extension we identified Cytochrome P450, which overlays with about half of the extension. Interestingly, RON13 has a cavity at the same position where heme binds Cytochrome P450 but lacks the crucial cysteine, and access to the cavity is hampered by the kinase domain.

5.1.3. A non-secreted rhoptry neck kinase

ROPKs are a coccidian family of protein kinases that localize to the rhoptry bulb, several of which are key virulence factors (Fox *et al.*, 2016). We systematically compared RON13 kinase domain sequence to known ROPKs as well as to other lineage-specific family of apicomplexan parasites such as FIKK kinases and to superfamilies of eukaryotic kinases. It revealed that RON13 clusters with the expanded family of ROPKs. But while ROPKs are known to be secreted into the host cells to manipulate host response and promote encystation, RON13 does not appear to be secreted into the host cell but is rather active in the parasite.

Whether phosphorylation of rhoptry proteins occurs along the trafficking route, in the rhoptry lumen or post-secretion, needs to be determined. There is no data available to confirm the presence or absence of ATP in the rhoptries. However, presence of luminal ATP in the ER, Golgi compartments, secretory vesicles and granules has been shown in several organisms, like yeast (Zhong *et al.*, 2003). This ATP is needed for trafficking, folding and phosphorylation of proteins. While it has not been demonstrated in apicomplexan parasites, organellar fractionation and rhoptries purification can help answer this question. The extensive phosphorylation observed in the rhoptry proteins is highly suggestive of the presence of ATP in the rhoptry or along the secretory pathway. This may indicate that phosphorylation could be an important trigger of a signaling cascade that eventually leads to the secretion of rhoptry proteins including the RON complex.

As most kinases, RON13 phosphorylates multiple substrates implying that the overall phenotype of RON13 depleted parasites might not be assigned to only one substrate. However, we can propose some putative RON13 substrate candidates in light of the phenotypes we observed.

5.1.4. A defect in MJ formation at the time of invasion

The strating goal of this project was to determine if RON13 was the ASP3 substrate responsible for the rhoptry secretion defect. Everything pointed to it: a rhoptry neck kinase, a mislocalization of the uncleaved protein, and a severe defect in invasion. Unfortunately, the answer is no. RON13 has no defect in rhoptry discharge. This result was received as kind of a disappointment at that time. However, looking at what we got with this protein, I think we are very satisfied with the outcome, at least I am. Dealing with a kinase crucial for invasion but with no defect in rhoptry secretion, made the project more challenging and amusing. In the case of RON13 depletion, the invasion impairment was due to a defect in the proper assembly of the MJ (made of the RON complex – RON2/4/5/8 and AMA1). The members of the RON complex are known to assemble prior rhoptry secretion and the complex already exists in the rhoptry organelle. By immunofluorescence assay and western blot, we validated that all the componements of the RON complex are properly expressed and localize to rhoptries. In addition, mass spectrometry results of RON4-co-immunoprecipitation indicated that the RON complex is inact prior secretion in both the control ΔKu80 and RON13-iKD. All these results demonstrate that RON13 kinase does not affect the trafficking and the assembly of the MJ complex prior secretion but plays a pivotal role in the RON complex stability once secreted, affecting dramatically the parasite invasion. The requirement of RON13 kinase activity to perform this essential step of the invasion indicates a crucial role of phosphorylation of the RON complex for the MJ assembly. Trying to understand more in depth this phenotype and the absence of the MJ, we studied *in vitro* and *in vivo* the impact of the phosphorylation on RON4 function but unfortunately, we were not able to mimic the phenotype observed in RON13-depeleted parasites. We opted to focus on RON4 due to its important role in the interaction with the host cell cytoskeleton (Guerin *et al.*, 2017) and its strong phosphorylation by RON13. But we could have also checked RON2 since its

phosphorylation might be important for its anchoring to the host membrane. So, without RON2 binding to AMA1, the RONs complex will just get diluted inside the host cytosol and can explain why we were not able to see a signal of the RONs complex at the moving junction.

What is interesting in these results, is that, in RON13-ikD, the subpopulation of parasites in the process of entry (in/out) shows a large proportion (74%) of RON13 depleted parasites with a complete absence of MJ while 20% present an abnormal staining using the antibodies raised against MJ components.

This suggest that parasites were still able to go halfway through the host cell PM even without the "conventional" MJ or with the presence of an aberrant structure.

Several possible explanations can be suggested. We already know that there is a redundancy in the components of the MJ, including AMA1 (Guérin *et al.*, 2017; Lamarque *et al.*, 2014; Parker *et al.*, 2016). It is possible then that other paralogs contribute to the invagination of the parasite in the absence of a conventional RONs complex without being sufficient for a successful invasion. It is also possible that there are other complexes and interacting partners that play a role during invasion. In *Plasmodium*¸ the SURGE complex can form a moving junction by binding to cytoskeletal RBC proteins linking the parasite PM to the host cytoskeleton (Quintana *et al.*, 2018; Zhu *et al.*, 2017). During the in/out experiments, we observed in some parasites, a staining of SAG1 in intracellular parasites (without permeabilization) **(Figure 5.1)**. SAG1 is a surface protein, and it should only stain extracellular parasites in absence of permeabilization agents (such us Triton X-100). This reflect that the interaction between the plasma membrane of the RON13-depleted parasites and the host cell, is loose comparing to the firm and tight attachment made by the MJ in wild-type parasites, and not sufficient to propel the parasite all the way in.

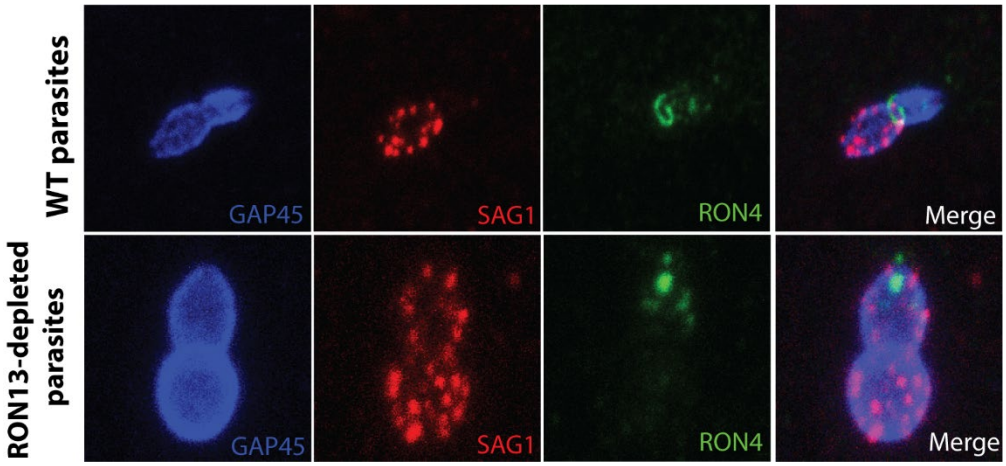

Figure 5.1 **SAG1 is observed in intracellular parasites**. Anti-SAG1 antibody (red) stain the extracellular part of the parasite and anti-GAP45 antibody (blue) stain both parts of the parasite.

Another explanation is the presence of another pathway that leads to a first step towards parasite invasion. In *Plasmodium* parasites, invasion can be achieved through the sialic acid-dependent pathway. The rhoptry bulb protein PfRA is an adhesin that is translocated to the merozoite surface upon invasion and interact with sialic acids on the RBC membrane driving the parasite invasion (Anand *et al.*, 2016). Rhoptry neck protein PfRh (reticulocyte binding protein homologue) play a key role during merozoites invasion with PfRh1 and PfRh4 that bind erythrocyte in a sialic-dependent manner (Triglia *et al.*, 2009; Wai-Hong *et al.*, 2009). Recent studies in *Toxoplasma* identified two novel micronemal proteins CRMPa and CRMPb that are essential for invasion and rhoptry secretion (Sparvoli *et al.*, 2022). Both proteins contain a carbohydrate-binding domain known to interact with sialic acids and CRMPs bears features of G protein-coupled receptor (GPCR). Additionally, the two micronemal proteins are part of a large complex that is translocated near the rhoptry secretion site at the time of invasion with the host cell-binding domain of CRMPs exposed in the extracellular milieu **(Figure 5.2)**. This suggests that the CRMP complex may bind to host ligands at the PM surface and can drive the first attachment and maybe the invagination of the parasite inside the host cell.

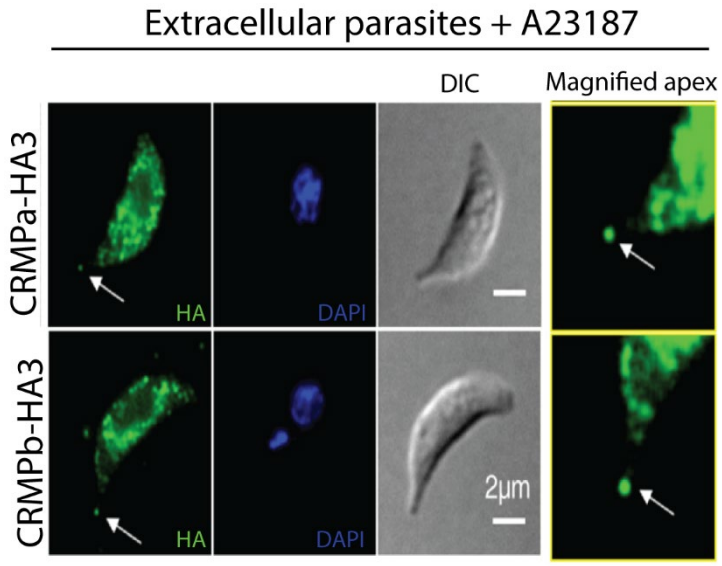

Figure 5.2 **CRMPa and CRMPb accumulate at the tip of the parasite.** Immunofluorescence images of extracellular parasites incubated with calcium ionophore A23187. The calcium ionophore is used to induce conoid extrusion. Image modified from (Sparvoli et al., 2022).

All these possible alternative complexes and pathways that can compensate the loss of the MJ could explain how the parasite is still able to penetrate to a certain level the host cell. The non-efficient invasion can be explained by the weak attachment between the parasite and the host that is not enough to fully push the parasite inside in absence of the active and firm attachment mediated by the MJ. Another explanation is that the parasite is still able to invade without the moving junction but is unable to detach from the PM. It was recently shown that the RONs complex plays a critical role in the pinching off of the tachyzoites PV (Pavlou *et al.*, 2018). The RONs complex plays a similar mechanical function to those of dynamin mechano-enzymes. Thus, without MJ, the parasite might be able to invade but incapable of separating from the host cell membrane. Another question that come to mind is the role of the MJ in the formation of the PV. Are the RON13-depeleted parasites able to form the PV while halfway inside? This could simply be addressed by immunofluorescence assay using an anti-ROP antibody during the invasion of the mutant.

5.1.5. So, who's the culprit?

As I mentioned at the start of this discussion, RON13 project is an example of how serendipity can be a driving force in research. After finding out that RON13 was not recapitulating the ASP3 phenotype, we kind of forgot about that goal and focused mainly on understanding RON13 function. Ultimately, not only RON13 turned out to have a very intriguing phenotype, but an innocent experiment (U-ExM) took us back to ASP3 and gave us a big step forward to understand the observed defect in rhoptry discharge.

ASP3 depleted parasites fail to invade due to a severe defect in rhoptry secretion. Some important players in the organelle's discharge were identified as substrates of ASP3. MIC8 is a micronemal protein that is essential for rhoptry secretion (Kessler *et al.*, 2008), however its role is still unknown. MIC8 forms a complex with another micronemal protein, MIC3 that possess an epidermal growth factor-like domain. It is possible that upon microneme secretion, this complex recognizes and interacts with an unknown ligand on the host cell triggering the rhoptry secretion. Both these proteins are processed by ASP3, but it was shown that the lack of processing does not impact the dimerization or the trafficking of these proteins to the micronemes (Dogga *et al.*, 2017) and MIC3 is predicted to be a dispensable gene based on its fitness score (Sidik *et al.*, 2016). Finally, in ASP3-iKD strain, there was no impact on the trafficking of proteins of the RON complex and RON2-RON4 interaction was normal (Dogga et al., 2017).

This left us with RON13 that was not our jackpot. However, the story took a new turn with the emergence of U-ExM that allows an increase in the resolution and to reveal new details that were not reachable with the conventional microscopy. We implemented this technique to assess in more details the localization of RON13 and other rhoptry proteins in presence or absence of ASP3. Our first observation was that the proteins in the rhoptry neck did not localize to the same space, with RON2 and RON4 found all along the neck whereas RON13 and RON9 were at the extreme tip of the rhoptry. This raises the question again on how and why these proteins are trafficked to different sub-compartments of the

organelle. Why a protein that is not secreted inside the host cell yet localizes to the tip of the organelle, and how is it prevented from being discharged along with the other proteins and lipids? So many questions that needs to be addressed to fully understand how these proteins are secreted. In *Plasmodium*, PfRh1 was shown to localize at the apical tip of the merozoite during invasion and a fraction of the protein was even observed at the MJ (Triglia *et al.*, 2009). PfRh and PfRA proteins are an example of the possible secretion of rhoptries on the surface of the parasite, which was never documented in *Toxoplasma*. It is possible that the first step of rhoptry discharge is the fusion of the docked rhoptries with the AV and RSA and a first secretion of some of the content in the restreint extracellular environment between the parasite and the host cell. Some of these proteins can play a role in the attachment and the fusion of the PM of the parasite to the host cell PM and then the release of the rest of the content inside the host cell. This can explain why proteins that are at the apical tip of the rhoptry neck such as RON13, RON9 and RON10 are not found secreted inside the host (Lamarque *et al.*, 2012).

The second observation was not expected and turned out to be the "easter egg" of the RON13 project. When depleting ASP3, we observed by U-ExM **(Figure 5.3 A)** that the neck of the organelle disappears, and the bulb seems closer to the conoid. This was then confirmed with FIB-SEM that showed that the rhoptry neck was morphologically aberrant and does not extend to the apical tip of the parasite **(Figure 5.3 B)**. This was our Eureka moment. This result now explains the rhoptry secretion defect observed in ASP3-depleted parasites. But that's not the end of it.

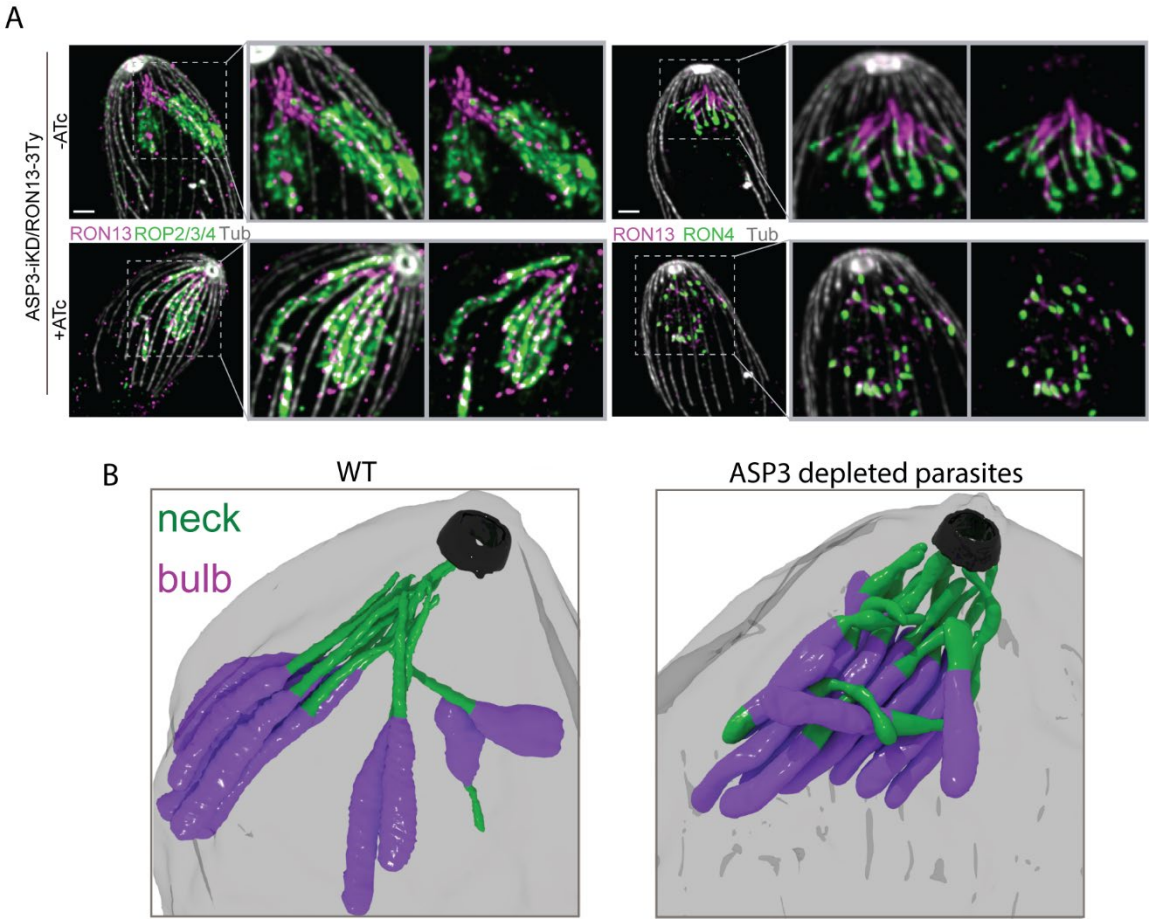

Figure 5.3 **Altered rhoptry neck structure in the absence of ASP3**. **A.** U-ExM images of rhoptries in presence or absence of ASP3. With ROP2/3/4 staining, we can see that the bulb seems very close from the apical tip of the parasite in ASP3-depleted parasites **B.** 3D reconstruction from FIB-SEM showing the aberrant structure of the rhoptry neck in absence of ASP3. Image modified from (Lentini et al., 2021).

The question now is, how can the un-processing of protein(s) be responsible of such a dramatic defect in the organelle biogenesis? This question is hard to answer because we don't know exactly how the rhoptry organelle is formed and what gives it this club-shape. Recently, cryo-ET of both *Cryptosporidium* and *T. gondii* rhoptries, uncovered new details on the structure of the rhoptry neck, results that took us a step forward to answering these questions. They showed that the rhoptry neck was subdivided to three distinct compartments, a short anterior tip followed by two type of membrane-associated helical

filaments that shape the neck to an anterior and a posterior region **(Figure 5.4)** (Mageswaran *et al.*, 2021) confirming our findings using U/ExM. Filaments on both anterior and posterior neck have different handedness and width which makes them unlikely to be composed of the same protein, but this needs to be established. Additionally, the rhoptry bulb seems devoid from filamentous lining supporting the contribution of these helical filaments in shaping the rhoptry organelle.

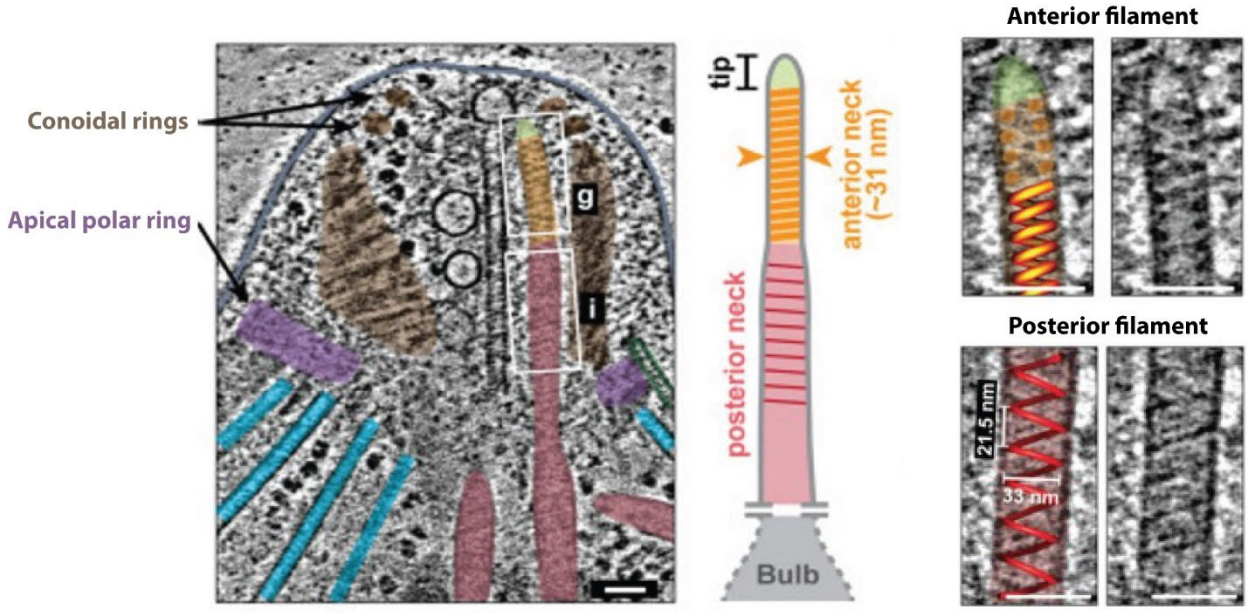

Figure 5.4 **Membrane-associated filaments shape the rhoptry neck in *T. gondii***. Image reproduced from the introduction (Figure 1.9). Image modified from (Mageswaran et al., 2021).

This definitely adds another layer to the complexity of the rhoptry organelle and these filamentous arrangements need to be studied further to confirm their contribution to the proper distribution of rhoptry proteins to the various sub-compartments. It will be very informative to assess these membrane-associated filaments in ASP3-depeleted parasites and if their absence is confirmed, to inspect closely the list of potential substrates that can explain such phenotype. It will be interesting to study in depth the distribution of the rhoptry neck proteins in absence of the neck itself. Do we still see some kind of sub-compartmentalization or the content of the rhoptry will be mixed? And what about the docked rhoptries? We already saw the bulbous part of the rhoptry very close to the conoid in ASP3-depleted parasites.

So, is the rhoptry shape important for its discharge even though the molecular content is preserved? All these questions can be addressed if we ever get to find the molecular identity of these filaments.

5.2. Discussion of chapter 2

While we were still wrapping the RON13 project and preparing our submission, I was already eager to move on to something new. I did not know that Dominique had already an idea about the next adventure. This was concurrent with the publication of the new dataset (LOPIT) where proteins were assigned to different subcellular compartment with what it seems to be a high accuracy (Barylyuk *et al.*, 2020). We knew that we were still eager to find new molecules essential for the rhoptry secretion and we were sure that there are plenty more fish in the sea. So, I embarked in this fishing expedition, and I started by looking at hypothetical rhoptry proteins that were assigned as rhoptry proteins in the LOPIT dataset. This of course gave too many candidates that needed to be shortlisted. The second filter was to make sure that all those candidates harbored either a signal peptide or a transmembrane domain that solidify their predicted rhoptry localization. In the LOPIT data set, the rhoptry compartment was sub-divided in “rhoptries 1” attributed to predicted soluble rhoptry protein and “rhoptries 2” predicted to be transmembrane proteins. Another filter was the gene essentiality. That was applied using the CRISPR loss of function screen (Sidik *et al.*, 2016) and we set our threshold to (≤ −2). The last filter was the expression profile of these proteins as we compared them to other profiles of characterized rhoptry proteins.
This gave us a list of 9 potential essential rhoptry proteins. This data-driven approach can be very helpful to discover novel rhoptry components. However, we also need to consider the pitfalls present in such approach. Firstly, this approach is based on experimental data of published genome-wide screens (localization and essentiality) and these datasets can introduce many false positive candidates in the shortlist. The datasets are based on the apicomplexan genome annotations that are constantly improved.

LOPIT dataset only represent a fraction of the annotated genes that were detected by this method. Only 3832 proteins out of 8158 were detected across all experiments and only 1916 were assigned to compartments with high confidence which mean that many other rhoptry proteins were excluded from our shortlist due to this limitation. The published CRISPR score presents 5 to 10% of false predictions which can also introduce false positive candidates.

For the functional characterization of the 9 candidates, we chose to use the U1 mediated downregulation approach in the DiCre-lox recombinase background that is regulated by the addition of rapamycin (Pieperhoff *et al.*, 2015). Tagging of the constructs was successful for all candidates except for LOPIT-7 and LOPIT-9 even after several trials. It is possible that a C-terminal tagging is not tolerated or the 3'UTR tag directly influence the level of gene expression resulting in a decrease in mRNA level and thus protein level. This was already reported in the U1 gene silencing study, where they failed to tag several proteins using this technique (Pieperhoff *et al.*, 2015). Additionally, geneome annotation on ToxoDB is regularly updated, and it is possible that these genes' annotation was not accurate.

Our results showed a downregulation of 6 genes over 7, observed after 48h or 72h of rapamycin treatment by both IFAs and western blots **(Figure 3.6 and 3.7)**. Western-Blot of LOPIT-8 still showed a band after 48h treatment while no protein was observed by IFA 72h post treatment. We need to assess the regulation after 72h using western blot to be able to interpret the results for this mutant. All the proteins showed a rhoptry localization, but LOPIT-8 that had a vesicular signal close to the rhoptries **(Figure 3.7)**. This confirms the high accuracy of the LOPIT dataset. However, to our surprise, only 1 candidate (LOPIT-1) showed a severe defect by plaque assay with no observable plaques, reflecting its essentiality **(Figure 3.8 A)**. LOPIT-2 annotated wrongly as RON3 had a mild defect. RON3 is a rhoptry bulb protein, already shown to interact with PfRON2 and PfRON4 in *Plasmodium* but it does not localize to the MJ (Ito *et al.*, 2011). This protein was also found in another complex interacting with rhoptry bulb protein PfRAMA (Ito *et al.*, 2021). PfRON3 is secreted into the host cell and RON3-deficient parasites failed to develop beyond the ring stage and glucose uptake was decreased (M *et al.*, 2019).

This phenotype is not yet confirmed in *Toxoplasma*, but it highlights the phenotype we observed by plaque assay. Depletion of the other 5 genes did not impact on parasite survival, contrasting with the data from the fitness conferring scores assigned in the CRISPR-Cas9 study **(Table 3)**.

Name	Gene ID	CRISPR score *Tg*	LOPIT Localisation	Signal Peptide	Transmembrane Domain (TM)	Molecular Weight (kDa)
LOPIT 3	TGGT1_297960	-3.48	rhoptries 1	YES	1	238.66
LOPIT 4	TGGT1_305590	-3.05	rhoptries 2	NO	9	206.11
LOPIT 5	TGGT1_276210	-2.94	rhoptries 1	YES	0	94.51
LOPIT 6	TGGT1_315470	-2.83	rhoptries 2	YES	2	135.83
LOPIT 8	TGGT1_225200	-2.54	rhoptries 1	YES	0	160.96

Table 3 **List of LOPITs that did not impact the parasite lytic cycle after their depletion**

There is no easy way to explain this and so many factors can interfere. To overcome this situation and to confirm these results, we could have made a clean knockout of these genes or chose another system that would give a clear result about their essentiality. Due to time concern and to the unpredicted confinement due to Covid, we had to prioritize the work and I chose to focus on LOPIT-1 (RAP1). This of course was a deviation from our initial plan, but our work was kindly paid-off by RAP1 project (no regret!). As stated before, CRISPR score is not an exact science even though it is a great indicator of essential genes in *Toxoplasma*. So, some of these genes can be part of the 5 to 10% (over 8150 genes) false positives of this study. Another plausible reason is about the chosen downregulation system. The combination of C-terminal tagging and U1 mediated knockdown with the regulated Dicre-mediated excision is not efficient for all genes and when it works, the excision rate is only 80 to 90%. That means that the remaining 20 or 10% of parasites with a non-excised gene are able to produce the protein. This can influence the results of a plaque assay since parasites with non-excised genes would form plaques. Hence, the “conventional” way we perform and analyze the results of plaque assay is not the best to really characterize proteins using this method. We should either use a tighter system such as the Tet-inducible (Meissner *et al.*, 2005) or monitor the number of parasites used in plaque assay and analyze not only the size of the plaques but also the number.

It is also important to look if the genes are well annotated and check the transcriptomics results from the tachyzoite nanopore long-read RNA seq. Doing this, we found that LOPIT-3 was not well annotated in ToxoDB and the RNA seq data show that a big portion of the protein was not transcribed **(Figure 5.5).**

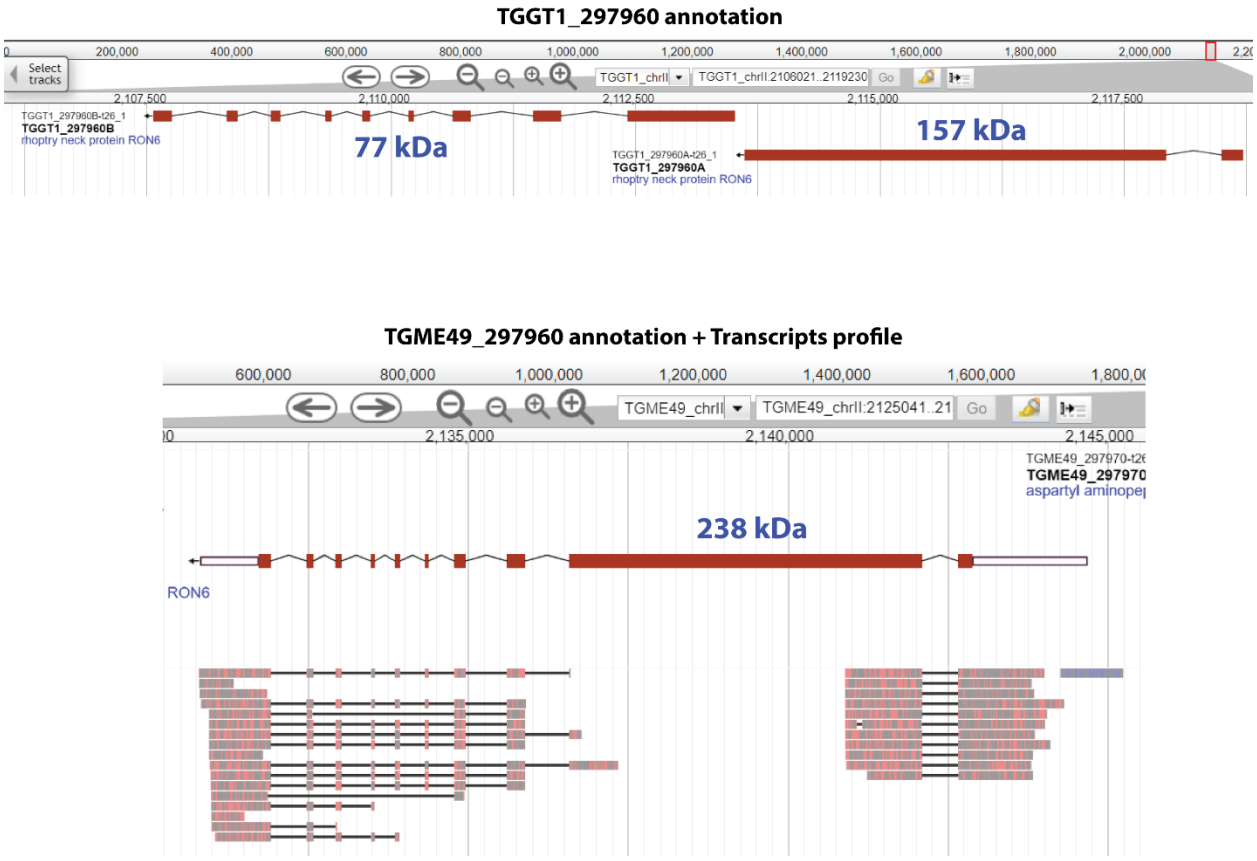

Figure 5.5 **Annotation of LOPIT-3 in ToxoDB.**

Additionally, in TGGT1 strain, LOPIT-3 was annotated as two separate genes with products of 77 kDa and 157 kDa **(Figure 5.5).** However, in TGME49, which usually has the accurate annotation, LOPIT-3 is annotated as one gene of 238 kDa **(Figure 5.5).** We tagged this protein at the C-terminal end that in TGGT1 (the strain used in the lab) correspond to the 77 kDa product. This was reflected in the western blot where it shows a band that migrates closely to 70 kDa, corresponding to TGGT1_297960B **(Chapter 2 - Figure 3.6 C).** Additionally, LOPIT-6 and LOPIT-8 showed multiple bands in the western blot showing either several protein

products due to processing or degradation of the proteins.

Altogether, these preliminary results need to be taking with a grain of salt and we need to perform more experiments to be able to validate and to interpret the observed phenotypes.

5.3. Discussion of chapter 3 on RAP1

5.3.1. Where to start?

Let's start by how all this took place. It all started with the screening discussed in the previous chapter, which started as Covid emerged and it was a bit of challenge to stay focused and to get to the end of it without wasting more time. As discussed in the previous chapter, the screening was not a big success unfortunately, but as we learn from all the experiences, it was indeed very eye-opening and also taught me that we should sometimes take a step back and look at the bigger picture. If I can go back in time, I think I would have done things differently and I would have taken my time to look closer at the results rather than jumping immediately on LOPIT-1 (RAP1) and leaving everything else behind (until now!). So as soon as I got the results from the plaque assays, I was so excited to look closely at LOPIT-1. I did all the necessary experiments that I knew will convince Dominique to let me run this project. The preliminary data at that time were the plaque assay, the localization, an invasion assay showing that this protein is important for this step and my favorite assay "the rhoptry secretion" that confirmed that LOPIT-1 plays a role in there. Coming to Dominique with those got me to start the journey with RAP1.

5.3.2. Is it a ROP or a RAP?

Working with this protein, was more challenging than I thought. Let's start with the localization issue. Results from immunofluorescence showed clearly that RAP1 localized to the bulb and colocalized well with markers of rhoptry bulb proteins (**Figure 3.9 C).**

So here we had in our hands the first rhoptry bulb in *Toxoplasma* that played a role in invasion and rhoptry secretion. This was exciting and intriguing at the same time. Why and how a protein that is localized in the bulb of the rhoptries being important for their discharge? In *Plasmodium* many rhoptry bulb proteins such as the rhoptry-associated adhesin PfRA, the rhoptry-associated membrane antigen PfRAMA and the RhopH complex contribute to parasite invasion but do not affect rhoptry secretion (Anand *et al.*, 2016; Sherling *et al.*, 2017, 2019). Additionally, like most content of the rhoptry bulb, these proteins are secreted outside of the parasite. To check if RAP1 is also secreted inside the host cell, we performed the same assay "e-vacuole assay" that we use to assess rhoptry secretion **(Figure 5.6 A)**. To do so, we treat extracellular parasites (in presence of host cells) with cytochalasin D (inhibitor of actin polymerization) that prevents invasion but not rhoptry secretion. Under these conditions, protein and lipid-rich vesicles called e-vacuoles, for empty vacuoles, are released into the host cell and visualized using anti-ROP1 antibody (Hakansson *et al.*, 2001). We observed that RAP1 is not released into the host cell in contrast to the visible trail of ROP1 **(Figure 5.6 B)** suggesting that RAP1 is not secreted during invasion. However, this method is not the most accurate because if RAP1 is secreted in a very small amounts it will get diluted within the host cell cytosol and cannot be visualized using conventional fluorescence microscopy imaging. Two other approaches were initiated to overcome this problem. The first one was by using a highly sensitive assay based on fluorescence resonance energy transfer (FRET) and βLactamase fused to the C-terminal of the protein of interest **(Figure 5.6 C)**. In this assay we use BLA substrate that links two fluorescent molecules: coumarin cephalosporin fluorescein (CCF2) that can detect the presence of BLA-fused proteins. The substrate is administered to host cells with an acetoxymethyl group (CCF2-AM). Host cell esterases will cleave this group resulting in retention of the substrate in the host cell cytosol. In the absence of BLA, the fluorophores are in close proximity and excitation at 407 nm results in a shift and emission of green fluorescent signal at 520 nm (fluorescein). However, when BLA is present, the substrate is cleaved, and the fluorophores are dissociated. In that case, excitation at 407 nm results in emission at 447 nm (coumarin) and a blue fluorescent signal as observed when rhoptry protein Toxofilin is secreted (Lodoen *et al.*, 2010). The second method was also used on Toxofilin where it is fused to Cre-recombinase **(Figure 5.6 D)** (Koshy et al., 2010).

This method is highly sensitive, and it monitors the excision of Cre following rhoptry secretion and can be measured by either fluorescence microscopy or fluorescence-activated cell sorting (FACS). We tried to tag RAP1 with either the βlactamase or the Cre-recombinase but unfortunately it was not possible as transfection using a big tag does not seem to work with such small protein (21 kDa).

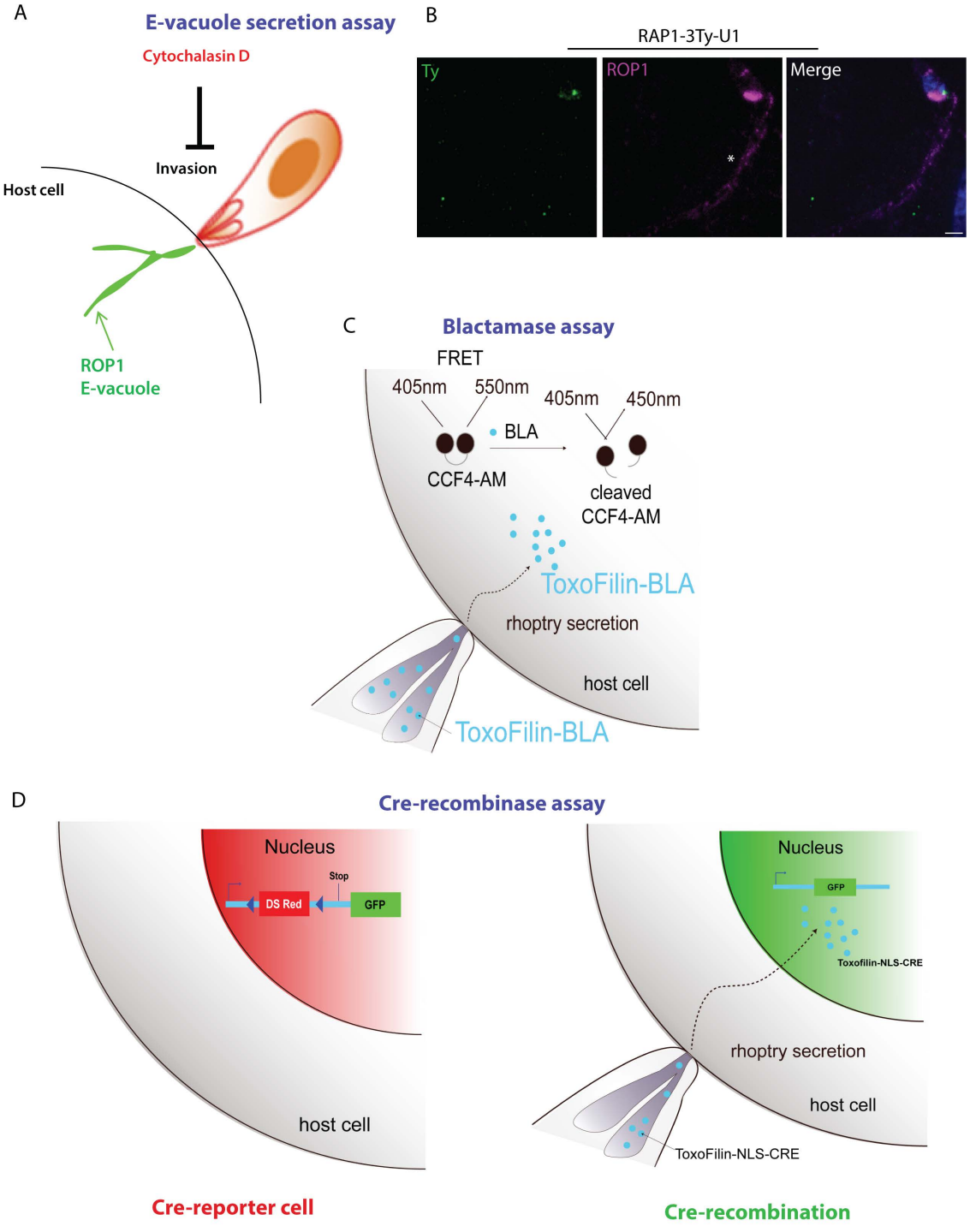

Figure 5.6 **Secretion of RAP1 inside the host cell. (A).** Schematic description of the E-vacuole assay. **(B).** IFAs showing that RAP1 is not secreted along with the E-vacuoles. Anti-Ty antibodies used to stain RAP1. Anti-ROP1 antibodies stain the E-vacuoles. White * shows the ROP1 trails. DAPI in blue is staining DNA. Scale bar = 2 µM. **(C).** Schematic representation of the Blactamase assay. **(D)** Schematic representation of the Cre-recombinase assay.

RAP1 is a soluble protein as observed in the fractionation assay **(Figure 3.9 D)**. However, we wanted to be sure if it is really inside the lumen of rhoptry bulb. To determine that we first tried to study its topology using proteinase K assay where we use a mild detergent such as digitonin to only permeabilize the parasite PM and then add proteinase K that will digest proteins found only in the cytosol or transmembrane proteins. Presence or absence of the protein is detected using western blot. Unfortunately, after several trials, this assay did not work (we also failed to implement it for RON13 in a previous time). Since the protein is fully soluble and is not predicted to have a transmembrane domain, we opted to answer this question using the mAID system (Brown *et al.*, 2017). Using this system, we showed that upon addition of auxin, RAP1 was not degraded (**Figure 3.15 A-C)** which mean that RAP1 C-terminal domain is not exposed to the cytosol. These results points towards RAP1 being inside the lumen. But looking at the dynamic localization of the protein during and after invasion **(discussed in detail in section 5.1.5)** and its importance for rhoptry secretion, this theory became more and more absurd. We tried to overcome this by using high level resolution methods. We first tried immunoelectron microscopy to try and localize more precisely the protein. Unfortunately, this technique was inconclusive and thus did not further clarify the localization of RAP1 in intracellular parasites. The second method was the use of U-ExM technique that can resolve protein localization at very high level of resolution (~60 to 70 nm). Results showed that the staining of RAP1 was different from ROP5 **(Figure 3.15 D)** and was visible as small dots likely corresponding to vesicles decorating the rhoptry bulb. Interestingly, observation on metal replicas of fractured parasites showed the presence of IMPs on both faces of the membrane with higher density in the bulb regions **(Figure 5.7)** (Lemgruber et al., 2011).

The IMPs were arranged in parallel rows around both bulb and neck and even though their molecular identity and function are not known, it was speculated that they may play a role in rhoptry positioning and/or the secretion of the rhoptry content.

Adding this to the fact that we see an apical localization at the tip of rhoptries and a punctuated signal of RAP1 upon invasion that do not colocalize with rhoptries, all this point to the hypothesis that RAP1 is not inside the rhoptry bulb lumen but probably in vesicles surrounding the bulb.

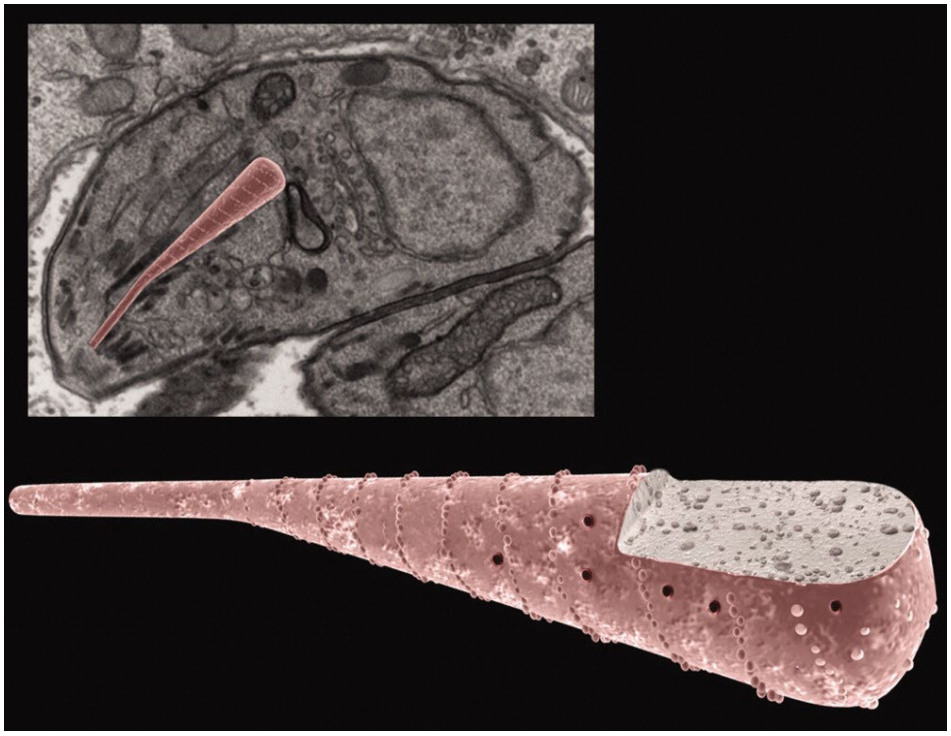

Figure 5.7 **Schematic model of the IMPS on the rhoptry organelle.** The pore like structures and the row of IMPs can be observed. Image from (Lemgruber et al., 2011).

5.3.3. About RAP1 structure: Uniqueness and talent

RAP1 is a small protein of only 200 amino acids (21 kDa), that has a signal peptide and no identified domain which made it extremely complicated to draw hypothesis. The AA sequence of RAP1 is intriguing with 38.5% of electrically charged residues (23% negatively charged) that are located mostly as patches of aspartic acid and lysine at the C-terminal end **(Figure 5.8 A)**

making it highly disordered. RAP1 seems to be only conserved in *Hammondia* and *Neospora* species only **(Figure 5.8 B)**. As stated before, some similarities are observed with *Plasmodium* PfASP protein that harbors patches of negatively charged residues in the C-terminal end but this do not recall for a conservation between both proteins (O'Keeffe *et al.*, 2005).

A

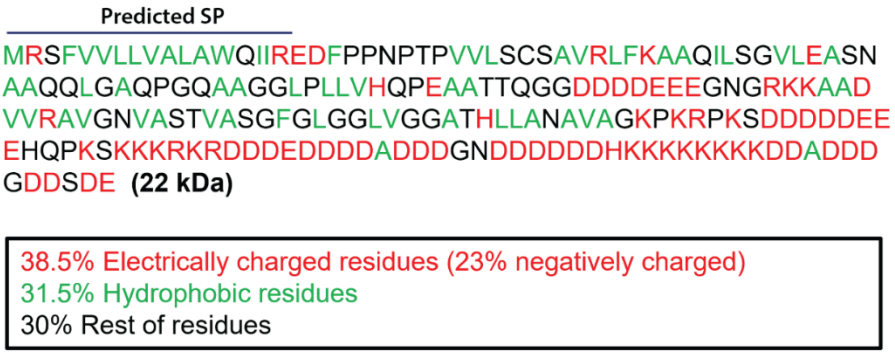

B

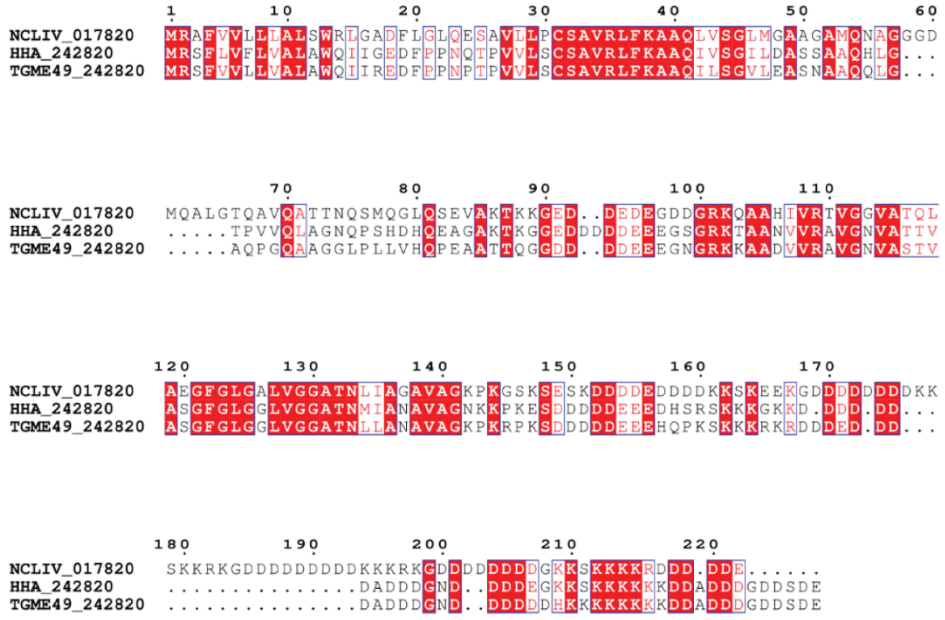

Figure 5.8 **RAP1 sequence and conservation. (A).** Sequence of RAP showing in different colors the different distribution of the residues. **(B).** The alignment of TgRAP1 with homologs in *Hammondia Hammondi* and *Neospora caninum.* Residues highlighted in red are conserved across the three species.

Other coccidian species are not as well studied as *Toxoplasma* making it hard to understand why such an important protein is only found in 3 species of this group. Digging up some papers about rhoptries in coccidia showed that what can be in common between *T. gondii, Neospora* and *Hammondia* is that three of them have more than two rhoptries. In a paper published in 1994 where they tried to identify antigens of *N. caninum,* immunogold electron micrographs showed the presence of at least 5 rhoptries per parasite (Bjerkas *et al.*, 1994). In *H. hammondi* electron microscopy showed the presence of multiple rhoptries at the apical pole of the parasite (Dubey and Ferguson, 2015). Concerning *E. tenella* and *S. muris* only two rhoptries were observed (Burrell *et al.*, 2022; Entzeroth, 1984). This can be an indication that RAP1 is only needed for parasites able to reload their rhoptries for multiple secretions. It was previously observed that *Toxoplasma* is even able to poke and secrete the rhoptries without invading the host cell (Koshy *et al.*, 2012) which can explain why the parasite secretes only two rhoptries per invasion tentative and keeps an arsenal of intact organelles. Assuming that the role of RAP1 is to dock rhoptry to the AV, then for parasites that only secrete once, it is possible that the rhoptries are already fused to the AV during biogenesis, as was observed for *Cryptosporidium* and *Plasmodium* (Mageswaran *et al.*, 2021; Martinez *et al.*, 2022), so there is no need for RAP1 function.

5.3.4. About RAP1 dynamic localization: Catch me if you can

If there is a feature of RAP1 that makes it very interesting, is its localization and the dynamic observed during invasion. I'm going to stop for a minute here and tell a short, but important story about the road I took to determine this localization. At the very start of the project and after knowing its importance in rhoptry secretion, I was so eager to check its localization in extracellular parasites in presence of cytD. I did this experiment hundred times during the RON13 project and I can do it blindfolded. I need to pinpoint here that at that time we did nosee any localization of RAP1 at the rhoptry tip since we were using the RAP1-3Ty-U1 strain. Doing so, we discovered that RAP1 changed localization and he staining at the bulb

disappeared and it accumulated at the rhoptry tip instead **(Figure 5.9 A).** Honestly, we were all excited about this result and we set up a preliminary model for RAP1 and based all the next experiments on this. To be sure about this fundamental result, I did it multiple times and I always got the same outcome. Until one day, I was in a hurry and instead of fixing the parasites for 20 minutes with paraformaldehyde as we are used to, I only fixed for 8 or 10 minutes. The next day I was puzzled looking at the IFAs slides under the microscope, because now the protein localized to both bulb and tip of the rhoptries. It directly hit me that the only difference was the fixation time, so I setup some IFAs for intracellular parasites fixing them at different time point. Indeed, when I fix for more than 10 minutes, the RAP1 staining starts to disappear **(Figure 5.9 B).** I don't want to spoil more details about this, but it changed a lot in the project and also taught me that protocols should not be taken as words on stones.

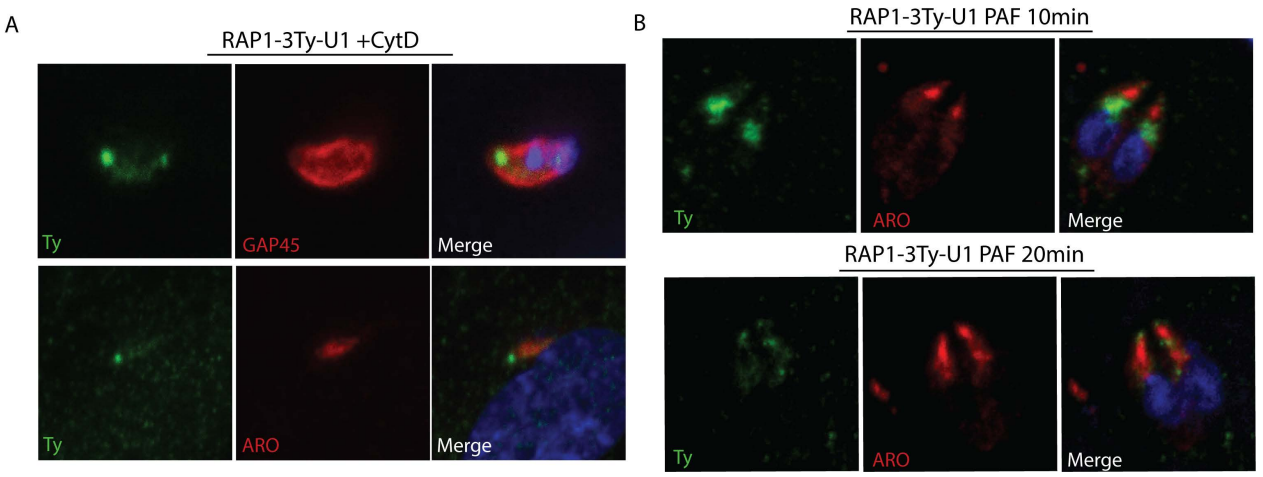

Figure 5.9 **RAP1 localization and impact of fixation. (A).** IFAs of extracellular RAP1-3Ty-U1 in presence of cytochalasin D. Anti-ty antibodies used to stain RAP1. Anti-GAP45 antibodies are used to stain the parasite. Anti-ARO antibodies stain the rhoptry organelle. DAPI in blue is staining DNA. **(B).** IFAs showing the impact of long fixation on RAP1 staining.

Our second misinterpretation of RAP1 localization was the fact that we didn't observe it at the rhoptry tip in RAP1-3Ty-U1 intracellular parasites. When we ectopically expressed a RAP1 second copy to try to complement the phenotypes observed in RAP1-depleted parasites, we discovered that even intracellular parasites showed a RAP1 staining at the tip of the rhoptries. This changed

all over again the model. This localization was by tagging the endogenous RAP1 with 2-Ty tag. The only explanation I see here, is that the introduction of loxP sequences at the 3'UTR of the gene influence the expression and the level of the protein. Maybe what we see at the tip of the rhoptries in intracellular parasites is already a small amount of RAP1 and modifying the 3'UTR makes the level drops even more and thus not detected by immunofluorescence.

So now we have, hopefully, our preliminary model where RAP1 is associated to the rhoptry organelle with a localization around the bulb and at the rhoptry tip. Unfortunately, we can't say for sure if the localization at the tip is inside or outside the rhoptries, however the staining seems to be higher than the stain of ARO, and we also used RON9 which is located at the very tip of the rhoptry, and RAP1 seems to be even more apical. In some IFAs on extracellular parasites in presence of cytD, we observed three distinct localizations of RAP1: bulb, neck and rhoptry tip. This can strengthen our model where we think that "RAP1 vesicles" located at the bulb, moves towards the tip of rhoptries for a probable replenishment, after secretion of rhoptries.

The localization of RAP1 post invasion was also studied. We found that 15 minutes to 1 hour post infection, RAP1 signal disappeared (in rare cases, the signal was extremely faint). Since only two rhoptries are discharged per invasion, we cannot imply that the protein is secreted, because in that case we would have seen a signal in the remaining rhoptries. The only plausible explanation is that the protein is degraded as soon as the parasite is inside. The fate of the RSA, AV, MVs and the key molecular player in rhoptry secretion, was not investigated yet due mostly to a lack of markers. We know that up to 5 minutes post invasion Nd6 signal is still present in the parasite, whereas CRMPs signal at the apical tip of the parasite disappears (Sparvoli *et al.*, 2022). It will be informative to check RAP1 after 5 minutes but also, to check what happens to CSCHAP and RASP2. Interestingly, 4 hours after invasion, RAP1 signal is back again but in 60% of counted parasites, the signal is vesicular and does not localize with rhoptries, whereas in almost the rest of the parasites, the signal is observed at the bulb. There was no localization observed at the tip

of the rhoptries. This means that sometime between 1 to 4 hours, we have again the expression of RAP1, producing vesicles that migrates towards the rhoptry bulb, which is observed 6 hours post invasion where we have an increase of the staining at the bulb (70% of parasites). The replenishment hypothesize was also discussed for the MVs, the vesicles that will replenish the AV and maybe the RSA. But we do not know when this replenishment happens. Is it directly after rhoptry secretion or it happens hours after invasion?

5.3.5. About RAP1 partners: All by myself

Rhoptry secretion mechanism is complex and relies on plenty of key molecular players that usually work in complexes or by binding, through their domains, to membranes or other proteins. Since RAP1 is devoid from any domain, we though to investigate its interaction with other proteins. To do so, we performed a pull-down assay followed by mass spectrometry. This did not help us advance on this part as few proteins were identified and none of them seemed to make sense in this context. This does not mean that there are no partners, but the dynamic localization of this protein might influence the results of the mass spectrometry making it hard to compare between one replicate to another. To overcome this, we tried to fuse RAP1 with either a TurboID, a miniID or even an UltraID but like with the βlactamase and Cre-recombinase the transfections were not successful leaving us with a big gap in this area.

5.3.6. About RAP1 function: the heart of the matter

So now, how do we apply all this knowledge about RAP1 to its function? The rhoptry secretion defect observed in RAP1-depleted parasites is very severe and resemble the one observed in ASP3-depleted parasites. To try to understand how RAP1 participate in this very complicated mechanism and to try to position it in the rhoptry secretion machinery we had to start by looking at its localization regarding the other proteins described before as implicated in rhoptry discharge and located to the apical tip of the parasite. We started with Nd6. This protein is detected at the site of secretion and the Nd6 mutant in *T. gondii* is unable

to secrete the rhoptries (Aquilini et al., 2021). We observed that RAP1 does not colocalize with Nd6 and disruption of the latter does not influence RAP1 localization **(Figure 3.18 B-C)**. The RAP1 signal seemed less apical than Nd6 and closer to rhoptries. The second target was RASP2. RASP2 is conserved in all apicomplexans, and it caps the extremity of the rhoptry neck and interacts with RASP1 and RASP3 (Suarez *et al.*, 2019). Depletion of RASP2 causes a severe defect in rhoptry secretion in both *T. gondii* and *Plasmodium* parasites (Suarez *et al.*, 2019). This protein is for now the best suited as a candidate that regulates the fusion between rhoptry neck and the AV thanks to its C2 domain (Ca2+-dependent lipid-binding) and PH-like domain. RASP2 is then able to bind to lipids such as PA and PIP2 that are known to participate in membrane fusion. However, the C2 domain of RASP2 is divergent and unable to bind calcium making the fusion, a calcium independent mechanism (Suarez *et al.*, 2019). Interestingly, in *Plasmodium*, PfRASP2 named CERLI1 for cytosolically exposed rhoptry-leaflet-interacting protein 1, localizes to the rhoptry bulb and also plays a role in rhoptry secretion (Liffner *et al.*, 2020). Our results show that RAP1 colocalizes with RASP2 at the rhoptry tip **(Figure 3.18 D-E)**. However, depletion of either RAP1 or RASP2 does not affect the localization of the other. Then we checked the colocalization between RAP1 and CSCHAP (Morlon-Guyot, Berry, *et al.*, 2018). This protein is very interesting but unfortunately it was not studied in depth. CSCHAP was shown to play a role in the apical positioning of rhoptries and parasite depleted in CSCHAP are unable to secrete their rhoptries and thus to invade (Morlon-Guyot, Berry, *et al.*, 2018). CSCHAP interacts with CORVET and HOPS tethering complexes and it also has two putative microtubule binding domains. This is different from ARO where positioning of rhoptries is an actomyosin-based process, involving MyoF (Mueller *et al.*, 2013). CSCHAP can contribute to another molecular machinery that depends on tubulin to position rhoptries to the apex. CSCHAP contains a putative dynactin domain that was already shown to interact with CORVET and HOPS during vesicular transport and fusion (van der Kant *et al.*, 2013; Xiang *et al.*, 2015). This imply that CSCHAP might ensure the link between rhoptries, CORVET/HOPS complexes and dynein and/or kinesin motors and probably fix the rhoptries to the ICMTs. Our results showed that RAP1 colocalizes with CSCHAP at the rhoptry tip and depletion of RAP1 does not affect CSCHAP localization **(Figure 3.18 F-G)**.

I2øŜØŜℕ øKŜy øŜ ŘŜLJfŜúŜŘ CSCHAP, rhoptry organelles did not localize apically as described before (Morlon-Guyot, Berry, *et al.*, 2018). We also showed that RAP1 staining followed the rhoptries confirming that this protein is indeed associated to the organelle. Interestingly, our results confirmed that RASP2 is also associated to rhoptries, since in CSCHAP depleted parasites, RASP2 signal was observed normally at the cap of dispersed rhoptries. All these results converge on the fact that these three proteins localize within the same vicinity between the rhoptry tip and the AV, but it is unlikely that they interact directly together since the removal of one does not affect the others.

So now let's put things into perspective. *Toxoplasma* invasion is a highly monitored event in time and space. Not only the parasite orchestrates its invasion at a precise time point but also this event only happens at the apical tip of the parasite. Just after egress from the host cell, microneme exocytosis takes place and persist during gliding and attachment of the parasite to a new cell (Bisio and Soldati-Favre, 2019). Rhoptry secretion is triggered just after, and the signal that triggers it is probably linked to the attachment of the parasite to the host cell through microneme proteins. We showed that in TFP1-depleted parasites, where microneme secretion is abrogated (Hammoudi *et al.*, 2018), RAP1 still localized to the tip of the rhoptries, implying that its localization and maybe function, are independent from microneme exocytosis **(Figure 3.20)**. Additionally, CRMPs and their associated factors are translocated to parasite surface and interact with surface ligands at the host cell PM. This can lead to the activation of a signaling cascade that triggers rhoptry secretion.

For rhoptry secretion to happen, rhoptries should already be docked to the apical tip. Then two crucial steps should follow: the fusion of the rhoptry neck with the AV and then the AV with the RSA at the PM. This will open a channel where the rhoptry content can be discharged. The fusion between the AV and the PM was deciphered using cryo-ET in both *Toxoplasma* and *Plasmodium* (Mageswaran *et al.*, 2021; Martinez *et al.*, 2022). Key molecular players were identified as well, such as Nd6 and Nd9 (Aquilini *et al.*, 2021). Interestingly, depletion of Nd9 leads to not only a decrease in the number of rosettes at the PM (Aquilini *et al.*, 2021) but also to structural defects of the AV and RSA anchoring (Mageswaran *et al.*, 2021). The assembly

and composition of the RSA is still not very well understood which makes it even complicated, to understand how the fusion occurs. Using cryo-ET, a distinct density was observed between the rhoptry neck and the AV **(Figure 1.13)** (Mageswaran *et al.*, 2021), exactly where RAP1, RASP2 and CSCHAP are located. Cryo-ET in absence of RAP1 can confirm if its role during invasion is to assist in the fusion between the neck and the AV explaining the defect in rhoptry secretion when depleted. The dynamic localization of RAP1 can speak for a replenishment process as the one proposed for the MVs. This hypothesis is reinforced by the RAP1-Mut1 mutant, where RAP1 signal is scattered through the cytosol, but the parasite was still able to rescue the invasion to 50% **(Figure 3.16).** In these parasites, the signal accumulated to the tip of the rhoptries in extracellular parasites. However, no signal was observed in the bulb. The hypothesis is that the parasite can secrete the content of the two docked rhoptries rhoptries, but if it does not invade, it does not get a second chance since there is no RAP1 to replenish and to fuse two other rhoptries to the AV.

6. General discussion

Before moving to the conclusion, I want to take a step back and look at the bigger picture that link both RON13 and RAP1 projects and try to summarize my opinion and the model I have in mind about rhoptry secretion mechanism before wrapping up.

It all starts with the end: egress or exit of the parasite from the host cell. At that time, the parasite is ready to reinvade. The secretion machinery is loaded, rhoptries are docked thanks to ARO and CSCHAP, and micronemes are secreted. RON13 was already processed in the ELC by ASP3 and now it is soluble inside the rhoptry neck. RON13 phosphorylates its substrates including the RONs complex, already assembled in the rhoptries and ready to be secreted.

The parasite attaches firmly to its prey thanks to adhesins and micronemes. CRMP complex is translocated to the surface where it binds its ligand on the host cell. This interaction is involved in the cascade that triggers rhoptry secretion. Now everything goes fast and there is

no room for mistakes. In 30 seconds, the parasite will be inside its host. The rhoptries running along the ICMTs will now fuse to the AV. This is done by RASP2 and RAP1 in an independent manner. Now rhoptries and AV need to fuse with the PM. This is done through the RSA that creates a tunnel allowing the opening of a pore at the apex of the parasite where rhoptries will be discharged. This is achieved thanks to the Alveolata-specific complex that include Nd6-Nd9-NdP1-NdP2 and FER2. At this moment, the parasite is attached but the road to the host cytosol is still far. I always thought about rhoptry discharge like trying to squeeze a toothpaste tube. From the bulb, a force drives the release of the rhoptry proteins. In this theory, all the content should be out, if not inside the host, then in the extracellular environment. And this is consolidated by the fact that rhoptries are observed electron-lucent, or empty after secretion. Therefor, content at the tip of the rhoptry neck including RON13, will be pushed out from the parasite. Probably, other rhoptry content are also discharged from the tip and play a role in the fusing with the host PM. Now the parasites have the road open in front of it to enter. But first, the RONs complex, phosphorylated by RON13, is secreted. The trojan horse is inside. The MJ is formed, and the parasite uses the host cytoskeleton to drive itself inside thanks to its glideosome machinery. In the meantime, ROPs are also secreted, and they will help to form the PV and modulate host function. As soon as it pinches out and now secure inside the PV, the parasite degrades RAP1, and the AV and RSA are probably gone as well. But anything can happen that can trigger the parasite to exit even before it starts to replicate. Hence, the machinery needs to be replenished and put together as fast as possible. The parasite then starts to produce RAP1 that is delivered to the remaining rhoptries, upon vesicular trafficking. Probably at this point, the parasite reloads its AV and RSA thanks to the MVs running along the ICMTs and starts to dock two new rhoptries for the subsequent invasion.

7. Concluding remarks

Overall, the projects presented in this thesis, offer an advance in our knowledge of parasite invasion as well as rhoptry secretion. These new data add novel details to these steps and allow broader speculations. RON13-dependent phosphorylation added a new layer of complexity in the build of the MJ and shed light on the importance of PTM during parasite invasion. The parasite seems to rely on multiple proteins, complexes, structures and pathways to invade. As an obligate intracellular organism, *Toxoplasma* needs to adapt and to create a solid machinery and mechanisms to allow it to invade any nucleated cell of all warm-blooded species. It is fascinating how sophisticated is the invasion in Apicomplexa. Even though the chapter for RAP1 is not closed yet, the preleminary data we provided show again, how complex the rhoptry discharge is. The recent technical breakthroughs including U-ExM and CryoET, as well as the emergence of reverse genetics toolbox has facilitated the study of the invasion in apicomplexan parasites and have helped to build the picture around the structures involved in this crucial step. Despite all these discoveries, a lot of questions still need to be addressed. What is the composition of the filaments that compose the rhoptry neck? Without these filaments, does the parasite secrete the rhoptries? How can the parasite breach the host PM without the RONs complex? What is responsible of the fusion of the rhoptries to the AV and RSA? What is exactly the role of the AV? What happens to the empty rhoptries after invasion? Are they degraded or recycled? What are the signaling cascades that trigger rhoptry secretion? All these remaining burning questions need more years and many enthusiastic scientists to answer them.

With all the ups and downs, the joys and disappointment during my PhD, I am very grateful to all the great and brilliant people I worked with and especially to the best supervisor **Dr. Gaelle Lentini** that shared this journey with me from its beginnings to this end, and together we made a golden team.

With my 4 years thesis on a 30 second invasion, I hope that my contribution can push forward the knowledge about this extremely fascinating parasite that I will definitely miss.

8. References

Adl, S.M., Simpson, A.G., Lane, C.E., Lukes, J., Bass, D., Bowser, S.S., Brown, M.W., *et al.* (2012), "The revised classification of eukaryotes", *J Eukaryot Microbiol*, Vol. 59 No. 5, pp. 429–493, doi: 10.1111/j.1550-7408.2012.00644.x.

Aikawa, M., Miller, L.H., Johnson, J. and Rabbege, J. (1978), "Erythrocyte entry by malarial parasites. A moving junction between erythrocyte and parasite", *J Cell Biol*, Vol. 77 No. 1, pp. 72–82.

Alaganan, A., Fentress, S.J., Tang, K., Wang, Q. and Sibley, L.D. (2014), "*Toxoplasma* GRA7 effector increases turnover of immunity-related GTPases and contributes to acute virulence in the mouse", *Proceedings of the National Academy of Sciences of the United States of America*, National Academy of Sciences, Vol. 111 No. 3, pp. 1126–1131, doi: 10.1073/pnas.1313501111.

Alexander, D.L., Mital, J., Ward, G.E., Bradley, P. and Boothroyd, J.C. (2005), "Identification of the moving junction complex of *Toxoplasma gondii*: a collaboration between distinct secretory organelles", *PLoS Pathog*, Vol. 1 No. 2, p. e17, doi: 10.1371/journal.ppat.0010017.

Anand, G., Reddy, K.S., Pandey, A.K., Mian, S.Y., Singh, H., Mittal, S.A., Amlabu, E., *et al.* (2016), "A novel *Plasmodium falciparum* rhoptry associated adhesin mediates erythrocyte invasion through the sialic-acid dependent pathway", *Sci Rep*, Vol. 6, p. 29185, doi: 10.1038/srep29185.

Aquilini, E., Cova, M.M., Mageswaran, S.K., dos Santos Pacheco, N., Sparvoli, D., Penarete-Vargas, D.M., Najm, R., *et al.* (2021), "An Alveolata secretory machinery adapted to parasite host cell invasion", *Nature Microbiology*, Vol. 6 No. 4, pp. 425–434, doi: 10.1038/s41564-020-00854-z.

Arenas, A.F., Osorio-Mendez, J.F., Gutierrez, A.J. and Gomez-Marin, J.E. (2010), "Genome-wide survey and evolutionary analysis of trypsin proteases in apicomplexan parasites", *Genomics Proteomics Bioinformatics*, Vol. 8 No. 2, pp. 103–112, doi: 10.1016/s1672-0229(10)60011-3.

Ayong, L., DaSilva, T., Mauser, J., Allen, C.M. and Chakrabarti, D. (2011), "Evidence for prenylation-dependent targeting of a Ykt6 SNARE in *Plasmodium falciparum*", *Molecular and Biochemical Parasitology*, Vol. 175 No. 2, pp. 162–168, doi: https://doi.org/10.1016/j.molbiopara.2010.11.007.

Bannister, L.H., Hopkins, J.M., Fowler, R.E., Krishna, S. and Mitchell, G.H. (2000), "Ultrastructure of rhoptry development in *Plasmodium falciparum* erythrocytic schizonts", *Parasitology*, Vol. 121 (Pt 3, pp. 273–287.

Bargieri, D.Y., Andenmatten, N., Lagal, V., Thiberge, S., Whitelaw, J.A., Tardieux, I., Meissner, M., *et al.* (2013), "Apical membrane antigen 1 mediates apicomplexan parasite attachment but is dispensable for host cell invasion", *Nat Commun*, Vol. 4, p. 2552, doi: 10.1038/ncomms3552.

Barylyuk, K., Koreny, L., Ke, H., Butterworth, S., Crook, O.M., Lassadi, I., Gupta, V., *et al.* (2020), "A Comprehensive Subcellular Atlas of the *Toxoplasma* Proteome via hyperLOPIT Provides

Spatial Context for Protein Functions", *Cell Host & Microbe*, Vol. 28 No. 5, pp. 752-766.e9, doi: https://doi.org/10.1016/j.chom.2020.09.011.

Beck, J.R., Chen, A.L., Kim, E.W. and Bradley, P.J. (2014), "RON5 is critical for organization and function of the *Toxoplasma* moving junction complex", *PLoS Pathog*, Vol. 10 No. 3, p. e1004025, doi: 10.1371/journal.ppat.1004025.

Beck, J.R., Fung, C., Straub, K.W., Coppens, I., Vashisht, A.A., Wohlschlegel, J.A. and Bradley, P.J. (2013), "A *Toxoplasma* palmitoyl acyl transferase and the palmitoylated armadillo repeat protein TgARO govern apical rhoptry tethering and reveal a critical role for the rhoptries in host cell invasion but not egress", *PLoS Pathog*, Vol. 9 No. 2, p. e1003162, doi: 10.1371/journal.ppat.1003162.

Behnke, M.S., Khan, A., Wootton, J.C., Dubey, J.P., Tang, K. and Sibley, L.D. (2011), "Virulence differences in *Toxoplasma* mediated by amplification of a family of polymorphic pseudokinases", *Proc Natl Acad Sci U S A*, Vol. 108 No. 23, pp. 9631–9636, doi: 10.1073/pnas.1015338108.

Behnke, M.S., Wootton, J.C., Lehmann, M.M., Radke, J.B., Lucas, O., Nawas, J., Sibley, L.D., *et al.* (2010), "Coordinated progression through two subtranscriptomes underlies the tachyzoite cycle of *Toxoplasma gondii*", *PLoS One*, Vol. 5 No. 8, p. e12354, doi: 10.1371/journal.pone.0012354.

Bertiaux, E., Balestra, A.C., Bournonville, L., Louvel, V., Maco, B., Soldati-Favre, D., Brochet, M., *et al.* (2021), "Expansion microscopy provides new insights into the cytoskeleton of malaria parasites including the conservation of a conoid", *PLoS Biology*, United States, Vol. 19 No. 3, pp. e3001020–e3001020, doi: 10.1371/journal.pbio.3001020.

Besteiro, S., Michelin, A., Poncet, J., Dubremetz, J.F. and Lebrun, M. (2009), "Export of a *Toxoplasma gondii* rhoptry neck protein complex at the host cell membrane to form the moving junction during invasion", *PLoS Pathog*, Vol. 5 No. 2, p. e1000309, doi: 10.1371/journal.ppat.1000309.

Bichet, M., Joly, C., Henni, A.H., Guilbert, T., Xémard, M., Tafani, V., Lagal, V., *et al.* (2014), "The *Toxoplasma*-host cell junction is anchored to the cell cortex to sustain parasite invasive force", *BMC Biol*, Vol. 12, p. 773, doi: 10.1186/s12915-014-0108-y.

Billker, O., Lourido, S. and Sibley, L.D. (2009), "Calcium-dependent signaling and kinases in apicomplexan parasites", *Cell Host & Microbe*, Vol. 5 No. 6, pp. 612–622, doi: 10.1016/j.chom.2009.05.017.

Bisio, H., Lunghi, M., Brochet, M. and Soldati-Favre, D. (2019), "Phosphatidic acid governs natural egress in *Toxoplasma gondii* via a guanylate cyclase receptor platform", *Nature Microbiology*, Vol. 4 No. 3, pp. 420–428, doi: 10.1038/s41564-018-0339-8.

Bisio, H. and Soldati-Favre, D. (2019), "Signaling Cascades Governing Entry into and Exit from Host Cells by *Toxoplasma gondii*", *Annual Review of Microbiology*, Annual Reviews, Vol. 73 No. 1, pp. 579–599, doi: 10.1146/annurev-micro-020518-120235.

Bjerkas, I., Jenkins, M.C. and Dubey, J.P. (1994), "Identification and characterization of *Neospora caninum* tachyzoite antigens useful for diagnosis of neosporosis", *Clinical Diagnostic*

Laboratory Immunology, American Society for Microbiology, Vol. 1 No. 2, pp. 214–221, doi: 10.1128/cdli.1.2.214-221.1994.

Boddey, J.A., Hodder, A.N., Gunther, S., Gilson, P.R., Patsiouras, H., Kapp, E.A., Pearce, J.A., *et al.* (2010), "An aspartyl protease directs malaria effector proteins to the host cell", *Nature*, Vol. 463 No. 7281, pp. 627–631, doi: 10.1038/nature08728.

Boothroyd, J.C. and Dubremetz, J.F. (2008), "Kiss and spit: the dual roles of *Toxoplasma* rhoptries", *Nat Rev Microbiol*, Vol. 6 No. 1, pp. 79–88, doi: 10.1038/nrmicro1800.

Boss, C., Richard-Bildstein, S., Weller, T., Fischli, W., Meyer, S. and Binkert, C. (2003), "Inhibitors of the *Plasmodium falciparum* parasite aspartic protease plasmepsin II as potential antimalarial agents", *Curr Med Chem*, Vol. 10 No. 11, pp. 883–907.

Bradley, P.J., Ward, C., Cheng, S.J., Alexander, D.L., Coller, S., Coombs, G.H., Dunn, J.D., *et al.* (2005), "Proteomic analysis of rhoptry organelles reveals many novel constituents for host-parasite interactions in *Toxoplasma gondii*", *J Biol Chem*, Vol. 280 No. 40, pp. 34245–34258, doi: 10.1074/jbc.M504158200.

Breinich, M.S., Ferguson, D.J., Foth, B.J., van Dooren, G.G., Lebrun, M., Quon, D. v, Striepen, B., *et al.* (2009), "A dynamin is required for the biogenesis of secretory organelles in *Toxoplasma gondii*", *Curr Biol*, Vol. 19 No. 4, pp. 277–286, doi: 10.1016/j.cub.2009.01.039.

Brochet, M., Collins, M.O., Smith, T.K., Thompson, E., Sebastian, S., Volkmann, K., Schwach, F., *et al.* (2014), "Phosphoinositide Metabolism Links cGMP-Dependent Protein Kinase G to Essential Ca2+ Signals at Key Decision Points in the Life Cycle of Malaria Parasites", *PLOS Biology*, Public Library of Science, Vol. 12 No. 3, pp. e1001806-.

Brown, K.M., Long, S. and Sibley, L.D. (2017), "Plasma Membrane Association by N-Acylation Governs PKG Function in *Toxoplasma gondii*", *MBio*, Vol. 8 No. 3, pp. e00375-17, doi: 10.1128/mBio.00375-17.

Bullen, H.E. and Soldati-Favre, D. (2016), "A central role for phosphatidic acid as a lipid mediator of regulated exocytosis in apicomplexa", *FEBS Lett*, Vol. 590 No. 15, pp. 2469–2481, doi: 10.1002/1873-3468.12296.

Burrell, A., Marugan-Hernandez, V., Wheeler, R., Moreira-Leite, F., Ferguson, D.J.P., Tomley, F.M. and Vaughan, S. (2022), "Cellular electron tomography of the apical complex in the apicomplexan parasite *Eimeria tenella* shows a highly organised gateway for regulated secretion", *PLOS Pathogens*, Public Library of Science, Vol. 18 No. 7, pp. e1010666-.

Caldas, L.A., Attias, M. and de Souza, W. (2018), "A structural analysis of the natural egress of *Toxoplasma gondii*", *Microbes and Infection*, Vol. 20 No. 1, pp. 57–62, doi: https://doi.org/10.1016/j.micinf.2017.09.006.

Carey, K.L., Jongco, A.M., Kim, K. and Ward, G.E. (2004), "The *Toxoplasma gondii* rhoptry protein ROP4 is secreted into the parasitophorous vacuole and becomes phosphorylated in infected cells", *Eukaryotic Cell*, United States, Vol. 3 No. 5, pp. 1320–1330, doi: 10.1128/EC.3.5.1320-1330.2004.

del Carmen, M.G., Mondragón, M., González, S. and Mondragón, R. (2009), "Induction and regulation of conoid extrusion in *Toxoplasma gondii*", *Cellular Microbiology*, John Wiley &

Sons, Ltd, Vol. 11 No. 6, pp. 967–982, doi: https://doi.org/10.1111/j.1462-5822.2009.01304.x.

Carruthers, V.B. and Sibley, L.D. (1997), "Sequential protein secretion from three distinct organelles of *Toxoplasma gondii* accompanies invasion of human fibroblasts", *Eur J Cell Biol*, Vol. 73 No. 2, pp. 114–123.

ben Chaabene, R., Lentini, G. and Soldati-Favre, D. (2021), "Biogenesis and discharge of the rhoptries: Key organelles for entry and hijack of host cells by the Apicomplexa", *Molecular Microbiology*, Vol. 115 No. 3, pp. 453–465, doi: https://doi.org/10.1111/mmi.14674.

ben Chaabene, R. and Soldati-Favre, D. (2023), "The Lytic Cycle of Human Apicomplexan Parasites", in Bradshaw, R.A., Hart, G.W. and Stahl, P.D. (Eds.), *Encyclopedia of Cell Biology (Second Edition)*, Academic Press, Oxford, pp. 356–370, doi: https://doi.org/10.1016/B978-0-12-821618-7.00073-0.

Charron, A.J. and Sibley, L.D. (2004), "Molecular Partitioning during Host Cell Penetration by *Toxoplasma gondii*", *Traffic*, John Wiley & Sons, Ltd, Vol. 5 No. 11, pp. 855–867, doi: https://doi.org/10.1111/j.1600-0854.2004.00228.x.

Ciana, C.L., Siegrist, R., Aissaoui, H., Marx, L., Racine, S., Meyer, S., Binkert, C., *et al.* (2013), "Novel in vivo active anti-malarials based on a hydroxy-ethyl-amine scaffold", *Bioorg Med Chem Lett*, Vol. 23 No. 3, pp. 658–662, doi: 10.1016/j.bmcl.2012.11.118.

Coffey, M.J., Sleebs, B.E., Uboldi, A.D., Garnham, A., Franco, M., Marino, N.D., Panas, M.W., *et al.* (2015), "An aspartyl protease defines a novel pathway for export of *Toxoplasma* proteins into the host cell", *Elife*, Vol. 4, doi: 10.7554/eLife.10809.

Cohen, P. (2002), "The origins of protein phosphorylation", *Nature Cell Biology*, Vol. 4 No. 5, pp. E127–E130, doi: 10.1038/ncb0502-e127.

Coleman, B.I., Saha, S., Sato, S., Engelberg, K., Ferguson, D.J.P., Coppens, I., Lodoen, M.B., *et al.* (2018), "A Member of the Ferlin Calcium Sensor Family Is Essential for *Toxoplasma gondii* Rhoptry Secretion", *MBio*, Vol. 9 No. 5, doi: 10.1128/mBio.01510-18.

Coombs, G.H., Goldberg, D.E., Klemba, M., Berry, C., Kay, J. and Mottram, J.C. (2001), "Aspartic proteases of *Plasmodium falciparum* and other parasitic protozoa as drug targets", *Trends Parasitol*, Vol. 17 No. 11, pp. 532–537.

Courret, N., Darche, S., Sonigo, P., Milon, G., Buzoni-Gatel, D. and Tardieux, I. (2006), "CD11c- and CD11b-expressing mouse leukocytes transport single *Toxoplasma gondii* tachyzoites to the brain", *Blood*, Vol. 107 No. 1, pp. 309–316, doi: 10.1182/blood-2005-02-0666.

Cova, M.M., Lamarque, M.H. and Lebrun, M. (2022), "How Apicomplexa Parasites Secrete and Build Their Invasion Machinery", *Annual Review of Microbiology*, Annual Reviews, Vol. 76 No. 1, pp. 619–640, doi: 10.1146/annurev-micro-041320-021425.

Curt-Varesano, A., Braun, L., Ranquet, C., Hakimi, M.A. and Bougdour, A. (2016), "The aspartyl protease TgASP5 mediates the export of the *Toxoplasma* GRA16 and GRA24 effectors into host cells", *Cell Microbiol*, Vol. 18 No. 2, pp. 151–167, doi: 10.1111/cmi.12498.

Darvill, N., Dubois, D.J., Rouse, S.L., Hammoudi, P.-M., Blake, T., Benjamin, S., Liu, B., *et al.* (2018), "Structural Basis of Phosphatidic Acid Sensing by APH in Apicomplexan Parasites", *Structure*

(London, England : 1993), Cell Press, Vol. 26 No. 8, pp. 1059-1071.e6, doi: 10.1016/j.str.2018.05.001.

Degrandi, D., Konermann, C., Beuter-Gunia, C., Kresse, A., Wurthner, J., Kurig, S., Beer, S., *et al.* (2007), "Extensive characterization of IFN-induced GTPases mGBP1 to mGBP10 involved in host defense", *J Immunol*, Vol. 179 No. 11, pp. 7729–7740, doi: 10.4049/jimmunol.179.11.7729.

Delgado, I.L.S., Zúquete, S., Santos, D., Basto, A.P., Leitão, A. and Nolasco, S. (2022), "The Apicomplexan Parasite *Toxoplasma gondii*", *Encyclopedia*, Vol. 2 No. 1, pp. 189–211, doi: 10.3390/encyclopedia2010012.

Delorme, V., Cayla, X., Faure, G., Garcia, A. and Tardieux, I. (2003), "Actin dynamics is controlled by a casein kinase II and phosphatase 2C interplay on *Toxoplasma gondii* Toxofilin", *Mol Biol Cell*, Vol. 14 No. 5, pp. 1900–1912, doi: 10.1091/mbc.e02-08-0462.

Delorme-Walker, V., Abrivard, M., Lagal, V., Anderson, K., Perazzi, A., Gonzalez, V., Page, C., *et al.* (2012), "Toxofilin upregulates the host cortical actin cytoskeleton dynamics, facilitating *Toxoplasma* invasion", *J Cell Sci*, Vol. 125 No. Pt 18, pp. 4333–4342, doi: 10.1242/jcs.103648.

Desai, S.A. and Rosenberg, R.L. (1997), "Pore size of the malaria parasite's nutrient channel", *Proc Natl Acad Sci U S A*, Vol. 94 No. 5, pp. 2045–2049.

Dogga, S.K., Mukherjee, B., Jacot, D., Kockmann, T., Molino, L., Hammoudi, P.M., Hartkoorn, R.C., *et al.* (2017), "A druggable secretory protein maturase of *Toxoplasma* essential for invasion and egress", *Elife*, Vol. 6, doi: 10.7554/eLife.27480.

Dou, Z. and Carruthers, V.B. (2011), "Cathepsin Proteases in *Toxoplasma gondii*", in Robinson, M.W. and Dalton, J.P. (Eds.), *Cysteine Proteases of Pathogenic Organisms*, Springer US, Boston, MA, pp. 49–61, doi: 10.1007/978-1-4419-8414-2_4.

Dowse, T.J., Koussis, K., Blackman, M.J. and Soldati-Favre, D. (2008), "Roles of Proteases during Invasion and Egress by *Plasmodium* and *Toxoplasma*", in Burleigh, B.A. and Soldati-Favre, D. (Eds.), *Molecular Mechanisms of Parasite Invasion: Subcellular Biochemistry*, Springer New York, New York, NY, pp. 121–139, doi: 10.1007/978-0-387-78267-6_10.

Drewry, L.L., Jones, N.G., Wang, Q., Onken, M.D., Miller, M.J. and Sibley, L.D. (2019), "The secreted kinase ROP17 promotes *Toxoplasma gondii* dissemination by hijacking monocyte tissue migration", *Nat Microbiol*, Vol. 4 No. 11, pp. 1951–1963, doi: 10.1038/s41564-019-0504-8.

Drewry, L.L. and Sibley, L.D. (2019), "The hitchhiker's guide to parasite dissemination", *Cellular Microbiology*, John Wiley & Sons, Ltd, Vol. 21 No. 11, p. e13070, doi: https://doi.org/10.1111/cmi.13070.

Dubey, J.P. and Ferguson, D.J.P. (2015), "Life Cycle of Hammondia hammondi (Apicomplexa: Sarcocystidae) in Cats", *Journal of Eukaryotic Microbiology*, John Wiley & Sons, Ltd, Vol. 62 No. 3, pp. 346–352, doi: https://doi.org/10.1111/jeu.12188.

Dubey, J.P., Lindsay, D.S. and Speer, C.A. (1998), "Structures of *Toxoplasma gondii* tachyzoites, bradyzoites, and sporozoites and biology and development of tissue cysts", *Clin Microbiol Rev*, Vol. 11 No. 2, pp. 267–299.

Dubois, D.J. and Soldati-Favre, D. (2019), "Biogenesis and secretion of micronemes in *Toxoplasma gondii*", *Cellular Microbiology*, John Wiley & Sons, Ltd, Vol. 21 No. 5, p. e13018, doi: https://doi.org/10.1111/cmi.13018.

Dubremetz, J.F. (2007), "Rhoptries are major players in *Toxoplasma gondii* invasion and host cell interaction", *Cell Microbiol*, Vol. 9 No. 4, pp. 841–848, doi: 10.1111/j.1462-5822.2007.00909.x.

Dubremetz, J.F. and Torpier, G. (1978), "Freeze fracture study of the pellicle of an eimerian sporozoite (Protozoa, Coccidia)", *J Ultrastruct Res*, Vol. 62 No. 2, pp. 94–109.

Dunn, J.D., Ravindran, S., Kim, S.-K. and Boothroyd, J.C. (2008), "The *Toxoplasma gondii* dense granule protein GRA7 is phosphorylated upon invasion and forms an unexpected association with the rhoptry proteins ROP2 and ROP4", *Infection and Immunity*, American Society for Microbiology (ASM), Vol. 76 No. 12, pp. 5853–5861, doi: 10.1128/IAI.01667-07.

Duraisingh, M.T., Triglia, T., Ralph, S.A., Rayner, J.C., Barnwell, J.W., McFadden, G.I. and Cowman, A.F. (2003), "Phenotypic variation of *Plasmodium falciparum* merozoite proteins directs receptor targeting for invasion of human erythrocytes", *EMBO J*, Vol. 22 No. 5, pp. 1047–1057, doi: 10.1093/emboj/cdg096.

Entzeroth, R. (1984), "Electron microscope study of host-parasite interactions of *Sarcocystis muris* (Protozoa, Coccidia) in tissue culture and in vivo", *Zeitschrift Für Parasitenkunde*, Vol. 70 No. 1, pp. 131–134, doi: 10.1007/BF00929582.

Etheridge, R.D., Alaganan, A., Tang, K., Lou, H.J., Turk, B.E. and Sibley, L.D. (2014), "The *Toxoplasma* pseudokinase ROP5 forms complexes with ROP18 and ROP17 kinases that synergize to control acute virulence in mice", *Cell Host Microbe*, Vol. 15 No. 5, pp. 537–550, doi: 10.1016/j.chom.2014.04.002.

Farrell, A., Thirugnanam, S., Lorestani, A., Dvorin, J.D., Eidell, K.P., Ferguson, D.J.P., Anderson-White, B.R., *et al.* (2012), "A DOC2 Protein Identified by Mutational Profiling Is Essential for Apicomplexan Parasite Exocytosis", *Science*, American Association for the Advancement of Science, Vol. 335 No. 6065, pp. 218–221, doi: 10.1126/science.1210829.

Fentress, S.J., Behnke, M.S., Dunay, I.R., Mashayekhi, M., Rommereim, L.M., Fox, B.A., Bzik, D.J., *et al.* (2010), "Phosphorylation of immunity-related GTPases by a *Toxoplasma gondii*-secreted kinase promotes macrophage survival and virulence", *Cell Host Microbe*, Vol. 8 No. 6, pp. 484–495, doi: 10.1016/j.chom.2010.11.005.

Ferguson DJP, D.J. (2013), *The Ultrastructure of Toxoplasma gondii. In: Toxoplasma gondii: The Model Apicomplexan—Perspectives and Methods*, Vol. 2nd ed.

Ferreira, J., Pražák, V., Vasishtan, D., Siggel, M., Hentzschel, F., Pietsch, E., Kosinski, J., *et al.* (2022), "Form follows function: Variable microtubule architecture in the malaria parasite", bioRxiv, doi: 10.1101/2022.04.13.488170.

Fox, B.A., Rommereim, L.M., Guevara, R.B., Falla, A., Hortua Triana, M.A., Sun, Y. and Bzik, D.J. (2016), "The *Toxoplasma gondii* rhoptry kinome is essential for chronic infection", *MBio*, Vol. 7 No. 3, pp. 1–12, doi: 10.1128/mBio.00193-16.

Frenal, K., Dubremetz, J.F., Lebrun, M. and Soldati-Favre, D. (2017), "Gliding motility powers invasion and egress in Apicomplexa", *Nat Rev Microbiol*, Vol. 15 No. 11, pp. 645–660, doi: 10.1038/nrmicro.2017.86.

Frenal, K., Tay, C.L., Mueller, C., Bushell, E.S., Jia, Y., Graindorge, A., Billker, O., *et al.* (2013), "Global analysis of apicomplexan protein S-acyl transferases reveals an enzyme essential for invasion", *Traffic*, Vol. 14 No. 8, pp. 895–911, doi: 10.1111/tra.12081.

Garg, S., Shivappagowdar, A., Hada, R.S., Ayana, R., Bathula, C., Sen, S., Kalia, I., *et al.* (2020), "*Plasmodium* Perforin-Like Protein Pores on the Host Cell Membrane Contribute in Its Multistage Growth and Erythrocyte Senescence", *Frontiers in Cellular and Infection Microbiology*, Frontiers Media S.A., Vol. 10, p. 121, doi: 10.3389/fcimb.2020.00121.

Geiger, M., Brown, C., Wichers, J.S., Strauss, J., Lill, A., Thuenauer, R., Liffner, B., *et al.* (2020), "Structural Insights Into PfARO and Characterization of its Interaction With PfAIP", *Journal of Molecular Biology*, Vol. 432 No. 4, pp. 878–896, doi: https://doi.org/10.1016/j.jmb.2019.12.024.

Gilberger, T.W., Thompson, J.K., Triglia, T., Good, R.T., Duraisingh, M.T. and Cowman, A.F. (2003), "A novel erythrocyte binding antigen-175 paralogue from *Plasmodium falciparum* defines a new trypsin-resistant receptor on human erythrocytes", *J Biol Chem*, Vol. 278 No. 16, pp. 14480–14486, doi: 10.1074/jbc.M211446200.

Giovannini, D., Spath, S., Lacroix, C., Perazzi, A., Bargieri, D., Lagal, V., Lebugle, C., *et al.* (2011), "Independent roles of apical membrane antigen 1 and rhoptry neck proteins during host cell invasion by apicomplexa", *Cell Host Microbe*, Vol. 10 No. 6, pp. 591–602, doi: 10.1016/j.chom.2011.10.012.

Gold, D.A., Kaplan, A.D., Lis, A., Bett, G.C., Rosowski, E.E., Cirelli, K.M., Bougdour, A., *et al.* (2015), "The *Toxoplasma* Dense Granule Proteins GRA17 and GRA23 Mediate the Movement of Small Molecules between the Host and the Parasitophorous Vacuole", *Cell Host Microbe*, Vol. 17 No. 5, pp. 642–652, doi: 10.1016/j.chom.2015.04.003.

Gonzalez, V., Combe, A., David, V., Malmquist, N.A., Delorme, V., Leroy, C., Blazquez, S., *et al.* (2009), "Host cell entry by apicomplexa parasites requires actin polymerization in the host cell", *Cell Host Microbe*, Vol. 5 No. 3, pp. 259–272, doi: 10.1016/j.chom.2009.01.011.

Griffith, M.B., Pearce, C.S. and Heaslip, A.T. (2022), "Dense granule biogenesis, secretion, and function in *Toxoplasma gondii*", *Journal of Eukaryotic Microbiology*, John Wiley & Sons, Ltd, Vol. n/a No. n/a, p. e12904, doi: https://doi.org/10.1111/jeu.12904.

Gubbels, M.J. and Duraisingh, M.T. (2012), "Evolution of apicomplexan secretory organelles", *Int J Parasitol*, Vol. 42 No. 12, pp. 1071–1081, doi: 10.1016/j.ijpara.2012.09.009.

Guerin, A., Corrales, R.M., Parker, M.L., Lamarque, M.H., Jacot, D., el Hajj, H., Soldati-Favre, D., *et al.* (2017), "Efficient invasion by *Toxoplasma* depends on the subversion of host protein networks", *Nat Microbiol*, Vol. 2 No. 10, pp. 1358–1366, doi: 10.1038/s41564-017-0018-1.

Guérin, A., el Hajj, H., Penarete-Vargas, D., Besteiro, S. and Lebrun, M. (2017), "RON4L1 is a new member of the moving junction complex in *Toxoplasma gondii*", *Scientific Reports*, Vol. 7 No. 1, pp. 1–11, doi: 10.1038/s41598-017-18010-9.

Gui, L., O'Shaughnessy, W.J., Cai, K., Reetz, E., Reese, M.L. and Nicastro, D. (2022), "Cryo-electron tomography of the apicomplexan invasion machinery in its native state reveals rigid body motion of the conoid and docked secretory machinery", *BioRxiv*, p. 2022.04.23.489287, doi: 10.1101/2022.04.23.489287.

el Hajj, H., Demey, E., Poncet, J., Lebrun, M., Wu, B., Galeotti, N., Fourmaux, M.N., *et al.* (2006), "The ROP2 family of *Toxoplasma gondii* rhoptry proteins: proteomic and genomic characterization and molecular modeling", *Proteomics*, Vol. 6 No. 21, pp. 5773–5784, doi: 10.1002/pmic.200600187.

Hakansson, S., Charron, A.J. and Sibley, L.D. (2001), "*Toxoplasma* evacuoles: a two-step process of secretion and fusion forms the parasitophorous vacuole", *EMBO J*, Vol. 20 No. 12, pp. 3132–3144, doi: 10.1093/emboj/20.12.3132.

Hakimi, M.-A. and Bougdour, A. (2015), "*Toxoplasma*'s ways of manipulating the host transcriptome via secreted effectors", *Current Opinion in Microbiology*, Vol. 26, pp. 24–31, doi: https://doi.org/10.1016/j.mib.2015.04.003.

Hakimi, M.-A., Olias, P. and Sibley, L.D. (2017), "*Toxoplasma* Effectors Targeting Host Signaling and Transcription", *Clinical Microbiology Reviews*, United States, Vol. 30 No. 3, pp. 615–645, doi: 10.1128/CMR.00005-17.

Hallee, S., Boddey, J.A., Cowman, A.F. and Richard, D. (2018), "Evidence that the *Plasmodium falciparum* Protein Sortilin Potentially Acts as an Escorter for the Trafficking of the Rhoptry-Associated Membrane Antigen to the Rhoptries", *MSphere*, Vol. 3 No. 1, doi: 10.1128/mSphere.00551-17.

Hammoudi, P.-M., Jacot, D., Mueller, C., di Cristina, M., Dogga, S.K., Marq, J.-B., Romano, J., *et al.* (2015), "Fundamental Roles of the Golgi-Associated *Toxoplasma* Aspartyl Protease, ASP5, at the Host-Parasite Interface", *PLOS Pathogens*, Public Library of Science, Vol. 11 No. 10, p. e1005211, doi: 10.1371/journal.ppat.1005211.

Hammoudi, P.M., Maco, B., Dogga, S.K., Frenal, K. and Soldati-Favre, D. (2018), "*Toxoplasma gondii* TFP1 is an essential transporter family protein critical for microneme maturation and exocytosis", *Mol Microbiol*, doi: 10.1111/mmi.13981.

Harker, K.S., Ueno, N. and Lodoen, M.B. (2015), "*Toxoplasma gondii* dissemination: a parasite's journey through the infected host", *Parasite Immunol*, Vol. 37 No. 3, pp. 141–149, doi: 10.1111/pim.12163.

Hayton, K., Gaur, D., Liu, A., Takahashi, J., Henschen, B., Singh, S., Lambert, L., *et al.* (2008), "Erythrocyte binding protein PfRH5 polymorphisms determine species-specific pathways of *Plasmodium falciparum* invasion", *Cell Host Microbe*, Vol. 4 No. 1, pp. 40–51, doi: 10.1016/j.chom.2008.06.001.

Heaslip, A.T., Ems-McClung, S.C. and Hu, K. (2009), "TgICMAP1 Is a Novel Microtubule Binding Protein in *Toxoplasma gondii*", *PLOS ONE*, Public Library of Science, Vol. 4 No. 10, pp. e7406-.

ten Hoeve, A.L., Braun, L., Rodriguez, M.E., Olivera, G.C., Bougdour, A., Belmudes, L., Couté, Y., *et al.* (2022), "The *Toxoplasma* effector GRA28 promotes parasite dissemination by inducing

dendritic cell-like migratory properties in infected macrophages", *Cell Host & Microbe*, doi: https://doi.org/10.1016/j.chom.2022.10.001.

Howard, B.L., Harvey, K.L., Stewart, R.J., Azevedo, M.F., Crabb, B.S., Jennings, I.G., Sanders, P.R., *et al.* (2015), "Identification of Potent Phosphodiesterase Inhibitors that Demonstrate Cyclic Nucleotide-Dependent Functions in Apicomplexan Parasites", *ACS Chemical Biology*, American Chemical Society, Vol. 10 No. 4, pp. 1145–1154, doi: 10.1021/cb501004q.

Hu, K., Mann, T., Striepen, B., Beckers, C.J., Roos, D.S. and Murray, J.M. (2002), "Daughter cell assembly in the protozoan parasite *Toxoplasma gondii*", *Mol Biol Cell*, Vol. 13 No. 2, pp. 593–606, doi: 10.1091/mbc.01-06-0309.

Hu, K., Roos, D.S. and Murray, J.M. (2002), "A novel polymer of tubulin forms the conoid of *Toxoplasma gondii*", *Journal of Cell Biology*, Vol. 156 No. 6, pp. 1039–1050, doi: 10.1083/jcb.200112086.

Hugo, B., Ben, C.R., Ricarda, S., Bohumil, M., Baptiste, M.J., Tim-Wolf, G., Tobias, S., *et al.* (2020), "The ZIP Code of Vesicle Trafficking in Apicomplexa: SEC1/Munc18 and SNARE Proteins", *MBio*, American Society for Microbiology, Vol. 11 No. 5, pp. e02092-20, doi: 10.1128/mBio.02092-20.

Hunt, A., Russell, M.R.G., Wagener, J., Kent, R., Carmeille, R., Peddie, C.J., Collinson, L., *et al.* (2019), "Differential requirements for cyclase-associated protein (CAP) in actin-dependent processes of *Toxoplasma gondii*", edited by Akhmanova, A., Frischknecht, F., Meissner, M., Insall, R. and Hu, K.*ELife*, eLife Sciences Publications, Ltd, Vol. 8, p. e50598, doi: 10.7554/eLife.50598.

Hunter, C.A. and Sibley, L.D. (2012), "Modulation of innate immunity by *Toxoplasma gondii* virulence effectors", *Nat Rev Microbiol*, Vol. 10 No. 11, pp. 766–778, doi: 10.1038/nrmicro2858.

Ito, D., Chen, J.-H., Takashima, E., Hasegawa, T., Otsuki, H., Takeo, S., Thongkukiatkul, A., *et al.* (2021), "Identification of a Novel RAMA/RON3 Rhoptry Protein Complex in *Plasmodium falciparum* Merozoites", *Frontiers in Cellular and Infection Microbiology*, Vol. 10.

Ito, D., Han, E.-T., Takeo, S., Thongkukiatkul, A., Otsuki, H., Torii, M. and Tsuboi, T. (2011), "Plasmodial ortholog of *Toxoplasma gondii* rhoptry neck protein 3 is localized to the rhoptry body", *Parasitology International*, Vol. 60 No. 2, pp. 132–138, doi: https://doi.org/10.1016/j.parint.2011.01.001.

Ito, D., Schureck, M.A. and Desai, S.A. (2017), "An essential dual-function complex mediates erythrocyte invasion and channel-mediated nutrient uptake in malaria parasites", edited by Clardy, J.*ELife*, eLife Sciences Publications, Ltd, Vol. 6, p. e23485, doi: 10.7554/eLife.23485.

Jacot, D., Frénal, K., Marq, J.-B., Sharma, P. and Soldati-Favre, D. (2014), "Assessment of phosphorylation in *Toxoplasma* glideosome assembly and function", *Cellular Microbiology*, John Wiley & Sons, Ltd, Vol. 16 No. 10, pp. 1518–1532, doi: https://doi.org/10.1111/cmi.12307.

Jacot, D., Tosetti, N., Pires, I., Stock, J., Graindorge, A., Hung, Y.F., Han, H., *et al.* (2016), "An Apicomplexan Actin-Binding Protein Serves as a Connector and Lipid Sensor to Coordinate

Motility and Invasion", *Cell Host Microbe*, Vol. 20 No. 6, pp. 731–743, doi: 10.1016/j.chom.2016.10.020.

Janouškovec, J., Paskerova, G.G., Miroliubova, T.S., Mikhailov, K. v, Birley, T., Aleoshin, V. v and Simdyanov, T.G. (2019), "Apicomplexan-like parasites are polyphyletic and widely but selectively dependent on cryptic plastid organelles", edited by McCutcheon, J., Weigel, D., Howe, C. and McFadden, G.*ELife*, eLife Sciences Publications, Ltd, Vol. 8, p. e49662, doi: 10.7554/eLife.49662.

Jia, Y., Marq, J.B., Bisio, H., Jacot, D., Mueller, C., Yu, L., Choudhary, J., *et al.* (2017), "Crosstalk between PKA and PKG controls pH-dependent host cell egress of *Toxoplasma gondii*", *EMBO J*, Vol. 36 No. 21, pp. 3250–3267, doi: 10.15252/embj.201796794.

Jiang, L., Duriseti, S., Sun, P. and Miller, L.H. (2009), "Molecular basis of binding of the *Plasmodium falciparum* receptor BAEBL to erythrocyte receptor glycophorin C", *Mol Biochem Parasitol*, Vol. 168 No. 1, pp. 49–54, doi: 10.1016/j.molbiopara.2009.06.006.

Jimenez-Ruiz, E., Morlon-Guyot, J., Daher, W. and Meissner, M. (2016), "Vacuolar protein sorting mechanisms in apicomplexan parasites", *Mol Biochem Parasitol*, Vol. 209 No. 1–2, pp. 18–25, doi: 10.1016/j.molbiopara.2016.01.007.

Jones, N.G., Wang, Q. and Sibley, L.D. (2017), "Secreted protein kinases regulate cyst burden during chronic toxoplasmosis", *Cell Microbiol*, Vol. 19 No. 2, doi: 10.1111/cmi.12651.

Jung, C., Lee, C.Y.-F. and Grigg, M.E. (2004), "The SRS superfamily of *Toxoplasma* surface proteins", *International Journal for Parasitology*, Vol. 34 No. 3, pp. 285–296, doi: https://doi.org/10.1016/j.ijpara.2003.12.004.

Kafsack, B.F., Pena, J.D., Coppens, I., Ravindran, S., Boothroyd, J.C. and Carruthers, V.B. (2009), "Rapid membrane disruption by a perforin-like protein facilitates parasite exit from host cells", *Science*, Vol. 323 No. 5913, pp. 530–533, doi: 10.1126/science.1165740.

van der Kant, R., Fish, A., Janssen, L., Janssen, H., Krom, S., Ho, N., Brummelkamp, T., *et al.* (2013), "Late endosomal transport and tethering are coupled processes controlled by RILP and the cholesterol sensor ORP1L", *Journal of Cell Science*, Vol. 126 No. 15, pp. 3462–3474, doi: 10.1242/jcs.129270.

Kats, L.M., Black, C.G., Proellocks, N.I. and Coppel, R.L. (2006), "*Plasmodium* rhoptries: how things went pear-shaped", *Trends Parasitol*, Vol. 22 No. 6, pp. 269–276, doi: 10.1016/j.pt.2006.04.001.

Kehrer, J., Singer, M., Lemgruber, L., Silva, P.A.G.C., Frischknecht, F. and Mair, G.R. (2016), "A Putative Small Solute Transporter Is Responsible for the Secretion of G377 and TRAP-Containing Secretory Vesicles during *Plasmodium* Gamete Egress and Sporozoite Motility", *PLOS Pathogens*, Public Library of Science, Vol. 12 No. 7, pp. e1005734-.

Kessler, H., Herm-Gotz, A., Hegge, S., Rauch, M., Soldati-Favre, D., Frischknecht, F. and Meissner, M. (2008), "Microneme protein 8--a new essential invasion factor in *Toxoplasma gondii*", *J Cell Sci*, Vol. 121 No. Pt 7, pp. 947–956, doi: 10.1242/jcs.022350.

Khalil, I.A., Troeger, C., Rao, P.C., Blacker, B.F., Brown, A., Brewer, T.G., Colombara, D. v, *et al.* (2018), "Morbidity, mortality, and long-term consequences associated with diarrhoea from *Cryptosporidium* infection in children younger than 5 years: a meta-analyses study.",

The Lancet. Global Health, Vol. 6 No. 7, pp. e758–e768, doi: 10.1016/S2214-109X(18)30283-3.

Kim, E.W., Nadipuram, S.M., Tetlow, A.L., Barshop, W.D., Liu, P.T., Wohlschlegel, J.A. and Bradley, P.J. (2016), "The Rhoptry Pseudokinase ROP54 Modulates *Toxoplasma gondii* Virulence and Host GBP2 Loading", *MSphere*, Vol. 1 No. 2, doi: 10.1128/mSphere.00045-16.

Konradt, C., Ueno, N., Christian, D.A., Delong, J.H., Pritchard, G.H., Herz, J., Bzik, D.J., *et al.* (2016), "Endothelial cells are a replicative niche for entry of *Toxoplasma gondii* to the central nervous system", *Nat Microbiol*, Vol. 1, p. 16001, doi: 10.1038/nmicrobiol.2016.1.

Koshy, A.A., Dietrich, H.K., Christian, D.A., Melehani, J.H., Shastri, A.J., Hunter, C.A. and Boothroyd, J.C. (2012), "*Toxoplasma* co-opts host cells it does not invade", *PLoS Pathogens*, Vol. 8 No. 7, p. 18, doi: 10.1371/journal.ppat.1002825.

Koshy, A.A., Fouts, A.E., Lodoen, M.B., Alkan, O., Blau, H.M. and Boothroyd, J.C. (2010), "*Toxoplasma* secreting Cre recombinase for analysis of host-parasite interactions", *Nat Methods*, Vol. 7 No. 4, pp. 307–309, doi: 10.1038/nmeth.1438.

Kremer, K., Kamin, D., Rittweger, E., Wilkes, J., Flammer, H., Mahler, S., Heng, J., *et al.* (2013), "An Overexpression Screen of *Toxoplasma gondii* Rab-GTPases Reveals Distinct Transport Routes to the Micronemes", *PLOS Pathogens*, Public Library of Science, Vol. 9 No. 3, pp. e1003213-.

Lamarque, M., Besteiro, S., Papoin, J., Roques, M., Vulliez-Le Normand, B., Morlon-Guyot, J., Dubremetz, J.F., *et al.* (2011), "The RON2-AMA1 interaction is a critical step in moving junction-dependent invasion by apicomplexan parasites", *PLoS Pathog*, Vol. 7 No. 2, p. e1001276, doi: 10.1371/journal.ppat.1001276.

Lamarque, M.H., Papoin, J., Finizio, A.-L., Lentini, G., Pfaff, A.W., Candolfi, E., Dubremetz, J.-F., *et al.* (2012), "Identification of a New Rhoptry Neck Complex RON9/RON10 in the Apicomplexa Parasite *Toxoplasma gondii*", *PLOS ONE*, Public Library of Science, Vol. 7 No. 3, pp. e32457-.

Lamarque, M.H., Roques, M., Kong-Hap, M., Tonkin, M.L., Rugarabamu, G., Marq, J.B., Penarete-Vargas, D.M., *et al.* (2014), "Plasticity and redundancy among AMA-RON pairs ensure host cell entry of *Toxoplasma* parasites", *Nature Communications*, Nature Publishing Group, Vol. 5 No. May, pp. 1–13, doi: 10.1038/ncomms5098.

Lammermann, T., Bader, B.L., Monkley, S.J., Worbs, T., Wedlich-Soldner, R., Hirsch, K., Keller, M., *et al.* (2008), "Rapid leukocyte migration by integrin-independent flowing and squeezing", *Nature*, Vol. 453 No. 7191, pp. 51–55, doi: 10.1038/nature06887.

Laporte, M.H., Klena, N., Hamel, V. and Guichard, P. (2022), "Visualizing the native cellular organization by coupling cryofixation with expansion microscopy (Cryo-ExM)", *Nature Methods*, United States, Vol. 19 No. 2, pp. 216–222, doi: 10.1038/s41592-021-01356-4.

Leander, B.S. (2008), "Marine gregarines: evolutionary prelude to the apicomplexan radiation?", *Trends in Parasitology*, Vol. 24 No. 2, pp. 60–67, doi: https://doi.org/10.1016/j.pt.2007.11.005.

Lebrun, M., Michelin, A., el Hajj, H., Poncet, J., Bradley, P.J., Vial, H. and Dubremetz, J.F. (2005), "The rhoptry neck protein RON4 re-localizes at the moving junction during *Toxoplasma*

gondii invasion", *Cell Microbiol*, Vol. 7 No. 12, pp. 1823–1833, doi: 10.1111/j.1462-5822.2005.00646.x.

Lefort-Tran, M., Aufderheide, K., Pouphile, M., Rossignol, M. and Beisson, J. (1981), "Control of exocytotic processes: cytological and physiological studies of trichocyst mutants in *Paramecium tetraurelia*", *The Journal of Cell Biology*, The Rockefeller University Press, Vol. 88 No. 2, pp. 301–311, doi: 10.1083/jcb.88.2.301.

Lemgruber, L., Lupetti, P., de Souza, W. and Vommaro, R.C. (2011), "New details on the fine structure of the rhoptry of *Toxoplasma gondii*", *Microsc Res Tech*, Vol. 74 No. 9, pp. 812–818, doi: 10.1002/jemt.20960.

Lentini, G., ben Chaabene, R., Vadas, O., Ramakrishnan, C., Mukherjee, B., Mehta, V., Lunghi, M., *et al.* (2021), "Structural insights into an atypical secretory pathway kinase crucial for *Toxoplasma* gondii invasion.", *Nature Communications*, England, Vol. 12 No. 1, p. 3788, doi: 10.1038/s41467-021-24083-y.

Lentini, G., el Hajj, H., Papoin, J., Fall, G., Pfaff, A.W., Tawil, N., Braun-Breton, C., *et al.* (2017), "Characterization of *Toxoplasma* DegP, a rhoptry serine protease crucial for lethal infection in mice", *PLoS One*, Vol. 12 No. 12, p. e0189556, doi: 10.1371/journal.pone.0189556.

Ley, K., Laudanna, C., Cybulsky, M.I. and Nourshargh, S. (2007), "Getting to the site of inflammation: the leukocyte adhesion cascade updated", *Nat Rev Immunol*, Vol. 7 No. 9, pp. 678–689, doi: 10.1038/nri2156.

Liffner, B., Frolich, S., Heinemann, G.K., Liu, B., Ralph, S.A., Dixon, M.W.A., Gilberger, T.W., *et al.* (2020), "PfCERLI1 is a conserved rhoptry associated protein essential for *Plasmodium falciparum* merozoite invasion of erythrocytes", *Nat Commun*, Vol. 11 No. 1, p. 1411, doi: 10.1038/s41467-020-15127-w.

Ling, I.T., Kaneko, O., Narum, D.L., Tsuboi, T., Howell, S., Taylor, H.M., Scott-Finnigan, T.J., *et al.* (2003), "Characterisation of the rhoph2 gene of *Plasmodium falciparum* and *Plasmodium* yoelii", *Mol Biochem Parasitol*, Vol. 127 No. 1, pp. 47–57, doi: 10.1016/s0166-6851(02)00302-x.

Lodoen, M.B., Gerke, C. and Boothroyd, J.C. (2010), "A highly sensitive FRET-based approach reveals secretion of the actin-binding protein toxofilin during *Toxoplasma gondii* infection", *Cell Microbiol*, Vol. 12 No. 1, pp. 55–66, doi: 10.1111/j.1462-5822.2009.01378.x.

Lourido, S., Shuman, J., Zhang, C., Shokat, K.M., Hui, R. and Sibley, L.D. (2010), "Calcium-dependent protein kinase 1 is an essential regulator of exocytosis in *Toxoplasma*", *Nature*, Vol. 465 No. 7296, pp. 359–362, doi: 10.1038/nature09022.

M, L.L., Yvonne, A., S, S.E., Matthias, G., Joshua, Z., Takafumi, T., Joseph, B., *et al.* (2019), "Deletion of *Plasmodium falciparum* Protein RON3 Affects the Functional Translocation of Exported Proteins and Glucose Uptake", *MBio*, American Society for Microbiology, Vol. 10 No. 4, pp. e01460-19, doi: 10.1128/mBio.01460-19.

M. Santos, J., Graindorge, A. and Soldati-Favre, D. (2012), "New insights into parasite rhomboid proteases", *Molecular and Biochemical Parasitology*, Vol. 182 No. 1, pp. 27–36, doi: https://doi.org/10.1016/j.molbiopara.2011.11.010.

Mageswaran, S.K., Guérin, A., Theveny, L.M., Chen, W.D., Martinez, M., Lebrun, M., Striepen, B., *et al.* (2021), "In situ ultrastructures of two evolutionarily distant apicomplexan rhoptry secretion systems", *Nature Communications*, Vol. 12 No. 1, p. 4983, doi: 10.1038/s41467-021-25309-9.

Manger, I.D., Hehl, A.B. and Boothroyd, J.C. (1998), "The surface of *Toxoplasma* tachyzoites is dominated by a family of glycosylphosphatidylinositol-anchored antigens related to SAG1", *Infection and Immunity*, American Society for Microbiology, Vol. 66 No. 5, pp. 2237–2244, doi: 10.1128/IAI.66.5.2237-2244.1998.

Marino, N.D., Panas, M.W., Franco, M., Theisen, T.C., Naor, A., Rastogi, S., Buchholz, K.R., *et al.* (2018), "Identification of a novel protein complex essential for effector translocation across the parasitophorous vacuole membrane of *Toxoplasma gondii*", *PLOS Pathogens*, Public Library of Science, Vol. 14 No. 1, p. e1006828, doi: 10.1371/journal.ppat.1006828.

Martin, T.F.J. (2015), "PI(4,5)P2-binding effector proteins for vesicle exocytosis", *Biochimica et Biophysica Acta (BBA) - Molecular and Cell Biology of Lipids*, Vol. 1851 No. 6, pp. 785–793, doi: https://doi.org/10.1016/j.bbalip.2014.09.017.

Martinez, M., Chen, W.D., Cova, M.M., Molnár, P., Mageswaran, S.K., Guérin, A., John, A.R.O., *et al.* (2022), "Rhoptry secretion system structure and priming in *Plasmodium falciparum* revealed using in situ cryo-electron tomography", *Nature Microbiology*, Vol. 7 No. 8, pp. 1230–1238, doi: 10.1038/s41564-022-01171-3.

McFadden, G.I. and Yeh, E. (2017), "The apicoplast: now you see it, now you don't", *International Journal for Parasitology*, Vol. 47 No. 2, pp. 137–144, doi: https://doi.org/10.1016/j.ijpara.2016.08.005.

McPhillie, M., Zhou, Y., el Bissati, K., Dubey, J., Lorenzi, H., Capper, M., Lukens, A.K., *et al.* (2016), "New paradigms for understanding and step changes in treating active and chronic, persistent apicomplexan infections", *Scientific Reports*, Vol. 6 No. 1, p. 29179, doi: 10.1038/srep29179.

Meissner, M., Krejany, E., Gilson, P.R., de Koning-Ward, T.F., Soldati, D. and Crabb, B.S. (2005), "Tetracycline analogue-regulated transgene expression in *Plasmodium falciparum* blood stages using *Toxoplasma gondii* transactivators", *Proceedings of the National Academy of Sciences*, Proceedings of the National Academy of Sciences, Vol. 102 No. 8, pp. 2980–2985, doi: 10.1073/pnas.0500112102.

Melo, M.B., Jensen, K.D. and Saeij, J.P. (2011), "*Toxoplasma gondii* effectors are master regulators of the inflammatory response", *Trends Parasitol*, Vol. 27 No. 11, pp. 487–495, doi: 10.1016/j.pt.2011.08.001.

Mercier, C., Dubremetz, J.-F., Rauscher, B., Lecordier, L., Sibley, L.D. and Cesbron-Delauw, M.-F. (2002), "Biogenesis of Nanotubular Network in *Toxoplasma*Parasitophorous Vacuole Induced by Parasite Proteins", *Molecular Biology of the Cell*, American Society for Cell Biology (mboc), Vol. 13 No. 7, pp. 2397–2409, doi: 10.1091/mbc.e02-01-0021.

Miller, S.A., Thathy, V., Ajioka, J.W., Blackman, M.J. and Kim, K. (2003), "TgSUB2 is a *Toxoplasma gondii* rhoptry organelle processing proteinase", *Mol Microbiol*, Vol. 49 No. 4, pp. 883–894.

Mital, J., Meissner, M., Soldati, D. and Ward, G.E. (2005), "Conditional Expression of *Toxoplasma gondii* Apical Membrane Antigen-1 (TgAMA1) Demonstrates That TgAMA1 Plays a Critical Role in Host Cell Invasion", *Mol Biol Cell*, The American Society for Cell Biology, Vol. 16 No. 9, pp. 4341–4349, doi: 10.1091/mbc.E05-04-0281.

Mondragon, R. and Frixione, E. (1996), "Ca(2+)-dependence of conoid extrusion in *Toxoplasma gondii* tachyzoites", *The Journal of Eukaryotic Microbiology*, Vol. 43 No. 2, pp. 120–127, doi: 10.1111/j.1550-7408.1996.tb04491.x.

Monteiro, V.G., de Melo, E.J.T., Attias, M. and de Souza, W. (2001), "Morphological Changes during Conoid Extrusion in *Toxoplasma gondii* Tachyzoites Treated with Calcium Ionophore", *Journal of Structural Biology*, Vol. 136 No. 3, pp. 181–189, doi: https://doi.org/10.1006/jsbi.2002.4444.

Morlon-Guyot, J., Berry, L., Sauquet, I., Singh Pall, G., el Hajj, H., Meissner, M. and Daher, W. (2018), "Conditional knock-down of a novel coccidian protein leads to the formation of aberrant apical organelles and abrogates mature rhoptry positioning in *Toxoplasma gondii*", *Mol Biochem Parasitol*, Vol. 223, pp. 19–30, doi: https://doi.org/10.1016/j.molbiopara.2018.06.003.

Morlon-Guyot, J., el Hajj, H., Martin, K., Fois, A., Carrillo, A., Berry, L., Burchmore, R., *et al.* (2018), "A proteomic analysis unravels novel CORVET and HOPS proteins involved in *Toxoplasma gondii* secretory organelles biogenesis", *Cell Microbiol*, Vol. 20 No. 11, p. e12870, doi: 10.1111/cmi.12870.

Morlon-Guyot, J., Pastore, S., Berry, L., Lebrun, M. and Daher, W. (2015), "*Toxoplasma gondii* Vps11, a subunit of HOPS and CORVET tethering complexes, is essential for the biogenesis of secretory organelles", *Cell Microbiol*, John Wiley & Sons, Ltd, Vol. 17 No. 8, pp. 1157–1178, doi: 10.1111/cmi.12426.

Morrissette, N.S. and Sibley, L.D. (2002), "Cytoskeleton of apicomplexan parasites", *Microbiol Mol Biol Rev*, Vol. 66 No. 1, pp. 21–38; table of contents.

Moudy, R., Manning, T.J. and Beckers, C.J. (2001), "The loss of cytoplasmic potassium upon host cell breakdown triggers egress of *Toxoplasma gondii*", *J Biol Chem*, Vol. 276 No. 44, pp. 41492–41501, doi: 10.1074/jbc.M106154200.

Mphande, F.A., Ribacke, U., Kaneko, O., Kironde, F., Winter, G. and Wahlgren, M. (2008), "SURFIN4.1, a schizont-merozoite associated protein in the SURFIN family of *Plasmodium falciparum*", *Malar J*, Vol. 7, p. 116, doi: 10.1186/1475-2875-7-116.

Mueller, C., Klages, N., Jacot, D., Santos, J.M., Cabrera, A., Gilberger, T.W., Dubremetz, J.F., *et al.* (2013), "The *Toxoplasma* protein ARO mediates the apical positioning of rhoptry organelles, a prerequisite for host cell invasion", *Cell Host Microbe*, Vol. 13 No. 3, pp. 289–301, doi: 10.1016/j.chom.2013.02.001.

Mueller, C., Samoo, A., Hammoudi, P.M., Klages, N., Kallio, J.P., Kursula, I. and Soldati-Favre, D. (2016), "Structural and functional dissection of *Toxoplasma gondii* armadillo repeats only protein", *J Cell Sci*, Vol. 129 No. 5, pp. 1031–1045, doi: 10.1242/jcs.177386.

Muñiz-Hernández, S., Carmen, M.G. del, Mondragón, M., Mercier, C., Cesbron, M.F., Mondragón-González, S.L., González, S., *et al.* (2011), "Contribution of the residual body in the spatial

organization of *Toxoplasma gondii* tachyzoites within the parasitophorous vacuole", *Journal of Biomedicine & Biotechnology*, United States, Vol. 2011, p. 473983, doi: 10.1155/2011/473983.

Nasamu, A.S., Glushakova, S., Russo, I., Vaupel, B., Oksman, A., Kim, A.S., Fremont, D.H., *et al.* (2017), "Plasmepsins IX and X are essential and druggable mediators of malaria parasite egress and invasion", *Science*, Vol. 358 No. 6362, pp. 518–522, doi: 10.1126/science.aan1478.

Nebl, T., Prieto, J.H., Kapp, E., Smith, B.J., Williams, M.J., Yates 3rd, J.R., Cowman, A.F., *et al.* (2011), "Quantitative in vivo analyses reveal calcium-dependent phosphorylation sites and identifies a novel component of the *Toxoplasma* invasion motor complex", *PLoS Pathog*, Vol. 7 No. 9, p. e1002222, doi: 10.1371/journal.ppat.1002222.

Ngo, H.M., Yang, M. and Joiner, K.A. (2004), "Are rhoptries in Apicomplexan parasites secretory granules or secretory lysosomal granules?", *Mol Microbiol*, Vol. 52 No. 6, pp. 1531–1541, doi: 10.1111/j.1365-2958.2004.04056.x.

Nichols, B.A. and Chiappino, M. louise. (1987), "Cytoskeleton of *Toxoplasma gondii*1", *The Journal of Protozoology*, John Wiley & Sons, Ltd, Vol. 34 No. 2, pp. 217–226, doi: https://doi.org/10.1111/j.1550-7408.1987.tb03162.x.

Nickerson, D.P., Brett, C.L. and Merz, A.J. (2009), "Vps-C complexes: gatekeepers of endolysosomal traffic", *Curr Opin Cell Biol*, Vol. 21 No. 4, pp. 543–551, doi: 10.1016/j.ceb.2009.05.007.

Nishi, M., Hu, K., Murray, J.M. and Roos, D.S. (2008), "Organellar dynamics during the cell cycle of *Toxoplasma gondii*", *J Cell Sci*, Vol. 121 No. Pt 9, pp. 1559–1568, doi: 10.1242/jcs.021089.

O'Keeffe, A.H., Green, J.L., Grainger, M. and Holder, A.A. (2005), "A novel Sushi domain-containing protein of *Plasmodium falciparum*", *Molecular and Biochemical Parasitology*, Vol. 140 No. 1, pp. 61–68, doi: https://doi.org/10.1016/j.molbiopara.2004.12.003.

Ong, Y.C., Reese, M.L. and Boothroyd, J.C. (2010), "*Toxoplasma* rhoptry protein 16 (ROP16) subverts host function by direct tyrosine phosphorylation of STAT6", *J Biol Chem*, Vol. 285 No. 37, pp. 28731–28740, doi: 10.1074/jbc.M110.112359.

Ouologuem, D.T. and Roos, D.S. (2014), "Dynamics of the *Toxoplasma gondii* inner membrane complex", *J Cell Sci*, Vol. 127 No. Pt 15, pp. 3320–3330, doi: 10.1242/jcs.147736.

Panas, M.W., Ferrel, A., Naor, A., Tenborg, E., Lorenzi, H.A. and Boothroyd, J.C. (2019), "Translocation of Dense Granule Effectors across the Parasitophorous Vacuole Membrane in *Toxoplasma*-Infected Cells Requires the Activity of ROP17, a Rhoptry Protein Kinase", edited by Sullivan, W.J.*MSphere*, Vol. 4 No. 4, pp. e00276-19, doi: 10.1128/mSphere.00276-19.

Paredes-Santos, T.C., de Souza, W. and Attias, M. (2012), "Dynamics and 3D organization of secretory organelles of *Toxoplasma gondii*", *Journal of Structural Biology*, Elsevier Inc., Vol. 177 No. 2, pp. 420–430, doi: 10.1016/j.jsb.2011.11.028.

Parker, M.L., Penarete-Vargas, D.M., Hamilton, P.T., Guérin, A., Dubey, J.P., Perlman, S.J., Spano, F., *et al.* (2016), "Dissecting the interface between apicomplexan parasite and host cell: Insights from a divergent AMA-RON2 pair", *Proceedings of the National Academy of Sciences*

of the United States of America, Vol. 113 No. 2, pp. 398–403, doi: 10.1073/pnas.1515898113.

Pavlou, G., Biesaga, M., Touquet, B., Lagal, V., Balland, M., Dufour, A., Hakimi, M. ali, *et al.* (2018), "*Toxoplasma* Parasite Twisting Motion Mechanically Induces Host Cell Membrane Fission to Complete Invasion within a Protective Vacuole", *Cell Host and Microbe*, Elsevier Inc., Vol. 24 No. 1, pp. 81-96.e5, doi: 10.1016/j.chom.2018.06.003.

Peixoto, L., Chen, F., Harb, O.S., Davis, P.H., Beiting, D.P., Brownback, C.S., Ouloguem, D., *et al.* (2010), "Integrative genomic approaches highlight a family of parasite-specific kinases that regulate host responses", *Cell Host and Microbe*, Elsevier Ltd, Vol. 8 No. 2, pp. 208–218, doi: 10.1016/j.chom.2010.07.004.

Periz, J., del Rosario, M., McStea, A., Gras, S., Loney, C., Wang, L., Martin-Fernandez, M.L., *et al.* (2019), "A highly dynamic F-actin network regulates transport and recycling of micronemes in *Toxoplasma gondii* vacuoles", *Nature Communications*, Vol. 10 No. 1, p. 4183, doi: 10.1038/s41467-019-12136-2.

Pieperhoff, M.S., Pall, G.S., Jiménez-Ruiz, E., Das, S., Melatti, C., Gow, M., Wong, E.H., *et al.* (2015), "Conditional U1 Gene Silencing in *Toxoplasma gondii*", *PLoS One*, Public Library of Science, Vol. 10 No. 6, p. e0130356, doi: 10.1371/journal.pone.0130356.

Pino, P., Caldelari, R., Mukherjee, B., Vahokoski, J., Klages, N., Maco, B., Collins, C.R., *et al.* (2017), "A multistage antimalarial targets the plasmepsins IX and X essential for invasion and egress", *Science*, Vol. 358 No. 6362, pp. 522–528, doi: 10.1126/science.aaf8675.

Plattner, H. and Kissmehl, R. (2003), "Molecular Aspects of Membrane Trafficking in *Paramecium*", *International Review of Cytology*, Vol. 232, pp. 185–216, doi: 10.1016/S0074-7696(03)32005-4.

Polonais, V., Shea, M. and Soldati-Favre, D. (2011), "*Toxoplasma gondii* aspartic protease 1 is not essential in tachyzoites", *Exp Parasitol*, Vol. 128 No. 4, pp. 454–459, doi: 10.1016/j.exppara.2011.05.003.

Porchet, E. and Torpier, G. (1977), "Etude du germe infectieux de *Sarcocystis tenella* et *Toxoplasma gondii* par la technique du cryodécapage", *Zeitschrift Für Parasitenkunde*, Vol. 54 No. 2, pp. 101–124, doi: 10.1007/BF00380795.

Porchet-Hennere, E. and Nicolas, G. (1983), "Are rhoptries of coccidia really extrusomes?", *Journal of Ultrastructure Research*, Vol. 84 No. 2, pp. 194–203, doi: https://doi.org/10.1016/S0022-5320(83)90130-2.

Possenti, A., di Cristina, M., Nicastro, C., Lunghi, M., Messina, V., Piro, F., Tramontana, L., *et al.* (2022), "Functional Characterization of the Thrombospondin-Related Paralogous Proteins Rhoptry Discharge Factors 1 and 2 Unveils Phenotypic Plasticity in *Toxoplasma gondii* Rhoptry Exocytosis", *Frontiers in Microbiology*, Vol. 13, doi: 10.3389/fmicb.2022.899243.

Proellocks, N.I., Coppel, R.L. and Waller, K.L. (2010), "Dissecting the apicomplexan rhoptry neck proteins", *Trends in Parasitology*, Vol. 26 No. 6, pp. 297–304, doi: https://doi.org/10.1016/j.pt.2010.02.012.

Qiu, W., Wernimont, A., Tang, K., Taylor, S., Lunin, V., Schapira, M., Fentress, S., *et al.* (2009), "Novel structural and regulatory features of rhoptry secretory kinases in *Toxoplasma*

gondii", *EMBO Journal*, Nature Publishing Group, Vol. 28 No. 7, pp. 969–979, doi: 10.1038/emboj.2009.24.

Quintana, M.D.P., Ch'ng, J.H., Zandian, A., Imam, M., Hultenby, K., Theisen, M., Nilsson, P., *et al.* (2018), "SURGE complex of *Plasmodium falciparum* in the rhoptry-neck (SURFIN4.2-RON4-GLURP) contributes to merozoite invasion", *PLoS One*, Vol. 13 No. 8, p. e0201669, doi: 10.1371/journal.pone.0201669.

Reese, M.L. and Boothroyd, J.C. (2011), "A conserved non-canonical motif in the pseudoactive site of the ROP5 pseudokinase domain mediates its effect on *Toxoplasma* virulence", *J Biol Chem*, Vol. 286 No. 33, pp. 29366–29375, doi: 10.1074/jbc.M111.253435.

Reiss, M., Viebig, N., Brecht, S., Fourmaux, M.N., Soete, M., di Cristina, M., Dubremetz, J.F., *et al.* (2001), "Identification and characterization of an escorter for two secretory adhesins in *Toxoplasma gondii*", *J Cell Biol*, Vol. 152 No. 3, pp. 563–578.

Roiko, M.S. and Carruthers, V.B. (2009), "New roles for perforins and proteases in apicomplexan egress", *Cellular Microbiology*, John Wiley & Sons, Ltd, Vol. 11 No. 10, pp. 1444–1452, doi: https://doi.org/10.1111/j.1462-5822.2009.01357.x.

Roiko, M.S., Svezhova, N. and Carruthers, V.B. (2014), "Acidification Activates *Toxoplasma gondii* Motility and Egress by Enhancing Protein Secretion and Cytolytic Activity", *PLoS Pathog*, Vol. 10 No. 11, p. e1004488, doi: 10.1371/journal.ppat.1004488.

Russo, I., Babbitt, S., Muralidharan, V., Butler, T., Oksman, A. and Goldberg, D.E. (2010), "Plasmepsin V licenses *Plasmodium* proteins for export into the host erythrocyte", *Nature*, Vol. 463 No. 7281, pp. 632–636, doi: 10.1038/nature08726.

Ryan, U., Paparini, A., Monis, P. and Hijjawi, N. (2016), "It's official – *Cryptosporidium* is a gregarine: What are the implications for the water industry?", *Water Research*, Vol. 105, pp. 305–313, doi: https://doi.org/10.1016/j.watres.2016.09.013.

Saeij, J.P., Boyle, J.P., Coller, S., Taylor, S., Sibley, L.D., Brooke-Powell, E.T., Ajioka, J.W., *et al.* (2006), "Polymorphic secreted kinases are key virulence factors in toxoplasmosis", *Science*, Vol. 314 No. 5806, pp. 1780–1783, doi: 10.1126/science.1133690.

Saeij, J.P., Coller, S., Boyle, J.P., Jerome, M.E., White, M.W. and Boothroyd, J.C. (2007), "*Toxoplasma* co-opts host gene expression by injection of a polymorphic kinase homologue", *Nature*, Vol. 445 No. 7125, pp. 324–327, doi: 10.1038/nature05395.

Sakura, T., Sindikubwabo, F., Oesterlin, L.K., Bousquet, H., Slomianny, C., Hakimi, M.-A., Langsley, G., *et al.* (2016), "A Critical Role for *Toxoplasma gondii* Vacuolar Protein Sorting VPS9 in Secretory Organelle Biogenesis and Host Infection", *Scientific Reports*, Vol. 6 No. 1, p. 38842, doi: 10.1038/srep38842.

dos Santos Pacheco, N. and Soldati-Favre, D. (2021), "Coupling Auxin-Inducible Degron System with Ultrastructure Expansion Microscopy to Accelerate the Discovery of Gene Function in *Toxoplasma gondii*", in de Pablos, L.M. and Sotillo, J. (Eds.), *Parasite Genomics: Methods and Protocols*, Springer US, New York, NY, pp. 121–137, doi: 10.1007/978-1-0716-1681-9_8.

dos Santos Pacheco, N., Tosetti, N., Koreny, L., Waller, R.F. and Soldati-Favre, D. (2020), "Evolution, Composition, Assembly, and Function of the Conoid in Apicomplexa", *Trends in Parasitology*, Vol. 36 No. 8, pp. 688–704, doi: https://doi.org/10.1016/j.pt.2020.05.001.

Sassmannshausen, J., Pradel, G. and Bennink, S. (2020), “Perforin-Like Proteins of Apicomplexan Parasites”, *Frontiers in Cellular and Infection Microbiology*, Vol. 10, p. 507.

Schwab, J.C., Beckers, C.J. and Joiner, K.A. (1994), “The parasitophorous vacuole membrane surrounding intracellular *Toxoplasma gondii* functions as a molecular sieve”, *Proc Natl Acad Sci U S A*, Vol. 91 No. 2, pp. 509–513.

Segev-Zarko, L., Dahlberg, P.D., Sun, S.Y., Pelt, D.M., Kim, C.Y., Egan, E.S., Sethian, J.A., *et al.* (2022), “Coupling cryo-electron tomography with mixed-scale dense neural networks reveals re-organization of the invasion machinery of *Toxoplasma gondii* upon ionophore-stimulation”, *BioRxiv*, p. 2022.01.12.476068, doi: 10.1101/2022.01.12.476068.

Segev-Zarko, L., Dahlberg, P.D., Sun, S.Y., Pelt, D.M., Sethian, J.A., Chiu, W. and Boothroyd, J.C. (2022), “Ionophore-stimulation promotes re-organization of the invasion machinery of *Toxoplasma gondii*”, *BioRxiv*, p. 2022.01.12.476068, doi: 10.1101/2022.01.12.476068.

Selleck, E.M., Fentress, S.J., Beatty, W.L., Degrandi, D., Pfeffer, K., Virgin, H.W. th, Macmicking, J.D., *et al.* (2013), “Guanylate-binding protein 1 (Gbp1) contributes to cell-autonomous immunity against *Toxoplasma gondii*”, *PLoS Pathog*, Vol. 9 No. 4, p. e1003320, doi: 10.1371/journal.ppat.1003320.

Shaw, M.K., Roos, D.S. and Tilney, L.G. (1998), “Acidic compartments and rhoptry formation in *Toxoplasma gondii*”, *Parasitology*, Vol. 117 (Pt 5), pp. 435–443.

Shaw, M.K. and Tilney, L.G. (1992), “How individual cells develop from a syncytium: merogony in Theileria parva (Apicomplexa)”, *J Cell Sci*, Vol. 101 (Pt 1, pp. 109–123.

Shea, M., Jakle, U., Liu, Q., Berry, C., Joiner, K.A. and Soldati-Favre, D. (2007), “A family of aspartic proteases and a novel, dynamic and cell-cycle-dependent protease localization in the secretory pathway of *Toxoplasma gondii*”, *Traffic*, Vol. 8 No. 8, pp. 1018–1034, doi: 10.1111/j.1600-0854.2007.00589.x.

Shen, B., Brown, K.M., Lee, T.D. and Sibley, L.D. (2014), “Efficient gene disruption in diverse strains of *Toxoplasma gondii* using CRISPR/CAS9”, *MBio*, United States, Vol. 5 No. 3, p. e01114, doi: 10.1128/mBio.01114-14.

Sherling, E.S., Knuepfer, E., Brzostowski, J.A., Miller, L.H., Blackman, M.J. and Ooij, C. van. (2017), “The *Plasmodium falciparum* rhoptry protein RhopH3 plays essential roles in host cell invasion and nutrient uptake”, edited by Soldati-Favre, D.*ELife*, eLife Sciences Publications, Ltd, Vol. 6, p. e23239, doi: 10.7554/eLife.23239.

Sherling, E.S., Perrin, A.J., Knuepfer, E., Russell, M.R.G., Collinson, L.M., Miller, L.H. and Blackman, M.J. (2019), “The *Plasmodium falciparum* rhoptry bulb protein RAMA plays an essential role in rhoptry neck morphogenesis and host red blood cell invasion”, *PLoS Pathog*, Vol. 15 No. 9, p. e1008049, doi: 10.1371/journal.ppat.1008049.

Shinuo, C., Juan, Y., Jiawen, F., Heming, C. and Honglin, J. (2021), “The Dissection of SNAREs Reveals Key Factors for Vesicular Trafficking to the Endosome-like Compartment and Apicoplast via the Secretory System in *Toxoplasma gondii*”, *MBio*, American Society for Microbiology, Vol. 12 No. 4, pp. e01380-21, doi: 10.1128/mBio.01380-21.

Sidik, S.M., Huet, D., Ganesan, S.M., Huynh, M.H., Wang, T., Nasamu, A.S., Thiru, P., *et al.* (2016), "A Genome-wide CRISPR Screen in *Toxoplasma* Identifies Essential Apicomplexan Genes", *Cell*, Vol. 166 No. 6, pp. 1423-1435.e12, doi: 10.1016/j.cell.2016.08.019.

Sim, B.K., Chitnis, C.E., Wasniowska, K., Hadley, T.J. and Miller, L.H. (1994), "Receptor and ligand domains for invasion of erythrocytes by *Plasmodium falciparum*", *Science*, Vol. 264 No. 5167, pp. 1941–1944, doi: 10.1126/science.8009226.

Sinai, A.P. (2014), "Chapter 11 - The *Toxoplasma gondii* Parasitophorous Vacuole Membrane: A Multifunctional Organelle in the Infected Cell", in Weiss, L.M. and Kim, K. (Eds.), *Toxoplasma gondii (Second Edition)*, Academic Press, Boston, pp. 375–387, doi: https://doi.org/10.1016/B978-0-12-396481-6.00011-8.

Singer, M., Simon, K., Forné, I. and Meissner, M. (2022), "A central protein complex essential for Invasion in *Toxoplasma gondii*", *BioRxiv*, Cold Spring Harbor Laboratory, doi: 10.1101/2022.02.24.481622.

Singh, S., Alam, M.M., Pal-Bhowmick, I., Brzostowski, J.A. and Chitnis, C.E. (2010), "Distinct External Signals Trigger Sequential Release of Apical Organelles during Erythrocyte Invasion by Malaria Parasites", *PLOS Pathogens*, Public Library of Science, Vol. 6 No. 2, pp. e1000746-.

Singh, S., Plassmeyer, M., Gaur, D. and Miller, L.H. (2007), "Mononeme: a new secretory organelle in *Plasmodium falciparum* merozoites identified by localization of rhomboid-1 protease", *Proceedings of the National Academy of Sciences of the United States of America*, United States, Vol. 104 No. 50, pp. 20043–20048, doi: 10.1073/pnas.0709999104.

Skariah, S., Walwyn, O., Engelberg, K., Gubbels, M.-J., Gaylets, C., Kim, N., Lynch, B., *et al.* (2016), "The FIKK kinase of *Toxoplasma gondii* is not essential for the parasite's lytic cycle", *International Journal for Parasitology*, Vol. 46 No. 5, pp. 323–332, doi: https://doi.org/10.1016/j.ijpara.2016.01.001.

Sleebs, B.E., Lopaticki, S., Marapana, D.S., O'Neill, M.T., Rajasekaran, P., Gazdik, M., Gunther, S., *et al.* (2014), "Inhibition of Plasmepsin V activity demonstrates its essential role in protein export, PfEMP1 display, and survival of malaria parasites", *PLoS Biol*, Vol. 12 No. 7, p. e1001897, doi: 10.1371/journal.pbio.1001897.

Sloves, P.J., Delhaye, S., Mouveaux, T., Werkmeister, E., Slomianny, C., Hovasse, A., Dilezitoko Alayi, T., *et al.* (2012), "*Toxoplasma* sortilin-like receptor regulates protein transport and is essential for apical secretory organelle biogenesis and host infection", *Cell Host Microbe*, Vol. 11 No. 5, pp. 515–527, doi: 10.1016/j.chom.2012.03.006.

Spang, A. (2016), "Membrane Tethering Complexes in the Endosomal System", *Front Cell Dev Biol*, Vol. 4, p. 35, doi: 10.3389/fcell.2016.00035.

Sparvoli, D., Delabre, J., Penarete-Vargas, D.M., Kumar Mageswaran, S., Tsypin, L.M., Heckendorn, J., Theveny, L., *et al.* (2022), "An apical membrane complex for triggering rhoptry exocytosis and invasion in *Toxoplasma*", *The EMBO Journal*, John Wiley & Sons, Ltd, Vol. n/a No. n/a, p. e111158, doi: https://doi.org/10.15252/embj.2022111158.

Sparvoli, D. and Lebrun, M. (2021), "Unraveling the Elusive Rhoptry Exocytic Mechanism of Apicomplexa", *Trends in Parasitology*, Elsevier Ltd, pp. 1–16, doi: 10.1016/j.pt.2021.04.011.

Steinfeldt, T., Konen-Waisman, S., Tong, L., Pawlowski, N., Lamkemeyer, T., Sibley, L.D., Hunn, J.P., *et al.* (2010), "Phosphorylation of mouse immunity-related GTPase (IRG) resistance proteins is an evasion strategy for virulent *Toxoplasma gondii*", *PLoS Biol*, Vol. 8 No. 12, p. e1000576, doi: 10.1371/journal.pbio.1000576.

Straub, K.W., Cheng, S.J., Sohn, C.S. and Bradley, P.J. (2009), "Novel components of the Apicomplexan moving junction reveal conserved and coccidia-restricted elements", *Cell Microbiol*, Vol. 11 No. 4, pp. 590–603, doi: 10.1111/j.1462-5822.2008.01276.x.

Straub, K.W., Peng, E.D., Hajagos, B.E., Tyler, J.S. and Bradley, P.J. (2011), "The moving junction protein RON8 facilitates firm attachment and host cell invasion in *Toxoplasma gondii*", *PLoS Pathogens*, Vol. 7 No. 3, doi: 10.1371/journal.ppat.1002007.

Su, C., Evans, D., Cole, R.H., Kissinger, J.C., Ajioka, J.W. and Sibley, L.D. (2003), "Recent Expansion of *Toxoplasma* Through Enhanced Oral Transmission", *Science*, American Association for the Advancement of Science, Vol. 299 No. 5605, pp. 414–416, doi: 10.1126/science.1078035.

Suarez, C., Lentini, G., Ramaswamy, R., Maynadier, M., Aquilini, E., Berry-Sterkers, L., Cipriano, M., *et al.* (2019), "A lipid-binding protein mediates rhoptry discharge and invasion in *Plasmodium falciparum* and *Toxoplasma gondii* parasites", *Nat Commun*, Vol. 10 No. 1, p. 4041, doi: 10.1038/s41467-019-11979-z.

Suss-Toby, E., Zimmerberg, J. and Ward, G.E. (1996), "*Toxoplasma* invasion: the parasitophorous vacuole is formed from host cell plasma membrane and pinches off via a fission pore", *Proc Natl Acad Sci U S A*, Vol. 93 No. 16, pp. 8413–8418.

Tagoe, D.N.A., Drozda, A.A., Coppens, I., Coleman, B.I. and Gubbels, M.-J. (2020), "*Toxoplasma* ferlin1 is a versatile and dynamic mediator of microneme trafficking and secretion", *BioRxiv*, p. 2020.04.27.063628, doi: 10.1101/2020.04.27.063628.

Tagoe, D.N.A., Drozda, A.A., Falco, J.A., Bechtel, T.J., Weerapana, E. and Gubbels, M.-J. (2021), "Ferlins and TgDOC2 in *Toxoplasma* Microneme, Rhoptry and Dense Granule Secretion", *Life*, Vol. 11 No. 3, doi: 10.3390/life11030217.

Talevich, E., Mirza, A. and Kannan, N. (2011), "Structural and evolutionary divergence of eukaryotic protein kinases in Apicomplexa", *BMC Evolutionary Biology*, Vol. 11 No. 1, p. 321, doi: 10.1186/1471-2148-11-321.

Talevich, E., Tobin, A.B., Kannan, N. and Doerig, C. (2012), "An evolutionary perspective on the kinome of malaria parasites", *Philosophical Transactions of the Royal Society B: Biological Sciences*, Royal Society, Vol. 367 No. 1602, pp. 2607–2618, doi: 10.1098/rstb.2012.0014.

Taylor, S., Barragan, A., Su, C., Fux, B., Fentress, S.J., Tang, K., Beatty, W.L., *et al.* (2006), "A secreted serine-threonine kinase determines virulence in the eukaryotic pathogen *Toxoplasma gondii*", *Science*, Vol. 314 No. 5806, pp. 1776–1780, doi: 10.1126/science.1133643.

Tenter, A.M., Heckeroth, A.R. and Weiss, L.M. (2000), "*Toxoplasma gondii*: from animals to humans", *Int J Parasitol*, Vol. 30 No. 12–13, pp. 1217–1258.

Tetley, L., Brown, S.M., McDonald, V. and Coombs, G.H. (1998), "Ultrastructural analysis of the sporozoite of *Cryptosporidium parvum*", *Microbiology (Reading)*, Vol. 144 (Pt 1, pp. 3249–3255, doi: 10.1099/00221287-144-12-3249.

Theveny, L.M., Mageswaran, S.K., Chen, W.D., Martinez, M., Guérin, A. and Chang, Y.-W. (2022), "Parasitology meets cryo-electron tomography – exciting prospects await", *Trends in Parasitology*, Vol. 38 No. 5, pp. 365–378, doi: https://doi.org/10.1016/j.pt.2022.01.006.

Tonkin, M.L., Roques, M., Lamarque, M.H., Pugnière, M., Douguet, D., Crawford, J., Lebrun, M., *et al.* (2011), "Host cell invasion by apicomplexan parasites: Insights from the co-structure of AMA1 with a RON2 peptide", *Science*, Vol. 333 No. 6041, pp. 463–467, doi: 10.1126/science.1204988.

Travier, L., Mondragon, R., Dubremetz, J.-F., Musset, K., Mondragon, M., Gonzalez, S., Cesbron-Delauw, M.-F., *et al.* (2008), "Functional domains of the *Toxoplasma* GRA2 protein in the formation of the membranous nanotubular network of the parasitophorous vacuole", *International Journal for Parasitology*, Vol. 38 No. 7, pp. 757–773, doi: https://doi.org/10.1016/j.ijpara.2007.10.010.

Treeck, M., Sanders, J.L., Elias, J.E. and Boothroyd, J.C. (2011), "The phosphoproteomes of *Plasmodium falciparum* and *Toxoplasma gondii* reveal unusual adaptations within and beyond the parasites' boundaries", *Cell Host Microbe*, Vol. 10 No. 4, pp. 410–419, doi: 10.1016/j.chom.2011.09.004.

Triglia, T., Duraisingh, M.T., Good, R.T. and Cowman, A.F. (2005), "Reticulocyte-binding protein homologue 1 is required for sialic acid-dependent invasion into human erythrocytes by *Plasmodium falciparum*", *Molecular Microbiology*, John Wiley & Sons, Ltd, Vol. 55 No. 1, pp. 162–174, doi: https://doi.org/10.1111/j.1365-2958.2004.04388.x.

Triglia, T., Tham, W.H., Hodder, A. and Cowman, A.F. (2009), "Reticulocyte binding protein homologues are key adhesins during erythrocyte invasion by *Plasmodium falciparum*", *Cell Microbiol*, Vol. 11 No. 11, pp. 1671–1687, doi: 10.1111/j.1462-5822.2009.01358.x.

Venugopal, K. and Marion, S. (2018), "Secretory organelle trafficking in *Toxoplasma gondii*: A long story for a short travel", *International Journal of Medical Microbiology*, Vol. 308 No. 7, pp. 751–760, doi: 10.1016/j.ijmm.2018.07.007.

Venugopal, K., Werkmeister, E., Barois, N., Saliou, J.-M., Poncet, A., Huot, L., Sindikubwabo, F., *et al.* (2017), "Dual role of the *Toxoplasma gondii* clathrin adaptor AP1 in the sorting of rhoptry and microneme proteins and in parasite division", *PLOS Pathogens*, Public Library of Science, Vol. 13 No. 4, p. e1006331, doi: 10.1371/journal.ppat.1006331.

Votypka, J., Modry, D., Oborník, M., Slapeta, J. and Lukeš, J. (2016), "Apicomplexa", pp. 1–58, doi: 10.1007/978-3-319-32669-6_20-1.

Wai-Hong, T., W, W.D., Linda, R., Lin, C., G, B.J. and F, C.A. (2009), "Antibodies to Reticulocyte Binding Protein-Like Homologue 4 Inhibit Invasion of *Plasmodium falciparum* into Human Erythrocytes", *Infection and Immunity*, American Society for Microbiology, Vol. 77 No. 6, pp. 2427–2435, doi: 10.1128/IAI.00048-09.

Wang, M., Cao, S., Du, N., Fu, J., Li, Z., Jia, H. and Song, M. (2017), "The moving junction protein RON4, although not critical, facilitates host cell invasion and stabilizes MJ members", *Parasitology*, Vol. 144 No. 11, pp. 1490–1497, doi: 10.1017/s0031182017000968.

Ward, P., Equinet, L., Packer, J. and Doerig, C. (2004), "Protein kinases of the human malaria parasite *Plasmodium falciparum*: the kinome of a divergent eukaryote", *BMC Genomics*, Vol. 5 No. 1, p. 79, doi: 10.1186/1471-2164-5-79.

Weiss, L.M. and Kim, K. (2000), "The development and biology of bradyzoites of *Toxoplasma gondii*", *Frontiers in Bioscience : A Journal and Virtual Library*, United States, Vol. 5, pp. D391–D405, doi: 10.2741/weiss.

Will, C.L. and Lührmann, R. (2011), "Spliceosome Structure and Function", *Cold Spring Harbor Perspectives in Biology*, Vol. 3 No. 7.

Winter, G., Kawai, S., Haeggstrom, M., Kaneko, O., von Euler, A., Kawazu, S., Palm, D., *et al.* (2005), "SURFIN is a polymorphic antigen expressed on *Plasmodium falciparum* merozoites and infected erythrocytes", *J Exp Med*, Vol. 201 No. 11, pp. 1853–1863, doi: 10.1084/jem.20041392.

Xiang, X., Qiu, R., Yao, X., Arst, H.N., Peñalva, M.A. and Zhang, J. (2015), "Cytoplasmic dynein and early endosome transport", *Cellular and Molecular Life Sciences*, Vol. 72 No. 17, pp. 3267–3280, doi: 10.1007/s00018-015-1926-y.

Yamamoto, M., Okuyama, M., Ma, J.S., Kimura, T., Kamiyama, N., Saiga, H., Ohshima, J., *et al.* (2012), "A cluster of interferon-gamma-inducible p65 GTPases plays a critical role in host defense against *Toxoplasma gondii*", *Immunity*, Vol. 37 No. 2, pp. 302–313, doi: 10.1016/j.immuni.2012.06.009.

Yamamoto, M., Standley, D.M., Takashima, S., Saiga, H., Okuyama, M., Kayama, H., Kubo, E., *et al.* (2009), "A single polymorphic amino acid on *Toxoplasma gondii* kinase ROP16 determines the direct and strain-specific activation of Stat3", *J Exp Med*, Vol. 206 No. 12, pp. 2747–2760, doi: 10.1084/jem.20091703.

Yap, A., Azevedo, M.F., Gilson, P.R., Weiss, G.E., O'Neill, M.T., Wilson, D.W., Crabb, B.S., *et al.* (2014), "Conditional expression of apical membrane antigen 1 in *Plasmodium falciparum* shows it is required for erythrocyte invasion by merozoites", *Cell Microbiol*, Vol. 16 No. 5, pp. 642–656, doi: 10.1111/cmi.12287.

Yarovinsky, F. (2014), "Innate immunity to *Toxoplasma gondii* infection", *Nat Rev Immunol*, Vol. 14 No. 2, pp. 109–121, doi: 10.1038/nri3598.

Yeoh, S., O'Donnell, R.A., Koussis, K., Dluzewski, A.R., Ansell, K.H., Osborne, S.A., Hackett, F., *et al.* (2007), "Subcellular Discharge of a Serine Protease Mediates Release of Invasive Malaria Parasites from Host Erythrocytes", *Cell*, Elsevier, Vol. 131 No. 6, pp. 1072–1083, doi: 10.1016/j.cell.2007.10.049.

Zhicheng, D., L, M.O., Manlio, D.C. and B, C.V. (2014), "*Toxoplasma gondii* Ingests and Digests Host Cytosolic Proteins", *MBio*, American Society for Microbiology, Vol. 5 No. 4, pp. e01188-14, doi: 10.1128/mBio.01188-14.

Zhong, X., Malhotra, R. and Guidotti, G. (2003), "ATP uptake in the Golgi and extracellular release require Mcd4 protein and the vacuolar H+-ATPase", *J Biol Chem*, Vol. 278 No. 35, pp. 33436–33444, doi: 10.1074/jbc.M305785200.

Zhu, X., He, Y., Liang, Y., Kaneko, O., Cui, L. and Cao, Y. (2017), “Tryptophan-rich domains of *Plasmodium falciparum* SURFIN4.2 and *Plasmodium* vivax PvSTP2 interact with membrane skeleton of red blood cell”, *Malar J*, Vol. 16 No. 1, p. 121, doi: 10.1186/s12936-017-1772-5.

Received: 4 November 2020 | Revised: 17 December 2020 | Accepted: 19 December 2020

DOI: 10.1111/mmi.14674

MICROREVIEW

WILEY

Biogenesis and discharge of the rhoptries: Key organelles for entry and hijack of host cells by the Apicomplexa

Rouaa Ben Chaabene | Gaëlle Lentini | Dominique Soldati-Favre

Department of Microbiology and Molecular Medicine, CMU, Faculty of Medicine, University of Geneva, Geneva, Switzerland

Correspondence
Rouaa Ben Chaabene, Department of Microbiology and Molecular Medicine, CMU, Faculty of Medicine, University of Geneva, 1211 Geneva 4, Switzerland.
Email: Rouaa.BenChaabene@unige.ch

Funding information
Schweizerischer Nationalfonds zur Förderung der Wissenschaftlichen Forschung, Grant/Award Number: 310030B_166678 and 310030_185325

Abstract

Rhoptries are specialized secretory organelles found in the Apicomplexa phylum, playing a central role in the establishment of parasitism. The rhoptry content includes membranous as well as proteinaceous materials that are discharged into the host cell in a regulated fashion during parasite entry. A set of rhoptry neck proteins form a RON complex that critically participates in the moving junction formation during invasion. Some of the rhoptry bulb proteins are associated with the membranous materials and contribute to the formation of the parasitophorous vacuole membrane while others are targeted into the host cell including the nucleus to subvert cellular functions. Here, we review the recent studies on *Toxoplasma* and *Plasmodium* parasites that shed light on the key steps leading to rhoptry biogenesis, trafficking, and discharge.

KEYWORDS

apical complex, Apicomplexa, effector molecules, exocytosis, invasion, moving junction, parasitophorous vacuole, rhoptries, secretory kinases, *Toxoplasma gondii*

1 | INTRODUCTION

The phylum of Apicomplexa includes a broad range of life-threatening protozoan pathogens for humans and animals, such as *Plasmodium* (malaria), *Toxoplasma gondii* (toxoplasmosis), and *Cryptosporidium* (cryptosporidiosis). Host cell invasion is a crucial step in the lytic cycle of these obligate intracellular parasites. Members of the Apicomplexa are characterized by several unifying features and most relevantly is the presence of an apical complex that gives the name to this phylum (Hu, 2006; Morrissette & Sibley, 2002). It is composed of an apical polar ring and a set of specialized secretory organelles, termed micronemes and rhoptries. Micronemes are crucial for motility, host cell attachment, invasion, and egress while the rhoptries are dedicated to invasion and establishment of intracellular parasitism (Boothroyd & Dubremetz, 2008; Dubois & Soldati-Favre, 2019). Additionally, the Coccidia subgroup of Apicomplexa possesses a dynamic apical structure made of tubulin fibers and called The conoid (Dos Santos Pacheco et al., 2020). In its center resides, a pair of intraconoidal microtubules of unknown function (Dos Santos et al., 2020). The parasites also possess dense granules randomly dispersed within the cytosol and once secreted, their content is implicated in remodeling of the parasitophorous vacuole membrane (PVM) as well as in subversion of host cell immune system and nutrient uptake (Cesbron-Delauw, 1994; Charnaud et al., 2018; Gold et al., 2015). As members of the Alveolata infrakingdom, the apicomplexan parasites possess a pellicle composed of the plasma membrane (PM) and apposed membrane cisternae that form the inner membrane complex (IMC), which is linked *via* proteinaceous alveolin network to the subpellicular microtubules (Kono et al., 2013).

T. gondii, like most of the Apicomplexa, actively penetrates the host cell by a process involving the sequential exocytosis of micronemes and rhoptries, two apical organelles that differ in shape and in function. Perforins and adhesins secreted by the micronemes

Abbreviations: ELC, endosome-like compartment; EM, electron microscopy; GRA, dense granules proteins; IMC, inner membrane complex; MIC, microneme adhesion; MJ, moving junction; PM, plasma membrane; PVM, parasitophorous vacuole membrane; RBC, red blood cell; RON, rhoptry neck protein; ROP, rhoptry bulb protein; TGN, trans-Golgi network.

are instrumental for parasite egress from infected cells and for motility and invasion, respectively (Dubois & Soldati-Favre, 2019). Discharge of the rhoptries depends on microneme exocytosis (Kessler et al., 2008), however, the signal and the machinery implicated in the release of their contents into the host cell, are poorly characterized. The rhoptries play a pivotal role in invasion and in subversion of host cellular functions. During host cell entry, the parasite induce the invagination of the host cell PM with the help of the rhoptry membranous material, form the PVM. The parasitophorous vacuole (PV) serves as a protective niche within the host cytoplasm, which is permeable to small molecules via the presence of a molecular sieve (Schwab et al., 1994) to ensure parasite proliferation. Intracellular parasites undergo several cycles of replication by endodyogeny and eventually actively egress from the infected cells, lysing the PVM and the host PM. *T. gondii* belongs to the tissue cyst-forming branch of the Coccidia and some secreted rhoptry proteins are important virulence factors that indirectly affect cyst burden influencing parasite persistence and transmission (Fox et al., 2016).

2 | RHOPTRY ULTRASTRUCTURE AND CONTENT

The rhoptries are large membrane-bound secretory organelles grouped together at the apical pole of the parasites (Figure 1a). While conserved in all the invasive stages of apicomplexan parasites that form a PV, the number of rhoptries varies not only between species, but also among the developmental varies stages. *Plasmodium falciparum* merozoites and sporozoites possess two rhoptries whereas the organelle is absent in ookinetes (Kats et al., 2006). *Theileria parva* merozoites exhibit six rhoptries (Shaw & Tilney, 1992) and *Cryptosporidium* sporozoites have only one rhoptry (Tetley et al., 1998). In *T. gondii*, the tachyzoites associated with the acute phase of the infection, have 10 to 12 rhoptries while the bradyzoites, responsible for chronic infection, possess only one to three rhoptries (Boothroyd & Dubremetz, 2008). Two main regions can be distinguished in the organelle that differ by their morphology and content. The rhoptry neck consists of an electron-dense apical duct oriented toward the conoid and which contains the rhoptry neck proteins (RONs). A larger electron-lucent basal region defines the bulb of the organelle where the rhoptry bulb proteins (ROPs) as well as membranous materials (Figure 1b) are found. Lipidomic analysis of the rhoptry compartment revealed a unique lipid composition with an unusual cholesterol to phospholipids ratio at 1.48, and phosphatidylcholine as major phospholipid (Coppens & Joiner, 2003; Foussard et al., 2009). These lipids are presumably important for the formation of the PVM upon invasion (Dluzewski et al., 1995). Rhoptry proteins are key players in the infection process mainly by operating invasion and by successfully establishing a permissive niche for parasite multiplication within the infected cells. The core RON complex composed of RON2/4/5 is conserved across the phylum (Table 1) and is implicated in the formation of a moving junction (MJ) during host cell entry. The MJ builds a tight connection between the parasite and host PMs that serves as a support to propel the parasite inside the host cell. In contrast, the ROPs are mostly species-specific with some of them well characterized as effector molecules contributing to the virulence of *T. gondii* whereas in *P. falciparum* the ROPs play a

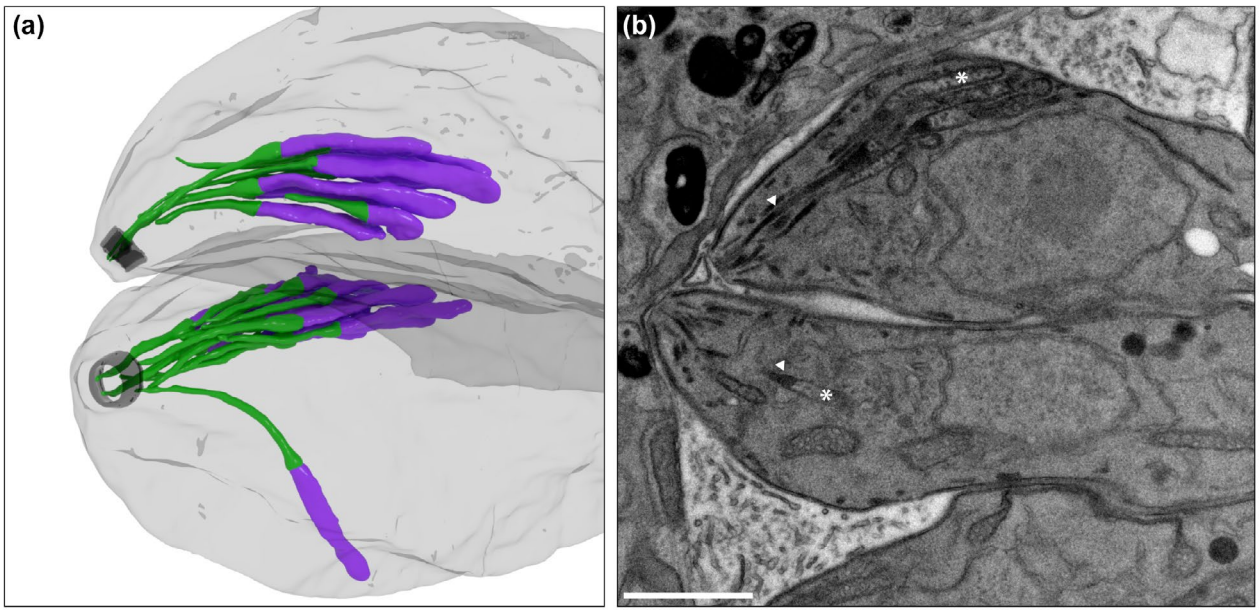

FIGURE 1 Ultrastructure of the rhoptries. A. 3D reconstruction from FIB-SEM images of the apical part of two intracellular parasites showing the rhoptries clustered together. The neck (green) and the bulb (violet) of the rhoptries are colored. The conoid is in black and the plasma membrane is shaded in grey. A couple of rhoptries are clearly seen inserted in the conoid. B. Transmission electron microscopy image of two intracellular parasites. The electron dense neck of the rhoptry (arrowhead) is found more apical that the electron-lucent bulb (asterisk). Scale bar = 1 μm. Image courtesy of Bohumil Maco from (Hammoudi et al., 2018)

TABLE 1 Table of rhoptry-related proteins

Category	Name	CRISPR score *Tg*	Fitness Score (MFS) *Pf*	Localisation	Tg	Hh	Nc	Sn	Et	Ta	Bb	Pf	Pb	Cp	G	Phenotype
Biogenesis and maturation	SRTLR	-3.67	-2.36	Golgi + post-Golgi	●	●	●	●	●	●	●	●	●	●	●	**Defect in motility, invasion and egress**-Disruption of rhoptries and micronemes biogenesis (89, 91)
	TFP1	-4.04	-2.21	Micronemes	●	●	●	●	●	●	●	●	●	●	●	Defect in microneme biogenesis (107)
	TFP2	0.14	-2.21	Rhoptry bulb	●	●	●	●	●	●	●	●	●	●	●	Elongated rhoptries (107)
	TFP3	-0.34	-0.99	Rhoptry	●	●	●	●	●	○	○	●	●	●	○	No impact (107)
	VPS8	N/A	N/A	Post-golgi	●	●	●	●	●	○	○	○	○	○	○	**Defect in invasion and egress**-Defect in rhoptry, microneme and dense granules biogenesis (96)
	VPS9	-3	N/A	ELC	●	●	●	●	●	○	○	○	○	○	○	**Invasion defect**-Defect in rhoptry proteins processing/matuation/sorting-Defect in micronemes biogenesis-Defect in dense granules secretion (94)
	VPS11	-4.09	-3.26	Golgi + Post-Golgi	●	●	●	●	●	●	●	●	●	●	●	**Defect invasion and egress**-Defect in rhoptry, microneme and dense granules biogenesis (95)
	AP1	-5.03	-3.15	TGN + secretory vesicles	●	●	●	●	●	●	●	●	●	●	●	**Defect in invasion, intracellular growth and egress**-Defect in rhoptry and microneme biogenesis (93)
	RAMA	N/A	-1.47	Rhoptry	○	○	○	○	○	○	○	●	●	○	○	**Invasion defect-** Defect in micronmes and rhoptries maturation (92)
Positioning	ARO	-2.1	-2.21	Rhoptry	●	●	●	●	●	●	●	●	●	●	●	**Invasion defect**-Dispersed and detached rhoptries-Rhoptry secretion defect (110, 111)
	AIP	-0.38	-3.28	Rhoptry	●	●	●	●	●	●	●	●	●	●	○	No impact (110, 112, 113)
	Acβ	-1.12	-2.68	Rhoptry	●	●	●	●	●	●	●	●	●	●	●	No impact (110, 112)
	CSCHAP	-0.18	N/A	Apical + rhoptries + micronemes + endomembrane system	●	●	●	○	○	○	○	○	○	○	○	**Invasion defect**-Formation of abberant apical organelles-Detached rhoptries-Rhoptry secretion defect (114)
PTMs	Plasmepsin X	N/A	-2.49	Exoneme	○	○	○	○	○	○	○	●	●	○	○	**Defect in invasion and egress-**Defect in rhoptry and micronemes maturation-Defect in rhoptry secretion (100, 101)
	Plasmepsin IX	N/A	-2.73	Novel apical organelles associated with rhoptries	○	○	○	○	○	○	○	●	●	○	○	**Defect in invasion and egress**-Defect in rhoptry and micronemes maturation-Defect in rhoptry secretion (100, 101)
	ASP3	-1.87	N/A	ELC	●	●	●	●	●	●	●	○	○	●	○	**Defect in invasion and egress**-Defect in rhoptry and micronemes maturation-Defect in rhoptry secretion (98)
Invasion / Secretion	AMA1	-2.86	-2.39	Micronemes	●	●	●	●	●	●	●	●	●	○	○	**Invasion defect**-Rhoptry secretion defect (132)
	MIC8	-1.71	N/A	Micronemes	●	●	●	●	●	○	○	○	○	○	○	**Invasion defect**-Rhoptry secretion defect (10)
	RASP1	0.91	N/A	Rhoptry Neck	●	●	●	●	●	●	●	●	●	●	○	No impact (127)
	RASP2	-3.5	-2.62	Rhoptry Neck	●	●	●	●	●	●	●	○	○	○	●	**Invasion defect**-Rhoptry secretion defect (127)
	RASP3	1.37	N/A	Rhoptry Neck	●	●	●	○	○	○	○	○	○	○	○	No impact (127)
	FER1	-4.77	-2.87	N/A	●	●	●	●	●	●	●	●	●	●	●	No impact (131)
	FER2	-5.03	-2.97	Apical + rhoptries + IMC	●	●	●	●	●	●	●	●	●	●	●	**Invasion defect**-Rhoptry secretion defect (131)
	FER3	0.77	N/A	N/A	●	●	●	●	●	○	○	○	○	○	○	No impact (131)
	RON5	-4.34	-2.85	Rhoptry Neck	●	●	●	●	●	○	○	●	●	○	○	**Invasion defect-**Rhoptry secretion defect (32)
	Nd6	-2.54	-2.7	Cytoplasme+Apical tip	●	●	●	●	●	●	●	●	●	●	○	**Invasion defect**-Rhoptry secretion defect (126)
	Nd9	-4.3	-2.85	Cytoplasme	●	●	●	●	●	●	●	●	●	●	○	**Invasion defect**-Rhoptry secretion defect (126)
	NdP1	-4.6	-3.07	Cytoplasme	●	●	●	●	●	●	●	●	●	●	○	**Invasion defect**-Rhoptry secretion defect (126)
	NdP2	-4.39	-2.71	Cytoplasme+Apical tip	●	●	●	●	●	●	●	●	●	●	○	**Invasion defect**-Rhoptry secretion defect (126)
Invasion	RON2	-4.63	-2.62	Rhoptry Neck	●	●	●	●	●	●	●	●	●	○	○	**Invasion defect**-Defective MJ formation (27, 37)
	RON4	-0.93	-2.54	Rhoptry Neck	●	●	●	●	●	○	○	●	●	○	○	**Invasion defect**-Defective MJ formation (33, 121)
	RON8	-3.26	N/A	Rhoptry Neck	●	●	●	●	●	○	○	○	○	○	○	Invasion defect (34)
	RON4L1	-0.24	N/A	Rhoptry Neck	●	●	●	●	●	○	○	○	○	○	○	No impact (35)
	SURFIN4.2	N/A	-1.17	Rhoptry Neck	○	○	○	○	○	○	○	●	○	○	○	Invasion defect (42-45)
	RhopH2	N/A	-3.01	Rhoptry Bulb	○	○	○	○	○	○	○	●	●	○	○	**Invasion defect**-Intracellular growth defect (53, 55)
	RhopH3	N/A	-2.74	Rhoptry Bulb	○	○	○	○	○	○	○	●	●	○	○	**Invasion defect**-Intracellular growth defect (56)
	RA	N/A	-2.88	Rhoptry Bulb	○	○	○	○	○	○	○	●	●	○	○	Sligh invasion defect (46)
	SUB2	0.3	-2.98	Rhoptries	●	●	●	●	●	○	○	●	●	○	○	**Invasion defect**-Intracellular growth defect (64)

Note: Reference table highlighting the relevant proteins discussed throughout the review. Fitness score (Sidik et al., 2016; Zhang et al., 2018), localization (Barylyuk et al., 2020), conservation throughout Apicomplexa and phenotype are mentioned. The presence of orthologs is indicated with a black dot while the absence is indicated by a white circle. *Toxoplasma gondii* (Tg), *Hammondia hammondia* (Hh), *Neospora caninum* (Nc), *Sarcocystis neurona* (Sn), *Eimeria tenella* (Et), *Theileria annulata* (Ta), *Babesia bovis* (Bb), *Plasmodium falciparum* (Pf), *Plasmodium berghei* (Pb), *Cryptosporidium parvum* (Cp), and *Gregarinicae* (G).

Abbreviations: ELC, endosome-like compartment; IMC, inner membrane complex; TGN, trans-Golgi network.

role in rhoptry biogenesis (Topolska et al., 2004), invasion (Werner et al., 1998), and PV formation (Hiller et al., 2003).

3 | MECHANISMS OF INVASION

Host cell entry is a vital, parasite-driven multisteps process. The first step is the attachment of the parasite to the host cell surface, mediated by members of the superfamily protein adhesins known as glycosylphosphatidylinositol (GPI)-anchored surface antigen glycoproteins (SAGs) related sequences (SRS) (Jung et al., 2004; Manger et al., 1998). A more intimate attachment is mediated by microneme proteins (MICs) (Frenal et al., 2017) that exocytose apically. MICs include transmembrane adhesins that recognize carbohydrates features on host cell receptors, thus, firmly attaching the parasite to the host cell (Reiss et al., 2001). The signaling cascade leading to microneme exocytosis has been largely dissected (Bisio et al., 2019). On the contrary and except for the fact that microneme secretion is required, little was known about the mechanism of rhoptry discharge (Kessler et al., 2008). Rhoptry proteins are injected into the host cytoplasm and the core RON complex (RON2/4/5) is inserted into the host PM to build the MJ. The composition and function of this complex are conserved in several apicomplexans parasites including malaria parasites (Cao et al., 2009; Richard et al., 2010). In *T. gondii*, the components of the RON complex are dependent on each other for their stability and trafficking to the rhoptries as observed in the individual knockdown (KD) (Beck et al., 2014; Wang et al., 2017). RON8 and RON4L1, two Coccidia-specific rhoptry proteins are also part of the RON complex but seem to traffic independently of the other RONs (Guérin et al., 2017; Straub et al., 2011). Once inserted in the host PM, the RON complex interacts with the microneme protein AMA1, which is anchored to the parasite PM after secretion. AMA1 directly interacts with the exposed C-terminal domain of RON2 at the host PM (Besteiro et al., 2009; Lamarque et al., 2011) and immunoprecipitation (IP) experiments showed that this binding does not require other RONs. A stage-specific redundancy is observed between *T. gondii* and *P. falciparum*, with paralogs of AMA1-RON2 also contributing to the invasion process (Lamarque et al., 2014; Parker et al., 2016; Poukchanski et al., 2013). This association generates a firm and irreversible link between the parasite and the host PM (Lamarque et al., 2014). The RON complex cooperatively interacts with cytoskeletal structures of the host cell, establishing a solid bridging interaction between the two cells (Guerin et al., 2017). Several cytosolic host adaptor proteins such as tumor susceptibility gene 101 protein (TSG101), ALG2-interacting protein X (ALIX), CD2-associated protein (CD2AP) and CBL-interacting protein of 85kDa (CIN85) are recruited to the MJ during invasion. However, the individual contribution of those factors have been shown to be dispensable for parasite invasion (Guerin et al., 2017; Pavlou et al., 2018) (Figure 2). As the parasite enters the host cell, the MJ moves toward the parasite basal pole leading to the invagination of the host cell PM to form the PVM. The apico-basal translocation of the MJ is powered by the actomyosin system, termed glideosome, with the glideosome-associated connector (GAC) connecting the MJ to the parasite F-actin (Bichet et al., 2014; Jacot et al., 2016).

Additionally, the malaria parasites also rely on a second complex to form the MJ. SURFIN4.2 is a merozoite rhoptry neck protein found at the surface of infected red blood cells (RBCs) (Mphande et al., 2008; Winter et al., 2005) and IP experiments showed that it forms a complex together with the parasite surface protein Glutamate Rich Protein (GLURP) and RON4 giving the name SURGE (SURFIN4.2-**R**ON4-**G**LURP compl**E**x) to this complex (Quintana et al., 2018). The Tryptophan-rich domain (WRD) of SURFIN4.2 might bind to cytoskeletal RBC proteins such as actin and spectrin (Zhu et al., 2017) linking the parasite PM to the RBC cytoskeleton. The rhoptry-associated Adhesin (PfRA) conserved across multiple *Plasmodium* species is a rhoptry bulb protein involved in the invasion (Anand et al., 2016). Upon secretion, this protein translocates to the merozoite surface and interacts with the sialic acids on the erythrocyte membrane, mediating parasite entry through the sialic acid-dependent pathway (Anand et al., 2016). Several other proteins were shown to interact with sialic acid such as EBA-175 (Sim et al., 1994), EBA-140 (Jiang et al., 2009), EBA-181 (Gilberger et al., 2003), and PfRH1 (Triglia et al., 2005) demonstrating that sialic acid-dependent and independent pathways are commonly used by *Plasmodium* to invade its host cells (Gaur & Chitnis, 2011; Paul et al., 2015). Additionally, a RhopH complex formed by RhopH2, RhopH3 and one member of the RhopH1/CLAG family has been reported to be important for invasion and nutrient uptake (Ito et al., 2017; Ling et al., 2003). The RhopH complex is secreted during the invasion process (Ling et al., 2003) and inserted in the PVM (Ito et al., 2017). A parallel study has consolidated the role of RhopH2 in parasite growth and replication via access to nutrients and disposal of waste products (Counihan et al., 2017). Depletion of RhopH3 prevents the formation of the complex resulting in a decrease in invasion and a complete block in intracellular growth at the trophozoite stage (Sherling et al., 2017). Finally, a subset of rhoptry neck proteins including Rh1, Rh4, and Rh5 are acting as adhesins by binding to host cell receptors (Duraisingh et al., 2003; Hayton et al., 2008; Kaneko et al., 2002; Rayner et al., 2000; Triglia et al., 2009). RONs have also been proposed to be involved in sporozoite invasion of the salivary glands, however, the mechanistic details are unknown (Ishino et al., 2019; Yang et al., 2017).

Once the parasite has entered the host cell, the PVM pinches off without leaving any breach into the host cell PM, by a rotational twisting motion independent from the host cell fission machinery (Pavlou et al., 2018).

Of relevance, a recent study in *P. falciparum* revealed the role of membrane-bound subtilisin protease SUB2, in merozoite surface protein shedding and sealing of the host RBC upon invasion (Collins et al., 2020). Depletion of SUB2 resulted in either abortive invasion along with a rapid RBC lysis, or developmental arrest of the intracellular parasite. A selective inhibition of the GPI-anchored surface protein MSP1 resulted in defective intracellular parasite development

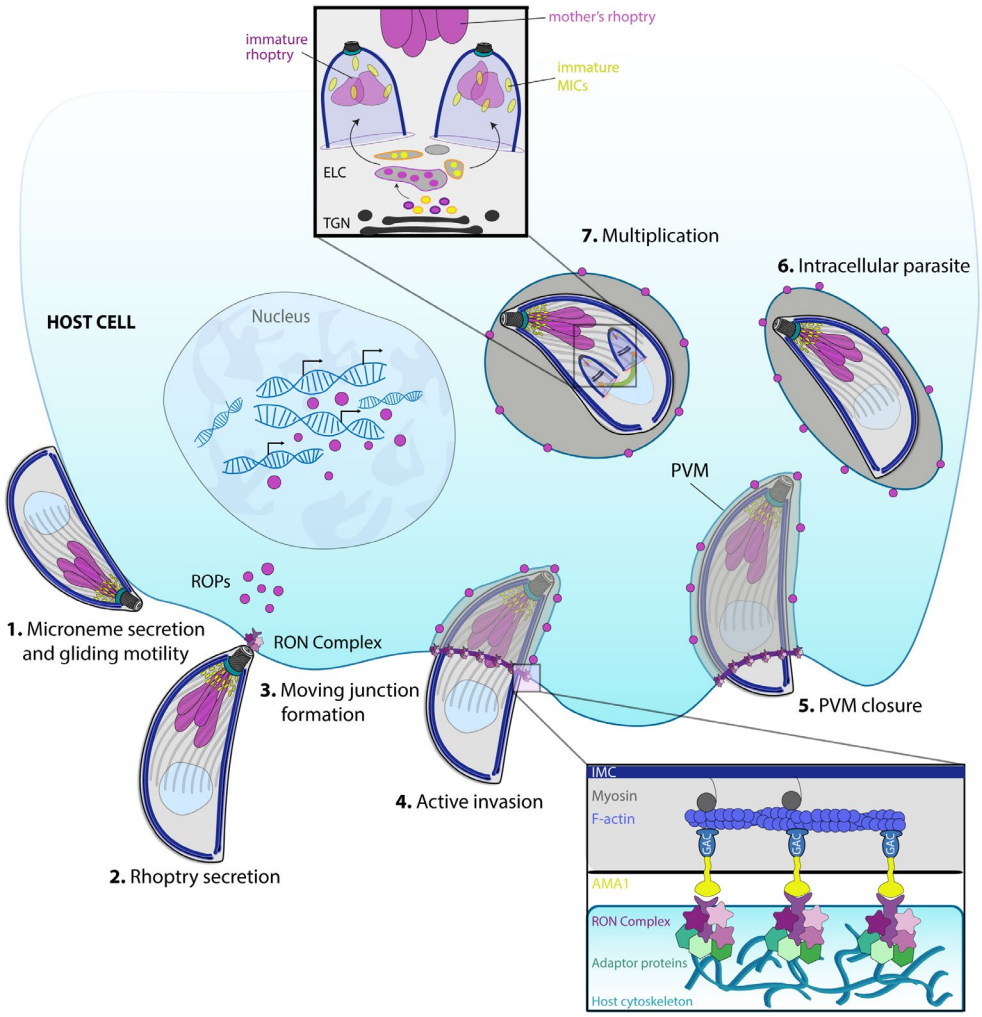

FIGURE 2 Journey of a rhoptry: fate and functions of rhoptry proteins; organelle biogenesis. Once attached to its host cell via microneme proteins (MIC) (1), the parasite discharges the rhoptry content into the host cytoplasm (2). A complex of RON proteins is insert into the host plasma membrane and interacts with AMA1 forming the moving junction (MJ) (3). ROPs are targeted to different compartments such as the host nucleus, cytoplasm, and parasitophorous vacuole membrane (PVM). Firmly anchored to the parasite actomyosin system on one side via the glideosome-associated protein (GAC) and to the host cytoskeleton on the other side, the MJ (inset A) supports active host cell invasion (4). Following PVM closure (5) and internalization (6), the intracellular parasite divides by endodyogeny with two daughter cells produced inside the mother cell (7). Pro-rhoptry proteins are packed and sorted in vesicles that emanate from the trans-Golgi network (TGN) and are then processed in an endosome-like compartment (ELC) prior to form the mature organelle (inset B)

similar to, although not as severe as SUB2-depleted parasites (Collins et al., 2020). The loss of AMA1, a known substrate of SUB2 (Howell et al., 2003), prevented invasion and produced host RBC lysis presumably due to a sealing defect.

4 | SUBVERSION OF HOST CELL AND VIRULENCE IN VIVO

Rhoptry membranous materials and ROPs do play a major role in the formation and remodeling of the PVM (Håkansson, 2001; Lingelbach & Joiner, 1998). First secreted as small vesicles inside the host cytoplasm, they then fuse with the invaginated host cell membrane and presumably contribute to PVM expansion (Håkansson, 2001). However, a mechanism of striping excludes host integral membrane proteins from the PVM (Charron & Sibley, 2004; Mordue et al., 1999). It was recently shown, using live cell imaging techniques, that secreted ROPs and dense granules proteins (GRAs) contribute to the redistribution and remodeling of the early PVM composition (Pavlou et al., 2018). As a result, the PVM is a unique compartment which does not fuse with the host cell endo-lysosomal system (Sinai et al., 2014).

Numerous ROPs harbor specialized enzymatic activities such as kinases, proteases, and phosphatases (Bradley et al., 2005). The ROP2 family, also known as ROP kinases (ROPK) possesses a conserved serine/threonine kinase domain and is the largest group of ROPs found so far (El Hajj et al., 2006). However, several members of this family lack the catalytic triad necessary for phosphorylation

activity and are, therefore, referred to as pseudo-kinases (Peixoto et al., 2010; Reese & Boothroyd, 2011; Talevich & Kannan, 2013). Several ROPK have been demonstrated to act as effectors modulating host responses to the benefit of the parasite, as discussed in recent reviews (Boothroyd & Dubremetz, 2008; Hakimi et al., 2017; Lim et al., 2012; Lima & Lodoen, 2019). The profiling of gene expression of ROPK family members showed a differentiation in the regulation of these genes between the tachyzoite stage and the bradyzoites stage and even between different type strains of *T. gondii* (Fox et al., 2016; Peixoto et al., 2010). Dense granules proteins (GRAs) are secreted throughout the lytic cycle and participate in PV and PVM maturation. Moreover, they facilitate host metabolite acquisition and in the case of the chronic infection participate to the formation of the cyst wall (Mercier & Cesbron-Delauw, 2015). Finally, some GRAs are also exported into the host cell and together with the ROPs constitute key players that tune parasite burden and dissemination modulating the host immune response (Cesbron-Delauw, 1994; Ong et al., 2010; Reese & Boothroyd, 2011; Saeij et al., 2006; Taylor et al., 2006).

5 | RHOPTRY ORGANELLE BIOGENESIS

During *T. gondii* endodyogeny, the secretory organelles are made de novo at a late stage of the division cycle, likely by vesicular trafficking generated from the late Golgi compartment (Nishi et al., 2008) (Figure 2). In addition to the de novo synthesis, daughter micronemes seem also to be recycled from the mother in an F-actin-dependent process (Periz et al., 2019). Rhoptry biogenesis relies on the acidification of an endosome-like compartment (ELC) found halfway between the Golgi apparatus and the apical pole of the parasite (Dubremetz, 2007; Shaw et al., 1998). ELC and pre-rhoptries contain pro-proteins that presumably transit via coated vesicles derived from the trans-Golgi network (TGN). The maturation of rhoptry organelles involves morphological changes such as elongation of the neck to adopt the distinctive club-shaped structure and condensation of rhoptry proteins (Shaw et al., 2002). Knowledge about the trafficking of secretory organelles in Apicomplexa has been deduced from functional investigations of factors conserved in model organisms (Venugopal & Marion, 2018). A sortilin-like receptor (SRTLR) was identified in *T. gondii* and *P. falciparum* as a cargo receptor to transport secreted proteins across the Golgi to the endosomal-related compartment (Hallee et al., 2018a; Sloves et al., 2012). Components of the retromer complex are then recruited for retrograde translocation and recycling to the Golgi (Sloves et al., 2012). Conditional depletion of TgSRTLR leads to parasites lacking micronemes and rhoptries (Sloves et al., 2012). In *P. falciparum*, knockdown of PfSRTLR results in accumulation of rhoptry and microneme proteins in the ER as well as disruption of IMC biogenesis (Hallee et al., 2018b). PfSRTLR interacts with the GPI-anchored rhoptry-associated membrane antigen (RAMA) also known to be important for rhoptry morphological maturation (Sherling et al., 2019). SRTLR clearly acts as a key escorter in the secretory pathway for several organelles proteins although the question remains on how the specificity is determined by this single escort protein. Heterotetrameric clathrin adaptor protein complexes (APs) are composed of four subunits that orchestrate the budding of coated vesicles from the TGN intended to fuse with organelles. In *T. gondii*, the adaptor protein 1 complex (AP1) has a dual role, being involved in trafficking of rhoptry and microneme proteins post-Golgi and implicated in the maturation of pre-rhoptry compartments to apically anchored mature organelles (Venugopal et al., 2017). The vacuolar protein sorting-associated protein 9 (Vps9), when conditionally depleted in *T. gondii* leads to mis-trafficking of rhoptry proteins, MICs and GRAs (Sakura et al., 2016). Similarly, conditional knock-down of Vps11, a common subunit of HOPS and CORVET complex leads to the mis-localization of Rab7 and a defect in micronemes, rhoptries, and dense granules biogenesis (Morlon-Guyot et al., 2015). In addition, two subunits belonging to the interacting network of Vps11, BEACH domain containing protein (BDCP) and Vps8 were recently discovered (Morlon-Guyot et al., 2018b). While depletion of Vps8 affects the biogenesis of dense granules, rhoptries and a subset of MICs, BDCP has a restricted function, affecting only the morphology of the rhoptries (Morlon-Guyot et al., 2018b). The description of an interaction between the C-terminal tail of SORTLR with AP1 and Vps proteins suggests a concerted role of these complexes in the trafficking of ROPs and MICs *via* a clathrin-dependent process (Sloves et al., 2012). A recent study shows that the trafficking of vesicles to their specialized compartments depends on SNARE proteins (Bisio et al., 2020). Syntaxin (Stx)-like SNARE protein 12 (Stx12) localizes to the ELC and is involved in the trafficking of proteins to rhoptries and micronemes as well as to the apicoplast. Disruption of Stx12 resulted in a decreased amount of mature microneme and rhoptry proteins along with a severe defect in invasion (Bisio et al., 2020).

Along the secretory pathway several rhoptry proteins undergo proteolytic cleavage by the aspartyl protease 3 (TgASP3) which is also involved in the maturation of the MICs (Dogga et al., 2017). Similarly, in *P. falciparum* rhoptries are formed de novo during schizogony (Margos et al., 2004). Two aspartyl proteases are responsible of the maturation of secreted proteins with Plasmepsin IX dedicated to rhoptry protein and Plasmepsin X dedicated to the microneme proteins (Nasamu et al., 2017; Pino et al., 2017). Genetic disruption or chemical inhibition of these maturases lead to severe blocks in invasion and egress (Nasamu et al., 2017; Pino et al., 2017). Of relevance, parasite depleted in vacuolar-proton ATPases (V-H+-ATPases) exhibited a delay in ASP3-dependent maturation and defective rhoptry function (Stasic et al., 2019), probably due to the absence of proper pre-rhoptry acidification (Yakubu et al., 2018) needed for protease activity and condensation of the organelle content. Another class of proteins has been recently described as being important for secretory organelles maturation and morphology. The major facilitator superfamily (MFS) is one of the largest group of membrane transporters (Pao et al., 1998) known to facilitate movement of small solutes across membranes (Law et al., 2008), playing an important role in the acidification process (Mellman et al., 1986) and nutrient

uptake. In *T. gondii*, four transporter family proteins (TFP1-4) belonging to the MFS family have been characterized (Hammoudi et al., 2018). TFP1 is associated with the microneme and the ELC, TFP2, and TFP3 are localized to the rhoptries and TFP4 is found at the Golgi apparatus (Hammoudi et al., 2018). Inducible depletion of TFP1 and TFP2 result in aberrant morphology of micronemes and rhoptries, respectively. Yet, the nature of the substrates transported by the TFPs is still unknown.

6 | RHOPTRY ORGANELLE POSITIONING

The apical positioning of rhoptries is crucial for the discharge of rhoptry content and consequently for successful invasion. A network of interacting proteins at the surface of the rhoptries has been described as key players for the clustering and anchoring of the rhoptries at the apical pole. Armadillo repeats only protein (ARO) is composed of five predicted armadillo motif (ARM) and anchored to the cytosolic face of the rhoptry membrane via N-terminal myristoylation and palmitoylation (Beck et al., 2013; Frenal et al., 2013). In *T. gondii* parasites depleted in ARO, the rhoptries are dispersed in the cytosol and some membranous structures of rhoptry origin accumulate (Mueller et al., 2016). Analysis of individual ARM deletions mutants showed that each motif is necessary for the proper folding of a functional ARO. Pull-down experiments identified partners of ARO such as myosin *F* (MyoF), adenylate cyclase beta (ACβ), and ARO Interacting Protein (AIP). TgMyoF is presumably implicated in the apical positioning of rhoptries (Mueller et al., 2013). While ARO homogeneously distributed on the rhoptry organelle, TgAIP and TgACβ are localized at a specific zone of the rhoptry positioned between the neck and the bulb and are dispensable for the parasite lytic cycle (Lemgruber et al., 2011; Mueller et al., 2016). Apart from its importance in positioning the rhoptries, TgARO also maintains the rhoptries in bundles. Successful trans-genera functional complementation between *T. gondii* and *P. falciparum* suggests that ARO functions and properties are conserved across the phylum (Mueller et al., 2016). The crystal structure of PfARO revealed that 5 tandem ARM repeats and the N-terminal region are highly flexible, allowing the protein to accommodate simultaneous interactions with multiple binding partners (Geiger et al., 2020). PfARO also interacts with PfAIP and PfACβ (Geiger et al., 2020), however, in contrast to TgAIP, PfAIP is essential for parasite survival and its mis-localization resulted in a decreased parasitemia due to impaired invasion (Geiger et al., 2020). This difference in phenotype reflects either additional functions for PfAIP in malaria parasites or that other proteins might compensate for the deletion of TgAIP in *T. gondii*. Finally and importantly, a protein predicted to interact with the CORVET and HOPS tethering complexes and referred to CORVET/HOPS-Associated Protein (TgCSCHAP) plays a central role in the apical positioning of rhoptries without contributing to their clustering (Morlon-Guyot et al., 2018a). TgCSCHAP is a conoid protein conserved only in the Coccidia. As TgCSCHAP possesses two putative microtubule binding domains, it might anchors the rhoptries apically to the intraconoidal microtubules positioned at the center of the conoid (Morlon-Guyot et al., 2018a), as discussed in the next section.

7 | MACHINERY OF RHOPTRY DISCHARGE

Rhoptry discharge that crosses both parasite and host cell PM is an enigmatic and yet crucial event in the parasite lytic cycle. This process requires a contact between parasite and its host and appears to be tightly linked to microneme secretion (Carruthers & Sibley, 1997). Unlike microneme exocytosis, rhoptry discharge cannot be triggered on purified extracellular parasites, however, several assays are available to monitor the ability of parasites to secrete their rhoptry content into the host cell (Suarez et al., 2020). Treatment of extracellular parasites with cytochalasin D, (an actin polymerization inhibitor) prevents invasion but allows rhoptry discharge. Under these conditions, lipid and protein-rich vesicles called evacuoles (empty-vacuoles) are released in the host cytosol and can be visualized using anti-ROP1 antibodies (Håkansson, 2001). A second method capitalizes on the role of ROP16 as an effector kinase that phosphorylates host cell transcriptional factors STAT3 and STAT6, negatively regulating the host inflammatory responses (Ong et al., 2010; Saeij et al., 2007). Anti-phosphoSTAT6/3 antibodies used by indirect immunofluorescence assay or western blot indirectly measure rhoptry discharge. Another approach relies on a fluorescence resonance energy transfer (FRET) assay and detects the secretion of parasite proteins into the host cell using beta-lactamase (BLA)-fused parasite protein and a FRET BLA substrate preloaded into the host cell cytoplasm. Successful secretion triggers a shift in host cell fluorescence from 520 nm (fluorescein) to 447 nm (coumarin) such as the one observed for when the rhoptry protein Toxofilin-BLA (Lodoen et al., 2010) is secreted. Finally, Toxofilin has been also used fused with Cre recombinase to develop a highly sensitive-method monitoring Cre excision following rhoptry discharge. Using an adequately responsive host cell lines, rhoptry-injected cells can be detected by either fluorescence-activated cell sorting (FACS) or fluorescence microscopy (Koshy et al., 2010). With this method, Koshy et al. showed that a large proportion of host cells is injected with rhoptry proteins without being infected. This phenomenon has been observed in vitro as well as in vivo where encysted parasites are surrounded by injected/uninfected cells (Koshy et al., 2012). Whether this subpopulation of cells participate in the modulation of the host immune response at the organism level remains to be investigated.

Following discharge, rhoptry organelles are observed empty (Lebrun et al., 2005) and of reduced size (Paredes-Santos et al., 2012) illustrating the mechanism of organelle discharge distinct from the exocytosis of the micronemes. In order to deliver its content into the host cytoplasm, the rhoptry organelles need to form successive pores or membrane fusions with the PMs of the parasite and the host cell. Previous patch-clamp experiments had recorded a break in the host PM at early time of invasion that presumably corresponds to the rhoptry discharge event (Suss-Toby et al., 1996). Ready for exocytosis, one or two rhoptries are often seen with their neck

traversing the conoid and reaching the PM at the apical tip of the parasites suggesting that they are primed and properly anchored for secretion (Figure 1a,b) (Jena, 2009; Paredes-Santos et al., 2012). An elegant ultrastructural study using focused ion beam-scanning electron microscopy described the elements surrounding the rhoptries that might participate in the secretion machinery (Paredes-Santos et al., 2012). In this paper, Paredes-Santos et al. described that the neck of the rhoptry primed for secretion runs along the pair of intraconoidal microtubules to reach a vesicle located just beneath the PM, at the apex of the parasites, called the apical vesicle. Four other vesicles of the same kind are aligned to the intraconoidal microtubules on the opposite side of the rhoptry neck (Paredes-Santos et al., 2012). Other studies have shown that the parasite PM over the conoid is decorated of a rosette of intramembranous particles such as the one observed in *Paramecium* at the site of trichocysts exocytosis (Dubremetz, 2007; Porchet & Torpier, 1977) (Figure 3). While the similarity with the *Paramecia* has been only descriptive so far, a recent functional study links the rosette to the rhoptry secretion. Recently, Aquilini et al. have identified a complex composed of TgNd6 and TgNd9, previously described in *Paramecium* as Non-discharge (Nd) as well as two Nd partners, TgNdP1 and TgNdP2 that are central for the assembly of the rosette and rhoptry discharge (Aquilini et al., 2020). Specifically, the depletion of TgNd6 or TgNd9 leads to impairment in rhoptry secretion and TgNd9 depletion additionally correlates with a decrease in the number of parasites possessing a rosette. This machinery is conserved in *P. falciparum* where rhoptry secretion is altered in the absence of PfNd9. While TgNd6 and TgNd9 are in the cytoplasm, TgNd6 also accumulates at the apical tip to the apical vesicle which is appears to be connected to the PM by the rosette from one side and to the tip of the rhoptries from the other side (Aquilini et al., 2020).

A small family of rhoptry apical surface proteins (RASPs) were described in *T. gondii* and *P. falciparum* to play a role in rhoptry discharge. The RASPs colocalize with ARO and cap the extremity of the rhoptry neck (Suarez et al., 2019) (Figure 3). In *T. gondii*, RASP1, RASP2, and RASP3 interact directly with each other to form a complex. RASP3 is only found in coccidians parasites and *P. falciparum* encodes only one RASP that has high similarities to TgRASP2. Depletion of RASP2 in both *T. gondii* and *P. falciparum*, results in a severe block in invasion due to a loss of rhoptry secretion without affecting the organelle targeting or morphology. PfRASP2 is also known as PfCERLI1 and found restricted to the rhoptry bulb (Liffner et al., 2020). RASP2 contains a C2 lipid binding domain and a PH-like domain. Both domains contribute to phosphatidic acid (PA) and phosphatidylinositol 4,5-biphosphate (PIP2) binding facilitating the docking of the rhoptry for fusion (Suarez et al., 2019). PA and PIP2 accumulation are important for membrane fusion during exocytosis (Martin, 2015) and more specifically, PA has been reported as lipid mediator of microneme secretion in *T. gondii* (Bullen et al., 2016). In their model, Suarez et al. proposed that following microneme exocytosis, RASP2 binds to the accumulated PIP2 and, or PA and facilitates the attachment between the rhoptry and the PM leading to the recruitment of a fusion machinery like SNARE proteins or other hypothetical proteins (Suarez et al., 2019). While microneme secretion is regulated by oscillations of intracellular Ca^{2+}, it was thought that rhoptry secretion was a Ca^{2+}-independent process (Mercier & Cesbron-Delauw, 2015). Recently, orthologs of Ca^{2+} sensing Ferlin proteins

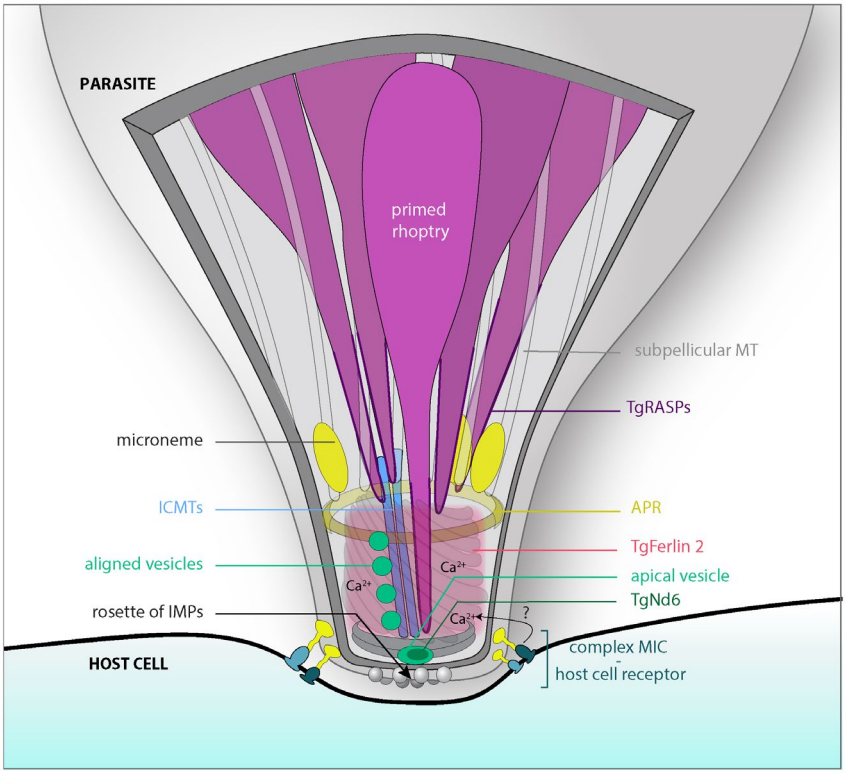

FIGURE 3 *T. gondii* rhoptry discharge machinery. Following microneme secretion, MICs interact with host cell receptors. A signaling cascade is initiated, possibly involving *Tg*Ferlin 2 (red) and Ca^{2+}. The rhoptry primed for discharge is largely inserted into the conoid with its neck running along the intraconoidal microtubules (ICMTs). The extreme tip of the rhoptry is found close to an apical vesicle located just beneath the plasma membrane at a site where a rosette of eight intramembranous particles (IMPs) is visible. Three to four vesicles sitting along the ICMTs are thought to replenish the apical vesicle, allowing consecutive rhoptry secretion. *Tg*RASPs coat the apical part of the rhoptry and are involved in their secretion. APR, apical polar ring; MT, microtubule

(FER) were identified in apicomplexan parasites. Ferlins are known to be involved in membrane trafficking and vesicle fusion and can bind calcium and phospholipids *via* their multiple C2 domains. TgFER1 and TgFER2 are conserved throughout the entire phylum, whereas TgFER3 is only found in Coccidia (Coleman et al., 2018). Conditional depletion of TgFER2 causes a severe defect in invasion due to a defect in rhoptry secretion but the role of Ca^{2+} in TgFER2 function is still uncertain (Figure 3) (Coleman et al., 2018). TgFER2 was also found to interact with TgNd6 and TgNd9 (Aquilini et al., 2020). Microneme proteins seem also to be part of the signaling cascade leading to rhoptry secretion as the depletion of MIC8 or AMA1 prevents rhoptry discharge (Kessler et al., 2008; Mital et al., 2005).

8 | CONCLUDING REMARKS AND PERSPECTIVES

Specialized secretory organelles in Apicomplexa have evolved to support the parasite in key steps of its lytic cycle, to ensure a proper proliferation and establishment of infection. In the recent years, considerable progress was achieved in deciphering the role of rhoptries. Despite the advance in our understanding of the biogenesis, trafficking and secretion of these organelles, many questions remain opened. Future challenges reside in the identification of the molecular mechanisms that orchestrate in time and space the rhoptry discharge. Additionally, the composition and structure of the MJ have not yet been fully elucidated. Host cell partners interacting with the RONs complex still need to be investigated and could help develop new effective drugs to disrupt the invasion. The involvement of secreted rhoptry proteins as effectors of virulence is a key step that add to the interest in these organelles. Our perception of the subversion of host cellular functions remains fractal. Finally, since these unique secretory organelles are shared in all Apicomplexa invasive stages, exciting new findings are to be anticipated about the role of the rhoptry content during encystation of *T. gondii* or liver development in *Plasmodium spp*.

ACKNOWLEDGMENTS

We are grateful for Bohumil Maco for generously sharing EM pictures. We thank Nicolas Dos Santos Pacheco for kindly helping with the figures. R.B.C and G.L were supported by the SNSF (310030B_166678 and 310030_185325). GL is supported by the faculty of medicine of the University of Geneva.

CONFLICT OF INTEREST

We declare to have no conflict of interest.

ORCID

Rouaa Ben Chaabene https://orcid.org/0000-0003-1617-6206
Gaëlle Lentini https://orcid.org/0000-0003-0836-9972
Dominique Soldati-Favre https://orcid.org/0000-0003-4156-2109

REFERENCES

Anand, G., Reddy, K.S., Pandey, A.K., Mian, S.Y., Singh, H., Mittal, S.A. et al. (2016) A novel *Plasmodium falciparum* rhoptry associated adhesin mediates erythrocyte invasion through the sialic-acid dependent pathway. *Scientific Reports*, *6*, 29185. Available from: https://doi.org/10.1038/srep29185

Aquilini, E., Cova, M.M., Mageswaran, S.K., Dos Santos Pacheco, N., Sparvoli, D., Penarete-Vargas, D.M. et al. (2020) An Alveolata secretory machinery adapted to parasite-host cell invasion. *Nature Microbiology*, 1–21. https://doi.org/10.1038/s41564-020-00854-z

Barylyuk, K., Koreny. L., Ke, H., Butterworth, S., Crook, O.M., Lassadi, I. et al. (2020) A comprehensive subcellular atlas of the toxoplasma proteome via hyperLOPIT provides spatial context for protein functions. *Cell Host & Microbe*, *28*(5), 752–766.e9. Available from: https://doi.org/10.1016/j.chom.2020.09.011

Beck, J.R., Chen, A.L., Kim, E.W. & Bradley, P.J. (2014) RON5 is critical for organization and function of the *Toxoplasma* moving junction complex. *PLoS Pathogens*, *10*(3), e1004025. Available from: https://doi.org/10.1371/journal.ppat.1004025

Beck, J.R., Fung, C., Straub, K.W., Coppens, I., Vashisht, A.A., Wohlschlegel, J.A. et al. (2013) A *Toxoplasma* palmitoyl acyl transferase and the palmitoylated armadillo repeat protein TgARO govern apical rhoptry tethering and reveal a critical role for the rhoptries in host cell invasion but not egress. *PLoS Pathogens*, *9*(2), e1003162. Available from: https://doi.org/10.1371/journal.ppat.1003162

Besteiro, S., Michelin, A., Poncet, J., Dubremetz, J.F. & Lebrun, M. (2009) Export of a *Toxoplasma gondii* rhoptry neck protein complex at the host cell membrane to form the moving junction during invasion. *PLoS Pathogens*, *5*(2), e1000309. Available from: https://doi.org/10.1371/journal.ppat.1000309

Bichet, M., Joly, C., Henni, A.H., Guilbert, T., Xemard, M., Tafani, V. et al. (2014) The *toxoplasma*-host cell junction is anchored to the cell cortex to sustain parasite invasive force. *BMC Biology*, *12*, 773. Available from: https://doi.org/10.1186/s12915-014-0108-y

Bisio, H., Chaabene, R.B., Sabitzki, R., Maco, B., Marq, J.B., Gilberger, T.W. et al. (2020) The ZIP code of vesicle trafficking in Apicomplexa: SEC1/Munc18 and SNARE proteins. *mBio*, *11*, e02092-20.

Bisio, H., Lunghi, M., Brochet, M. & Soldati-Favre, D. (2019) Phosphatidic acid governs natural egress in *Toxoplasma gondii* via a guanylate cyclase receptor platform. *Nature Microbiology*, *4*(3), 420–428. Available from: https://doi.org/10.1038/s41564-018-0339-8

Boothroyd, J.C. & Dubremetz, J.F. (2008) Kiss and spit: The dual roles of *Toxoplasma* rhoptries. *Nature Reviews Microbiology*, *6*(1), 79–88. Available from: https://doi.org/10.1038/nrmicro1800

Bradley, P.J., Ward, C., Cheng, S.J., Alexander, D.L., Coller, S., Coombs, G.H. et al. (2005) Proteomic analysis of rhoptry organelles reveals many novel constituents for host-parasite interactions in *Toxoplasma gondii*. *The Journal of Biological Chemistry*, *280*(40), 34245–34258. Available from: https://doi.org/10.1074/jbc.M504158200

Bullen, H.E., Jia, Y., Yamaryo-Botte, Y., Bisio, H., Zhang, O., Jemelin, N.K. et al. (2016) Phosphatidic acid-mediated signaling regulates microneme secretion in *Toxoplasma*. *Cell Host & Microbe*, *19*(3), 349–360. Available from: https://doi.org/10.1016/j.chom.2016.02.006

Cao, J., Kaneko, O., Thongkukiatkul, A., Tachibana, M., Otsuki, H., Gao, Q. et al. (2009) Rhoptry neck protein RON2 forms a complex with microneme protein AMA1 in *Plasmodium falciparum* merozoites. *Parasitology International*, *58*(1), 29–35. Available from: https://doi.org/10.1016/j.parint.2008.09.005

Carruthers, V.B. & Sibley, L.D. (1997) Sequential protein secretion from three distinct organelles of *Toxoplasma gondii* accompanies invasion of human fibroblasts. *European Journal of Cell Biology*, *73*(2), 114–123.

Cesbron-Delauw, M.F. (1994) Dense-granule organelles of *Toxoplasma gondii*: Their role in the host-parasite relationship. *Parasitology Today*, *10*(8), 293–296. Available from: https://doi.org/10.1016/0169-4758(94)90078-7

Charnaud, S.C., Kumarasingha, R., Bullen, H.E., Crabb, B.S. & Gilson, P.R. (2018) Knockdown of the translocon protein EXP2 in *Plasmodium falciparum* reduces growth and protein export. *PLoS ONE*, *13*(11), e0204785. Available from: https://doi.org/10.1371/journal.pone.0204785

Charron, A.J. & Sibley, L.D. (2004) Molecular partitioning during host cell penetration by *Toxoplasma gondii*. *Traffic*, *5*(11), 855–867. Available from: https://doi.org/10.1111/j.1600-0854.2004.00228.x

Coleman, B.I., Saha, S., Sato, S., Engelberg, K., Ferguson, D.J.P., Coppens, I. et al. (2018) A member of the ferlin calcium sensor family is essential for *Toxoplasma gondii* rhoptry secretion. *mBio*, *9*(5), 1–14.

Collins, C.R., Hackett, F., Howell, S.A., Snijders, A.P., Russell, M.R.G., Collinson, L.M. et al. (2020) The malaria parasite sheddase SUB2 governs host red blood cell membrane sealing at invasion. *eLife*, *9*. Available from: https://doi.org/10.7554/elife.61121

Coppens, I. & Joiner, K.A. (2003) Host but not parasite cholesterol controls *Toxoplasma* cell entry by modulating organelle discharge. *Molecular Biology of the Cell*, *14*(9), 3804–3820.

Counihan, N.A., Chisholm, S.A., Bullen, H.E., Srivastava, A., Sanders, P.R., Jonsdottir, T.K. et al. (2017) *Plasmodium falciparum* parasites deploy RhopH2 into the host erythrocyte to obtain nutrients, grow and replicate. *eLife*, *6*, 1–31. Available from: https://doi.org/10.7554/eLife.23217

Dluzewski, A.R., Zicha, D., Dunn, G.A. & Gratzer, W.B. (1995) Origins of the parasitophorous vacuole membrane of the malaria parasite: Surface area of the parasitized red cell. *European Journal of Cell Biology*, *68*(4), 446–449.

Dogga, S.K., Mukherjee, B., Jacot, D., Kockmann, T., Molino, L., Hammoudi, P.M. et al. (2017) A druggable secretory protein maturase of *Toxoplasma* essential for invasion and egress. *eLife*, *6*, 1–35. Available from: https://doi.org/10.7554/eLife.27480.

Dos Santos, P.N., Tosetti, N., Koreny, L., Waller, R.F. & Soldati-Favre, D. (2020) Evolution, composition, assembly, and function of the conoid in Apicomplexa. *Trends in Parasitology*, *36*(8), 688–704. Available from: https://doi.org/10.1016/j.pt.2020.05.001

Dubois, D.J. & Soldati-Favre, D. (2019) Biogenesis and secretion of micronemes in *Toxoplasma gondii*. *Cell Microbiology*, *21*(5), e13018.

Dubremetz, J.F. (2007) Rhoptries are major players in *Toxoplasma gondii* invasion and host cell interaction. *Cellular Microbiology*, *9*(4), 841–848. Available from: https://doi.org/10.1111/j.1462-5822.2007.00909.x

Duraisingh, M.T., Triglia, T., Ralph, S.A., Rayner, J.C., Barnwell, J.W., McFadden, G.I. et al. (2003) Phenotypic variation of *Plasmodium falciparum* merozoite proteins directs receptor targeting for invasion of human erythrocytes. *The EMBO Journal*, *22*(5), 1047–1057. Available from: https://doi.org/10.1093/emboj/cdg096

El Hajj, H., Demey, E., Poncet, J., Lebrun, M., Wu, B., Galeotti, N. et al. (2006) The ROP2 family of *Toxoplasma gondii* rhoptry proteins: Proteomic and genomic characterization and molecular modeling. *Proteomics*, *6*(21), 5773–5784. Available from: https://doi.org/10.1002/pmic.200600187

Foussard, F., Leriche, M.A. & Dubremetz, J.F. (2009) Characterization of the lipid content of *Toxoplasma gondii* rhoptries. *Parasitology*, *102*(3), 367–370.

Fox, B.A., Rommereim, L.M., Guevara, R.B., Falla, A., Hortua Triana, M.A., Sun, Y. et al. (2016) The *Toxoplasma gondii* rhoptry kinome is essential for chronic infection. *mBio*, *7*(3), 1–12.

Frenal, K., Dubremetz, J.F., Lebrun, M. & Soldati-Favre, D. (2017) Gliding motility powers invasion and egress in Apicomplexa. *Nature Reviews Microbiology*, *15*(11), 645–660. Available from: https://doi.org/10.1038/nrmicro.2017.86

Frenal, K., Tay, C.L., Mueller, C., Bushell, E.S., Jia, Y., Graindorge, A. et al. (2013) Global analysis of apicomplexan protein S-acyl transferases reveals an enzyme essential for invasion. *Traffic*, *14*(8), 895–911. Available from: https://doi.org/10.1111/tra.12081

Gaur, D. & Chitnis, C.E. (2011) Molecular interactions and signaling mechanisms during erythrocyte invasion by malaria parasites. *Current Opinion in Microbiology*, *14*(4), 422–428. Available from: https://doi.org/10.1016/j.mib.2011.07.018

Geiger, M., Brown, C., Wichers, J.S., Strauss, J., Lill, A., Thuenauer, R. et al. (2020) Structural insights Into PfARO and characterization of its interaction with PfAIP. *Journal of Molecular Biology*, *432*(4), 878–896. Available from: https://doi.org/10.1016/j.jmb.2019.12.024

Gilberger, T.W., Thompson, J.K., Triglia, T., Good, R.T., Duraisingh, M.T. & Cowman, A.F. (2003) A novel erythrocyte binding antigen-175 paralogue from *Plasmodium falciparum* defines a new trypsin-resistant receptor on human erythrocytes. *The Journal of Biological Chemistry*, *278*(16), 14480–14486. Available from: https://doi.org/10.1074/jbc.M211446200

Gold, D.A., Kaplan, A.D., Lis, A., Bett, G.C., Rosowski, E.E., Cirelli, K.M. et al. (2015) The *Toxoplasma* dense granule proteins GRA17 and GRA23 mediate the movement of small molecules between the host and the parasitophorous vacuole. *Cell Host & Microbe*, *17*(5), 642–652. Available from: https://doi.org/10.1016/j.chom.2015.04.003

Guerin, A., Corrales, R.M., Parker, M.L., Lamarque, M.H., Jacot, D., El Hajj, H. et al. (2017) Efficient invasion by *Toxoplasma* depends on the subversion of host protein networks. *Nature Microbiology*, *2*(10), 1358–1366. Available from: https://doi.org/10.1038/s41564-017-0018-1

Guérin, A., El Hajj, H., Penarete-Vargas, D., Besteiro, S. & Lebrun, M. (2017) RON4L1 is a new member of the moving junction complex in *Toxoplasma gondii*. *Scientific Reports*, *7*(1), 17907. Available from: https://doi.org/10.1038/s41598-017-18010-9

Håkansson, S. (2001) Toxoplasma evacuoles: A two-step process of secretion and fusion forms the parasitophorous vacuole. *The EMBO Journal*, *20*(12), 3132–3144. Available from: https://doi.org/10.1093/emboj/20.12.3132

Hakimi, M.-A., Olias, P. & Sibley, L.D. (2017) Effectors targeting host signaling and transcription. *Clinical Microbiology Reviews*, *30*(3), 615–645.

Hallee, S., Boddey, J.A., Cowman, A.F. & Richard, D. (2018a) Evidence that the *Plasmodium falciparum* protein sortilin potentially acts as an escorter for the trafficking of the rhoptry-associated membrane antigen to the rhoptries. *mSphere*, *3*(1), 1–10. Available from: https://doi.org/10.1128/mSphere.00551-17

Hallee, S., Counihan, N.A., Matthews, K., de Koning-Ward, T.F. & Richard, D. (2018b) The malaria parasite *Plasmodium falciparum* Sortilin is essential for merozoite formation and apical complex biogenesis. *Cellular Microbiology*, *20*(8), e12844.

Hammoudi, P.M., Maco, B., Dogga, S.K., Frenal, K. & Soldati-Favre, D. (2018) *Toxoplasma gondii* TFP1 is an essential transporter family protein critical for microneme maturation and exocytosis. *Molecular Microbiology*, *109*(2), 225–244. Available from: https://doi.org/10.1111/mmi.13981

Hayton, K., Gaur, D., Liu, A., Takahashi, J., Henschen, B., Singh, S. et al. (2008) Erythrocyte binding protein PfRH5 polymorphisms determine species-specific pathways of *Plasmodium falciparum* invasion. *Cell Host & Microbe*, *4*(1), 40–51. Available from: https://doi.org/10.1016/j.chom.2008.06.001

Hiller, N.L., Akompong, T., Morrow, J.S., Holder, A.A. & Haldar, K. (2003) Identification of a stomatin orthologue in vacuoles induced in human erythrocytes by malaria parasites. A role for microbial raft proteins in apicomplexan vacuole biogenesis. *The Journal of Biological Chemistry*, *278*(48), 48413–48421. Available from: https://doi.org/10.1074/jbc.M307266200

Howell, S.A., Well, I., Fleck, S.L., Kettleborough, C., Collins, C.R. & Blackman, M.J. (2003) A single malaria merozoite serine protease mediates shedding of multiple surface proteins by juxtamembrane cleavage. *Journal of Biological Chemistry*, *278*(26), 23890–23898. Available from: https://doi.org/10.1074/jbc.M302160200

Hu, K. (2006) Cytoskeletal components of an invasion machine—The apical complex of *Toxoplasma gondii*. *PLoS Pathogens*, *2*(2), 1–18. https://doi.org/10.1371/journal.ppat.0020013

Ishino, T., Murata, E., Tokunaga, N., Baba, M., Tachibana, M., Thongkukiatkul, A. et al. (2019) Rhoptry neck protein 2 expressed in *Plasmodium* sporozoites plays a crucial role during invasion of mosquito salivary glands. *Cellular Microbiology*, *21*(1), e12964.

Ito, D., Schureck, M.A. & Desai, S.A. (2017) An essential dual-function complex mediates erythrocyte invasion and channel-mediated nutrient uptake in malaria parasites. *eLife*, *6*, 1–24. https://doi.org/10.7554/eLife.23485

Jacot, D., Tosetti, N., Pires, I., Stock, J., Graindorge, A., Hung, Y.F. et al. (2016) An apicomplexan actin-binding protein serves as a connector and lipid sensor to coordinate motility and invasion. *Cell Host & Microbe*, *20*(6), 731–743. Available from: https://doi.org/10.1016/j.chom.2016.10.020

Jena, B.P. (2009) Porosome: The secretory portal in cells. *Biochemistry*, *48*(19), 4009–4018. Available from: https://doi.org/10.1021/bi900 2698

Jiang, L., Duriseti, S., Sun, P. & Miller, L.H. (2009) Molecular basis of binding of the *Plasmodium falciparum* receptor BAEBL to erythrocyte receptor glycophorin C. *Molecular and Biochemical Parasitology*, *168*(1), 49–54. Available from: https://doi.org/10.1016/j.molbiopara.2009.06.006

Jung, C., Lee, C.Y.F. & Grigg, M.E. (2004) The SRS superfamily of *Toxoplasma* surface proteins. *International Journal for Parasitology*, *34*(3), 285–296. Available from: https://doi.org/10.1016/j.ijpara.2003.12.004

Kaneko, O., Mu, J., Tsuboi, T., Su, X. & Torii, M. (2002) Gene structure and expression of a *Plasmodium falciparum* 220-kDa protein homologous to the *Plasmodium* vivax reticulocyte binding proteins. *Molecular and Biochemical Parasitology*, *121*(2), 275–278. Available from: https://doi.org/10.1016/S0166-6851(02)00042-7

Kats, L.M., Black, C.G., Proellocks, N.I. & Coppel, R.L. (2006) *Plasmodium* rhoptries: How things went pear-shaped. *Trends in Parasitology*, *22*(6), 269–276. Available from: https://doi.org/10.1016/j.pt.2006.04.001

Kessler, H., Herm-Gotz, A., Hegge, S., Rauch, M., Soldati-Favre, D., Frischknecht, F. et al. (2008) Microneme protein 8–a new essential invasion factor in *Toxoplasma gondii*. *Journal of Cell Science*, *121*(Pt 7), 947–956. Available from: https://doi.org/10.1242/jcs.022350

Kono, M., Prusty, D., Parkinson, J. & Gilberger, T.W. (2013) The apicomplexan inner membrane complex. *Frontiers in Bioscience*, *18*, 982–992.

Koshy, A.A., Dietrich, H.K., Christian, D.A., Melehani, J.H., Shastri, A.J., Hunter, C.A. et al. (2012) *Toxoplasma* co-opts host cells it does not invade. *PLoS Pathogens*, *8*(7), e1002825. Available from: https://doi.org/10.1371/journal.ppat.1002825

Koshy, A.A., Fouts, A.E., Lodoen, M.B., Alkan, O., Blau, H.M. & Boothroyd, J.C. (2010) *Toxoplasma* secreting Cre recombinase for analysis of host-parasite interactions. *Nature Methods*, *7*(4), 307–309. Available from: https://doi.org/10.1038/nmeth.1438

Lamarque, M., Besteiro, S., Papoin, J., Roques, M., Vulliez-Le Normand, B., Morlon-Guyot, J. et al. (2011) The RON2-AMA1 interaction is a critical step in moving junction-dependent invasion by apicomplexan parasites. *PLoS Pathogens*, *7*(2), e1001276. Available from: https://doi.org/10.1371/journal.ppat.1001276

Lamarque, M.H., Roques, M., Kong-Hap, M., Tonkin, M.L., Rugarabamu, G., Marq, J.B. et al. (2014) Plasticity and redundancy among AMA-RON pairs ensure host cell entry of *Toxoplasma* parasites. *Nature Communications*, *5*, 4098. Available from: https://doi.org/10.1038/ncomms5098

Law, C.J., Maloney, P.C. & Wang, D.N. (2008) Ins and outs of major facilitator superfamily antiporters. *Annual Review of Microbiology*, *62*, 289–305. Available from: https://doi.org/10.1146/annurev.micro.61.080706.093329

Lebrun, M., Michelin, A., El Hajj, H., Poncet, J., Bradley, P.J., Vial, H. et al. (2005) The rhoptry neck protein RON4 re-localizes at the moving junction during *Toxoplasma gondii* invasion. *Cellular Microbiology*, *7*(12), 1823–1833. Available from: https://doi.org/10.1111/j.1462-5822.2005.00646.x

Lemgruber, L., Lupetti, P., De Souza, W. & Vommaro, R.C. (2011) New details on the fine structure of the rhoptry of *Toxoplasma gondii*. *Microscopy Research and Technique*, *74*(9), 812–818.

Liffner, B., Frolich, S., Heinemann, G.K., Liu, B., Ralph, S.A., Dixon, M.W.A. et al. (2020) PfCERLI1 is a conserved rhoptry associated protein essential for *Plasmodium falciparum* merozoite invasion of erythrocytes. *Nature Communications*, *11*(1), 1411–1424. Available from: https://doi.org/10.1038/s41467-020-15127-w

Lim, D.C., Cooke, B.M., Doerig, C. & Saeij, J.P. (2012) *Toxoplasma* and *Plasmodium* protein kinases: Roles in invasion and host cell remodelling. *International Journal for Parasitology*, *42*(1), 21–32. Available from: https://doi.org/10.1016/j.ijpara.2011.11.007

Lima, T.S. & Lodoen, M.B. (2019) Mechanisms of human innate immune evasion by *Toxoplasma gondii*. *Frontiers in Cellular and Infection Microbiology*, *9*(103), 1–8. https://doi.org/10.3389/fcimb.2019.00103

Ling, I.T., Kaneko, O., Narum, D.L., Tsuboi, T., Howell, S., Taylor, H.M. et al. (2003) Characterisation of the rhoph2 gene of *Plasmodium falciparum* and *Plasmodium yoelii*. *Molecular and Biochemical Parasitology*, *127*(1), 47–57. Available from: https://doi.org/10.1016/S0166-6851(02)00302-X

Lingelbach, K. & Joiner, K.A. (1998) The parasitophorous vacuole membrane surrounding *Plasmodium* and *Toxoplasma*: An unusual compartment in infected cells. *Journal of Cell Science*, *111*(Pt 11), 1467–1475.

Lodoen, M.B., Gerke, C. & Boothroyd, J.C. (2010) A highly sensitive FRET-based approach reveals secretion of the actin-binding protein toxofilin during *Toxoplasma gondii* infection. *Cellular Microbiology*, *12*(1), 55–66.

Manger, I.D., Hehl, A.B. & Boothroyd, J.C. (1998) The surface of *Toxoplasma* tachyzoites is dominated by a family of glycosylphosphatidylinositol-anchored antigens related to SAG1. *Infection and Immunity*, *66*(5), 2237–2244. Available from: https://doi.org/10.1128/IAI.66.5.2237-2244.1998

Margos, G., Bannister, L.H., Dluzewski, A.R., Hopkins, J., Williams, I.T. & Mitchell, G.H. (2004) Correlation of structural development and differential expression of invasion-related molecules in schizonts of *Plasmodium falciparum*. *Parasitology*, *129*(Pt 3), 273–287.

Martin, T.F.J. (2015) PI(4,5)P_2-binding effector proteins for vesicle exocytosis. *Biochimica et Biophysica Acta*, *1851*(6), 785–793.

Mellman, I., Fuchs, R. & Helenius, A. (1986) Acidification of the endocytic and exocytic pathways. *Annual Review of Biochemistry*, *55*, 663–700. Available from: https://doi.org/10.1146/annurev.bi.55.070186.003311

Mercier, C. & Cesbron-Delauw, M.F. (2015) *Toxoplasma* secretory granules: One population or more? *Trends in Parasitology*, *31*(2), 60–71. https://doi.org/10.1016/j.pt.2014.12.002

Mital, J., Meissner, M., Soldati, D. & Ward, G.E. (2005) Conditional expression of *Toxoplasma gondii* apical membrane antigen-1 (TgAMA1) demonstrates that TgAMA1 plays a critical role in host cell invasion. *Molecular Biology of the Cell*, *16*(9), 4341–4349.

Mordue, D.G., Desai, N., Dustin, M. & Sibley, L.D. (1999) Invasion by *Toxoplasma gondii* establishes a moving junction that selectively excludes host cell plasma membrane proteins on the basis of their membrane anchoring. *The Journal of Experimental Medicine*, *190*(12), 1783–1792. Available from: https://doi.org/10.1084/jem.190.12.1783

Morlon-Guyot, J., Berry, L., Sauquet, I., Singh Pall, G., El Hajj, H., Meissner, M. et al. (2018a) Conditional knock-down of a novel coccidian protein leads to the formation of aberrant apical organelles and abrogates mature rhoptry positioning in *Toxoplasma gondii*. *Molecular and Biochemical Parasitology*, *223*, 19–30. Available from: https://doi.org/10.1016/j.molbiopara.2018.06.003

Morlon-Guyot, J., El Hajj, H., Martin, K., Fois, A., Carrillo, A., Berry, L. et al. (2018b) A proteomic analysis unravels novel CORVET and HOPS proteins involved in *Toxoplasma gondii* secretory organelles biogenesis. *Cellular Microbiology*, *20*(11), e12870.

Morlon-Guyot, J., Pastore, S., Berry, L., Lebrun, M. & Daher, W. (2015) *Toxoplasma gondii* Vps11, a subunit of HOPS and CORVET tethering complexes, is essential for the biogenesis of secretory organelles. *Cellular Microbiology*, *17*(8), 1157–1178.

Morrissette, N.S. & Sibley, L.D. (2002) Cytoskeleton of apicomplexan parasites. *Microbiology and Molecular Biology Reviews*, *66*(1), 21–38; table of contents. Available from: https://doi.org/10.1128/MMBR.66.1.21-38.2002

Mphande, F.A., Ribacke, U., Kaneko, O., Kironde, F., Winter, G. & Wahlgren, M. (2008) SURFIN4.1, a schizont-merozoite associated protein in the SURFIN family of *Plasmodium falciparum*. *Malaria Journal*, *7*(1), 116. Available from: https://doi.org/10.1186/1475-2875-7-116

Mueller, C., Klages, N., Jacot, D., Santos, J.M., Cabrera, A., Gilberger, T.W. et al. (2013) The *Toxoplasma* protein ARO mediates the apical positioning of rhoptry organelles, a prerequisite for host cell invasion. *Cell Host & Microbe*, *13*(3), 289–301. Available from: https://doi.org/10.1016/j.chom.2013.02.001

Mueller, C., Samoo, A., Hammoudi, P.M., Klages, N., Kallio, J.P., Kursula, I. et al. (2016) Structural and functional dissection of *Toxoplasma gondii* armadillo repeats only protein. *Journal of Cell Science*, *129*(5), 1031–1045.

Nasamu, A.S., Glushakova, S., Russo, I., Vaupel, B., Oksman, A., Kim, A.S. et al. (2017) Plasmepsins IX and X are essential and druggable mediators of malaria parasite egress and invasion. *Science*, *358*(6362), 518–522. https://doi.org/10.1126/science.aan1478

Nishi, M., Hu, K., Murray, J.M. & Roos, D.S. (2008) Organellar dynamics during the cell cycle of *Toxoplasma gondii*. *Journal of Cell Science*, *121*(Pt 9), 1559–1568. Available from: https://doi.org/10.1242/jcs.021089

Ong, Y.C., Reese, M.L. & Boothroyd, J.C. (2010) *Toxoplasma* rhoptry protein 16 (ROP16) subverts host function by direct tyrosine phosphorylation of STAT6. *The Journal of Biological Chemistry*, *285*(37), 28731–28740. Available from: https://doi.org/10.1074/jbc.M110.112359

Pao, S.S., Paulsen, I.T. & Saier, M.H., Jr. (1998) Major facilitator superfamily. *Microbiology and Molecular Biology Reviews*, *62*(1), 1–34. Available from: https://doi.org/10.1128/MMBR.62.1.1-34.1998

Paredes-Santos, T.C., de Souza, W. & Attias, M. (2012) Dynamics and 3D organization of secretory organelles of *Toxoplasma gondii*. *Journal of Structural Biology*, *177*(2), 420–430. Available from: https://doi.org/10.1016/j.jsb.2011.11.028

Parker, M.L., Penarete-Vargas, D.M., Hamilton, P.T., Guerin, A., Dubey, J.P., Perlman, S.J. et al. (2016). Dissecting the interface between apicomplexan parasite and host cell: Insights from a divergent AMA–RON2 pair. *Proceedings of the National Academy of Sciences*, *113*(2), 398–403. Available from: https://doi.org/10.1073/pnas.1515898113

Paul, A.S., Egan, E.S. & Duraisingh, M.T. (2015) Host-parasite interactions that guide red blood cell invasion by malaria parasites. *Current Opinion in Hematology*, *22*(3), 220–226. Available from: https://doi.org/10.1097/MOH.0000000000000135

Pavlou, G., Biesaga, M., Touquet, B., Lagal, V., Balland, M., Dufour, A. et al. (2018) *Toxoplasma* parasite twisting motion mechanically induces host cell membrane fission to complete invasion within a protective vacuole. *Cell Host & Microbe*, *24*(1), 81–96 e5. Available from: https://doi.org/10.1016/j.chom.2018.06.003

Peixoto, L., Chen, F., Harb, O.S., Davis, P.H., Beiting, D.P., Brownback, C.S. et al. (2010) Integrative genomic approaches highlight a family of parasite-specific kinases that regulate host responses. *Cell Host & Microbe*, *8*(2), 208–218. Available from: https://doi.org/10.1016/j.chom.2010.07.004

Periz, J., Del Rosario, M., McStea, A., Gras, S., Loney, C., Wang, L. et al. (2019) A highly dynamic F-actin network regulates transport and recycling of micronemes in *Toxoplasma gondii* vacuoles. *Nature Communications*, *10*(1), 1–16. Available from: https://doi.org/10.1038/s41467-019-12136-2

Pino, P., Caldelari, R., Mukherjee, B., Vahokoski, J., Klages, N., Maco, B. et al. (2017) A multistage antimalarial targets the plasmepsins IX and X essential for invasion and egress. *Science*, *358*(6362), 522–528.

Porchet, E. & Torpier, G. (1977) Etude du germe infectieux de Sarcocystis tenella et *Toxoplasma gondii* par la technique du cryodécapage. *Zeitschrift für Parasitenkunde*, *54*(2), 101–124.

Poukchanski, A., Fritz, H.M., Tonkin, M.L., Treeck, M., Boulanger, M.J. & Boothroyd, J.C. (2013) *Toxoplasma gondii* sporozoites invade host cells using two novel paralogues of RON2 and AMA1. *PLoS ONE*, *8*(8), e70637. Available from: https://doi.org/10.1371/journal.pone.0070637

Quintana, M.D.P., Ch'ng, J.H., Zandian, A., Imam, M., Hultenby, K., Theisen, M. et al. (2018) SURGE complex of *Plasmodium falciparum* in the rhoptry-neck (SURFIN4.2-RON4-GLURP) contributes to merozoite invasion. *PLoS ONE*, *13*(8), e0201669. Available from: https://doi.org/10.1371/journal.pone.0201669

Rayner, J.C., Galinski, M.R., Ingravallo, P. & Barnwell, J.W. (2000) Two *Plasmodium falciparum* genes express merozoite proteins that are related to *Plasmodium vivax* and *Plasmodium yoelii* adhesive proteins involved in host cell selection and invasion. *Proceedings of the National Academy of Sciences of the United States of America*, *97*(17), 9648–9653. Available from: https://doi.org/10.1073/pnas.160469097

Reese, M.L. & Boothroyd, J.C. (2011) A conserved non-canonical motif in the pseudoactive site of the ROP5 pseudokinase domain mediates its effect on *Toxoplasma* virulence. *The Journal of Biological Chemistry*, *286*(33), 29366–29375. Available from: https://doi.org/10.1074/jbc.M111.253435

Reiss, M., Viebig, N., Brecht, S., Fourmaux, M.N., Soete, M., Di Cristina, M. et al. (2001) Identification and characterization of an escorter for two secretory adhesins in *Toxoplasma gondii*. *Journal of Cell Biology*, *152*(3), 563–578. Available from: https://doi.org/10.1083/jcb.152.3.563

Richard, D., MacRaild, C.A., Riglar, D.T., Chan, J.A., Foley, M., Baum, J. et al. (2010) Interaction between *Plasmodium falciparum* apical membrane antigen 1 and the rhoptry neck protein complex defines a key step in the erythrocyte invasion process of malaria parasites. *The Journal of Biological Chemistry*, *285*(19), 14815–14822. Available from: https://doi.org/10.1074/jbc.M109.080770

Saeij, J.P., Boyle, J.P., Coller, S., Taylor, S., Sibley, L.D., Brooke-Powell, E.T. et al. (2006) Polymorphic secreted kinases are key virulence factors in toxoplasmosis. *Science*, *314*(5806), 1780–1783. Available from: https://doi.org/10.1126/science.1133690

Saeij, J.P., Coller, S., Boyle, J.P., Jerome, M.E., White, M.W. & Boothroyd, J.C. (2007) *Toxoplasma* co-opts host gene expression by injection of a polymorphic kinase homologue. *Nature*, *445*(7125), 324–327. Available from: https://doi.org/10.1038/nature05395

Sakura, T., Sindikubwabo, F., Oesterlin, L.K., Bousquet, H., Slomianny, C., Hakimi, M.-A. et al. (2016) A critical role for *Toxoplasma gondii* vacuolar protein sorting VPS9 in secretory organelle biogenesis and host infection. *Scientific Reports*, *6*(1), 38842.

Schwab, J.C., Beckers, C.J. & Joiner, K.A. (1994) The parasitophorous vacuole membrane surrounding intracellular *Toxoplasma gondii* functions as a molecular sieve. *Proceedings of the National Academy of Sciences of the United States of America*, *91*(2), 509–513. Available from: https://doi.org/10.1073/pnas.91.2.509

Shaw, M.K., Roos, D.S. & Tilney, L.G. (1998) Acidic compartments and rhoptry formation in *Toxoplasma gondii*. *Parasitology*, *117*(Pt 5), 435–443.

Shaw, M.K., Roos, D.S. & Tilney, L.G. (2002) Cysteine and serine protease inhibitors block intracellular development and disrupt the secretory pathway of *Toxoplasma gondii*. *Microbes and Infection*, *4*(2), 119–132. Available from: https://doi.org/10.1016/S1286-4579(01)01520-9

Shaw, M.K. & Tilney, L.G. (1992) How individual cells develop from a syncytium: Merogony in *Theileria parva* (Apicomplexa). *Journal of Cell Science*, *101*(Pt 1), 109–123.

Sherling, E.S., Knuepfer, E., Brzostowski, J.A., Miller, L.H., Blackman, M.J. & van Ooij, C. (2017) The *Plasmodium falciparum* rhoptry protein RhopH3 plays essential roles in host cell invasion and nutrient uptake. *eLife*, *6*, 1–23. Available from: https://doi.org/10.7554/eLife.23239

Sherling, E.S., Perrin, A.J., Knuepfer, E., Russell, M.R.G., Collinson, L.M., Miller, L.H. et al. (2019) The *Plasmodium falciparum* rhoptry bulb protein RAMA plays an essential role in rhoptry neck morphogenesis and host red blood cell invasion. *PLoS Pathogens*, *15*(9), e1008049.

Sidik, S.M., Huet, D., Ganesan, S.M., Huynh, M.H., Wang, T., Nasamu, A.S. et al. (2016) A genome-wide CRISPR screen in *Toxoplasma* identifies essential apicomplexan genes. *Cell*, *166*(6), 1423–1435.e12. Available from: https://doi.org/10.1016/j.cell.2016.08.019

Sim, B.K., Chitnis, C.E., Wasniowska, K., Hadley, T.J. & Miller, L.H. (1994) Receptor and ligand domains for invasion of erythrocytes by *Plasmodium falciparum*. *Science*, *264*(5167), 1941–1944. Available from: https://doi.org/10.1126/science.8009226

Sinai, A.P. (2014) Chapter 11—The *Toxoplasma gondii* parasitophorous vacuole membrane: A multifunctional organelle in the infected cell. In: Weiss, L.M. & Kim, K. (Eds.) *Toxoplasma gondii*, 2nd edition, Academic Press, pp. 375–387.

Sloves, P.J., Delhaye, S., Mouveaux, T., Werkmeister, E., Slomianny, C., Hovasse, A. et al. (2012) *Toxoplasma* sortilin-like receptor regulates protein transport and is essential for apical secretory organelle biogenesis and host infection. *Cell Host & Microbe*, *11*(5), 515–527. Available from: https://doi.org/10.1016/j.chom.2012.03.006

Stasic, A.J., Chasen, N.M., Dykes, E.J., Vella, S.A., Asady, B., Starai, V.J. et al. (2019) The *Toxoplasma* vacuolar H(+)-ATPase regulates intracellular pH and impacts the maturation of essential secretory proteins. *Cell Reports*, *27*(7), 2132–2146.e7. Available from: https://doi.org/10.1016/j.celrep.2019.04.038

Straub, K.W., Peng, E.D., Hajagos, B.E., Tyler, J.S. & Bradley, P.J. (2011) The moving junction protein RON8 facilitates firm attachment and host cell invasion in *Toxoplasma gondii*. *PLoS Pathogens*, *7*(3), e1002007. Available from: https://doi.org/10.1371/journal.ppat.1002007

Suarez, C., Lentini, G., Ramaswamy, R., Maynadier, M., Aquilini, E., Berry-Sterkers, L. et al. (2019) A lipid-binding protein mediates rhoptry discharge and invasion in *Plasmodium falciparum* and *Toxoplasma gondii* parasites. *Nature Communications*, *10*(1), 1–14. Available from: https://doi.org/10.1038/s41467-019-11979-z

Suarez, C., Lodoen, M.B. & Lebrun, M. (2020) Assessing rhoptry secretion in *T. gondii*. *Methods in Molecular Biology*, *2071*, 143–155.

Suss-Toby, E., Zimmerberg, J. & Ward, G.E. (1996) *Toxoplasma* invasion: The parasitophorous vacuole is formed from host cell plasma membrane and pinches off via a fission pore. *Proceedings of the National Academy of Sciences of the United States of America*, *93*(16), 8413–8418. Available from: https://doi.org/10.1073/pnas.93.16.8413

Talevich, E. & Kannan, N. (2013) Structural and evolutionary adaptation of rhoptry kinases and pseudokinases, a family of coccidian virulence factors. *BMC Evolutionary Biology*, *13*(1), 117. Available from: https://doi.org/10.1186/1471-2148-13-117

Taylor, S., Barragan, A., Su, C., Fux, B., Fentress, S.J., Tang, K. et al. (2006) A secreted serine-threonine kinase determines virulence in the eukaryotic pathogen *Toxoplasma gondii*. *Science*, *314*(5806), 1776–1780. Available from: https://doi.org/10.1126/science.1133643

Tetley, L., Brown, S.M., McDonald, V. & Coombs, G.H. (1998) Ultrastructural analysis of the sporozoite of *Cryptosporidium parvum*. *Microbiology*, *144*(Pt 12), 3249–3255. Available from: https://doi.org/10.1099/00221287-144-12-3249

Topolska, A.E., Lidgett, A., Truman, D., Fujioka, H. & Coppel, R.L. (2004) Characterization of a membrane-associated rhoptry protein of *Plasmodium falciparum*. *The Journal of Biological Chemistry*, *279*(6), 4648–4656. Available from: https://doi.org/10.1074/jbc.M307859200

Triglia, T., Duraisingh, M.T., Good, R.T. & Cowman, A.F. (2005) Reticulocyte-binding protein homologue 1 is required for sialic acid-dependent invasion into human erythrocytes by *Plasmodium falciparum*. *Molecular Microbiology*, *55*(1), 162–174. Available from: https://doi.org/10.1111/j.1365-2958.2004.04388.x

Triglia, T., Tham, W.H., Hodder, A. & Cowman, A.F. (2009) Reticulocyte binding protein homologues are key adhesins during erythrocyte invasion by *Plasmodium falciparum*. *Cellular Microbiology*, *11*(11), 1671–1687.

Venugopal, K. & Marion, S. (2018) Secretory organelle trafficking in *Toxoplasma gondii*: A long story for a short travel. *International Journal of Medical Microbiology*, *308*(7), 751–760. Available from: https://doi.org/10.1016/j.ijmm.2018.07.007

Venugopal, K., Werkmeister, E., Barois, N., Saliou, J.M., Poncet, A., Huot, L. et al. (2017) Dual role of the *Toxoplasma gondii* clathrin adaptor AP1 in the sorting of rhoptry and microneme proteins and in parasite division. *PLoS Pathogens*, *13*(4), e1006331.

Wang, M., Cao, S., Du, N., Fu, J., Li, Z., Jia, H. et al. (2017) The moving junction protein RON4, although not critical, facilitates host cell invasion and stabilizes MJ members. *Parasitology*, *144*(11), 1490–1497. Available from: https://doi.org/10.1017/S0031182017000968

Werner, E.B., Taylor, W.R. & Holder, A.A. (1998) A *Plasmodium* chabaudi protein contains a repetitive region with a predicted spectrin-like structure. *Molecular and Biochemical Parasitology*, *94*(2), 185–196.

Winter, G., Kawai, S., Haeggstrom, M., Kaneko, O., von Euler, A., Kawazu, S. et al. (2005) SURFIN is a polymorphic antigen expressed on *Plasmodium falciparum* merozoites and infected erythrocytes. *The Journal of Experimental Medicine*, *201*(11), 1853–1863. Available from: https://doi.org/10.1084/jem.20041392

Yakubu, R.R., Weiss, L.M. & Silmon de Monerri, N.C. (2018) Post-translational modifications as key regulators of apicomplexan biology: Insights from proteome-wide studies. *Molecular Microbiology*, *107*(1), 1–23. Available from: https://doi.org/10.1111/mmi.13867

Yang, A.S.P., Lopaticki, S., O'Neill, M.T., Erickson, S.M., Douglas, D.N., Kneteman, N.M. et al. (2017) AMA1 and MAEBL are important for *Plasmodium falciparum* sporozoite infection of the liver. *Cellular Microbiology*, *19*(9), 1–14. Available from: https://doi.org/10.1111/cmi.12745

Zhang, M., Wang, C., Otto, T.D., Oberstaller, J., Liao, X., Adapa, S.R. et al. (2018) Uncovering the essential genes of the human malaria parasite *Plasmodium falciparum* by saturation mutagenesis. *Science*, *360*(6388), 1–12.

Zhu, X., He, Y., Liang, Y., Kaneko, O., Cui, L. & Cao, Y. (2017) Tryptophan-rich domains of *Plasmodium falciparum* SURFIN4.2 and *Plasmodium* vivax PvSTP2 interact with membrane skeleton of red blood cell. *Malaria Journal*, *16*(1), 1–12. Available from: https://doi.org/10.1186/s12936-017-1772-5

How to cite this article: Ben Chaabene R, Lentini G, Soldati-Favre D. Biogenesis and discharge of the rhoptries: Key organelles for entry and hijack of host cells by the Apicomplexa. *Mol Microbiol*. 2021;115:453–465. https://doi.org/10.1111/mmi.14674

The Lytic Cycle of Human Apicomplexan Parasites

Rouaa Ben Chaabene and Dominique Soldati-Favre, Department of Microbiology and Molecular Medicine, University of Geneva, Geneva, Switzerland

Abstract

The phylum of Apicomplexa groups important eukaryotic pathogens that are responsible for life threatening diseases in human and livestock. These intracellular parasites actively enter into host cells and reside safely in a parasitophorous vacuole. To escape host cell defense mechanisms and access nutrients, parasites secrete effectors to hijack host cellular functions. Novel technologies in recent years helped to deeply dissect each step of their lytic cycle. This article focuses on the lytic cycle of *Toxoplasma gondii*, *Plasmodium falciparum*, and *Cryptosporidium parvum* and aims at comparing and contrasting their strategies toward establishment of intracellular parasitism.

Key Points

- The phylum of Apicomplexa groups unicellular eukaryotic parasites that cause important and life-threatening veterinary and human diseases, such as toxoplasmosis, malaria and cryptosporidiosis.
- *Toxoplasma*, *Plasmodium* and *Cryptosporidium* share numerous common features but occupy distinct niches in the host.
- Invasion of host cells involves secretory organelles and an actomyosin system that are conserved across the phylum.
- *Toxoplasma*, *Plasmodium* and *Cryptosporidium* multiply within a parasitophorous vacuole that serves as physical barrier against the host immune system.
- Apicomplexans replicate within their host cells generating in some species thousands of progeny.
- Apicomplexans egress from host cell in a timely manner that is governed by signaling cascade leading to exocytosis of micronemes. This results in the lysis of the parasitophorous vacuole membrane and host plasma membrane causing damage to tissues and inflammatory responses.
- This Review summarizes our current knowledge of the life cycle of three apicomplexans, *Toxoplasma. Plasmodium* and *Cryptosporidium*.

Introduction

The Phylum of Apicomplexa comprises a large group of unicellular organisms such as coccidia, gregarines, piroplasms, haemogregarines, and plasmodia that are of medical and veterinary importance. The human parasites of the phylum cause devastating diseases, including toxoplasmosis, malaria and cryptosporidiosis that affect millions of people each year and kill hundreds of thousands of individuals globally. The most ubiquitous parasite, *Toxoplasma gondii*, infects about one third of the human population and can cause miscarriage or stillbirth if primary infection occurs during pregnancy. Even though toxoplasmosis is well controlled by a healthy immune system, immunocompromised patients are most vulnerable to the development of acute toxoplasmosis upon a new infection or reactivation of a chronic infection, which can lead to fatal encephalitis (Halonen and Weiss, 2013). *Plasmodium falciparum* is the deadliest parasite responsible for malaria, an uncontrolled disease with 200 million new cases each year and over 500,000 deaths, primarily in young children in sub-Saharan Africa (World Health Organ. WHO, 2021) *Cryptosporidium* infection in livestock animals causes severe intestinal disease and has only recently been fully recognized as a leading cause of diarrhea-associated mortality in immunocompromised patients and young children worldwide (Khalil *et al.*, 2018).

Apicomplexans have opted for an intracellular lifestyle, one of the best adapted and effective strategy for microorganisms to escape the animal immune system, avoid clearance and at the same time more directly access host metabolites and nutrients (Plattner and Soldati-Favre, 2008; Roy and Mocarski, 2007). Given their size and in order to expand the range of infectable host cells the apicomplexans have evolved an active process of entry that results in the formation of a unique parasitophorous vacuole (PV) (Pavlou *et al.*, 2018). To optimize intracellular survival and replication, these parasites remodel the parasitophorous vacuole membrane (PVM) to salvage host metabolites and to evade host cell-autonomous defense mechanisms (Pavlou *et al.*, 2018).

Methodological and technological advances over the last decade have led to the dissection of molecular mechanisms and to an improved understanding of the strategies that govern each step of their lytic cycle. This review compares and contrasts the life cycle of three major human apicomplexan parasites, *T. gondii, P. falciparum*, and *Cryptosporidium parvum*. Theses parasites undergo multiple lytic cycles in host cells that can be decomposed in three main steps, invasion, intracellular replication and egress that are dissected here.

Species of Human Apicomplexan Parasites Occupy Very Different Niches

T. gondii is a ubiquitous parasite infecting all warm-blooded animals and virtually any nucleated cell type. This parasite, frequently viewed as a model organism for the Apicomplexa, belongs to the coccidian subgroup together with *Eimeria* (causative agent of chicken coccidiosis), *Neospora* (causing disease in cattle), *Sarcocystis* (causing disease in sheep) and *Besnoitia spp*. *T. gondii* has a complex life cycle that consists of several distinct developmental stages. Two distinct infective stages are of relevance for enteric transmission. The sporozoites in oocysts shed in the feces of the definitive host (felines) and slow growing bradyzoites within the cysts in the tissues of infected intermediate hosts. Upon infection, both sporozoites and bradyzoites convert into fast-replicating

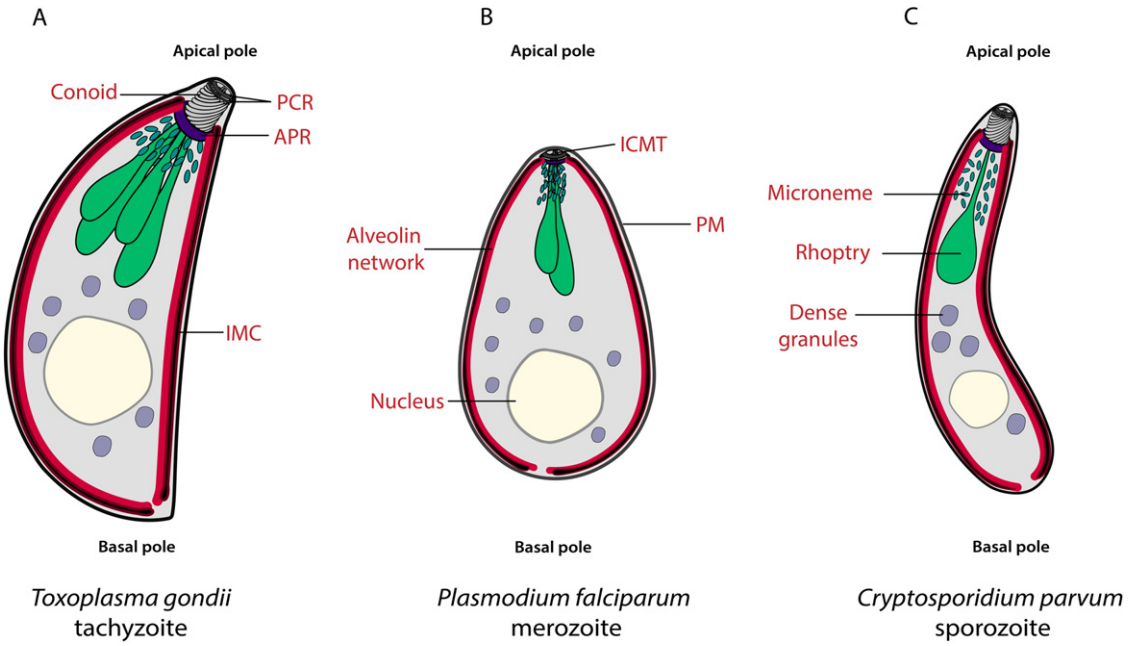

Fig. 1 Schematic representation of (A) *Toxoplasma* tachyzoite (B) *Plasmodium* merozoite and (C) *Cryptosporidium* sporozoites. The polarized organization of the zoite includes the apical complex with a cytoskeletal part: Conoid, PCR, preconoidal rings; APR, apical polar rings; and two ICMT, intraconoidal microtubules; and apical secretory organelles: micronemes, and rhoptries. IMC, inner membrane complex; PM, Plasma membrane.

tachyzoites that disseminate in the host and are responsible for acute infection prior to establishment of a chronic infection (Fox *et al.*, 2016; Halonen and Weiss, 2013).

The main species responsible for malaria and causing benign or severe forms of malaria in humans are *P. falciparum*, *P. vivax*, *P. malariae*, *P. knowlesi* and *P. ovale*. Infection begins with a direct transmission of sporozoites during blood feeding from the female *Anopheles* mosquito that serves as a vector and as definitive host. Sporozoites asymptomatically infect liver cells and mature into schizonts, which rupture and release merozoites into the bloodstream. Merozoites invade red blood cells (RBCs) to initiate erythrocytic development. Several lytic cycles lead to cycles of fever as well as the severe symptoms of malaria. Some of the infected blood cells leave the cycle of asexual multiplication to develop into sexual forms and ensure transmission via mosquito bites (Meibalan and Marti, 2017).

Cryptosporidium hominis infects only humans whereas *C. parvum* infect both humans and animals (Xiao, 2010). The asexual and sexual stages of *Cryptosporidium* life cycle are completed within one unique host, targeting the intestinal epithelial cells (Bouzid *et al.*, 2013). Infection occurs through the ingestion of oocysts, each containing four sporozoites (Guérin and Striepen, 2020). Sporozoites are released through excystation, immediately invade enterocytes and transform into trophozoites. Trophozoites undergo several rounds of asexual replication generating merozoites that transform into sexual stages. Sexual replication results into four haploid sporozoites within an oocyst that is passed in the feces to be ingested by another host continuing the cycle (Guérin and Striepen, 2020; Pinto and Vinayak, 2021). *Cryptosporidium* belongs to the epicellular species that develop extra-cytoplasmically in host cells (Bartošová-Sojková *et al.*, 2015).

The Apicomplexan Zoites are Polarized and Professional Secretory Cells

Although these parasites infect distinctive hosts, occupy unique niches and harbor diverse strategies to ensure transmission, they have in common multiple morphological features (**Fig. 1**) (Dos Santos Pacheco *et al.*, 2020). They also share high similarity at the genome level with the conservation of a large set of apicomplexan specific genes as well as development of distinctive adaptations via lineage-specific gene loss and innovation that took place during divergence from a common parasitic ancestor (Janouškovec *et al.*, 2019).

Together with ciliates and dinoflagellates, apicomplexans belong to the superphylum of Alveolata (Adl *et al.*, 2012), sharing with them a peripheral alveolar membrane system called inner membrane complex (IMC). Members of Apicomplexa are also unified by sharing an apical complex structure composed of structural and secretory elements (Dos Santos Pacheco *et al.*, 2020). The cytoskeletal part of the apical complex is composed of the apical polar ring (APR) a structure that appears to serve as microtubule-organizing center (MTOC), nucleating subpellicular microtubules (SPMTs) that form a basket covering two third of the parasite length (Dos Santos Pacheco *et al.*, 2020). The APR marks the apical extremity of the IMC. An additional tubulin-rich structure, the conoid, is a dynamic organelle that sits within the APR (Hu *et al.*, 2002; Morrissette and Sibley, 2002) and is extruded from the parasite body during invasion. In the coccidian subgroup of Apicomplexa, the conoid complex is composed of two preconoidal rings, a cone made of spiraling tubulin fibers and a pair of short intraconoidal microtubules (ICMTs) (Dos Santos Pacheco *et al.*, 2020). In *Plasmodium* species, the conoid is made of a single tubulin ring and the ICMTs are absent (Dos Santos Pacheco *et al.*, 2020).

Zoites are highly polarized cells with an apical complex, an apical tip, and a conoid positioned at a focal point to discharge specialized and regulated secretory organelles, rhoptries and micronemes. Micronemes are small, rod-shaped organelles and about 50–100 micronemes can be found at the apical pole of *T. gondii* tachyzoites and invading zoites (**Fig. 1**(A)) (Dubois and Soldati-Favre, 2019). Micronemes exocytose proteins including notably adhesins, proteases and perforins in a regulated fashion in response to changes in intracellular calcium (Bisio and Soldati-Favre, 2019; Dubois and Soldati-Favre, 2019). The content of the micronemes is strikingly conserved across members of the phylum. Rhoptries are large, club-shaped organelles formed of a bulb and a neck and are positioned at the apical pole of the parasite with their neck traversing the conoid (Ben Chaabene *et al.*, 2021). Even though rhoptries are well conserved across the Apicomplexa, their number and content vary not only between different species but also between different developmental stages within the same species. In *Plasmodium* (**Fig. 1**(B)), merozoites harbor only two rhoptries while ookinete stage lacks them entirely (Kats *et al.*, 2006). On the other hand, *Cryptosporidium* sporozoites (**Fig. 1**(C)) possess one rhoptry (Tetley *et al.*, 1998) whereas *T. gondii* tachyzoites has 10–12 rhoptries (Boothroyd and Dubremetz, 2008). Some rhoptry neck proteins (RONs) are well conserved among members of the phylum and are involved in the formation of the moving junction (MJ) during the invasion step. The content of the rhoptry bulb (ROPs) is more divergent among apicomplexans. Notably, *T. gondii* possesses a large family of secreted rhoptry protein kinases that act as effector molecules playing important role in subversion of host cellular functions and virulence (Ben Chaabene *et al.*, 2021; Hakimi *et al.*, 2017; Lima and Lodoen, 2019).

Host Cell Entry

The mechanism of host cell invasion is shared to a large extent among apicomplexans and involves invagination of the host cell plasma membrane (PM). *Cryptosporidium* differs significantly and leads to an intracellular but extra-cytoplasmic niche. While micronemes critically participate in motility, host cell recognition as well as lysis of the PVM and host cell PM during egress, rhoptry discharge is dedicated to invasion and contributes to formation and modification of the PVM.

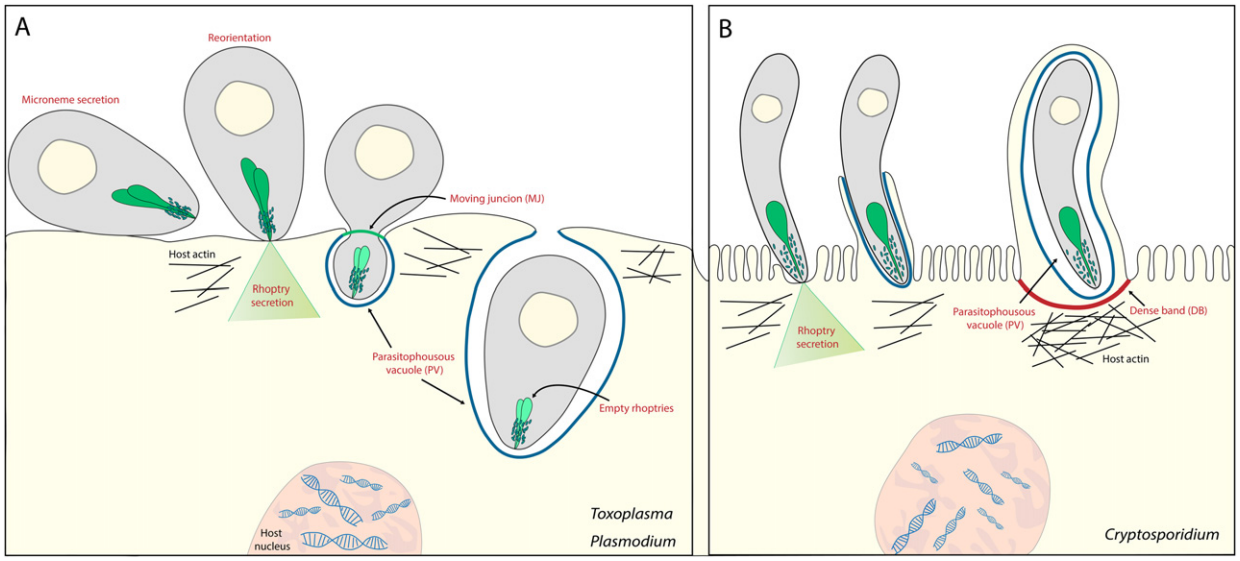

Fig. 2 Host cell invasion by Apicomplexa. (A) *Toxoplasma* and *Plasmodium*: the invasion process starts with host cell adhesion followed by secretion of the content of micronemes onto parasite surface and the subsequent reorientation of the parasite. Once attached, the parasite discharges the rhoptry content inside the host cell. Rhoptry neck proteins (RONs) enable the formation of the moving junction (MJ) whereas rhoptry bulb proteins (ROPs) are targeted to the parasitophorous vacuole membrane (PVM), the host nucleus and cytoplasm. Following the discharge, empty rhoptry organelles are observed. (B) *Cryptosporidium*: Micronemes and rhoptry proteins are secreted during invasion. Remodeling of the host cell actin cytoskeleton is observed around the invading parasite. The host microvilli elongate and surround the parasite while fusing with the parasitophorous vacuole (PV). The active entry leads to the formation of an extracytoplasmic vacuole.

Host Cell Recognition and Attachment

Host cell invasion is a vital and active process distinct from phagocytosis, that has been extensively studied in *T. gondii* and shown to share many characteristics in *P. falciparum* and other apicomplexans. Entry of tachyzoites into host cell is very fast (ca. 30 s) and driven by parasite motility. Polarized invading parasites, also called zoites, penetrate their host with the apical end of the parasite leading. The first step required for the invasion process is attachment of the parasite to the host cell PM, mediated by members of the glycosylphosphatidylinositol (GPI)-anchored surface antigen glycoproteins (SAGs) related sequence (SRS) (Jung *et al.*, 2004). These proteins are present abundantly on the parasite surface and bind specifically host cell receptors. Next, a tighter connection is mediated by exocytosed microneme proteins (MICs) at the apical tip of the parasite. Some of the MICs contain adhesive and transmembrane domains that interact with host cell receptors and firmly attach the parasite to the host cell (Reiss *et al.*, 2001). The signaling cascade behind this exocytosis has been dissected and reviewed (Bisio *et al.*, 2019; Bisio and Soldati-Favre, 2019; Bullen *et al.*, 2016; Dubois and Soldati-Favre, 2019; Jia *et al.*, 2017). MICs include the family of surface-associated TRAP (thrombospondin-related anonymous protein) conserved across Apicomplexa and play a role in *Plasmodium* parasite motility and invasion by acting as a bridge between the erythrocyte surface and the parasite actomyosin machinery (Bargieri *et al.*, 2016; Morahan *et al.*, 2009). In *Plasmodium*, merozoites invade erythrocytes but do not exhibit gliding motility. Merozoite TRAP is not involved in invasion but plays a central role in gamete egress from the PVM (Bargieri *et al.*, 2016).

In *Cryptosporidium*, the molecular content of micronemes remains poorly understood. Only eight proteins were confirmed as MICs in sporozoites using either immunofluorescence or/and immunogold electron microscopy (Gao *et al.*, 2021; Lendner and Daugschies, 2014). The peptidase S54 belonging to the rhomboid family (CpROM1) was localized to micronemes in *Cryptosporidium* sporozoites and merozoites (Gao *et al.*, 2021). CpROM1 also localizes to the host cell-parasite interface during invasion as well as the PVM and the feeder organelle (Gao *et al.*, 2021) suggesting a role in cleavage of MICs during invasion as well as proteostasis of membrane proteins in the PVM and feeder organelle.

Active Host Cell Invasion is Powered by Myosin Motors

Gliding motility of the parasite is an indispensable feature for invasion (reviewed (Frenal *et al.*, 2017)) that contrasts with crawling of amoebae or propelling via cilia and flagella, except for the microgamete stage (King, 1988). This substrate-dependent mode of locomotion is powered by the parasite actomyosin system, located underneath the PM and named the glideosome (Frenal *et al.*, 2010). In *T. gondii*, gliding involves myosin motors and secreted transmembrane proteins that are translocated with F-actin to the posterior end of the parasite. Myosin A is found along the periphery of the parasite, while Myosin H is restricted to the conoid, and both are indispensable for motility, invasion, and egress (Graindorge *et al.*, 2016; Yusuf *et al.*, 2015). Motility and invasion rely on the

indispensable contribution of the glideosome-associated connector (GAC) (Jacot *et al.*, 2016). During host cell penetration a ring-shaped structure called the moving junction (MJ) is formed and serves as a support to propel the parasite into the host cell (Alexander *et al.*, 2005; Besteiro *et al.*, 2011; Lebrun *et al.*, 2005). This structure is translocated towards the posterior pole of the parasite thanks to the actomyosin system, with GAC presumably connecting the adhesin complex to F-actin (Jacot *et al.*, 2016). Formation and stability of the MJ are crucial for efficient invasion of the parasite and for rhoptry secretion (**Fig. 2**(A)). A rhoptry neck kinase protein TgRON13, was shown to play a crucial role during invasion. This kinase phosphorylates several rhoptry proteins, including components of the MJ. TgRON13 is important for anchoring and stabilization of the MJ at the parasite-host interface (Lentini *et al.*, 2021).

In *Plasmodium*, sporozoites and ookinetes rely on gliding to move through tissues, whereas in merozoites the actomyosin system was thought to be required for invasion (Tardieux and Baum, 2016). More recently, *P. falciparum* and *P. knowlesi* merozoites were shown to be capable of gliding and moving across erythrocytes (Yahata *et al.*, 2021). Gliding motility was confirmed to be important during several steps of invasion and is powered by the glideosome machinery and a complex signaling cascade (Yahata *et al.*, 2021).

Cryptosporidium is more related to gregarines than coccidia and *Plasmodium*, due to early branching in Apicomplexa (Carreno *et al.*, 1999). *Cryptosporidium* is known to rely on the conserved glideosome machinery (Wetzel *et al.*, 2005) and secreted proteins from the apical organelles, for invasion and to be enveloped within the host PM (Chen *et al.*, 2004). The invasion process does not involve a MJ as the parasite lacks homologous proteins needed to form the structure (**Fig. 2**(B)). To date, molecular mechanisms and key players from both host and the parasite during invasion are still not fully identified. Recently, ROP1 was described as a key player during *Cryptosporidium* invasion. It is injected into the host and accumulates in the terminal web of enterocytes and directly interact with host protein LIM domain only 7 (LMO7) (Guérin *et al.*, 2021).

The Machinery for Rhoptry Discharge

Successful invasion needs orchestrated secretion of MICs followed by injection of rhoptry proteins inside the host cell, as described in depth in recent reviews (Ben Chaabene *et al.*, 2021; Sparvoli and Lebrun, 2021). Following their discharges, the rhoptries are observed empty (Lebrun *et al.*, 2005), which emphasizes the difference between exocytosis of micronemes and rhoptry discharge mechanisms (**Fig. 2**). To successfully discharge rhoptry content inside the host cell, the parasite needs to either form pores or fuse its membrane with the host PM. Even though *T. gondii* possess several rhoptry organelles, only one or two are discharged during invasion. Rhoptries dock to the apical tip of the parasite, with their neck traversing the conoid, being properly anchored for discharge (Paredes-Santos *et al.*, 2012). It was observed that the neck of these primed rhoptries, runs along the pair of ICMTs to reach an apical vesicle located underneath the PM at the apex of the parasite (Paredes-Santos *et al.*, 2012).

Above the apical vesicle, the PM of the parasite is decorated with a rosette of intramembranous particles (Dubremetz, 2007). This structure is similar to the rosette observed in *Paramecium* at the site of trichocysts exocytosis (Plattner and Kissmehl, 2003) and it is conserved across the superphylum of Alveolates. Recently, these structures were functionally linked to rhoptry protein injection in *T. gondii and P. falciparum* (Aquilini *et al.*, 2020) and were structurally described in *Cryptosporidium* using cryo-electron tomography (Mageswaran *et al.*, 2021). The presence of the apical vesicle only in Apicomplexa might be an adaptation of these organisms towards parasitism and an additional layer of complexity to this secretory mechanism, where the content of rhoptries needs to be injected through two membranes. Moreover, the apical vesicle was described in *Perkinsus marinus*, a parasite that possesses rhoptries and is viewed as an example of early adaptation to parasitism (Perkins, 1976). Non-discharge (Nd) proteins were first identified in *Paramecium tetraurelia* and they are important for trichocysts exocytosis and rosette formation (Lefort-Tran *et al.*, 1981). These proteins are conserved in ciliates, dinoflagellates and apicomplexans. Recently, these proteins as well as two partners NdP1 and NdP2 were shown to be involved in the rhoptry protein injection machinery, and are important for the assembly of rosette in *T. gondii* and *P. falciparum* (Aquilini *et al.*, 2020).

Formation of a Unique Parasitophorous Vacuole

During invasion, the host PM is invaginated forming the PVM, which ultimately pinches off from the host PM (Suss-Toby *et al.*, 1996). Importantly, rhoptry membranous materials and conserved ROPs are secreted inside the host cell and contribute to formation and remodeling of the PVM in *T. gondii* (Hakansson *et al.*, 2001; Hiller *et al.*, 2003). This secreted material contributes to the expansion of the PVM (**Fig. 2**). The host membrane proteins are stripped from the forming PVM during invasion (Mordue *et al.*, 1999) and secreted ROPs and dense granule proteins (GRAs) additionally remodel the composition of the PVM (Culvenor *et al.*, 1991; Pavlou *et al.*, 2018). The resulting PVM is a unique compartment unable to fuse with the lysosome. The PVM serves as a platform for parasite effector proteins like ROPs, that subvert host cell functions, and along with GRAs, protect intracellular parasites from host cell defense mechanisms (Bradley *et al.*, 2005; Hakansson *et al.*, 2001). The PVM is also important for acquisition of many essential nutrients, through pore-like system, mediated by GRAs (Gold *et al.*, 2015).

In contrast to *T. gondii* and *Plasmodium*, *Cryptosporidium* parasites reside in an extracytosolic niche at the apical side of infected enterocytes (**Fig. 2**(B)). The contact site between the parasite and the host cell has been studied and described by electron microscopy. During invasion, microvilli of the host cell engulf the parasite and fuse with it to form the PVM. A dense band of an unknown composition and a ring-shaped structure are observed at the basal end of the PVM. Just underneath, a host actin pedestal is observed but its function is still unknown.

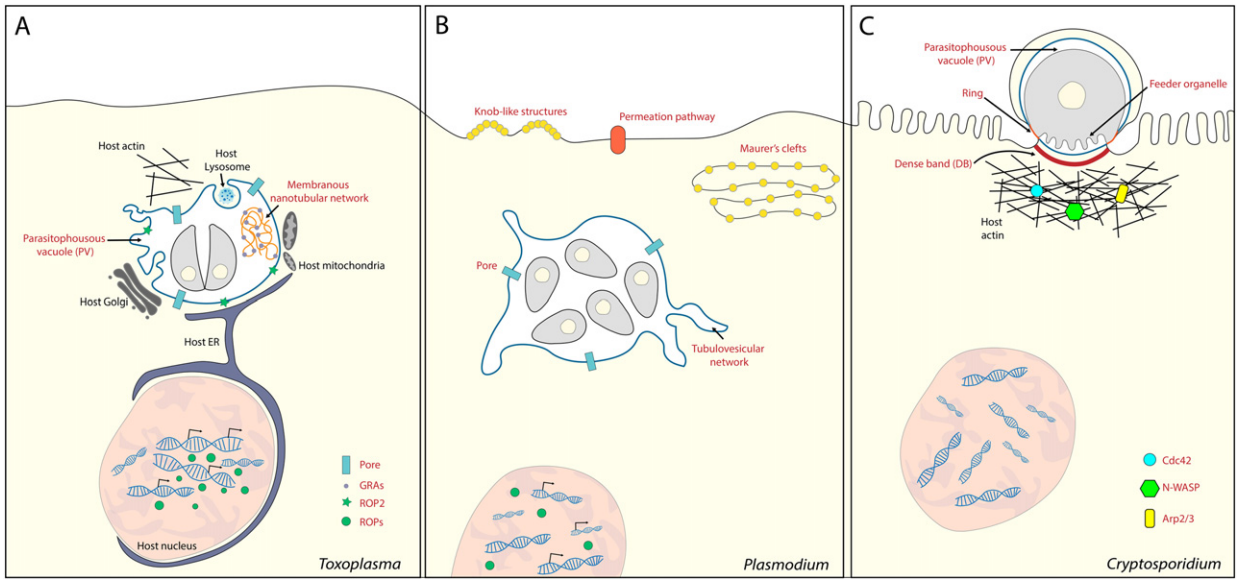

Fig. 3 Host cell remodeling and subversion by Apicomplexa. (A) *Toxoplasma gondii* recruits the host endoplasmic reticulum and mitochondria. Host lysosomes are internalized into the PV. A pore traversing the PVM allows the uptake of small molecules and nutrients. GRAs proteins form a membranous nanotubular network inside the PV. (B) In *Plasmodium* parasites, the new permeation pathway (NPP) increases the permeability of the erythrocyte to metabolites and nutrients. A pore in the PVM is allow the uptake of small molecules. Formation of knob-like structures at the surface of the infected erythrocyte and Maurer's cleft in the cytoplasm. (C) *Cryptosporidium* invasion induces a major remodeling of the host cytoskeleton at the invasion site. The host PI3K is recruited and activated which subsequently activates Cdc42, N-WASP and Arp273 to mediate actin remodeling and formation of an actin pedestal.

Intracellular Survival in a Protected Niche

Intracellular survival of parasites is a challenging mission. The parasite needs not only to take up nutrients to survive and replicate, but it also needs to find an escape from the constant threat of host autonomous defense mechanisms. The PVM function is indispensable for overcoming all these challenges. However, other species such as the related apicomplexan parasite *Babesia*, loses its PVM just after its formation (Repnik *et al.*, 2015). Thus, the PVM is not an essential structure for all intracellular parasites but its conservation in a multitude of species indicates its selective advantage. Ultimately, the PVM constitutes a physical barrier for replication of daughter cells, and it plays a role not only in the uptake of nutrients but also in excretion of waste and export of effectors to manipulate and reprogram the host cell.

The apicomplexans have a high capacity to modulate host innate defense and to interfere with the host signaling and lipid trafficking pathways to their benefits (**Fig. 3**).

Modification of the Parasitophorous Vacuole Membrane

The major task for the parasite upon entry, is to modify the PVM to avoid degradation in lysosomes and start nutrient uptake for survival. The newly formed PVM of *T. gondii* is modified immediately after invasion allowing the uptake of small molecules like amino acids and simple sugars (**Fig. 3**(A)). Using labeled peptides and small fluorescent dyes, presence of pores at the PVM was confirmed (Schwab *et al.*, 1994). These pores allow the passage of small molecules inside the PV. Once inside, these molecules are taken up by the parasite by either endocytosis or substrate-specific transporters. Not only the membrane of the PV that undergoes modifications, the inside of the PV also goes through major changes. During intracellular development of *T. gondii*, a multilamellar structure eventually assembles to build up a membranous nanotubular network (MNN) inside the lumen of the PV (Sibley *et al.*, 1995). The MNN plays a role in increasing membrane surface across which the parasite takes up metabolites (**Fig. 3**(A)). This network is formed by secreted GRAs (Travier *et al.*, 2008). In addition to PVM modification, malaria parasites induce morphological changes inside infected erythrocyte starting with formation of a tubulovesicular network referred to as Maurer's clefts (MC) that stretches from the PVM to the periphery of infected RBCs (**Fig. 3**(B)) (Warncke and Beck, 2019). *Cryptosporidium* hijacks the host actin polymerization at the infection site (**Fig. 3**(C)). Two signaling pathways involving Arp 2/3 complex were identified for this localized actin polymerization. One is orchestrated by phosphoinositide 3-kinase (PI3K) that activates Cdc42, N-WASP, and the Arp2/3 complex (Chen *et al.*, 2004; Forney *et al.*, 1999). The second pathways relies on the tyrosine kinase c-Src, that phosphorylates cortactin, and induces activation of the Arp2/3 complex (Chen *et al.*, 2003).

Resistance to the Host Autonomous Defense Mechanisms

Survival of intracellular organisms depends on their efficiency to manipulate host signaling pathways to hide from and survive the immune system and control host cell death. To overcome this barrier, parasites need to alter host gene expression. Previous studies helped in shedding light on the function and importance of several rhoptry proteins. Some of these proteins harbor specialized functions such as kinases, proteases, and phosphatases. For example, the ROP2 family, also known as ROP kinases (ROPK), possess a conserved serine threonine (S/K) kinase domain (el Hajj *et al.*, 2006). However, several proteins of ROPK family do not possess the catalytic triad necessary for phosphorylation activity and are referred to as pseudo-kinases. Some members of the ROPK are important mediators in modulating host cells for the parasite's benefit. The population genetic structure of *T. gondii* consists of three clonal lineages that differ in their virulence phenotype depending on the host. Type I strains (RH) are highly virulent in mice, while type II (ME49) and type III (CTG) are less virulent and can differentiate into latent forms (Behnke *et al.*, 2011). ROP16 and ROP18 are active kinases responsible for the parasite virulence and their catalytic activity is a key determinant that modulates host-signaling pathways. ROP16 is secreted into the cytosol of the host cell at time of invasion and translocates to the host cell nucleus. ROP16 activates signal transducer and activator of transcription 3 (STAT3) and STAT6 that lead to repression of *T. gondii* -induced pro-inflammatory cytokines (Ong *et al.*, 2010; Yamamoto *et al.*, 2009). Moreover, combined activity of ROP5, a pseudo-kinase, and ROP18, phosphorylate Irga6 and Irgb6, two members of p47 immunity related GTPases (IRGs), which results in blocking their recruitment to the PV surface for parasite clearance (Fentress *et al.*, 2010; Steinfeldt *et al.*, 2010). Taken together, ROPK family includes some key players that balance the rate of parasite replication versus parasite control by the host immune system, in a strain-specific manner. GRA proteins are also important effectors for modulation of the cell host immune system. Secretion of GRAs occurs at the end of invasion following PV formation (Panas and Boothroyd, 2021). These proteins are found post-secretion inside the PV and in the PVM and are crucial for its maturation into a metabolically active compartment and for its subsequent transformation into a cyst wall (Panas and Boothroyd, 2021). It was also shown that some GRAs traffic to the host cell and can modulate gene expression and cellular functions (Bougdour *et al.*, 2013; Braun *et al.*, 2013).

In *P. falciparum*, over 30 proteins have been described as rhoptry proteins (Kats *et al.*, 2006; Sam-Yellowe *et al.*, 2004). ROPs are mostly species-specific, and contrary to what is observed in *T. gondii*, none of the *Plasmodium* ROPs described so far have a kinase activity. Profiling and characterization of *P. falciparum* kinases is a high priority to develop potent anti-malarial drugs. FIKK kinases represent one of the 27 distinct protein families including known exported proteins (Schneider and Mercereau-Puijalon, 2005). FIKK kinases are highly atypical kinases with no orthologs in any other eukaryote, with only FIKK8 present in all apicomplexans. Most of exported FIKKs in *P. falciparum* play a primary role in remodeling of the infected RBC and are involved in parasite pathogenicity and virulence. Infected erythrocytes are subjected to splenic clearance. To avoid this, *P. falciparum* induces cytoadherence of the host to the endothelium of blood vessels. This is achieved by secretion of adhesion molecules such as ICAM-1 across the PVM and targeted to the host PM. These proteins are subjected to antigenic variation to avoid being targets of the immune system when exposed to the host blood circulation. Other proteins that mediate the cytoadherence, are sent to the infected erythrocyte surface, through the MC, and induce the formation of knobs (Haeggström *et al.*, 2004). The MC is a Golgi-like membranous structure with an electron-dense surface and translucent lumen (Spycher *et al.*, 2006). The MC is deposited in the host cytosol during infection and has a major role in trafficking and targeting of parasite proteins to the surface of infected erythrocytes (Tilley *et al.*, 2008). Another strategy used by malaria parasites to avoid the host immune system, is to send proteins to the surface of the infected cell that will eventually bind to an uninfected erythrocyte. This mechanism called rosetting is not well understood but it was shown to have a role in parasitemia (Rowe *et al.*, 2002).

Metabolites Exchanges With The Host Cell

To survive inside their restricted niche, intracellular parasites need to scavenge metabolites and acquire essential nutrients from the infected host. Apicomplexans have mastered different strategies to acquire essential nutrients to sustain rapid growth within their respective hosts. Nutrients from the external medium need to cross three different membranes before reaching the parasite, the host PM, the PVM and the parasite PM that harbor distinct permeability properties and transporters (Kirk, 2001).

T. gondii infect all types of nucleated cells that are metabolically actives, giving access to a great metabolite diversity. The PVM is permeable for small molecules such us carbohydrates, nucleotides, and amino acids up to 1.9 kDa (Clough and Frickel, 2017; Schwab *et al.*, 1994). Secreted GRAs are key players in this passive transport. TgGRA17 is related to PfEXP2, a protein implicated in the translocon machinery in *Plasmodium*. Together with TgGRA23, they function to facilitate sieving of nutrients from the infected host (Gold *et al.*, 2015).

In a similar way as the intracellular bacterium *Chlamydia trachomatis*, *T. gondii* modifies the cytoskeletal architecture and the endomembrane system of its host during replication (Romano and Coppens, 2013). These two pathogens share similar strategies to modify the structure of the host MTOC, mitochondria, ER and Golgi apparatus. Golgi recruitment to the PVM is the way for *T. gondii* to salvage lipids, mainly sphingolipids. Fast and active recruitment of host mitochondria is mediated by GRAs protein TgMAF1 (Pernas *et al.*, 2014) whereas recruitment of ER is not understood. This close interaction with the host ER and mitochondria facilitates the scavenging of lipids by the parasite. Additionally, by modulating the host microtubule-dependent transport, *T. gondii* recruit the host endolysosome system to target vesicles loaded with cholesterol and other small molecules (Coppens *et al.*, 2006).

Cryptosporidium lacks enzymes for synthesis of sugars, nucleotides, and amino acids and has a reduced metabolism comparing to other apicomplexan parasites. To get essential nutrients to survive, the parasite relies on a special cellular structure, called feeder organelle, to take up host metabolites (**Fig. 3**(C)). This structure is a convoluted set of membrane invagination that increases the surface across which the parasite takes in nutrients. In addition, *Cryptosporidium* has also lost the apicoplast and thus lacks isoprenoids, fatty

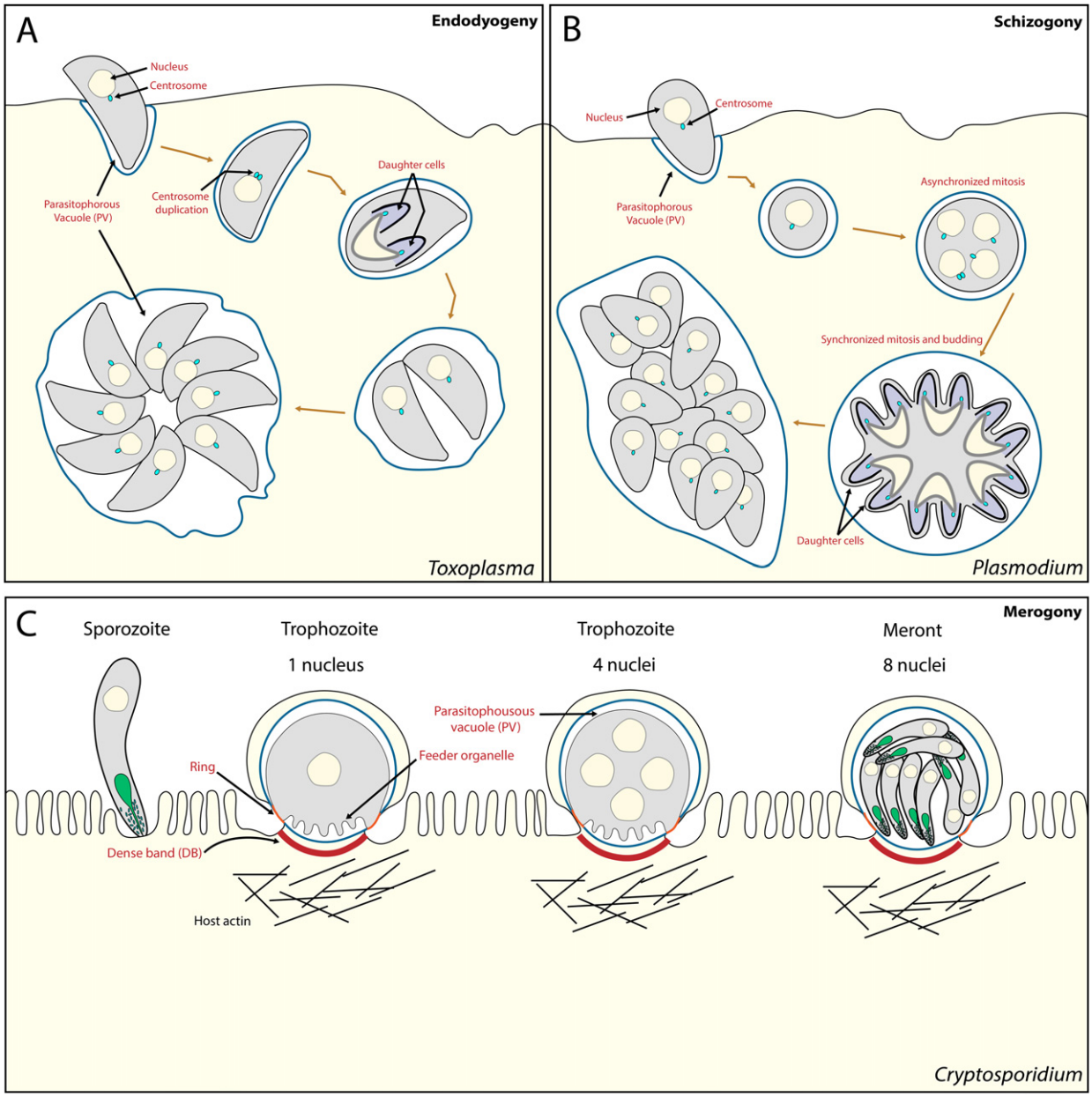

Fig. 4 Flexibility of different apicomplexan replication cycles. Schematic representation of (A) *Toxoplasma* (endodyogeny). Each DNA replication is followed by mitosis and budding of daughter cells within the mother cell. (B) *Plasmodium* (schizogony). Nuclei start multiplying by asynchronized rounds of mitosis. The last round is synchronized for all nuclei with budding and emergence of daughter cells. (C) *Cryptosporidium* (merogony). After invasion, the sporozoite forms a trophozoite that undergo merogony to transform into meront I with eight merozoites.

acids, and heme synthesis pathways. Glycose and amylopectin are important for the oocyst (Tandel *et al.*, 2019). To get these metabolites, the parasite relies on glycolysis and fermentation as its only source of energy (Witola *et al.*, 2017; Zhang *et al.*, 2015).

Cell Division and Organelles Biogenesis

During most parts of their life cycle apicomplexan parasites possess a haploid genome and are known to change the replication mode in different stages of transmission which allows them to infect different host cell types (Francia and Striepen, 2014). However, the beginning and end point of all division is a zoite that harbors the apical complex needed for invasion.

Cell division in Apicomplexa differs fundamentally from what we know from eukaryotic model organisms. In mammalian cells, the nuclear envelope disintegrates as soon as the mitotic spindle is formed, and chromosomes migrate during mitosis. This is followed by fission and cytokinesis to give rise to two daughter cells. In contrast, apicomplexans use closed mitosis leaving the

nuclear envelope intact and are able to uncouple the karyokinesis from the cytokinesis. The number of offsprings can vary from two to 100,000, the disassembly of the mother cytoskeleton can be the first or last step of the division, and budding of daughter cells can happen either at the surface of the parasite (external budding) or deep in its cytoplasm (internal budding) (Gubbels *et al.*, 2020).

Divide and Conquer

Within tissues of its intermediate hosts, *T. gondii* tachyzoites engage in cycles of internal budding process called endodyogeny, where two daughter cells are formed within the boundaries of the parent parasite that is consumed at the end (**Fig. 4**(A)) (Francia and Striepen, 2014). The tachyzoite has a haploid genome that is duplicated during S phase to give 1.8 N DNA. At this time, the mitotic spindle starts to appear, meaning that the G2 phase is missing. Also, cytokinesis and daughter budding start when 1.8 N DNA is reached. Cell cycle progression is also monitored by cyclins and CDKs. In addition to endodyogeny, *T. gondii* uses schizogony to divide in intestinal epithelia of its definitive feline host (Attias *et al.*, 2020). This flexibility suggests the existence of an overlap of regulators between these different cell division modes.

Plasmodium parasite undergoes schizogony, an asynchronized form of division and replication that occurs during hepatic and erythrocytic infections in mammalian hosts, while sporogony, an analog process occurs in the mosquito vector. During schizogony, schizonts, a multinucleate syncytium, are formed before budding and cytokinesis (**Fig. 4**(B)) (Francia and Striepen, 2014). Even though these multiple nuclei share the same cytoplasm, their division is asynchronized resulting in a non-geometric expansion. The last round of mitosis is however synchronous and coincide with assembly of daughter cells. A defining feature of schizogony is the immediate disassembly of the mother's cytoskeleton just after invasion which results in a pleomorphic cell that undergoes cycles of nuclear division and DNA replication (Francia and Striepen, 2014). Another intriguing fact about *Plasmodium* cell division, is the remarkably fast process of male gamete formation where gametocytes undergo three rounds of DNA replication in a few minutes to give rise to eight male gametes (Billker *et al.*, 2004).

In contrast to *Toxoplasma* and *Plasmodium*, we know little about the molecular mechanisms behind the asexual development of *Cryptosporidium*. This parasite has a highly reduced genome and yet it is capable to differentiate through multiple stages that amplify asexually and then transform into gametes that undergo sexual fertilization, building a flexible and strong spore (**Fig. 4**(C)) (Tandel *et al.*, 2019). The asexual multiplication (schizogony or merogony) starts 24 h after ingestion of the oocyst. The trophozoite stage 3 divides to give two meronts. These cells are haploid and divide asexually very rapidly. Merozoites are formed from meront II, a second-generation haploid stage of *C. parvum* (Borowski *et al.*, 2008). These cells grow and develop to form microgamonts (male) or macrogamonts (female) that undergo sexual division (gametogony) (Borowski *et al.*, 2008).

Checkpoints Controlling Division in Apicomplexa

The molecular mechanisms regulating the different division modes and how they contribute to the budding process that characterizes Apicomplexa are less understood. Progress of cell cycle is controlled tightly by cyclin-cyclin dependent kinases (CDKs) activities that are conserved among all eukaryotic cells, as described in recent reviews (Gubbels *et al.*, 2021; Matthews *et al.*, 2018; White and Suvorova, 2018).

With such a complex life cycle, sophisticated regulators and refined checkpoints and DNA repair mechanisms are in place to ensure a proper replication. However, cell cycle regulators are different from their mammalian counterparts (Roques *et al.*, 2015) and from host organisms, making them a suitable drug target. In eukaryotic cells, the cell cycle is regulated by cyclins and CDKs and synchronization between regulatory and catalytic players is needed for progression through G1, S, G2 and M phases. In Apicomplexa, the cell cycle is composed of only three phases, G1, S and M (Striepen *et al.*, 2007). Additionally, the repertoire of cyclins in Apicomplexa is different from the canonical cyclins of other eukaryotes such us mammalian Cyc D, E and A and they are expressed constitutively rather than "cycling" as seen in mammalian cells (Merckx *et al.*, 2003). Calcium-dependent protein kinases (CDPKs) are another specific apicomplexan regulator that play multiple roles during the parasite life cycle and are considered an attractive parasite-specific drug target (Ghartey-Kwansah *et al.*, 2020). Homologs of the centrosome-associated NIMA kinase were found in both *Plasmodium and Toxoplasma*, and they play a major role in cell cycle progression (Reininger *et al.*, 2005). Apicomplexa engage in several division patterns dependent on their environment and developmental stage. This plasticity suggests the existence of a master regulator that controls the budding time and promote and/or inhibit differentiation pathways. Apicomplexan parasites express homologs of Apetala 2 (AP2) transcription factors known as ApiAP2s. These transcription factors were identified in both *P. falciparum* and *T. gondii*, and they bind to several promoters of multiple co-regulated genes controlling activation of the budding-specific cell cycle expression pattern (Painter *et al.*, 2011; Radke *et al.*, 2013). Recently, transcription factor Api2IX-5 was identified in *T. gondii*, and it regulates expression of genes important for completion of budding and ensures the continuity of asexual division by inhibiting the differentiation pathway (Khelifa *et al.*, 2021).

Organelle Segregation During Division

In Apicomplexa, the first steps of daughter formation start with a polarized microtubule scaffold that is further elaborated by other cytoskeleton and membrane elements. The daughter cell conoid and MTOC are assembled forming nucleating points for daughter IMCs and subpellicular microtubules (Nishi *et al.*, 2008a). The next steps are replication of centrioles, elongation of the Golgi and

apicoplast that divide and segregate into daughter scaffolds. This is trailed by sequential segregation of the nucleus, ER, and mitochondrion. The IMC is part of the cortical cytoskeleton of the parasite. It is a double membrane that consists of a membrane cisterna supported by a membrane skeleton of alveolin network and 22 SPMTs that start from the apical tip reaching the two-third length of the parasite (Mann and Beckers, 2001). The IMC prepares the scaffold for correct partition of nuclei and organelles (Anderson-White *et al.*, 2012). Separation between the mother material and forming daughter cells is guaranteed by elongation of the IMC (Nishi *et al.*, 2008b; Stanway *et al.*, 2011).

Exit From the Infected Cells

Following multiple rounds of replication, parasites eventually egress from the host cell by lysing the PVM and the host PM, contributing to disease pathology, including damage to tissues and inflammatory responses. This active process of egress requires secretion of micronemes and parasite motility. Mobilization of these proteins is induced notably by increased cytosolic calcium (reviewed in (Blackman and Carruthers, 2013; Lourido and Moreno, 2015).

Secreted perforins permeabilize the PVM and the host cell PM and help motile parasites to mechanically rupture the fragile PVM (Sassmannshausen *et al.*, 2020). Egress can be stimulated by several inducers that converge to a rise in cyclic guanosine monophosphate (cGMP) leading to an increase in intracellular Ca^{2+}. In *T. gondii*, the compromised integrity of the host cell PM leads to a drop in intracellular K^{+} which is sensed by the parasite and causes a release of intracellular calcium from storage triggering egress (Moudy *et al.*, 2001). Additionally, acidification of the PV can trigger secretion of micronemes and activation of perforin-like protein 1 (PLP1) that forms a pore complex in membranes (Kafsack *et al.*, 2009; Roiko *et al.*, 2014).

All these events are the result of either environmental signals from infected host cells or regulated egress initiated by the parasite itself after an optimal number of replication cycles (reviewed (Bisio and Soldati-Favre, 2019; Tan and Blackman, 2021). Following egress, parasites glide and reach neighboring host cells to invade and initiate a new infection cycle.

Sensing Intrinsic and Extrinsic Factors for Egress

Egress from the host cell is highly regulated and controlled and can be triggered by extrinsic factors such as the host immune response or limitation in nutrients, which leads to microneme secretion. The parasite can also respond to intrinsic signals that trigger a non-stimulated egress called natural egress (Caldas *et al.*, 2018). This type of stimulation controls the number of division cycles that the parasite undergoes before egress. In recent years, many candidates were proposed to trigger natural egress in *T. gondii*. Abscisic acid (ABA) is produced continuously by the parasite during intracellular division until it reaches a threshold at which the parasite egresses (Nagamune *et al.*, 2008). A family of nucleotide triphosphate-degrading enzymes (NTPases) were also associated to natural egress (Stommel *et al.*, 1997) but their role is not yet understood. Recently, Diacylglycerol kinase 2 (DGK2) was proposed as a plausible candidate for natural egress in member of coccidia subgroup. DGK2 localizes to dense granules and is secreted and accumulates into the PV lumen. This active kinase produces phosphatidic acid (PA) and parasites with deleted DGK2 exhibit a defect in natural egress (Bisio *et al.*, 2019). Other dense granules proteins, GRA41 and GRA22 were also shown as intrinsic triggers for natural egress through calcium signaling (LaFavers *et al.*, 2017; Okada *et al.*, 2013). While tachyzoites egress after five to six rounds of replication, bradyzoites grow very slowly and develop within a cyst wall and tissue cysts persist a very long time during the chronic phase.

When intracellular parasites face an unhealthy or dangerous host environment, they egress immediately. This can happen when the pH of the PV decreases due to an outward flow of K^{+} ions, triggering microneme secretion (Roiko *et al.*, 2014). This low pH activates protein kinase A catalytic subunit 1 (PKAc1) (Moudy *et al.*, 2001) and phosphoinositide phospholipase C (PI-PLC) (Fang *et al.*, 2006) by G protein-coupled receptor (GPCR). Increase in intracellular Ca^{2+} can originate from the extracellular environment and contribute to egress, invasion, and motility (Borges-Pereira *et al.*, 2015; Pace *et al.*, 2014). Signals that modulate host Ca^{2+} were shown to be implicated in parasite egress (Persson *et al.*, 2007) and calcium-dependent enzymes, such as CDPKs that resemble plant enzymes, are conserved among apicomplexan parasites (Nagamune and Sibley, 2006). Another inducer of egress is nitric oxide (NO) that induces heme-dependent soluble guanylate cyclase leading to an increase in the host Ca^{2+} (Denninger and Marletta, 1999).

In *Plasmodium*, blood stage merozoites egress is apparently controlled by unidentified intrinsic factors that trigger the activation of cGMP-dependent protein kinase G (PKG). A study has shown that exogenous phosphatidylcholine triggers egress, but more research is needed to understand the regulation of this pathway (Paul *et al.*, 2020). Moreover, xanthurenic acid, a tryptophan metabolite, induces release of motile male gametes in both *P. falciparum and P. berghei* by activating the cGMP signaling pathway (Brochet *et al.*, 2021; Muhia *et al.*, 2001).

Release of Perforins, Lipases and Proteases

Microneme secretion is initiated by production of cGMP by GC (Bisio *et al.*, 2019). Ca^{2+} is then mobilized by induction of PKG (M *et al.*, 2021) that phosphorylates key enzymes, forming phosphatidylinositol 3,4,5 triphosphate that eventually is converted by PI-PLC (Brochet *et al.*, 2014) into inositol triphosphate (IP3) and diacylglycerol (DAG) (Singh *et al.*, 2010). In *T. gondii*, IP3

induces release of Ca^{2+} from unknown stores (Lourido and Moreno, 2015). CDPK1 and CDPK3 are activated through this intracellular Ca^{2+} increase (Lourido *et al.*, 2010).

DAG is next converted into PA that contribute to microneme exocytosis (Bullen *et al.*, 2016). In *Plasmodium*, PfCDPK5, a homolog of TgCDPK3, was also shown to regulate egress of merozoites from both infected RBCs and liver cells. However, the PfCDPK cascade differs from the one observed in *T. gondii* since it appears to function downstream of PKG (Dvorin *et al.*, 2010).

Micronemes secrete perforins, lipases and proteases that will directly contribute to exit from the host cell. Importantly, PLP1 is activated after a decrease in pH. PLP1 is imbedded in membranes and has a crucial role in pore formation in the PV and host PM to make a path out of the infected cell (Kafsack *et al.*, 2009). PLPs are expressed in different life stages and can lyse different cell membranes (Garg *et al.*, 2020; Sassmannshausen *et al.*, 2020). *P. falciparum* subtilisin-like serine protease 1 (PfSUB1) plays an important role during egress. It is secreted from exonemes, a secretory organelle distinct from rhoptries, micronemes and dense granules, into the PV space (Yeoh *et al.*, 2007) and cleaves putative proteases called SERA, which degrade the PVM, host cytoskeleton and host PM (Yeoh *et al.*, 2007). When parasites are depleted from SUB1, egress is inhibited in the same manner as in PKG knock-out parasites (Thomas *et al.*, 2018) which places SUB1 as an early effector in the egress machinery. The aspartic protease Plasmepsin X (PMX) plays an important role in egress and invasion in intraerythrocytic parasites by controlling the maturation of SUB1 (Pino *et al.*, 2017).

While invasion was extensively studied in *Cryptosporidium*, little is known about molecular mechanisms behind egress. Homologs of TgCDPK3 and PfSUB1 were identified in *Cryptosporidium* and shown to play a role during invasion (Castellanos-Gonzalez *et al.*, 2016; Wanyiri *et al.*, 2009). A recent work reported that silencing of CpSUB1 led to a severe decrease in egress with an increase in trapped parasites within the host (Samantha *et al.*, 2021). Further studies are needed to identify substrates of CpSUB1 and whether they are secreted into the PV lumen as in *Plasmodium*. CpCDPK5 does affect parasite egress either due to a limited role of CpCDPK5 during egress or compensation of other pathways. *Cryptosporidium* genome encodes seven CDPKs. CpCDPK3 is expressed prior to egress and has a 14% sequence homology with TgCDPK3, which may indicate a role at this step (Etzold *et al.*, 2014).

Additionally, an ortholog of TgPKG and PfPKG was found in *Cryptosporidium* (Nava *et al.*, 2020). Decreasing the level of CpPKG affected merozoites exit by completely blocking egress (Nava *et al.*, 2020).

Conclusion

Emergence of a reverse genetics toolbox has promoted and facilitated the study of the cell biology of apicomplexans by offering robust experimental approaches to test the function of essential genes. Efforts still need to be directed towards developing effective drugs to block parasites' dissemination and to prevent the devastating diseases caused by these human pathogens.

Acknowledgments

RBC is supported by a Swiss National Foundation grant to D.S.-F. (310030_185325).

References

Adl, S.M., Simpson, A.G., Lane, C.E., *et al.*, 2012. The revised classification of eukaryotes. Journal of Eukaryotic Microbiology 59 (5), 429–493.
Alexander, D.L., Mital, J., Ward, G.E., Bradley, P., Boothroyd, J.C., 2005. Identification of the moving junction complex of *Toxoplasma gondii*: A collaboration between distinct secretory organelles. PLOS Pathogens 1 (2), e17.
Anderson-White, B., Beck, J.R., Chen, C.T., *et al.*, 2012. Cytoskeleton assembly in *Toxoplasma gondii* cell division. International Review of Cell and Molecular Biology 298, 1–31.
Aquilini, E., Cova, M.M., *et al.*, 2020. An Alveolata secretory machinery adapted to parasite-host cell invasion. Nature Microbiology 6.
Attias, M., Teixeira, D.E., Benchimol, M., *et al.*, 2020. The life-cycle of *Toxoplasma gondii* reviewed using animations. Parasites & Vectors 13 (1), 588.
Bargieri, D.Y., Thiberge, S., Tay, C.L., *et al.*, 2016. *Plasmodium* merozoite TRAP family protein is essential for vacuole membrane disruption and gamete egress from erythrocytes. Cell Host & Microbe 20 (5), 618–630. (Elsevier).
Bartošová-Sojková, P., Oppenheim, R.D., Soldati-Favre, D., Lukeš, J., 2015. Epicellular apicomplexans: Parasites 'on the way in'. PLOS Pathogens 11 (9), e1005080.
Behnke, M.S., Khan, A., Wootton, J.C., *et al.*, 2011. Virulence differences in *Toxoplasma* mediated by amplification of a family of polymorphic pseudokinases. Proceedings of the National Academy of Sciences of the United States of America 108 (23), 9631–9636.
Ben Chaabene, R., Lentini, G., Soldati-Favre, D., 2021. Biogenesis and discharge of the rhoptries: Key organelles for entry and hijack of host cells by the Apicomplexa. Molecular Microbiology 115 (3), 453–465.
Besteiro, S., Dubremetz, J.F., Lebrun, M., 2011. The moving junction of apicomplexan parasites: A key structure for invasion. Cellular Microbiology 13 (6), 797–805.
Billker, O., Dechamps, S., Tewari, R., *et al.*, 2004. Calcium and a calcium-dependent protein kinase regulate gamete formation and mosquito transmission in a malaria parasite. Cell 117 (4), 503–514.
Bisio, H., Soldati-Favre, D., 2019. Signaling cascades governing entry into and exit from host cells by *Toxoplasma gondii*. Annual Review of Microbiology 73 (1), 579–599. (Annual Reviews).
Bisio, H., Lunghi, M., Brochet, M., Soldati-Favre, D., 2019. Phosphatidic acid governs natural egress in *Toxoplasma gondii* via a guanylate cyclase receptor platform. Nature Microbiology 4 (3), 420–428.
Blackman, M.J., Carruthers, V.B., 2013. Recent insights into apicomplexan parasite egress provide new views to a kill. Current Opinion in Microbiology 16 (4), 459–464.
Boothroyd, J.C., Dubremetz, J.F., 2008. Kiss and spit: The dual roles of *Toxoplasma* rhoptries. Nature Reviews Microbiology 6 (1), 79–88.
Borges-Pereira, L., Budu, A., McKnight, C.A., *et al.*, 2015. Calcium signaling throughout the *Toxoplasma gondii* lytic cycle: A study using genetically encoded calcium indicators. Journal of Biological Chemistry 290 (45), 26914–26926. (Elsevier).

Borowski, H., Clode, P.L., Thompson, R.C., 2008. Active invasion and/or encapsulation? A reappraisal of host-cell parasitism by *Cryptosporidium*. Trends in Parasitology 24 (11), 509–516.
Bougdour, A., Durandau, E., Brenier-Pinchart, M.-P., *et al*., 2013. Host cell subversion by toxoplasma GRA16, an exported dense granule protein that targets the host cell nucleus and alters gene expression. Cell Host & Microbe 13. (available at). https://doi.org/10.1016/j.chom.2013.03.002.
Bouzid, M., Hunter, P.R., Chalmers, R.M., Tyler, K.M., 2013. *Cryptosporidium* pathogenicity and virulence. Clinical Microbiology Reviews 26 (1), 115–134. (American Society for Microbiology).
Bradley, P.J., Ward, C., Cheng, S.J., *et al*., 2005. Proteomic analysis of rhoptry organelles reveals many novel constituents for host-parasite interactions in *Toxoplasma gondii*. Journal of Biological Chemistry 280 (40), 34245–34258.
Braun, L., Brenier-Pinchart, M.P., Yogavel, M., *et al*., 2013. A *Toxoplasma* dense granule protein, GRA24, modulates the early immune response to infection by promoting a direct and sustained host p38 MAPK activation. Journal of Experimental Medicine 210 (10), 2071–2086.
Brochet, M., Balestra, A.C., Brusini, L., 2021. cGMP homeostasis in malaria parasites – The key to perceiving and integrating environmental changes during transmission to the mosquito. Molecular Microbiology 115 (5), 829–838. John Wiley & Sons, Ltd.
Brochet, M., Collins, M.O., Smith, T.K., *et al*., 2014. Phosphoinositide metabolism Links cGMP-dependent protein kinase G to essential Ca2 + signals at key decision points in the life cycle of malaria parasites. PLOS Biology 12 (3), e1001806.
Bullen, H.E., Jia, Y., Yamaryo-Botte, Y., *et al*., 2016. Phosphatidic acid-mediated signaling regulates microneme secretion in *Toxoplasma*. Cell Host & Microbe 19 (3), 349–360.
Caldas, L.A., Attias, M., de Souza, W., 2018. A structural analysis of the natural egress of *Toxoplasma gondii*. Microbes and Infection 20 (1), 57–62.
Carreno, R.A., Martin, D.S., Barta, J.R., 1999. *Cryptosporidium* is more closely related to the gregarines than to coccidia as shown by phylogenetic analysis of apicomplexan parasites inferred using small-subunit ribosomal RNA gene sequences. Parasitology Research 85 (11), 899–904. (Springer Verlag).
Castellanos-Gonzalez, A., Perry, N., Nava, S., White Jr, A.C., 2016. Preassembled single-stranded RNA-argonaute complexes: A novel method to silence genes in *Cryptosporidium*. The Journal of Infectious Diseases 213 (8), 1307–1314. (Oxford University Press).
Chen, X.M., Splinter, P.L., Tietz, P.S., *et al*., 2004. Phosphatidylinositol 3-kinase and frabin mediate *Cryptosporidium parvum* cellular invasion via activation of Cdc42. Journal of Biological Chemistry 279 (30), 31671–31678.
Chen, X.-M., Huang, B.Q., Splinter, P.L., *et al*., 2003. *Cryptosporidium parvum* invasion of biliary epithelia requires host cell tyrosine phosphorylation of cortactin via c-Src. Gastroenterology 125 (1), 216–228.
Chen, X.-M., O'Hara, S.P., Huang, B.Q., *et al*., 2004. Apical organelle discharge by *Cryptosporidium parvum* is temperature, cytoskeleton, and intracellular calcium dependent and required for host cell invasion. Infection and Immunity 72 (12), 6806–6816. (American Society for Microbiology).
Clough, B., Frickel, E.M., 2017. The *Toxoplasma* parasitophorous vacuole: An evolving host–parasite frontier. Trends in Parasitology 33 (6), 473–488. (Elsevier Ltd).
Coppens, I., Dunn, J.D., Romano, J.D., *et al*., 2006. *Toxoplasma gondii* sequesters lysosomes from mammalian hosts in the vacuolar space. Cell 125 (2), 261–274. (Elsevier B.V.).
Culvenor, J.G., Day, K.P., Anders, R.F., 1991. *Plasmodium falciparum* ring-infected erythrocyte surface antigen is released from merozoite dense granules after erythrocyte invasion. Infection and Immunity 59 (3), 1183–1187. (American Society for Microbiology).
Denninger, J.W., Marletta, M.A., 1999. Guanylate cyclase and the ·NO/cGMP signaling pathway. Biochimica et Biophysica Acta - Bioenergetics 1411 (2), 334–350.
Dos Santos Pacheco, N., Tosetti, N., Koreny, L., Waller, R.F., Soldati-Favre, D., 2020. Evolution, composition, assembly, and function of the conoid in apicomplexa. Trends in Parasitology 36 (8), 688–704.
Dubois, D.J., Soldati-Favre, D., 2019. Biogenesis and secretion of micronemes in *Toxoplasma gondii*. Cellular Microbiology 21 (5), e13018. John Wiley & Sons, Ltd.
Dubremetz, J.F., 2007. Rhoptries are major players in *Toxoplasma gondii* invasion and host cell interaction. Cellular Microbiology 9 (4), 841–848.
Dvorin, J.D., Martyn, D.C., Patel, S.D., *et al*., 2010. A plant-like kinase in *Plasmodium falciparum* regulates parasite egress from erythrocytes. Science 328 (5980), 910–912.
el Hajj, H., Demey, E., Poncet, J., *et al*., 2006. The ROP2 family of *Toxoplasma gondii* rhoptry proteins: Proteomic and genomic characterization and molecular modeling. Proteomics 6 (21), 5773–5784.
Etzold, M., Lendner, M., Daugschies, A., Dyachenko, V., 2014. CDPKs of *Cryptosporidium parvum*—stage-specific expression in vitro. Parasitology Research 113 (7), 2525–2533.
Fang, J., Marchesini, N., Moreno, S.N.J., 2006. A *Toxoplasma gondii* phosphoinositide phospholipase C (TgPI-PLC) with high affinity for phosphatidylinositol. The Biochemical Journal 394 (Pt 2), 417–425. (Portland Press Ltd.).
Fentress, S.J., Behnke, M.S., Dunay, I.R., *et al*., 2010. Phosphorylation of immunity-related GTPases by a *Toxoplasma gondii*-secreted kinase promotes macrophage survival and virulence. Cell Host & Microbe 8 (6), 484–495.
Forney, J.R., DeWald, D.B., Yang, S., Speer, C.A., Healey, M.C., 1999. A role for host phosphoinositide 3-kinase and cytoskeletal remodeling during *Cryptosporidium parvum* infection. Infection and Immunity 67 (2), 844–852. (American Society for Microbiology).
Fox, B.A., Rommereim, L.M., Guevara, R.B., *et al*., 2016. The *Toxoplasma gondii* rhoptry kinome is essential for chronic infection. MBio 7 (3), 1–12.
Francia, M.E., Striepen, B., 2014. Cell division in apicomplexan parasites. Nature Reviews Microbiology 12, 125. (Nature Publishing Group, a division of Macmillan Publishers Limited. All Rights Reserved).
Frenal, K., Dubremetz, J.F., Lebrun, M., Soldati-Favre, D., 2017. Gliding motility powers invasion and egress in Apicomplexa. Nature Reviews Microbiology 15 (11), 645–660.
Frenal, K., Polonais, V., Marq, J.B., *et al*., 2010. Functional dissection of the apicomplexan glideosome molecular architecture. Cell Host & Microbe 8 (4), 343–357.
Gao, X., Yin, J., Wang, D., *et al*., 2021. Discovery of new microneme proteins in *Cryptosporidium parvum* and Implication of the roles of a rhomboid membrane protein (CpROM1) in host–parasite interaction. Frontiers in Veterinary Science 8, 1466.
Garg, S., Shivappagowdar, A., Hada, R.S., *et al*., 2020. *Plasmodium* perforin-like protein pores on the host cell membrane contribute in its multistage growth and erythrocyte senescence. Frontiers in Cellular and Infection Microbiology 10, 121.
Ghartey-Kwansah, G., Yin, Q., Li, Z., *et al*., 2020. Calcium-dependent protein kinases in malaria parasite development and infection. Cell Transplantation 29. 0963689719884888.
Gold, D.A., Kaplan, A.D., Lis, A., *et al*., 2015. The *Toxoplasma* dense granule proteins GRA17 and GRA23 mediate the movement of small molecules between the host and the parasitophorous vacuole. Cell Host & Microbe 17 (5), 642–652.
Graindorge, A., Frénal, K., Jacot, D., *et al*., 2016. The conoid associated motor MyoH is indispensable for *Toxoplasma gondii* entry and exit from host cells. PLoS Pathogens 12 (1), e1005388.
Gubbels, M.-J., Coppens, I., Zarringhalam, K., Duraisingh, M.T., Engelberg, K., 2021. The modular circuitry of apicomplexan cell division plasticity. Frontiers in Cellular and Infection Microbiology 11, 283.
Gubbels, M.-J., Keroack, C.D., Dangoudoubiyam, S., *et al*., 2020. Fussing about fission: Defining variety among mainstream and exotic apicomplexan cell division modes. Frontiers in Cellular and Infection Microbiology 10, 269.
Guérin, A., Striepen, B., 2020. The biology of the intestinal intracellular parasite *Cryptosporidium*. Cell Host & Microbe 28 (4), 509–515. (Elsevier).
Guérin, A., Roy, N.H., Kugler, E.M., *et al*., 2021. A screen for *Cryptosporidium* rhoptry proteins identifies ROP1 as an effector targeting the host cytoskeletal modulator LMO7. Cell Host & Microbe 29 (9), 1407–1420.
Haeggström, M., Kironde, F., Berzins, K., *et al*., 2004. Common trafficking pathway for variant antigens destined for the surface of the *Plasmodium falciparum*-infected erythrocyte. Molecular and Biochemical Parasitology 133 (1), 1–14.

Hakansson, S., Charron, A.J., Sibley, L.D., 2001. *Toxoplasma* evacuoles: A two-step process of secretion and fusion forms the parasitophorous vacuole. EMBO Journal 20 (12), 3132–3144.
Hakimi, M., Olias, P., David, L., 2017. crossm *Toxoplasma* effectors targeting host. Clinical Microbiology Reviews 30 (3), 615–645.
Halonen, S.K., Weiss, L.M., 2013. Chapter 8 - Toxoplasmosis. In: Garcia, H.H., Tanowitz, H.B., del Brutto, O.H. (Eds.), Handbook of Clinical Neurology 114. Elsevier, pp. 125–145.
Hiller, N.L., Akompong, T., Morrow, J.S., Holder, A.A., Haldar, K., 2003. Identification of a stomatin orthologue in vacuoles induced in human erythrocytes by malaria parasites. A role for microbial raft proteins in apicomplexan vacuole biogenesis. Journal of Biological Chemistry 278 (48), 48413–48421.
Hu, K., Roos, D.S., Murray, J.M., 2002. A novel polymer of tubulin forms the conoid of *Toxoplasma gondii*. Journal of Cell Biology 156 (6), 1039–1050.
Jacot, D., Tosetti, N., Pires, I., *et al*., 2016. An apicomplexan actin-binding protein serves as a connector and lipid sensor to coordinate motility and invasion. Cell Host and Microbe 20 (6), 731–743.
Janouškovec, J., Paskerova, G.G., Miroliubova, T.S., *et al*., 2019. Apicomplexan-like parasites are polyphyletic and widely but selectively dependent on cryptic plastid organelles. eLife 8, e49662.
Jia, Y., Marq, J.B., Bisio, H., *et al*., 2017. Crosstalk between PKA and PKG controls pH-dependent host cell egress of *Toxoplasma gondii*. EMBO Journal 36 (21), 3250–3267.
Jung, C., Lee, C.Y.-F., Grigg, M.E., 2004. The SRS superfamily of *Toxoplasma* surface proteins. International Journal for Parasitology 34 (3), 285–296.
Kafsack, B.F., Pena, J.D., Coppens, I., *et al*., 2009. Rapid membrane disruption by a perforin-like protein facilitates parasite exit from host cells. Science 323 (5913), 530–533.
Kats, L.M., Black, C.G., Proellocks, N.I., Coppel, R.L., 2006. *Plasmodium* rhoptries: How things went pear-shaped. Trends in Parasitology 22 (6), 269–276.
Khalil, I.A., Troeger, C., Rao, P.C., *et al*., 2018. Morbidity, mortality, and long-term consequences associated with diarrhoea from *Cryptosporidium* infection in children younger than 5 years: A meta-analyses study. The Lancet Global Health 6 (7), e758–e768.
Khelifa, A.S., Guillen Sanchez, C., Lesage, K.M., *et al*., 2021. TgAP2IX-5 is a key transcriptional regulator of the asexual cell cycle division in *Toxoplasma gondii*. Nature Communications 12 (1), 116.
King, C.A., 1988. Cell motility of sporozoan protozoa. Parasitology Today 4 (11), 315–319.
Kirk, K., 2001. Membrane transport in the malaria-infected erythrocyte. Physiological Reviews 81 (2), 495–537. (American Physiological Society).
LaFavers, K.A., Márquez-Nogueras, K.M., Coppens, I., Moreno, S.N.J., Arrizabalaga, G., 2017. A novel dense granule protein, GRA41, regulates timing of egress and calcium sensitivity in *Toxoplasma gondii*. Cellular Microbiology 19 (9), 1–20.
Lebrun, M., Michelin, A., el Hajj, H., *et al*., 2005. The rhoptry neck protein RON4 re-localizes at the moving junction during *Toxoplasma gondii* invasion. Cellular Microbiology 7 (12), 1823–1833.
Lefort-Tran, M., Aufderheide, K., Pouphile, M., Rossignol, M., Beisson, J., 1981. Control of exocytotic processes: Cytological and physiological studies of trichocyst mutants in Paramecium tetraurelia. The Journal of Cell Biology 88 (2), 301–311. (The Rockefeller University Press).
Lendner, M., Daugschies, A., 2014. *Cryptosporidium* infections: Molecular advances. Parasitology 141 (11), 1511–1532. (Cambridge University Press).
Lentini, G., ben Chaabene, R., Vadas, O., *et al*., 2021. Structural insights into an atypical secretory pathway kinase crucial for *Toxoplasma gondii* invasion. Nature Communications 12 (1), 3788. (England).
Lima, T.S., Lodoen, M.B., 2019. Mechanisms of human innate immune evasion by *Toxoplasma gondii*. Frontiers in Cellular and Infection Microbiology 9, 103.
Lourido, S., Moreno, S.N.J., 2015. The calcium signaling toolkit of the Apicomplexan parasites *Toxoplasma gondii* and *Plasmodium* spp. Cell Calcium 57 (3), 186–193.
Lourido, S., Shuman, J., Zhang, C., *et al*., 2010. Calcium-dependent protein kinase 1 is an essential regulator of exocytosis in *Toxoplasma*. Nature 465 (7296), 359–362.
M, B.K., Shaojun, L., David, S.L., M, W.L., 2021. Plasma membrane association by N-acylation governs PKG function in *Toxoplasma gondii*. MBio 8 (3), e00375–17. (American Society for Microbiology).
Mageswaran, S.K., Guérin, A., Theveny, L.M., *et al*., 2021. In situ ultrastructures of two evolutionarily distant apicomplexan rhoptry secretion systems. Nature Communications 12 (1), 4983.
Mann, T., Beckers, C., 2001. Characterization of the subpellicular network, a filamentous membrane skeletal component in the parasite *Toxoplasma gondii*. Molecular and Biochemical Parasitology 115 (2), 257–268.
Matthews, H., Duffy, C.W., Merrick, C.J., 2018. Checks and balances? DNA replication and the cell cycle in *Plasmodium*. Parasites & Vectors 11 (1), 216.
Meibalan, E., Marti, M., 2017. Biology of malaria transmission. Cold Spring Harbor Perspectives in Medicine 7 (3), a025452. (Cold Spring Harbor Laboratory Press).
Merckx, A., le Roch, K., Nivez, M.-P., *et al*., 2003. Identification and initial characterization of three novel cyclin-related proteins of the human malaria parasite *Plasmodium falciparum* *. Journal of Biological Chemistry 278 (41), 39839–39850.
Morahan, B.J., Wang, L., Coppel, R.L., 2009. No TRAP, no invasion. Trends in Parasitology 25 (2), 77–84. (Elsevier).
Mordue, D.G., Desai, N., Dustin, M., Sibley, L.D., 1999. Invasion by *Toxoplasma gondii* establishes a moving junction that selectively excludes host cell plasma membrane proteins on the basis of their membrane anchoring. Journal of Experimental Medicine 190 (12), 1783–1792.
Morrissette, N.S., Sibley, L.D., 2002. Cytoskeleton of apicomplexan parasites. Microbiology and Molecular Biology Reviews 66 (1), 21–38. (table of contents).
Moudy, R., Manning, T.J., Beckers, C.J., 2001. The loss of cytoplasmic potassium upon host cell breakdown triggers egress of *Toxoplasma gondii*. Journal of Biological Chemistry 276 (44), 41492–41501.
Muhia, D.K., Swales, C.A., Deng, W., Kelly, J.M., Baker, D.A., 2001. The gametocyte-activating factor xanthurenic acid stimulates an increase in membrane-associated guanylyl cyclase activity in the human malaria parasite *Plasmodium falciparum*. Molecular Microbiology 42 (2), 553–560. John Wiley & Sons, Ltd.
Nagamune, K., Sibley, L.D., 2006. Comparative genomic and phylogenetic analyses of calcium atpases and calcium-regulated proteins in the apicomplexa. Molecular Biology and Evolution 23 (8), 1613–1627.
Nagamune, K., Hicks, L.M., Fux, B., *et al*., 2008. Abscisic acid controls calcium-dependent egress and development in *Toxoplasma gondii*. Nature 451 (7175), 207–210.
Nava, S., Sadiqova, A., Castellanos-Gonzalez, A., White Jr., A.C., 2020. *Cryptosporidium parvum* cyclic GMP-dependent protein kinase (PKG): An essential mediator of merozoite egress. Molecular and Biochemical Parasitology 237, 111277. (Elsevier/North-Holland Biomedical Press).
Nishi, M., Hu, K., Murray, J.M., Roos, D.S., 2008a. Organellar dynamics during the cell cycle of *Toxoplasma gondii*. Journal of Cell Science 121 (Pt 9), 1559–1568.
Nishi, M., Hu, K., Murray, J.M., Roos, D.S., 2008b. Organellar dynamics during the cell cycle of *Toxoplasma gondii*. Journal of Cell Science 121 (Pt 9), 1559–1568.
Okada, T., Marmansari, D., Li, Z., *et al*., 2013. A novel dense granule protein, GRA22, is involved in regulating parasite egress in *Toxoplasma gondii*. Molecular and Biochemical Parasitology 189 (1), 5–13.
Ong, Y.C., Reese, M.L., Boothroyd, J.C., 2010. *Toxoplasma* rhoptry protein 16 (ROP16) subverts host function by direct tyrosine phosphorylation of STAT6. Journal of Biological Chemistry 285 (37), 28731–28740.
Pace, D.A., McKnight, C.A., Liu, J., Jimenez, V., Moreno, S.N.J., 2014. Calcium entry in *Toxoplasma gondii* and its enhancing effect of invasion-linked traits. Journal of Biological Chemistry 289 (28), 19637–19647.
Painter, H.J., Campbell, T.L., Llinás, M., 2011. The apicomplexan AP2 family: Integral factors regulating *Plasmodium* development. Molecular and Biochemical Parasitology 176 (1), 1–7.
Panas, M.W., Boothroyd, J.C., 2021. Seizing control: How dense granule effector proteins enable *Toxoplasma* to take charge. Molecular Microbiology 115 (3), 466–477.
Paredes-Santos, T.C., de Souza, W., Attias, M., 2012. Dynamics and 3D organization of secretory organelles of *Toxoplasma gondii*. Journal of Structural Biology 177 (2), 420–430.
Paul, A.S., Miliu, A., Paulo, J.A., *et al*., 2020. Co-option of *Plasmodium falciparum* PP1 for egress from host erythrocytes. Nature Communications 11 (1), 3532.
Pavlou, G., Biesaga, M., Touquet, B., *et al*., 2018. *Toxoplasma* parasite twisting motion mechanically induces host cell membrane fission to complete invasion within a protective vacuole. Cell Host and Microbe 24 (1), 81–96. e5.

Perkins, F.O., 1976. Zoospores of the oyster pathogen, dermocystidium marinum. I. Fine structure of the conoid and other sporozoan-like organelles. The Journal of Parasitology 62 (6), 959–974. ([The American Society of Parasitologists, Allen Press]).
Pernas, L., Adomako-Ankomah, Y., Shastri, A.J., *et al.*, 2014. *Toxoplasma* effector MAF1 mediates recruitment of host mitochondria and impacts the host response. PLoS Biology 12 (4), e1001845.
Persson, E.K., Agnarson, A.M., Lambert, H., *et al.*, 2007. Death receptor ligation or exposure to perforin trigger rapid egress of the intracellular parasite *Toxoplasma gondii*. The Journal of Immunology 179 (12), 8357.
Pino, P., Caldelari, R., Mukherjee, B., *et al.*, 2017. A multistage antimalarial targets the plasmepsins IX and X essential for invasion and egress. Science 358 (6362), 522–528.
Pinto, D.J., Vinayak, S., 2021. *Cryptosporidium*: Host-parasite interactions and pathogenesis. Current Clinical Microbiology Reports. 1–6.
Plattner, F., Soldati-Favre, D., 2008. Hijacking of host cellular functions by the apicomplexa. Annual Review of Microbiology 62 (1), 471–487.
Plattner, H., Kissmehl, R., 2003. Molecular aspects of membrane trafficking in paramecium. International Review of Cytology 232, 185–216.
Radke, J.B., Lucas, O., de Silva, E.K., *et al.*, 2013. ApiAP2 transcription factor restricts development of the *Toxoplasma* tissue cyst. Proceedings of the National Academy of Sciences of the United States of America 110 (17), 6871.
Reininger, L., Billker, O., Tewari, R., *et al.*, 2005. A NIMA-related protein kinase is essential for completion of the sexual cycle of malaria parasites*. Journal of Biological Chemistry 280 (36), 31957–31964.
Reiss, M., Viebig, N., Brecht, S., *et al.*, 2001. Identification and characterization of an escorter for two secretory adhesins in *Toxoplasma gondii*. Journal of Cell Biology 152 (3), 563–578.
Repnik, U., Gangopadhyay, P., Bietz, S., *et al.*, 2015. The apicomplexan parasite Babesia divergens internalizes band 3, glycophorin A and spectrin during invasion of human red blood cells. Cellular Microbiology 17 (7), 1052–1068.
Roiko, M.S., Svezhova, N., Carruthers, V.B., 2014. Acidification activates *Toxoplasma gondii* motility and egress by enhancing protein secretion and cytolytic activity. PLOS Pathogens 10 (11), e1004488.
Romano, J.D., Coppens, I., 2013. Host organelle hijackers: A similar modus operandi for *Toxoplasma gondii* and Chlamydia trachomatis: Co-infection model as a tool to investigate pathogenesis. Pathogens and Disease 69 (2), 72–86.
Roques, M., Wall, R.J., Douglass, A.P., *et al.*, 2015. *Plasmodium* P-Type Cyclin CYC3 modulates endomitotic growth during oocyst development in mosquitoes. PLOS Pathogens 11 (11), e1005273.
Rowe, J.A., Obiero, J., Marsh, K., Raza, A., 2002. Short report: Positive correlation between rosetting and parasitemia in Plasmodium falciparum clinical isolates. The American Journal of Tropical Medicine and Hygiene 66.
Roy, C.R., Mocarski, E.S., 2007. Pathogen subversion of cell-intrinsic innate immunity. Nature Immunology 8 (11), 1179–1187.
Samantha, N., Clinton, W.A., Alejandro, C.-G., H, A.J., 2021. *Cryptosporidium parvum* subtilisin-like serine protease (SUB1) is crucial for parasite egress from host cells. Infection and Immunity 87 (5), e00784–18. (American Society for Microbiology).
Sam-Yellowe, T.Y., Florens, L., Wang, T., *et al.*, 2004. Proteome analysis of rhoptry-enriched fractions isolated from *Plasmodium* merozoites. Journal of Proteome Research 3 (5), 995–1001.
Sassmannshausen, J., Pradel, G., Bennink, S., 2020. Perforin-like proteins of apicomplexan parasites. Frontiers in Cellular and Infection Microbiology 10, 507.
Schneider, A.G., Mercereau-Puijalon, O., 2005. A new Apicomplexa-specific protein kinase family: Multiple members in *Plasmodium falciparum*, all with an export signature. BMC Genomics 6, 30.
Schwab, J.C., Beckers, C.J., Joiner, K.A., 1994. The parasitophorous vacuole membrane surrounding intracellular *Toxoplasma gondii* functions as a molecular sieve. Proceedings of the National Academy of Sciences of the United States of America 91 (2), 509–513.
Sibley, L.D., Niesman, I.R., Parmley, S.F., Cesbron-Delauw, M.F., 1995. Regulated secretion of multi-lamellar vesicles leads to formation of a tubulo-vesicular network in host-cell vacuoles occupied by *Toxoplasma gondii*. Journal of Cell Science 108 (Pt 4), 1669–1677.
Singh, S., Alam, M.M., Pal-Bhowmick, I., Brzostowski, J.A., Chitnis, C.E., 2010. Distinct external signals trigger sequential release of apical organelles during erythrocyte invasion by malaria parasites. PLOS Pathogens 6 (2), e1000746. (Public Library of Science).
Sparvoli, D., Lebrun, M., 2021. Unraveling the elusive rhoptry exocytic mechanism of apicomplexa. Trends in Parasitology. 1–16. (Elsevier Ltd).
Spycher, C., Rug, M., Klonis, N., *et al.*, 2006. Genesis of and trafficking to the Maurer's clefts of *Plasmodium falciparum*-infected erythrocytes. Molecular and Cellular Biology 26 (11), 4074–4085. (American Society for Microbiology).
Stanway, R.R., Mueller, N., Zobiak, B., *et al.*, 2011. Organelle segregation into *Plasmodium* liver stage merozoites. Cellular Microbiology 13 (11), 1768–1782. John Wiley & Sons, Ltd.
Steinfeldt, T., Konen-Waisman, S., Tong, L., *et al.*, 2010. Phosphorylation of mouse immunity-related GTPase (IRG) resistance proteins is an evasion strategy for virulent *Toxoplasma gondii*. PLOS Biology 8 (12), e1000576.
Stommel, E.W., Ely, K.H., Schwartzman, J.D., Kasper, L.H., 1997. *Toxoplasma gondii*:Dithiol-induced Ca2 + Flux causes egress of parasites from the parasitophorous vacuole. Experimental Parasitology 87 (2), 88–97.
Striepen, B., Jordan, C.N., Reiff, S., van Dooren, G.G., 2007. Building the perfect parasite: Cell division in apicomplexa. PLOS Pathogens 3 (6), e78. (Public Library of Science).
Suss-Toby, E., Zimmerberg, J., Ward, G.E., 1996. *Toxoplasma* invasion: The parasitophorous vacuole is formed from host cell plasma membrane and pinches off via a fission pore. Proceedings of the National Academy of Sciences of the United States of America 93 (16), 8413–8418.
Tan, M.S.Y., Blackman, M.J., 2021. Malaria parasite egress at a glance. Journal of Cell Science 134 (5), jcs257345.
Tandel, J., English, E.D., Sateriale, A., *et al.*, 2019. Life cycle progression and sexual development of the apicomplexan parasite *Cryptosporidium parvum*. Nature Microbiology 4 (12), 2226–2236.
Tardieux, I., Baum, J., 2016. Reassessing the mechanics of parasite motility and host-cell invasion. The Journal of Cell Biology 214 (5), 507–515. (The Rockefeller University Press).
Tetley, L., Brown, S.M., McDonald, V., Coombs, G.H., 1998. Ultrastructural analysis of the sporozoite of *Cryptosporidium parvum*. Microbiology 144 (Pt 1), 3249–3255.
Thomas, J.A., Tan, M.S.Y., Bisson, C., *et al.*, 2018. A protease cascade regulates release of the human malaria parasite *Plasmodium falciparum* from host red blood cells. Nature Microbiology 3 (4), 447–455.
Tilley, L., Sougrat, R., Lithgow, T., Hanssen, E., 2008. The twists and turns of maurer's cleft trafficking in *P. falciparum*-infected erythrocytes. Traffic 9 (2), 187–197.
Travier, L., Mondragon, R., Dubremetz, J.-F., *et al.*, 2008. Functional domains of the *Toxoplasma* GRA2 protein in the formation of the membranous nanotubular network of the parasitophorous vacuole. International Journal for Parasitology 38 (7), 757–773.
Wanyiri, J.W., Techasintana, P., O'Connor, R.M., *et al.*, 2009. Role of CpSUB1, a subtilisin-like protease, in *Cryptosporidium parvum* infection in vitro. Eukaryotic Cell 8 (4), 470–477.
Warncke, J.D., Beck, H.-P., 2019. Host cytoskeleton remodeling throughout the blood stages of *Plasmodium falciparum*. Microbiology and Molecular Biology Reviews 83 (4), e00013–e00019.
Wetzel, D.M., Schmidt, J., Kuhlenschmidt, M.S., Dubey, J.P., Sibley, L.D., 2005. Gliding motility leads to active cellular invasion by *Cryptosporidium parvum* sporozoites. Infection and Immunity 73 (9), 5379–5387.
White, M.W., Suvorova, E.S., 2018. Apicomplexa cell cycles: Something old, borrowed, lost, and new. Trends in Parasitology 34 (9), 759–771.
Witola, W.H., Zhang, X., Kim, C.Y., 2017. Targeted gene knockdown validates the essential role of lactate dehydrogenase in *Cryptosporidium parvum*. International Journal for Parasitology 47 (13), 867–874.

World Health Organ. (WHO), 2021. World Malaria Report. Geneva: WHO, https://www.who.int/teams/global-malaria-programme/reports/world-malaria-report-2021.
Xiao, L., 2010. Molecular epidemiology of cryptosporidiosis: An update. Experimental Parasitology 124 (1), 80–89.
Yahata, K., Hart, M.N., Davies, H., *et al*., 2021. Gliding motility of *Plasmodium* merozoites. Proceedings of the National Academy of Sciences of the United States of America 118 (48), e2114442118.
Yamamoto, M., Standley, D.M., Takashima, S., *et al*., 2009. A single polymorphic amino acid on *Toxoplasma gondii* kinase ROP16 determines the direct and strain-specific activation of Stat3. Journal of Experimental Medicine 206 (12), 2747–2760.
Yeoh, S., O'Donnell, R.A., Koussis, K., *et al*., 2007. Subcellular discharge of a serine protease mediates release of invasive malaria parasites from host erythrocytes. Cell 131 (6), 1072–1083.
Yusuf, N.A., Green, J.L., Wall, R.J., *et al*., 2015. The *Plasmodium* Class XIV myosin, MyoB, has a distinct subcellular location in invasive and motile stages of the malaria parasite and an unusual light chain*. Journal of Biological Chemistry 290 (19), 12147–12164.
Zhang, H., Guo, F., Zhu, G., 2015. *Cryptosporidium* lactate dehydrogenase is associated with the parasitophorous vacuole membrane and is a potential target for developing therapeutics. PLOS Pathogens 11 (11), e1005250. (Public Library of Science).